Experimental Measurements and Modeling of Liquid-Liquid Taylor Flow in Mini-Scale Tubing

by

© Wesam Adrugi

A thesis submitted to the School of Graduate Studies in partial fulfillment of the requirements for the degree of Doctor of Philosophy

Department of Mechanical Engineering
Faculty of Engineering and Applied Science
Memorial University of Newfoundland

October 2019

St. John's, Newfound and Labrador, Canada

Abstract

Immiscible two-phase segmented flow in a mini / micro scale channel is a promising area for heat transfer enhancement. A segmented flow, also known as a slug flow, plug flow or Taylor flow is a series of moving liquid segments separated by a liquid medium. A literature review of the research reveals large gaps in the knowledge base of liquid-liquid Taylor flows and calls for further investigation. Earlier studies have reported that introducing two immiscible liquids into mini / micro scale channels significantly increases heat transfer rate. The main focus of this research is on modeling liquid-liquid Taylor flows using an experimental approach based on the concept of the internal fluid flow and a dimensionless analysis for reducing experimental data. The purpose of this study is to investigate the fluid dynamic and thermal characteristics of liquid-liquid Taylor flows in small-scale tubes that will lead to better understanding on this process. Therefore, the heat transfer and pressure drop in two-phase liquid-liquid Taylor flows inside mini-scale tubing have been examined using a wide range of geometrical and operational parameters such as Capillary number, Prandtl number and minichannel geometries. Proposed models for each of these geometries have been developed to predict the heat transfer behaviors and pressure drop for low Reynolds number flow conditions. The effect of internal circulation and boundary layer renewal within the flow components is clearly presented. Namely, it is shown that cause significant thermal enhancement. The intensity of these circulations is a function of different parameters, including the flow conditions, channel geometry, and liquids employed. The effects of all of these parameters on heat transfer and pressure drop have

been studied experimentally and are presented in this dissertation. Furthermore, this study demonstrates how heat transfer enhancement results due to varying the slug lengths of each phase in the liquid-liquid Taylor flow. New experimental data for liquid-liquid Taylor flows in straight, curved, and coiled mini scale tubes were obtained using low viscosity silicone oils segmented by water at varying volume fractions. The results of this thesis are of fundamental and practical relevance for the analysis and design of small systems and devices incorporating liquid-liquid Taylor flow regimes. The novel results were obtained with carefully controlled flow cell slug lengths and volume fractions, which show a significant impact on the rate of laminar heat transfer and pressure drop. Analytical models for each of these geometries have been developed. Dimensionless heat transfer rate and pressure drop results show good agreement with proposed analytical models. The proposed models' predictions for the heat transfer and pressure drop agree with the new experimental data within ± 20% or less.

Acknowledgements

I would like to express the deepest appreciation to my supervisor, Prof. Dr. Yuri S. Muzychka, who has the attitude and the substance of a great mentor, as well as his support in terms of providing the required equipment in the laboratory to conduct this work. Without his guidance and persistent help, this dissertation would not have been possible.

I would also like to express my gratitude to Dr. Kevin Pope, the co-supervisor of this thesis, for his useful comments, remarks, and engagement.

I gratefully acknowledge the Natural Sciences and Engineering Research Council of Canada (NSERC) for providing financial assistance under the Discovery Grants program. The financial support of the Libyan Ministry of Higher Education and Scientific Research is also gratefully acknowledged.

Last but not least, I am especially beholden to my lovely wife, Esra for her continuous support and sacrifice.

Finally, I would like to dedicate this work to the soul of my beloved mother, my dear father, and to all my precious family members.

Table of Contents

List of Tables

List of Figures

Nomenclature

A	=	Area, m^2
Bo	=	Bond number, $\equiv gD_h^2(\rho_1 - \rho_2)/\sigma$
Ca	=	Capillary number, $\equiv \mu U/\sigma$
c_p	=	Specific heat, J/kgK
D	=	Diameter, m
D_h	=	Hydraulic diameter, m
De	=	Dean number, $\equiv Re\sqrt{D/2R}$
f	=	Fanning frication factor, $\equiv \tau_w/\frac{1}{2}\rho U^2$
G	=	Mass flux, kg/m^2s
Gr	=	Graetz number, $\equiv Pe/L/D$
h	=	Thermal convection coefficient, W/m^2K
k	=	Thermal conductivity, W/mK
L	=	Length, m
L^*	=	Dimensionless thermal length, $\equiv {L/D}/{Pe}$
$\dot{m}$	=	Liquid mass flow rate, kg/s
Nu	=	Nusselt number, $\equiv hD/k$
P	=	Perimeter, m

p = Pressure, N/m^2

Pe = Peclet number, $\equiv UD/\alpha$

Pr = Prandtl number, $\equiv c_p\,\mu/k$

$\dot{Q}$ = Volumetric flow rate, m^3/s

Q = Heat transfer, W

$\bar{q}$ = Mean heat flux, W/m^2

q^* = Dimensionless heat flux

R = Radius, m

R_c = Effective radius of curvature, m

Re = Reynolds number, $\equiv UD/v$

t = Tube wall thickness, m

T = Temperature, K

u = Velocity, m/s

U = Average velocity, m/s

We = Weber number, $\equiv \rho U^2 D/\sigma$

Greek Symbols

α = Thermal diffusivity, m^2/s

α_L = Liquid fraction

μ	=	Dynamic viscosity, Ns/m^2
ρ	=	Density, kg/m^3
ν	=	Kinematic viscosity, m^2/s
x	=	Two-phase quality
δ	=	Film thickness, m
σ	=	Interfacial tension, N/m
θ	=	Contact angle, rad
τ	=	Shear stress, Pa
Δ	=	Difference

Subscripts

1	=	Phase 1
2	=	Phase 2
a	=	Advancing
c	=	Continuous phase (Carrier phase)
$d\ (s)$	=	Dispersed phase (Segmented phase)
e	=	Effective
g	=	Gas
i	=	Inlet

Int	=	Interface
l	=	Liquid
m	=	Mean
o	=	Outlet
r	=	Receding
$slug$	=	Slug
Sp	=	Single-phase
Tp	=	Two-phase
T	=	Total
t	=	Wall thickness of tubing
w	=	Wall

Superscripts

*	=	Dimensionless
$\overline{(\cdot)}$	=	Mean value

CHAPTER 1

Introduction and Background

1.1 Overview

Liquid-liquid Taylor flow in small scale tubing is a two-phase flow pattern encountered in a wide range of applications such as electronics cooling systems, pharmacology industry, microfluidics, biological engineering, and chemical micro processing. Following the emergence of small-scale channels as an attractive technology for single-phase flow applications, research has been conducted on the thermo-fluid fundamentals and applications of two-phase flows. Such research has increased the demand for details of flow hydrodynamics, pressure drop, and heat transfer characteristics in the analysis and design of small devices [1 – 4].

There are several motivating factors for transferring existing technologies into small-scale designs, and some of these include device portability and cost reduction for manufacturers and consumers. Since the past decades, there has been a lot of interest in developing miniature mechanical systems, electronic and computer devices, and MEMS (Micro-Electro-Mechanical-Systems). Recent developments in a microelectronics passive

cooling system ignited the need to create two-phase flows in small scale, such as the adiabatic and non-adiabatic gas-liquid, and liquid-liquid two-phase flows. As a result, two-phase flows have become an active research area. They can be found in applications such as microfluidic sensors and biological diagnostic tools, especially lab-on-a-chip devices [5, 6].

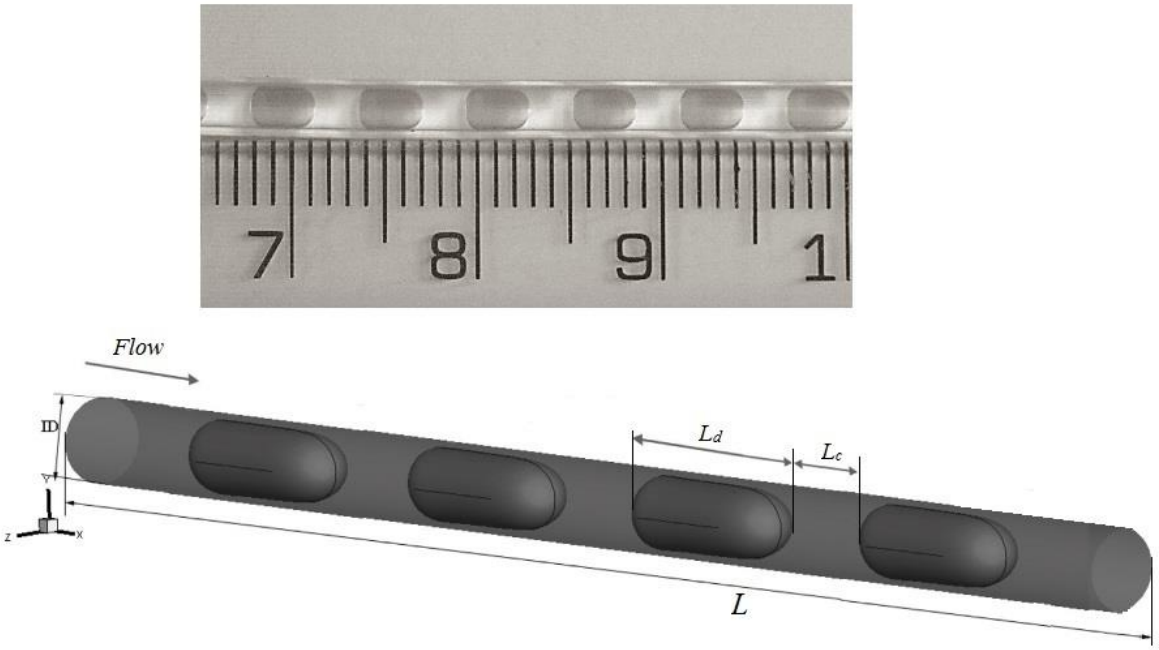

Fig. 1. 1 - Liquid-liquid Taylor flow of dyed water (dispersed phase)-oil (carrier phase) in a mini-scale tube.

This thesis is concerned with the development of models for predicting the liquid-liquid Taylor flow characteristics in mini-scale tubing. It presents a fundamental investigation of the thermal and hydrodynamic characteristics of liquid-liquid slug flow regime confined to mini / micro channel geometries. Liquid-liquid Taylor flow has potential use in a variety of

applications, however, this thesis is focused on assessing the thermal performance of the heat sinks, as well as determining the complex fluid dynamics that govern liquid-liquid Taylor flow. The aim of this chapter is to provide an overview of the fundamentals and applications of two-phase flows in mini / micro-channels.

Details of flow hydrodynamics, pressure drop, and heat transfer characteristics in Taylor flow are required in the analysis and design of devices used for these applications. The flow regime is characterized by segmenting the fluid stream into a series of shorter liquid plugs surrounded by a thin liquid film at the tube wall. A two-phase slug flow contains a series of elongated plugs (carrier phase / dispersed phase) in a mini / micro channel, usually with a plug length greater than the hydraulic diameter of the tube, as shown in Fig. (1.1). Taylor flow is commonly referred to as segmented flow, slug flow or plug flow.

1.2 Flow Patterns

This section provides an overview of two-phase regimes encountered for horizontal flow in a small diameter channel, which is similar to the flow in this research. A flow pattern or regime is a specific type of geometric distribution of components, and there are several standard names for these flow patterns. Even though the visual inspection is the most commonly used technique for visualizing or mapping flow regimes, there exists other means including analysis of the spectral content of the unsteady pressures or the fluctuations of the volume fraction. A wide variety of two-phase flow patterns in relatively small-scale channels were noted and described in the literature. The different names given to the same geometric flow patterns and the subjective nature of defining flow patterns are responsible for these variations. Knowing the two-phase flow pattern can help in predicting

proper models for mass momentum, heat transfer, and pressure drop, which are important in the design process [7, 8]. When gas-liquid or liquid-liquid mixtures flow in a horizontal mini / micro channel, the two phases may distribute into different patterns. Most researchers now recognize the existence of four flow patterns: bubble flow, slug flow, ring or churn flow, and annular flow (see Fig. 1.2). Slug-annular flow is the term used to refer to the combination of slug and churn flows. Some researchers have named annular flow as mist or annular-mist flow [9].

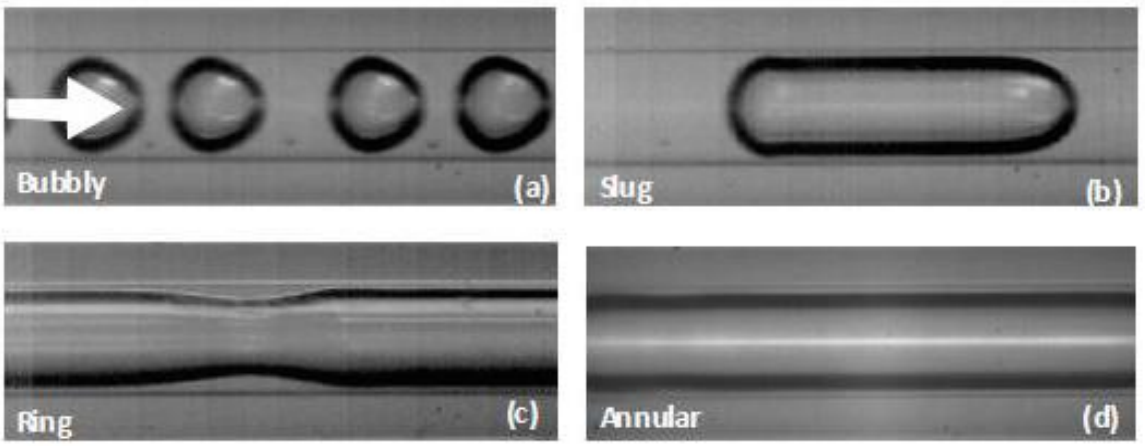

Fig. 1. 2 - Two-phase flow patterns in micro-tubes (D = 324 μm) [7].

In mini / micro channels, there are various types of flow pattern maps of two-phase flow. With the help of these maps, transition boundaries can be determined in a two-dimensional coordinate system. The type of flow pattern that would occur as well as the system geometry and phase velocities can be predicted by using a flow map. Also, a flow map gives the required model and the type of flow pattern can be obtained based on combination of

different flow rates. There are differences in both absolute value and trend when various maps are compared. Presently, the transition boundaries are not determined via physical models but through empirical techniques. The transport rates of heat, mass, and momentum can better be predicted by having a detailed understanding of the flow characteristics of various flow regimes. Thus, this thesis is focused on examining the heat transfer and pressure drop in the slug flow regime, where a well-defined interface separates two phases. While the slug flow regimes occupy a large portion of the flow regime map, it also has several industrial applications [2]. A number of articles, which studies have been published on liquid-liquid flow pattern, such as Dessimoz et al. [10], Salim et al. [11], Kumar et al. [12], Kashid and Kiwi-Minsker [8], Tsaoulidis et al. [13], Biswas et al. [14], Wu et al. [15]. Given the different operating conditions in these studies, the primary task is to predict the flow pattern and value of characteristic fluid as well as the flow parameters at which the transition from one flow-pattern to another will take place.

1.3 Dimensionless Groups

A significant quantity of dimensionless groups exists to assist two-phase flow researchers in developing more general results and models. There are a lot of dimensionless groups that can be used to convert Taylor flow data into more convenient forms. Dimensionless numbers provide a means of assessing the relative magnitudes of these interacting forces. In addition to using classical dimensionless groups, like hydrodynamic and thermal groups, to characterize two-phase Taylor flow models, there are also a series of groups used in the fundamental relations characterization of Taylor flow in micro and mini channels.

1.3.1 Dimensionless Hydrodynamic and Thermal Groups

This subsection presents a brief overview of the dimensionless groups used in the hydrodynamic and thermal characterization of Taylor flows.

Reynolds Number

The Reynolds number is the ratio of inertial and viscous forces, which is traditionally defined as:

$$Re = \frac{\rho U D_h}{\mu} \tag{1.1}$$

The low value of the Reynolds number indicates that viscous forces dominate inertial forces, which results in laminar flow in mini and micro channels. For two-phase flow, the Reynolds number depends upon the flow rates and physical properties of the two phases.

Capillary Number

The Capillary number is the ratio of the viscous and surface tension forces and is an important dimensionless number in two-phase Taylor flow with decreasing channel size.

$$Ca = \frac{\mu U}{\sigma} \tag{1.2}$$

In the above equation, σ is the surface tension between the two phases. In the case of liquid plugs in a capillary tube, the Capillary number (Ca) can be viewed as a measure of the scaled axial viscous drag force and the capillary or wetting force. For two-phase flow in mini / micro scale channels, Ca is expected to play a critical role because both the surface tension and the viscous forces are important in narrow channel flows. The Capillary number (Ca) also controls principally the liquid film thickness (δ) surrounds the immiscible liquid phase in liquid-liquid two-phase slug flows.

Weber Number

The Weber number is the ratio of the inertial and surface tension forces, which can also be expressed as the product of the Reynolds and Capillary numbers. It is defined as:

$$We = Re\ Ca = \frac{\rho U^2 D_h}{\sigma} \tag{1.3}$$

For liquid-liquid flow, where there is an interface between the liquid phases, the Weber number plays an important role in determining surface tension effects and the formation of slug in a mini and micro scale channel. If the surface tension of the fluid decreases, slugs will have the tendency to decrease because of higher momentum transfer between the phases.

Bond Number

It represents the ratio of gravitational (buoyancy) and capillary force scales. The Bond number is defined as

$$Bo = \frac{g {D_h}^2 (\rho_1 - \rho_2)}{4\,\sigma} \tag{1.4}$$

The gravitational force can be neglected in two-phase flow in micro-channels if Bo < 1. As a result, the other forces like surface tension force, the inertial and the viscous shear force exerted by the liquid phase are found to be the most critical forces in the formation of two-phase flow patterns.

Froude Number

The Froude number is defined as the ratio of inertial and gravitational forces, as given below

$$Fr = \frac{\rho U^2}{\rho g D_h} = \frac{U^2}{g D_h} \tag{1.5}$$

Although the dominance of the inertia force in mini-scale channels, the gravitational force could play an important role in some flow conditions. When Fr < 1, small surface waves can move upstream; when Fr > 1, they will be carried downstream; and when Fr = 1 (said to be the critical Froude number), the velocity of flow is equal to the velocity of surface waves.

Dean Number

The Dean number (De) depends on the Reynolds number (Re) as well as on the channel geometry. It is defined as

$$De = Re\sqrt{D_h/2R_c} \tag{1.6}$$

It serves as a dimensionless group that accounts for the secondary flow patterns in curved or coiled tubes or ducts.

Nusselt Number

It represents the ratio of convective to conductive heat transfer across (normal to) the boundary. The Nusselt number is defined as

$$Nu = \frac{(Q/A)D_h}{k(T_w - T_m)} = \frac{h\, D_h}{k} \tag{1.7}$$

It can be viewed as either the dimensionless heat transfer rate, defined based on the difference between wall temperature (T_w) , and fluid bulk temperature (T_m) , or dimensionless heat transfer coefficient. $Nu \sim 1$, namely convection and conduction of similar magnitude, is characteristic of "slug flow" or laminar flow.

Dimensionless Heat Transfer

Another approach exists for defining a dimensionless heat transfer (q^*), as follows:

$$q^* = \frac{(Q/A)D_h}{k(T_w - T_i)} \tag{1.8}$$

It is based on the difference between wall temperature (T_w) and inlet temperature (T_i), leading to a dimensionless wall flux (q^*).

Prandtl Number

The Prandtl number is a measure of the rate of momentum diffusion to that of thermal diffusion. It is defined as follows

$$Pr = \frac{\nu}{\alpha} = \frac{c_p \mu}{k} \tag{1.9}$$

These diffusion rates determine the relative thickness of the thermal and hydrodynamic boundary layer.

Peclet Number

This dimensionless number represents the ratio of thermal energy convection to the fluid (advection) to thermal energy conduction within the fluid (diffusion). It is defined as

$$Pe = \frac{UD_h}{\alpha} = Re\ Pr \tag{1.10}$$

It is used in calculations involving heat convection and α is the thermal diffusivity of the fluid.

1.3.2 Dimensionless Taylor Flow Groups

In two-phase Taylor flow, several dimensionless numbers are critical to the thermal and hydrodynamic characterization. The mass flow rate of two-phase flow is:

$$\dot{m}_T = \dot{m}_1 + \dot{m}_2 = \rho_1 \dot{Q}_1 + \rho_2 \dot{Q}_2 \tag{1.11}$$

The mass fraction or mixture quality, in the case of a two-phase flow, is defined as

$$x = \frac{\dot{m}_2}{\dot{m}_1 + \dot{m}_2} \tag{1.12}$$

such that when $x = 0$, only phase 1 is present, and when $x = 1$, only phase 2 is present. For Taylor flow, these correspond to all-carrier phase and all-dispersed phase, respectively. The void fraction of the flow is a ratio of volumetric flow rates within the system, which is defined as

$$\beta = \frac{\dot{Q}_2}{\dot{Q}_1 + \dot{Q}_2} \tag{1.13}$$

This parameter is more commonly encountered in Taylor flows. The volume fraction of a two-phase flow (void fraction in a gas / liquid flow or liquid fraction in a liquid / liquid flow) gives the fraction of the dispersed phase.

1.4 Taylor / Slug Flows

One of the common two-phase flow patterns encountered is Taylor (slug) flow in narrow tubes. Taylor flow is characterized by splitting the fluid stream in the channel or tube into a series of shorter elements or slugs (plugs) and surrounded by a thin liquid film at the tube wall. One phase is termed the carrier or base fluid while the other phase is termed the segmenting media or dispersed phase, as shown in Fig. (1.3).

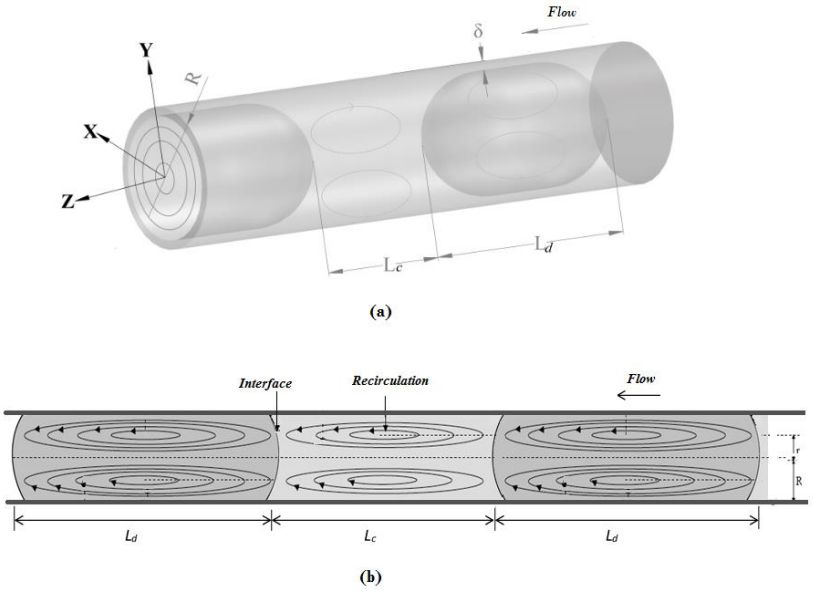

Fig. 1. 3 - Schematic of internal circulations in moving plugs: (a) 3D and (b) 2D.

Researchers often refer to Taylor flow as segmented flow, slug flow or plug flow, and Taylor [16] who examined two-phase plug flows with a view to understanding film thickness and deposition at the wall. It is straightforward to produce and examine slug flow on micro-scale systems where surface tension force is a dominating factor on gravity force. However, it is almost impossible to create a steady train of slugs at macro-scale due to surface tension being a non-dominant factor.

Internal circulations arise within liquid slugs of Taylor flow, due to liquid-liquid interfaces or gas-liquid interfaces and these internal circulations (circulation eye) are shown in Fig. (1.3). As the slug moves forward, there are two dominating symmetrical vortices that affect the flow field in a normal liquid plug of Taylor flow. When the liquid in the slug moves towards the front of the slug, the liquid is blocked by the front interface, which

changes the flow direction towards the wall of the channel, and then the liquid moves backward due to the friction with the wall of the channel. At the rear of the liquid slug, fluid moves from the wall of the micro channels to the center of the slug due to the presence of the rear interface. Therefore, a recirculating flow pattern is produced in the liquid plug as a result of the front / rear interfaces. Heat transfer between the liquid and the wall is enhanced by the transverse flow of the vortices circulating in the slug. Similarly, the same process also takes place within the carrier phase, which likewise produces a circulating flow pattern [17].

The hydrodynamic studies of the flow are essential for both segmented flow and curved geometry to understand the nature of the flow, as well as the effect of secondary flow, which is the main reason for the augmentation of mass and heat transfer. Particle image velocimetry (PIV) is a well-established technique for measuring flow in mini / micro scale channels.

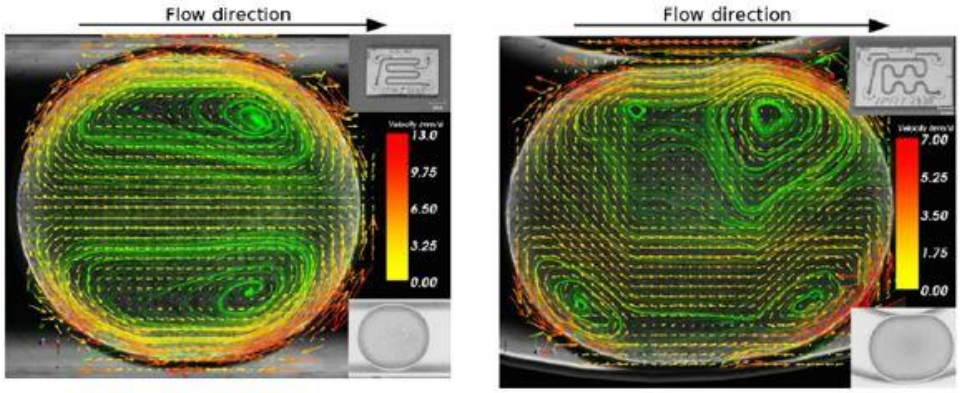

Fig. 1. 4 - Instantaneous velocity vector and streamline in liquid plugs for (a) straight micro channel, and (b) winding micro channel [18].

Significant success has been achieved in developing micro resolution PIV (micro-PIV) systems. In particular, Malsch et al. [18] used the micro-PIV technique to measure Taylor flows and demonstrated the existence of internal circulation structures in both straight and winding small-scale tubes, as shown in Fig. (1.4). Micro-PIV is the most promising visualization technique since it can produce high-quality results with spatial and temporal resolutions.

1.4.1 Taylor/Slug Flow Generation

Segmental flow can be produced in channels or ducts in several ways; however, a T-junction is the most common method. The segments are generated as each phase cuts the flow of the other as the phases merge at the junction. Additionally, the slug flow regime depends upon stabilities at the interface between two immiscible phases in narrow horizontal channels. In mini or micro size tubes, the surface forces are higher than gravitational forces, resulting in a segmented slug flow regime.

The techniques employed in generating a slug flow regime and their associated fluid dynamics can be found in Christopher and Anna [19], Gunther and Jensen [20], Kawakami et al. [21] and Collins et al. [22], among others. The following is a brief summary of these techniques and devices, which are used in the formation of Taylor flow and their associated fluid dynamics.

The different techniques used to produce Taylor flow can be summarized and classified in two approaches: active or passive. Both methods employ two immiscible phases, in specified segments, which allow the breaking of one of the streams into discrete droplets.

To obtain precise control over the slugs' parameters (size and frequency) while using these methods, a very accurate flow control system is essential. Active techniques rely upon an external force to control slug size and frequency. Typically, an actuation mechanism utilizes a flexible membrane or micro-valve that is deflected using a piezoelectric transducer. The timing, amplitude and duration of a pressure pulse can be controlled to produce various slug formations. Passive techniques are more common for generating uniform liquid slugs. These methods take advantage of the flow field to deform the interface and promote the natural growth of interfacial instabilities, without the influence of external actuations [23, 24]. Typically, the force driving fluid flow to the segmentation device is an externally driven pressure source, such as a syringe or pressure-driven pump.

Passive approaches could be classified into several groups, in these categories, the formation of the slugs is described by the nature of the flow near the slug break-off point. Geometries commonly employed for passive droplet generators include (i) co-flowing streams (Fig. 1.5 - a), (ii) cross-flowing (T-junctions, X-junctions or Y-junction) (Fig. 1.5 - b) and (iii) flow-focusing (Fig. 1.5 - c). However, uniform slugs can be produced over a range of sizes by changing the ratio of liquid flow rates.

Two methods are used in this thesis to generate a segmented slug flow regime: (1) T-junctions, whereby slug form due to break up in cross-flowing streams, as shown in the Fig. (1.5 – b). (2) The segmenters, whereby slug form due to break up in a flow focusing geometry as shown in Fig. (1.5 – c). The segmenters principle operation is through the liquid bridge ruptures between the two opposing capillary points by another liquid periodically. The design of these segmenters was based on a previous study by Curran et

al. [25] to dispense the sub-microliter volumes of reagents used as microfluidic chemical reactors in a polymerase chain reaction process.

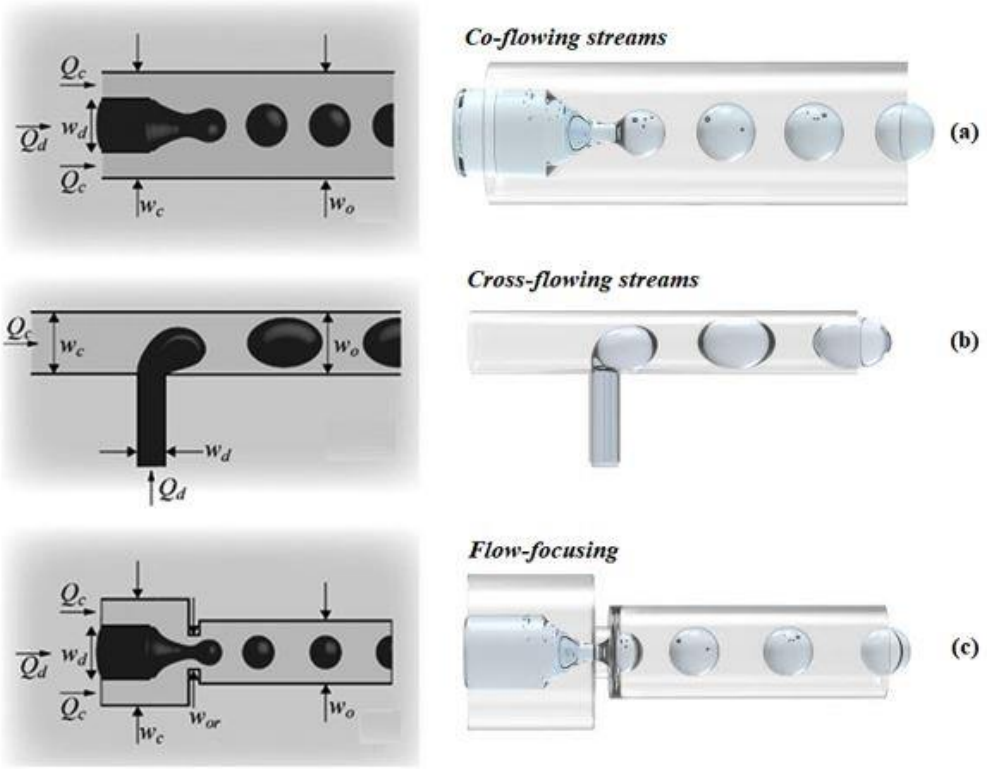

Fig. 1. 5 - Schematic illustration and images of the three types of passive slug generators for liquid-liquid Taylor flow: (a) co-flowing streams, (b) cross-flowing streams and (c) flow-focusing geometry [19].

1.4.2 Mechanisms of Heat Transfer

The thermal enhancement occurs in small-scale tubing using liquid-liquid Taylor flow due to internal circulation within liquid plugs, which is mainly caused by shear forces of the fluids in addition to increasing the flow rate of injected liquids. As illustrated in Fig.

(1.4), the internal circulations within the liquid slugs bring fresh liquid from the center of the slug to the wall through linear and winding micro channels, where the heat transfer process occurs. This provides a renewal mechanism to the thermal boundary layer and increases heat transfer. However, since diffusion is also important in this process, the boundary layer grows until the circulation center (circulation eye) receives the thermal energy. The effects of the internal circulations on the heat removal process at a wall were demonstrated by Fischer et al. [26], as shown in Fig. (1.6).

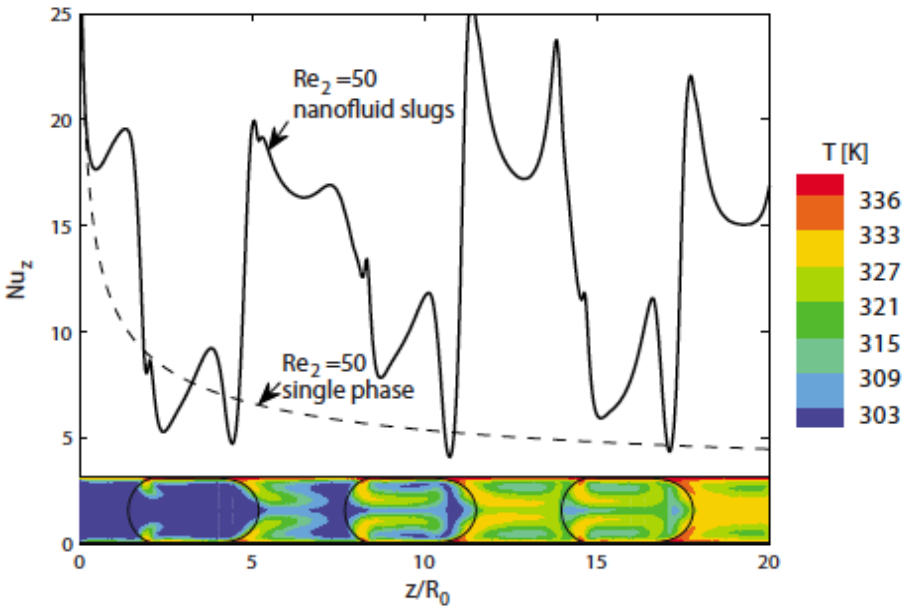

Fig. 1. 6 - Local Nusselt number and Temperature field in axial direction for liquid-liquid flow with elongated droplets and compared with single fluid flow [26].

For Poiseuille flow, the flow through the circular heated channel would follow the well known Graetz problem of a thermally developing and hydrodynamically fully developed laminar flow. However, for slug flow (Taylor flow), the presence of these toroidal vortices

results in significant changes to the development of the thermal boundary layer. According to Che et al. [27], the heat transfer process begins immediately after the plug is inserted into the channel, and there are three stages of convective heat transfer that occur between the heated wall and the slug. These stages include:

(i) The development of the thermal boundary layer: the liquid in the continuous phase touches the heated wall, which causes a rapid increase in the temperature of the thin liquid layer surrounding the wall, and thus, leading to the formation of a thermal boundary layer. While the thermal boundary appears thinner at the front of the slug, it is thicker at the rear due to the relative flow fields, as illustrated in Fig. (1.6).

(ii) Advection of heated / fresh fluid in the plug: cooler fluid moves towards the heated wall due to the presence of the front interface. Warmer fluid is transported to the capillary centerline from the wall at the rear interface, which leads to a reformation of the thermal boundary layer.

(iii) Thermally fully developed flow: this stage is formed due to the absolute value of the slug temperature gradually approaches the temperature of the capillary wall.

1.4.3 Pressure Drop

Pressure drop is one of the most important parameters needed for the design of process equipment. It is considered as an important parameter because it affects the sizing of the pumps, stability and flow rates as well as the total cost of the system. However, despite several theoretical and experimental studies, significant gaps exist for two-phase frictional pressure drop in small channels. Models are needed to accurately predict the pressure drop in two-phase Taylor flow ducts for the design of process devices. Typically, two-phase flow

pressure gradient in tubes occurs due to friction, acceleration, and gravitation. For single-phase laminar flow in small-scale horizontal channels, the pressure drop is determined using a friction factor. However, the frictional pressure gradient for Taylor flow is due to the mixture of shear stress at the tube wall and interfacial effects between phases. Compared to single-phase flow, there is an appreciable increase in pressure drop when a second immiscible phase is added to the flow.

There are limited analytical approaches used for pressure drop modeling in two phase Taylor flow. The two most widely applied approaches are homogeneous flow and separated flow models. In the homogeneous flow model, mixture properties are utilized with traditional single-phase flow pressure drop. In the separated flow model, each phase is modeled separately based on hydrodynamic properties and different velocities. However, these methods do not differentiate between the different physics associated with different flow regimes. Hence, without specific knowledge of the flow patterns, these models are generally not suitable for Taylor flow regime applications. There are several models developed specifically for Taylor flow regimes. These models are presented in the following subsections.

1.4.3.1 Homogeneous Flow Modeling

The homogeneous modeling approach is the most straightforward means of analyzing the pressure drop associated with a two-phase flow regime. This modeling technique assumes that the two-phase flow behaves as a pseudo single-phase fluid with average or mixture defined thermo-physical properties, i.e., McAdams model, Dukler model, and

Cicchitti model [28], [29]. The pressure drop per unit length, $\Delta P/L$, in capillary tubes or channels is calculated using models from single-phase flow theory:

$$\Delta P = 4f\frac{L}{D}\frac{1}{2}\bar{\rho}_e U^2 \tag{1.14}$$

Using the appropriate mixture and friction models from single-phase flow theory, one can easily calculate the two-phase flow multiplier. A review of some simple models used for mixture properties of two-phase Taylor flow will be given later.

1.4.3.2 Separated Flow Modeling

Unlike homogeneous flow modeling, separated flow modeling takes into account that the two-phases have different hydrodynamic properties and flow with different velocities. Several approaches with various degrees of sophistication have been developed, and typical examples include the Lockhart-Martinelli correlation, Chisholm correlation and Friedel correlation [29], [30]. In the separated approach, both phases are considered independently, and the resultant pressure drop is predicted as the sum of their single-phase contributions. Although the interfaces between the two phases may cause additional pressure drop, this is not accounted for in this model. Thus, Lockhart and Martinelli [31] added an empirical parameter to the separated flow model to account for this additional pressure drop that may occur between the two phases. The basic formulation of a separated flow model is similar to that of a two-phase frictional multiplier, ϕ, which defines the ratio of the two-phase flow pressure gradient to a reference single-phase pressure gradient.

$$\phi = \sqrt{\frac{(\Delta P/L)_{TP}}{(\Delta P/L)_{SP}}} \tag{1.15}$$

The Martinelli parameter X is defined as:

$$X = \sqrt{\frac{(\Delta P/L)_d}{(\Delta P/L)_c}} = \frac{\phi_c}{\phi_d} \tag{1.16}$$

where c, d refer to the carrier and dispersed phases respectively, and X is a reference scale that defines the extent to which either the carrier or dispersed phase dominate the two-phase pressure drop. Most of the available separated flow models for large channels do not include surface tension effects, which are important in small channels. Therefore, it is imperative to study hydrodynamics in these flow patterns.

1.4.3.3 Taylor / Slug Flow Modeling

The unique hydrodynamic features of liquid-liquid Taylor flows are not captured in both the homogeneous and separated flow models previously discussed. Nevertheless, various models have specifically been developed for Taylor flow regimes [32]. These models consist of the frictional pressure drop of the individual phases (ΔP_f) and the pressure drop due to the interfacial effects (ΔP_{Int}). This approach assumes that a fully developed laminar flow separates the slugs from the capillary wall with or without liquid film. The interfacial pressure is calculated using the Young-Laplace equation by Bretherton's solution [33, 34]. The overall pressure drop is

$$\Delta P_{Slug} = \Delta P_f + \Delta P_{Int} \tag{1.17}$$

Introducing a second phase into laminar flow in a small channel to create a slug flow regime, which significantly alters the hydrodynamic characteristics of the flow, results in an increase in the pressure drop over the single-phase flow case. Consequently, the sum of

the contribution of each phase (i.e., the single-phase pressure drops of the various phases and the additional interfacial pressure drop) can be used to calculate the total pressure drop of Taylor flow in the channel.

1.4.4 Film Thickness

Another important characteristic of Taylor flow is liquid film thickness, δ, between the slug and the channel wall, which affects the mass, heat and momentum transfer within the carrier fluid and the slug by circulation and bypass. In applications such as heat and mass transfer from the channel wall, the thickness of this liquid film is considered essential [32, 35, 36] The change in liquid film thickness depends on the capillary number, as reported by Fairbrother and Stubbs [37], Bretherton [38], and Taylor et al. [16]. There are several models for film thickness in a Taylor flow, as presented in Table (1.1).

Table 1. 1 - Correlations of film thickness (δ) for two-phase Taylor flow.

Author(s)	**Correlation**	**Flow conditions**
Fairbrother and Stubbs (1935)	$\delta/_R = 0.5\ Ca^{1/2}$	$5.0 \times 10^{-5} < \mathrm{Ca} < 3.0 \times 10^{-3}$ Liquid-gas Taylor flow
Bretherton (1960)	$\delta/_R = 0.66\ Ca^{2/3}$	$10^{-3} < \mathrm{Ca} < 10^{-2}$ Liquid-gas Taylor flow
Taylor (1961)	$\delta/_R = \frac{1.34\ \mathrm{Ca}^{2/3}}{1 + 3.35\ \mathrm{Ca}^{2/3}}$	$10^{-3} < \mathrm{Ca} < 1.4$ Liquid-gas Taylor flow
Irandoust and Andersson (1989)	$\delta/_R = 0.335\ [1 - \exp(-3.08\ Ca^{0.79})]$	$9.5 \times 10^{-4} < \mathrm{Ca} < 1.9$ Liquid-gas Taylor flow
Han and Shikazono (2009)	$\delta/_R = \frac{1.34\ \mathrm{Ca}^{2/3}}{1 + +3.13\ \mathrm{Ca}^{2/3} + 0.54\ \mathrm{Ca}^{0.672}\mathrm{Re}^{0.589} - 0.352\ \mathrm{Ca}^{0.629}}$	$\mathrm{Ca} < 4.0 \times 10^{-1}$ Liquid-gas Taylor flow
Dore et al. (2012)	$\delta/_R = 0.3\ [1 - \exp(-6.9\ Ca^{0.54})]$	$7.0 \times 10^{-3} < \mathrm{Ca} < 1.59 \times 10^{-1}$ Liquid-liquid Taylor flow

Eain et al. (2013)	$\delta/_R = 0.35\, Ca^{0.354}\, We^{0.097}$	$2.0 \times 10^{-3} < \mathrm{Ca} < 1.19 \times 10^{-1}$ $4.7 \times 10^{-2} < \mathrm{We} < 6.97 \times 10^{-1}$ Liquid-liquid Taylor flow
Tsaoulidis and Angeli (2015)	$\delta/_R = 0.658\, Ca^{0.6409}\, Re^{0.1067}$	$3.0 \times 10^{-2} < \mathrm{Ca} < 1.8$ Liquid-liquid Taylor flow

When film thickness increases, more fluid bypasses through the film and limits recirculation in the liquid plugs. Whereas, a decrease in film thickness leads to recirculation of streamlines in the liquid plugs, as illustrated in Fig. (1.7). There are two different classes of experimental methods for estimating the film thickness:

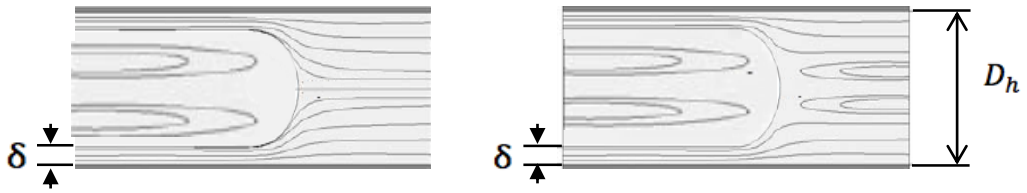

Fig. 1. 7 - Streamlines in liquid plugs film thickness (δ) for complete bypass flow and recirculation of streamline.

(i) Direct methods: high-quality images, for which optical properties are either not affected by the curved channel wall [39] or corrected for optical distortion [17], [40] to measure the film thickness directly.

(ii) Indirect methods: an experimental approach is used to determine the bubble velocity, and continuity is then applied to calculate the film thickness. Adequate knowledge of the velocity profile in the liquid film is needed [2].

1.5 Curved or Coiled Geometry

The geometry of ducts may significantly affect the behavior of two-phase Taylor flow and subsequently the transport phenomena (mass and heat) within the plugs. A particular surface geometry such as a bend or coiled geometries in thermal applications is one of the passive techniques for heat transfer enhancement as well as fluid additives using fluid properties or segmented flow. The various types of curved or coiled tube geometries and twisted tubes are shown in Fig. (1.8).

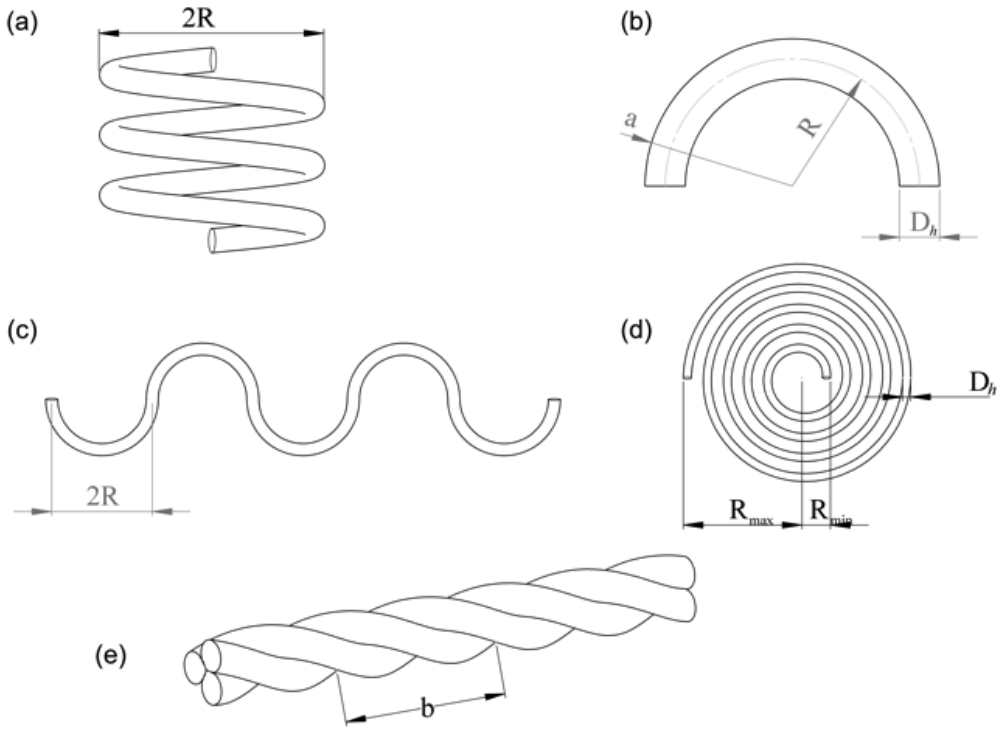

Fig. 1. 8 - Different type of curved tube geometries: (a) helical coil, (b) bend tube, (c) serpentine rube, (d) spiral and (e) twisted tubes [41].

The importance and use of curved or coiled channels in heating applications and mass transfer applications due to the secondary flow are by providing the high heat and mass transfer area per unit volume. Taylor flow in curved channels can give rise to a recirculating motion in the streamwise direction (as seen in Taylor flow in straight channels), as well as in the spanwise direction (originating from the centrifugal force) and can therefore have very high rates of heat and mass transfer. Unlike the flow in a straight channel, flow induction is asymmetric as a result of the channel curvature. This leads to more complex flow fields, which results in a faster mass and heat transfer over the whole segment, as well as improved mixing efficiency in curved channels [18].

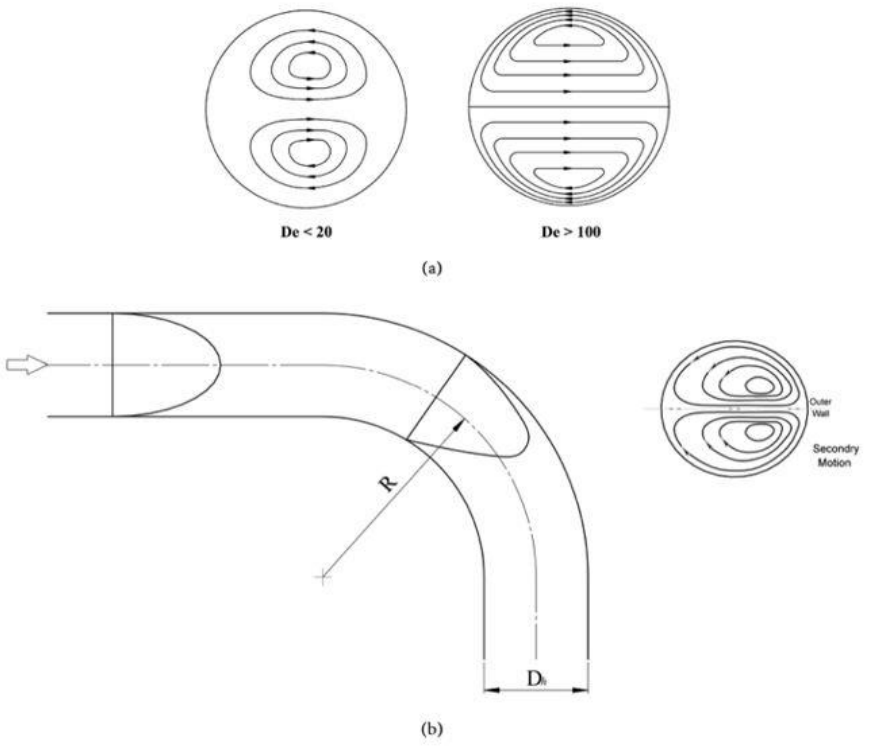

Fig. 1. 9 - Secondary flow field at (a) vertical cross section with low and high Dean numbers; (b) curved tube with axial velocity profile.

As indicated in Fig. (1.9), for flow in a curved channel, the secondary flow, which consists of a pair of longitudinal vortex rolls, appears in the passage due to the effect of the centrifugal force. The value of the Dean number ($De = Re\sqrt{D/2R}$) determines the secondary flow intensity, where R is the radius of curvature, Re is the Reynolds number, and *D* is the hydraulic diameter of the channel. Several authors have used the definition of the Dean number to measure the secondary flow intensity and for curved tube studies. It was reported that, for low Dean numbers, the axial-velocity profile was parabolic and unaltered from the fully developed flow in a straight tube. As the Dean number is increased, the maximum velocity began to be skewed toward the outer periphery. Similarly, for low values of curvature ratio, the secondary flow intensity is very high while for high values of curvature ratio the secondary flow intensity is much less [41].

1.6 Effective Fluids Properties of Taylor Flow

The thermodynamic properties of the test fluids, such as density, viscosity, and thermal conductivity are essential for an experimental analysis of Taylor flow. The flow physics of liquid-liquid Taylor flows can be characterized by non-dimensional numbers: Reynolds, Capillary, Nusselt and Prandtl numbers. The fluid properties of interest are density, viscosity, interfacial tension, thermal conductivity and specific heat capacity of the liquid phases.

The models form can vary depending on the application (i.e., gas-liquid, and liquid-liquid mixtures). Several models that are entirely based on experimental and theoretical data have been proposed, however, such models are very specific to a given regime or material. Generic models have been developed by various researchers through equations

derived based on a theoretical parent model, which is modified to accommodate changes in composition and structure. Notwithstanding, some of these models still contain empirical parameters. The appropriate models are working on interpreting the structure-property relations in two-phase flow based on the phase structure, fluid distribution and certain connectivity posterns. The most commonly used formulas in two-phase flows are the McAdams model, Cicchitti model, and Dukler model [29], [42].

1.6.1 Effective Density

The effective density of two-phase Taylor flow in a channel can be calculated using the void fraction, or liquid fraction of the dispersed phase. In terms of the volume fraction of the segmented or continuous phase, the effective density is

$$\bar{\rho}_e = \rho_1 \, (1 - \alpha_L) + \rho_2 \, \alpha_L \tag{1.18}$$

or if written in terms of the mass fraction x, the effective density is

$$\bar{\rho}_e = \left[\frac{1 - x}{\rho_1} + \frac{x}{\rho_2}\right]^{-1} \tag{1.19}$$

1.6.2 Effective Viscosity

One effective viscosity model of Taylor flow, which has been traditionally attributed to McAdams model, calculates the average effective viscosity in the following way,

$$\bar{\mu}_e = \left[\frac{1 - x}{\mu_1} + \frac{x}{\mu_2}\right]^{-1} \tag{1.20}$$

This is a series combination of the two-phase viscosities, weighted by mass quality.

Field and Hrnjak [43] then applied this framework to develop a new model by

combining the viscosities in series and using volume fraction to weight them:

$$\bar{\mu}_e = \left[\frac{1 - \alpha_L}{\mu_1} + \frac{\alpha_L}{\mu_2}\right]^{-1} \tag{1.21}$$

The phase viscosities were also combined in a model developed by Dukler et al. [44], but volume was used to weigh their contributions

$$\bar{\mu}_e = \mu_1 (1 - \alpha_L) + \mu_2 \alpha_L \tag{1.22}$$

Cicchitti et al. [45] formulated the effective viscosity with mass weighting:

$$\bar{\mu}_e = \mu_1 (1 - x) + \mu_2 x \tag{1.23}$$

1.6.3 Effective Thermal Conductivity

Based on the previous approach, these models can also be used to estimate effective thermal conductivity of liquid-liquid two-phase flow. Some of the models consider parameters such as the shape of the phases inside a channel, orientation and distribution of the liquids particles, as well as contact between phases (resistance). The structure in Fig. (1.10) represents a material in which the two components are distributed, with neither phase being necessarily carrier or segmented.

For the prediction of effective thermal conductivity for Taylor flow, various models and formulas have been proposed. The proposed models give the prediction of effective thermal conductivity of two-phase Taylor flow regime as a function of the thermal conductivity of each phase and volume fraction. Additionally, each phase is defined by the ratio of fluid volume to the aggregate volume. Awad and Muzychka [28] used an analogy between thermal conductivity modes in porous media and viscosity in two-phase flow, to propose

new definitions for two-phase viscosity. For example, the series and parallel combination (phases) rules were analogous to existing rules proposed by Cicchitti et al. [45] and, McAdams et al. [46] for two-phase viscosity.

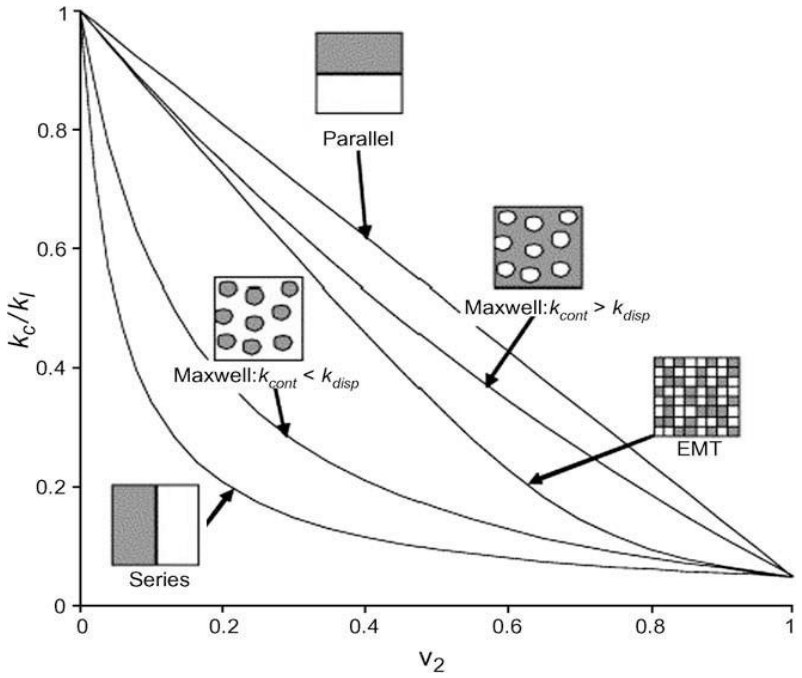

Fig. 1. 10 - Schematic representations of the structure assumed by each model [47].

1.7 Laminar Single-Phase Flow in Mini / Micro Scale Tubing

The principles of single-phase flow in circular capillaries are detailed, from a hydrodynamic and thermal perspective, in this section. These principles provide an insight into the flow conditions encountered within the capillaries used during experimentation in this thesis. The analysis begins by focusing on the formation of the hydrodynamic boundary layer and is followed by a brief description of the relevant modes of heat transfer and

thermal boundary layer development. There are two distinct flow regions in an internal flow, which are the developing region and the fully developed region. Developing flow occurs throughout the flow length in short tubes, while the flow field remains unchanged throughout the duct length in a fully developed flow. The bulk or mixed mean fluid temperature (T_m) and the mean flow velocity ($\bar{u}$) are two important parameters in internal flow, which can be used to model internal forced convection and pressure drop. The mass flow rate is defined as:

$$\dot{m} = \rho\, \bar{u}\, A \tag{1.24}$$

where

$$\bar{u} = \frac{1}{A} \iint_A u\, dA \tag{1.25}$$

while the bulk or mixed mean temperature is defined as:

$$T_m = \frac{1}{\bar{u}\, A} \iint_A u\, T\, dA \tag{1.26}$$

Since temperature is increasing as the fluid flows downstream, we must use alternate approaches to formulate the Nusselt number and heat transfer rate.

1.7.1 Pressure Drop (Fluid Friction)

Pressure drop in single-phase flow in small scales is a well-studied phenomenon. Pressure drop is traditionally determined using the concept of a friction factor for fully developed flows and apparent friction for a developing laminar flow. When the characteristic transversal scale is small enough to yield a small Reynolds number or when the duct length is longer than the entrance length (i.e., $L >> L_h$), it results in a fully

developed fluid flow. The flow through the entire duct may be regarded as fully developed under these conditions. These fully developed flow conditions can be created by the small size of the flow channel in many engineering systems, such as micro-coolers and compact heat exchangers used in electronics packaging. However, in many modern systems, the flow length is generally not very large, $L \sim L_h$ or $L << L_h$, and developing flow prevails over most of the duct length. In these situations, a model capable of predicting the hydrodynamic characteristic usually denoted as fRe (i.e., the product of the friction factor and the Reynolds number), is required, where f is the Fanning friction factor defined as:

$$f = \frac{\bar{\tau}_w}{\frac{1}{2}\rho\bar{u}^2} \tag{1.27}$$

The mean wall shear stress ($\bar{\tau}_w$) is then related through a simple pressure-force balance on the duct wall:

$$\bar{\tau}_w = \frac{A\ \Delta P}{P\ L} \tag{1.28}$$

The pressure drop in a section of duct may now be related to the mean fluid velocity, fluid properties, and geometry by means of Eqs. (1.27) and (1.28):

$$\Delta P = f\,\frac{\rho\bar{u}^2\ L\ P}{2\ A} \tag{1.29}$$

where $P/A = 4/D$ for tubes.

1.7.2 Heat Transfer

This subsection presents a category of internal flow heat transfer problems, popularly known as Graetz or Graetz–Nusselt problems, which involve solving the energy equation

for either fully developed Poiseuille flow or for a uniform velocity distribution.

$$\nabla^2 T = \frac{u}{\alpha}\frac{\partial T}{\partial x} \tag{1.30}$$

where the inlet temperature is constant at $x = 0$, and either the wall temperature (T_w) or heat flux (q_w) is constant at the duct periphery, as shown in Fig. (1.11). Along the axis of the duct or channel, an adiabatic symmetry condition is prescribed.

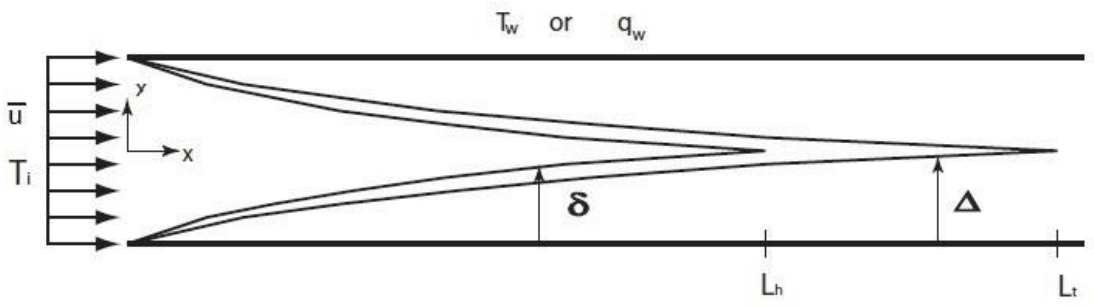

Fig. 1. 11 – Internal Flow Problems.

Given that we are examining laminar developing flow in a tube at constant wall temperature, it is appropriate to make reference to the fundamental Graetz theory for both Poisueille and Slug flow for isothermal boundary condition. The following fundamental correlations are applicable [48, 49]. The specific problem under investigation analyzes thermal boundary layer development in a hydrodynamically developed laminar flow with constant wall heat flux. Heat transfer in tubes at constant wall temperature can be analyzed using a dimensionless heat transfer coefficient or Nusselt number, or we maybe consider a dimensionless mean wall flux [50]. The heat transfer rate is nondimensionalized using a mean Nusselt number defined as

$$\overline{Nu}_D = \frac{\bar{q}\, D}{k\, \Delta T_{lm}} = \frac{\bar{h}\, D}{k} \tag{1.31}$$

where $\bar{q} = Q/A$ is the average heat flux.

In the case of a mean heat transfer coefficient, $\bar{h}$, defined on the basis of the wall to bulk fluid temperature difference, this requires the use of the log mean temperature difference

$$\Delta T_{lm} = \frac{(T_w - T_i) - (T_w - T_o)}{ln\frac{(T_w - T_i)}{(T_w - T_o)}} \tag{1.32}$$

where T_i and T_o are the inlet and outlet bulk temperatures, respectively, and T_w is the constant wall temperature.

Alternatively, using the wall to inlet temperature difference, $(T_w - T_i)$, the dimensionless mean wall heat flux is defined

$$q^* = \frac{\bar{q}\, D}{k(T_w - T_i)} \tag{1.33}$$

The mean Nusselt number and dimensionless mean wall heat flux are related through the following expression:

$$q^* = \frac{1}{L^*}[1 - exp(-4\overline{Nu}_D L^*)] \tag{1.34}$$

where $L^* = L/D\ Pe_D$ is the dimensionless thermal tube length or inverse Graetz number.

Heat Transfer Models

Based on the general Graetz flow behavior, general models, which combine the expected behavior for the boundary layer and fully developed regions of Graetz flow in isothermal tubes and ducts were proposed by Muzychka et al. [50]. They used the Churchill–Usagi

asymptotic approach [51] and the models take the form of

$$Nu = [(Nu)_0^n + (Nu)_\infty^n]^{1/n} \tag{1.35}$$

where *n* can be a positive or negative constant depending on the concavity of the curve to be fit. A similar model can be developed for q^*.

In the case of a Graetz-Poiseuille flow in a circular tube, one obtains for $\overline{Nu}_D$ and q^* the following:

$$\overline{Nu}_D = \left[\left(\frac{1.614}{L^{*1/3}}\right)^5 + 3.65^5\right]^{1/5} \tag{1.36}$$

and

$$q^* = \left[\left(\frac{1.614}{L^{*1/3}}\right)^{-3/2} + \left(\frac{1}{4L^*}\right)^{-3/2}\right]^{-2/3} \tag{1.37}$$

In the case of a Graetz-slug flow in a circular tube, one obtains for $\overline{Nu}_D$ and q^* the following:

$$\overline{Nu}_D = \left[\left(\frac{1.128}{L^{*1/2}}\right)^2 + 5.78^2\right]^{1/2} \tag{1.38}$$

and

$$q^* = \left[\left(\frac{1.128}{L^{*1/2}}\right)^{-2} + \left(\frac{1}{4L^*}\right)^{-2}\right]^{-1/2} \tag{1.39}$$

The above expressions are used for comparing the experimental data and to provide a convenient nondimensional reference to measure heat transfer enhancement regardless of the type of flow or flow rates. The limit of $q^* = 1/(4L^*)$ is the maximum heat transfer rate which can be achieved by a fluid passing through a long isothermal duct, and hence, measured q^* should be asymptotic to this limit as L^* increases.

1.8 Thesis Structure

This thesis is divided into eight chapters, including six papers and organized as follows:

Chapter 2 reviews the available literature pertaining to non-boiling liquid-liquid Taylor flow in mini / micro-scale channels and objectives of this research. A series of numerical and experimental studies of liquid-liquid Taylor flow are also thoroughly assessed in the chapter. Furthermore, the Chapter 2 reviews the analytical and empirical correlations from the literature on heat transfer, pressure drop, and film thickness. Based on the literature review, the gaps which can be addressed in this thesis are discussed also as objectives in this chapter.

Chapter 3 address the experimental investigation of laminar heat transfer for liquid-liquid segmented (Taylor) flow in mini-scale tubes with a constant wall temperature boundary condition is examined. New experimental data for liquid-liquid Taylor flow in heated copper tubes were obtained using silicone oils of 0.65 cSt, 1 cSt, and 3 cSt viscosity and segmented by water at varying volume fractions. The heat transfer enhancement is observed from the data reduction from the experimental results. The results also were showed a significant impact of the slug length on the rate of heat transfer. Chapter 3 was published on ASME 2015 13th International Conference on Nanochannels, Microchannels, and Minichannels, San Francisco, California, USA; ICNMM2015-48272; and submitted to Journal of Heat Transfer for publication.

Chapter 4 includes an experimental and theoretical study on the pressure drop of liquid-liquid Taylor flow in mini-scale tubing. A new approach is developed to introduce the pressure drop as a sum of two separated contributions: the frictional pressure drop of the

individual phases and the pressure drop due to the interfacial effects. Experimental data for liquid-liquid Taylor flow in mini scale tubes were obtained using three silicone oils of 1, 3, and 5 cSt viscosity and segmented by water at different volume fractions. Pressure drop results for the dimensionless approach, show good agreement with a proposed model with varying slug lengths. The results were obtained with carefully controlled flow slug lengths and volume fractions show a significant impact on pressure drop. Chapter 4 is submitted to ASME Journal of Fluids Engineering for publication.

Chapter 5 shows an experimental study on the effect of entrance region and curvature on heat transfer enhancement in mini-scale curved tubing using liquid-liquid Taylor flow. The experiments were performed on heated copper tubing in a constant temperature bath with different radii of curvature and lengths. Experimental data for two liquid-liquid Taylor flow were carefully obtained using two different silicone oils segmented by water with liquid fraction maintained constant at 0.5 and low Reynolds numbers. Hence, the effect of curvature and changing the length on heat transfer enhancement at a constant length can be studied as well as the effect of Prandtl number on curved tubing heat transfer augmentation. This Chapter is published on Journal of Electronic Packaging by ASME; 2017; Vol. 139 / 020909-1.

Chapter 6 presents an experimental study heat transfer enhancement in coiled mini-scale tubing using liquid-liquid Taylor flow. An experimental setup with a constant temperature boundary condition was used to collect data with small diameter coiled copper tubes were heated in a constant temperature bath. Slug flows which three low viscosity silicone oils segmented by water were used to examine the effect of Prandtl number on heat transfer

rates in coiled tubing. Heat transfer rate was determined by a dimensionless approach at different flow rates for coiled copper tubes with a different number of turns and different radii of curvature. An asymptotic model is developed based on the experimental results to predict the heat transfer rate based on Dean number and Prandtl number. Chapter 6 is published on ASME 2018 16th International Conference on Nanochannels, Microchannels, and Minichannels, Dubrovnik, Croatia; ICNMM2018-7743.

Chapter 7 determined pressures drop in curved and coiled mini-scale tubing experimentally for liquid-liquid segmented (Taylor) flow in an experimental study. An experimental setup for the steady-state laminar two-phase flow was assembled. A set of narrow coiled and could tubes were used as test sections with different radii of curvature and overall lengths. Two immiscible liquids (water / 1 cSt silicone oil) formed Taylor flow with liquid fraction at 0.5. According to the experimental results, an asymptotic model was developed as a function to Dean number and dimensionless slug length. The effect of secondary flow on pressure drop using liquid-liquid Taylor flow in mini scale systems was also studied. This Chapter is accepted for publication ASME 2019 17th International Conference on Nanochannels, Microchannels, and Minichannels, St. John's, NL, Canada; ICNMM2019-4219.

Finally, Chapter 8 summarizes the primary conclusions from this thesis as well as provides several recommendations for further research. Appendix A contains the experimental facilities and measurement techniques used in this thesis and Appendix B presents an uncertainty analysis of the experimental results.

1.9 References

[1] Angeli, P., and Gavriilidis, A., 2008, "Hydrodynamics of Taylor Flow in Small Channels: A Review," Proc. Inst. Mech. Eng. Part C J. Mech. Eng. Sci., 222, pp. 737–751.

[2] Gupta, R., Fletcher, D. F., and Haynes, B. S., 2010, "Taylor Flow in Microchannels: A Review of Experimental and Computational Work," J. Comput. Multiph. Flows, 2(1), pp. 1–31.

[3] Muzychka, Y. S., Walsh, E., Walsh, P., and Egan, V., 2011, "Non-Boiling Two Phase Flow in Microchannels," *Microfluidics and Nanofluidics Handbook: Chemistry, Physics, and Life Science Principles*, S.K. Mitra, and S. Chakraborty, eds., CRC Press, Taylor & francis group, Boca Raton, FL.

[4] Abdollahi, A., Sharma, R. N., and Vatani, A., 2017, "Fluid Flow and Heat Transfer of Liquid-Liquid Two Phase Flow in Microchannels: A Review," Int. Commun. Heat Mass Transf., 84, pp. 66–74.

[5] Berthier, J., and Silberzan, P., 2006, *Microfluidics for Biotechnology*, Artech House, London.

[6] Temiz, Y., Lovchik, R. D., Kaigala, G. V., and Delamarche, E., 2015, "Lab-on-a-Chip Devices: How to Close and Plug the Lab?," Microelectron. Eng., 132, pp. 156–175.

[7] Sur, A., and Liu, D., 2012, "Adiabatic Air-Water Two-Phase Flow in Circular Microchannels," Int. J. Therm. Sci., 53, pp. 18–34.

[8] Kashid, M., and Kiwi-Minsker, L., 2011, "Quantitative Prediction of Flow Patterns in Liquid-Liquid Flow in Micro-Capillaries," Chem. Eng. Process. Process Intensif., 50(10), pp. 972–978.

[9] Triplett, K. a., Ghiaasiaan, S. M., Abdel-Khalik, S. I., and Sadowski, D. L., 1999, "Gas–Liquid Two-Phase Flow in Microchannels Part I: Two-Phase Flow Patterns," Int. J. Multiph. Flow, 25(3), pp. 377–394.

[10] Dessimoz, A. L., Cavin, L., Renken, A., and Kiwi-Minsker, L., 2008, "Liquid-Liquid Two-Phase Flow Patterns and Mass Transfer Characteristics in Rectangular Glass Microreactors," Chem. Eng. Sci., 63(16), pp. 4035–4044.

[11] Salim, A., Fourar, M., Pironon, J., and Sausse, J., 2008, "Oil-Water Two-Phase Flow in Microchannels: FLow Patterns and Pressure Drop Measurements," Can. J. Chem. Eng., 86(6), pp. 978–988.

[12] Kumar, S., Cherlo, R., Kariveti, S., and Pushpavanam, S., 2010, "Experimental and Numerical Investigations of Two-Phase (Liquid - Liquid) Flow Behavior in Rectangular Microchannels," Ind. Eng. Chem. Fundam., 49, pp. 893–899.

[13] Tsaoulidis, D., Dore, V., Angeli, P., Plechkova, N. V., and Seddon, K. R., 2013, "Flow Patterns and Pressure Drop of Ionic Liquid-Water Two-Phase Flows in Microchannels," Int. J. Multiph. Flow, 54, pp. 1–10.

[14] Biswas, K. G., Patra, R., Das, G., Ray, S., and Basu, J. K., 2015, "Effect of Flow Orientation on Liquid-Liquid Slug Flow in a Capillary Tube," Chem. Eng. J., 262, pp. 436–446.

[15] Wu, Z., Cao, Z., and Sundén, B., 2017, "Liquid-Liquid Flow Patterns and Slug Hydrodynamics in Square Microchannels of Cross-Shaped Junctions," Chem. Eng. Sci., 174, pp. 56–66.

[16] Taylor, G. I., Eaboratory, C., 1961, "Deposition of a Viscous Fluid on the Wall of a Tube," J. Fluid Mech., 10(September), pp. 161–165.

[17] Howard, J. A., and Walsh, P. A., 2013, "Review and Extensions to Film Thickness and Relative Bubble Drift Velocity Prediction Methods in Laminar Taylor or Slug Flows," Int. J. Multiph. Flow, 55, pp. 32–42.

[18] Malsch, D., Kielpinski, M., Merthan, R., Albert, J., Mayer, G., Köhler, J. M., Süße, H., Stahl, M., and Henkel, T., 2008, "MPIV-Analysis of Taylor Flow in Micro Channels," Chem. Eng. J., 135(SUPPL. 1), pp. 166–172.

[19] Christopher, G. F., and Anna, S. L., 2007, "Microfluidic Methods for Generating Continuous Droplet Streams," J. Phys. D. Appl. Phys.

[20] Günther, A., and Jensen, K. F., 2006, “Multiphase Microfluidics: From Flow Characteristics to Chemical and Materials Synthesis,” Lab Chip.

[21] Kawakami, Y., Nobuhiro, K., and Koichi, S., 2011, “A New Sliding Micro Valve Generating/Separating Slug Flow in Micro Chemical Process,” pp. 321–326.

[22] Collins, D. J., Neild, A., deMello, A., Liu, A. Q., and Ai, Y., 2015, “The Poisson Distribution and beyond: Methods for Microfluidic Droplet Production and Single Cell Encapsulation,” Lab Chip, 15(17), pp. 3439–3459.

[23] Baroud, C. N., Delville, J. P., Gallaire, F., and Wunenburger, R., 2007, “Thermocapillary Valve for Droplet Production and Sorting,” Phys. Rev. E - Stat. Nonlinear, Soft Matter Phys.

[24] Seemann, R., Brinkmann, M., Pfohl, T., and Herminghaus, S., 2012, “Droplet Based Microfluidics,” Reports Prog. Phys.

[25] Curran, K., Colin, S., Baldas, L., and Davies, M., 2005, “Liquid Bridge Instability Applied to Microfluidics,” Microfluid. Nanofluidics, 1(4), pp. 336–345.

[26] Fischer, M., Juric, D., and Poulikakos, D., 2010, “Large Convective Heat Transfer Enhancement in Microchannels With a Train of Coflowing Immiscible or Colloidal Droplets,” J. Heat Transfer, 132(11), p. 112402.

[27] Che, Z., Wong, T. N., and Nguyen, N. T., 2013, “Heat Transfer in Plug Flow in Cylindrical Microcapillaries with Constant Surface Heat Flux,” Int. J. Therm. Sci., 64, pp. 204–212.

[28] Awad, M. M., and Muzychka, Y. S., 2008, “Effective Property Models for Homogeneous Two-Phase Flows,” Exp. Therm. Fluid Sci., 33(1), pp. 106–113.

[29] Muzychka, Y. S., John, S., Walsh, E. J., Walsh, P., and Egan, V., 2011, “Non-Boiling Two Phase Flow in Microchannels,” S. K. Mitra, and S. Chakraborty, eds., CRC Press, Boca Raton, FL.

[30] Chisholm, D., 1967, “A Theoretical Basis for the Lockhart-Martinelli Correlation for Two-Phase Flow,” Int. J. Heat Mass Transf., 10(12), pp. 1767–1778.

[31] Lockhart, R. W., and Martinelli, R. C., 1949, “Proposed Correlation of Data for Isothermal Two-Phase, Two-Component Flow in Pipes,” Chem. Eng. Prog., 45(1), pp. 39–48.

[32] Kreutzer, M. T., Kapteijn, F., Moulijn, J. A., Kleijn, C. R., and Heiszwolf, J. J., 2005, “Inertial and Interfacial Effects on Pressure Drop of Taylor Flow in Capillaries,” AIChE J., 51(9), pp. 2428–2440.

[33] Aota, A., Mawatari, K., Takahashi, S., Matsumoto, T., Kanda, K., Anraku, R., Tokeshi, M., and Kitamori, T., 2009, “Phase Separation of Gas-Liquid and Liquid-Liquid Microflows in Microchips,” Microchim. Acta, 164(3–4), pp. 249–255.

[34] Warnier, M. J. F., De Croon, M. H. J. M., Rebrov, E. V., and Schouten, J. C., 2010, “Pressure Drop of Gas-Liquid Taylor Flow in Round Micro-Capillaries for Low to Intermediate Reynolds Numbers,” Microfluid. Nanofluidics, 8(1), pp. 33–45.

[35] Zhang, J., Fletcher, D. F., and Li, W., 2016, “Heat Transfer and Pressure Drop Characteristics of Gas-Liquid Taylor Flow in Mini Ducts of Square and Rectangular Cross-Sections,” Int. J. Heat Mass Transf., 103, pp. 45–56.

[36] Di Miceli Raimondi, N., Prat, L., Gourdon, C., and Tasselli, J., 2014, “Experiments of Mass Transfer with Liquid-Liquid Slug Flow in Square Microchannels,” Chem. Eng. Sci., 105, pp. 169–178.

[37] Fairbrother, F., and Stubbs, A. E., 1935, “Studies in Electro-Endosmosis. Part VI. The ‘Bubble-Tube’ Method of Measurement,” J. Chem. Soc., pp. 527–529.

[38] Bretherton, F. P., 1961, “The Motion of Long Bubbles in Tubes of Square Cross Section*,” Phys. Fluids A Fluid Dyn., 5(7), pp. 1549–1557.

[39] Aussillous, P., and Quere, D., 2000, “Quick Deposition of a Fluid on the Wall of a Tube,” Phys. Fluids, 12(10), pp. 2367–2371.

[40] Han, Y., and Shikazono, N., 2009, “Measurement of the Liquid Film Thickness in Micro Tube Slug Flow,” Int. J. Heat Fluid Flow.

[41] Vashisth, S., Kumar, V., and Nigam, K. D. P., 2008, “A Review on the Potential Applications of Curved Geometries in Process Industry,” Ind. Eng. Chem. Res.,

47(10), pp. 3291–3337.

[42] Levy, S., 1999, “Two-Phase Flow in Complex Systems,” p. 425.

[43] Field, B. S., and Hrnjak, P. S., 2007, “Two-Phase Pressure Drop and Flow Regime of Refrigerants and Refrigerant-Oil Mixtures in Small Channels.”

[44] Dukler, A. E., Wicks, M., and Cleveland, R. G., 1964, “Frictional Pressure Drop in Two-Phase Flow. Part A: A Comparison of Existing Correlations for Pressure Loss and Holdup, and Part B: An Approach through Similarity Analysis,” AIChE J., 10(1), pp. 38–51.

[45] Cicchitti, A., Lombardi, C., Silvestri, M., Soldaini, G., and Zavattarelli, R., 1960, “Two-Phase Cooling Experiments: Pressure Drop, Heat Transfer and Burnout Measurements,” Energ. Nucl.

[46] McAdams, W. H., Woods, W. K., Heroman Jr, L. C., and Heroman L C, J., 1942, “Vaporization inside Horizontal Tubes II-Benzene-Oil Mixtures,” Trans. ASME, 64(3), pp. 193–200.

[47] Carson, J. K., Lovatt, S. J., Tanner, D. J., and Cleland, A. C., 2005, “Thermal Conductivity Bounds for Isotropic, Porous Materials,” Int. J. Heat Mass Transf., 48(11), pp. 2150–2158.

[48] Muzychka, Y. S., Walsh, E. J., and Walsh, P., 2011, “Heat Transfer Enhancement Using Laminar Gas-Liquid Segmented Plug Flows,” J. Heat Transfer, 133(4), p. 041902.

[49] Muzychka, Y. S., 2014, “Laminar Heat Transfer for Gas-Liquid Segmented Flows in Circular and Non-Circular Ducts with Constant Wall Temperature,” Int. Conf. Nanochannels, Microchannels, Minichannels, (FEDSM2014-21087), pp. 1–10.

[50] Muzychka, Y. S., Walsh, E., and Walsh, P., 2010, “Simple Models for Laminar Thermally Developing Slug Flow in Noncircular Ducts and Channels,” J. Heat Transfer, 132(111702–1).

[51] Churchill, S. W., and Usagi, R., 1972, “A General Expression for the Correlation of Rates of Transfer and Other Phenomena,” AIChE J., 18(6), pp. 1121–1128.

CHAPTER 2

Literature Review of Liquid-Liquid Taylor Flow in Mini / Micro Channels

2.1 Introduction

In this chapter, a review of previous studies on non-boiling liquid-liquid Taylor flows in small-scale channels is presented. In non-boiling liquid-liquid Taylor flows in micro/mini channels, there are substantial changes in the fluid flow and heat transfer behaviors compared for the properties of single-phase flow. This chapter provides a review of both the numerical and experimental studies of the hydrodynamics and heat transfer rate of liquid-liquid Taylor flows. The chapter is divided into subsections addressing various topics associated with flow geometry such as heat transfer, pressure drop, film thickness and slug formation (slug shape). A general overview of the hydrodynamic and thermal properties of liquid-liquid Taylor flow in small-scale channels is also included in this chapter along with a summary of information pertaining to the correlations commonly used for calculating the pressure drop and heat transfer coefficient. Lastly, objectives and conclusions of this research are provided at the end of the chapter.

2.2 Heat Transfer

While there has been a lot of research aimed at understanding the hydrodynamics and mass transfer behavior in Taylor flow, very few researchers have studied heat transfer without phase change in liquid-liquid slug flows in mini / microchannels [1-3]. The impact of various parameters, such as bulk fluid and near-wall properties as well as geometry dimensions and fluid properties have been discussed in the literature on heat transfer of liquid-liquid Taylor flow [4].

Only three experimental studies have addressed this topic to date [5, 7, 8]. Heat transfer enhancement in a circular microchannel was experimentally investigated by Eain et al. [5]. They highlighted the heat transfer characteristics of two-phase liquid-liquid slug flow with a varying the Reynolds number, Capillary number, slug length, and slug spacing. Experiments were conducted in a 1.5 mm circular tube under constant heat flux boundary conditions with oil as the carrier fluid, segmented by water droplets. High-resolution infrared thermography was utilized to obtain the external temperatures of the surface. The slug length as accounted by the results affects attainable heat transfer rates. This is due to a change in the internal circulations in the slugs, and changes in slug length. The correlation was developed based on Muzychka's [6] model for gas-liquid slug flow to describe the thermal behaviour of liquid-liquid Taylor flow for fully developed and entrance regions with deviations of 10% and 30%, respectively, as follows:

$$Nu_{x(Slug)} = \left(\left(Nu_{x(Slug,Ent)}\right)^4 + \left(Nu_{x(Slug,Dev)}\right)^4\right)^{1/4} \tag{2.1}$$

They observed a heat transfer enhancement of up to 600%. The heat transfer rate increased as the segmented phase length was increased, and the carrier phase length was decreasing. As stated, the heat transfer augmentation of flow is maximized when carrier slug length approaching the channel diameter. Moreover, enhancing liquid film thickness decreases the heat transfer percentage.

Asthana et al. [7] studied the convective heat transfer rate in micro-channels with segmented liquid-liquid flows. They used Laser Induced Fluorescence (*LIF*) and micro-PIV to visualize the temperature and the velocity field of the coolant with and without droplets. Their calculations of the Nusselt number show that the heat sinks in the micro channel are significantly enhanced compared to single phase liquid cooling.

In an initial study, Janes et al. [8] experimentally investigated the heat transfer rate of liquid-liquid Taylor flow (water-canola oil) in two different miniature heat sinks. All their experimental data were presented graphically with dimensionless heat transfer q^* vs. dimensionless length L^*, and that indicated an overall enhancement in heat transfer.

With numerical methods, Urbant et al. [9] investigated the heat transfer enhancement with mineral oil and water droplets in a circular microchannel was by. They observed that mixing oil drops with water significantly enhanced the heat transfer rate, while increasing the size of the oil droplet increased the Nusselt number. The flow disturbance caused by the droplets in the carrier fluid as well as the flow recirculation in the droplets was the cause of enhancement.

Che et al. [10] numerically examined the heat transfer rate of liquid slug flow through a microchannel at the isothermal boundary condition. They identified the convective heat

transfer process between the slug and the heated wall channel by three stages: (i) development of thermal boundary layer; (ii) advection of heated / fresh fluid in the slug, and (iii) thermally fully developed flow. The effects of the Peclet number and slug length on the heat transfer process were investigated. They showed that short slugs provided high Nusselt numbers and enhanced heat transfer compared to long slugs due to the higher transverse velocity. By using 3D simulations, the effects of droplet length, aspect ratio of the channel cross sections, and Peclet number on heat transfer enhancement of liquid-liquid two-phase flow in a rectangular microchannel was studied by Che et al. [11]. There was an increase in the Nusselt number when the Peclet number was changed from 25 to 800. The rate of the heat transfer process decreased as the Peclet number increased. Fresh fluid moved to the high temperature wall from the middle of the plug at a high Peclet number, which caused the Nusselt numbers to exhibit oscillatory behavior.

Fischer et al. [12] have conducted numerical simulations of heat transfer in slug flows at different flow conditions such as velocity, slug size, and liquid type (with and without the use of nanoparticles). The local Nusselt number was used to determine the effect of different flow conditions and fluid systems on heat transfer with single-phase flow.

By performing both experiments and numerical simulations (CFD), Dai et al. [13] have studied the heat transfer for 1 and 2 mm vertical tubes with constant wall heat flux boundary conditions using water / hexadecane slug flow with Reynolds numbers between 4.9 and 21.9. The heat transfer of gas-liquid and liquid-liquid Taylor flows was predicted using a mechanistic model. They also established a connection between the heat transfer from the film itself, as well as from the continuous film area of the droplets and slug. Table (2.1)

presents the numerical and experimental studies on the thermal characteristics of liquid-liquid Taylor flow in mini / micro channels.

Table 2. 1 - Summarizes studies on the thermal behavior of liquid-liquid Taylor flow in mini / micro channels.

Author(s)	Mode of study	Flow conditions	Geometry	Working liquids	Remarks
Urbant et al. 2008	Numerical (VOF)	$Ca \leq 0.15$, $Re \leq 0.1$ $Pe = 69.6$ & 160.8 Droplet radius, $a/R = 0.4 - 0.7$ $T_w = Constant$	Cylindrical capillary, $Di = 100\ \mu m - 1000\ \mu m$	Water / Mineral oil	Enhancement in heat transfer rates over conventional Poiseuille flow. Nu augmented by increasing the droplets size.
Fischer et al. 2010	Numerical	$0.01 \leq Re \leq 100$ $1.1 \times 10^{-4} \leq We \leq 1.9 \times 10^{-1}$ $3.5 \leq Pe \leq 700$ T_w = *Constant*	Circular microchannel, $Di = 0.1\ mm - 1\ mm$	Water / 5 cS Silicon oil, PAO, AI2O3	400% enhancement in thermal performance over single-phase flow without unacceptably large pressure losses.
Janes et al. 2010	Experimental	$Q' < 180$ ml/min $q_w = Constant$	Minichannel heat sinks Square CS $= 1\ mm \times 1\ mm$	Water / Oil	Taylor flows enhance radial transport of heat and mass in circular tubes.
Asthana et al. 2011	Experimental (LIF & Micro-PIV)	$0.001 \leq$ Ca ≤ 0.120 $Q' < 130$ µl/min $q_w = Constant$	Minichannel chip $D_h = 100\ \mu m \times 100\ \mu m$ X-junction	Water / Oil	Significant Nu enhancement in Taylor flow compared to single-phase flow with a penalty of increased pressure drop.
Eain et al. 2015	Experimental (Bulk heat transfer setup & IR image system)	$2.3 <$ Re < 92.1 $4.49 \times 10^{-5} < Ca < 0.052$ $23.6 \leq Pr \leq 265.4$ $q_w = Constant$	Mini circular tubing 0.3 < L < 1 m, Di=1.5 mm Segmenters & T-junctions	Water / Pd5, Dodecane, AR20, FC40	L-L Taylor flow regimes induce significant heat transfer enhancements with the effects of slug length.
Bandara et al. 2015	Review & Theoretical	$Q^{*}_{water} = 1206 - 2413$ µl/min $Q^{*}_{oil} = 302 - 2715$ µl/min $6.6 \times 10^{-4} \leq Ca \leq 8.8 \times 10^{-3}$ $56.4 \leq Re \leq 1127$ $q_w = Constant$	Circular microchannel $Di = 800$ µm $L = 50\ D$	Water / 1.5 cSt Silicon oil	There are discrepancies of over 500% between previous Nu correlation results. Nu increases up to 200% by using L-L Taylor flow compared to single-phase flow; and the Nu decreased with increasing slug length.
Dai et al. 2015	Experimental & Numerical (VOF)	$15 \leq Re \leq 48$ $0.0013 \leq Ca \leq 0.0043$ $23.6 \leq Ca \leq 265.4$ $q_w = Constant$	Stainless-steel circular channel *Di*=2 mm T-junctions	Water / Hexadecane	Heat transfer model was developed for L-L and G-L Taylor flow and found the experimental data were in good agreement with predictions of numerical ones.
Che et al. 2015	Numerical (FVM & LSM)	$25 \leq Pe \leq 800$ $T_w = Constant$	Microchannels 200 µm × (200–800) × 800 µm Aspect ratio (AR)= 1- 4	Water / Mineral oil	Heat transfer rate increased by recirculation flow in droplet and the continuous phase. Existing liquid between the corner of channel and droplet delays the heat transfer. Nu decreases by increasing *Pe* number and decreasing aspect ratio.

2.3 Pressure Drop

Several numerical and experimental investigations have been performed to examine the pressure drop of Taylor flow in mini / micro channels. However, only a few studies have been conducted on liquid-liquid Taylor flows, as most researchers has focus on gas-liquid

Taylor flows. The pressure drop of a liquid-liquid Taylor flow regime can be modeled with various approaches. The homogeneous flow model is the simplest approach and is based on the assumption that the behavior of the two-phase flow mixture is similar to that of a pseudo-fluid with average defined characteristics. Single-phase flow theory is then used to calculate the pressure drop. The separated flow model is another direct approach. It considers the contributions of each phase separately and thereby predicts the resulting pressure drop as the sum of single-phase contributions, hence including an empirical parameter to account for the interfacial effects. Developed models have been published specifically for Taylor flow regimes. Taylor flow was considered as a series of the unit cells which suggested a pressure drop equal to the frictional pressure drop of in both phases and the interfacial pressure drop. Specifically, the liquid-liquid Taylor flow regime has only been addressed by a few studies in the literature which are presented in Table (2.2), and some of these studies are discussed below.

Kashid and Agar [14] experimentally studied the effect of various operating conditions on flow regimes, including slug size, interfacial area and pressure drop for different Y-junction mixing elements. A snapshot approach is used under the operating conditions which were similar and corresponded to the interfacial area used to measure the slug length and contact angles. They developed a theoretical prediction for pressure drop along the slug flow capillary based on the capillary pressure and hydrodynamic pressure drop without a wall film and compared it with experimental data. Per unit capillary length, the model for the pressure drop without film is:

$$\frac{\Delta P}{L} = \left(\frac{\Delta P_W + \Delta P_{CH}}{l_U}\right) + \left(\frac{2L - l_U}{l_U}\right)\left(\frac{P_C}{L}\right) \tag{2.2}$$

where W, CH, L, U and C relate to water slug, cyclohexane, length of micro-reactor, slug unit and capillary, respectively. The overall pressure drop, which is due to the film region is

$$\frac{\Delta P}{L} = \left(\frac{\alpha}{1 - k^4}\right)\left(\frac{\Delta P}{L}\right)_{CH} \tag{2.3}$$

where $k = (R - \delta)/R$. The prediction agrees well with experimental data when a film thickness was taken into consideration in an improved model.

Aota et al. [15] proposed that for gas-liquid and liquid-liquid flows laminar pipe flow theory predicts the pressure within each phase with reasonable accuracy when the pressure drop at the interface is balanced by the Laplace pressure. The technique demonstrated good agreement with measured data.

The hydrodynamics and pressure drop of liquid-liquid flow of water / toluene and ethylene glycol-water / toluene were experimentally and numerically investigated by Jovanovic et al. [16]. They made use of microtubes with an internal diameter of 248 μm and 498 μm. The pressure drop was calculated as the addition of the interface pressure drop and the frictional pressure drop. A thin film was inserted between the channel wall and the slugs to depict the moving film and the stagnant film models. The flow ratio of two-phases, slug velocity, capillary diameter and viscosity were found to influence the sizes of the dispersed and continuous phase slugs. The impact of the film velocity on the pressure drop was reported to be insignificant. In conformity with experimental data, the pressure drop (Eqs.

2.4 and 2.5) in liquid-liquid slug flow was accurately predicted by the moving film (MF) and stagnant film (SF) model with an average error of less than 7%.

$$\Delta P_{SF} = \frac{8U_{slug}\mu_d \alpha L}{(R-\delta)^2} + \frac{8U_{TP}\mu_c(1-\alpha)L}{R^2} + \frac{L}{l_U}7.16(3Ca)^{2/3}\frac{\sigma}{D} \tag{2.4}$$

and

$$\Delta P_{MF} = \frac{4U_{slug}\alpha L}{(R^2-(R-\delta)^2)/\mu_c + (0.5(R-\delta)^2)/\mu_d} + \frac{8U_{TP}\mu_c(1-\alpha)L}{R^2} + \frac{L}{l_U}7.16(3Ca)^{2/3}\frac{\sigma}{D} \tag{2.5}$$

where α, R, L and l_U are void fraction, internal radius of the channel, length of capillary and unit cell length, respectively.

Both CFD and experimental techniques were used by Gupta et al. [17] to examine the pressure drop in liquid-liquid flows in a circular channel with a diameter of 1.06 *mm*. Droplet and two adjacent halves of liquid slugs were used to create a fully-formed unit cell whose pressure drop was calculated using a developed model by Jovanovic et al. [16]. By adding up the individual contributions of pressure drop in the slug region, the model was able to predict about 25% of the total pressure obtained using the CFD simulations over a unit cell.

Eain et al. [18] identified the lack of data for calculating pressure drop of liquid-liquid slug flow, which was a result of experimentally studying the pressure drop of liquid-liquid slug flow in a hard-walled FEP Teflon circular capillary of 1.59 *mm* inner diameter. The experiment revealed a lack of data when a comparison was canducted between the previous correlations and experimental data. The effect of flow physics was mentioned in the

experiment, and it was concluded that these correlations were not applicable for liquid-liquid slug flow. A new model was developed to estimate the friction factor:

$$f_{exp_{Tp}} = \frac{P/L}{(\frac{1}{2}\rho_c U^2)(\frac{4}{D})\left(\frac{Q_c}{Q_T}\right) + (\frac{1}{2}\rho_d U^2)(\frac{4}{D})\left(\frac{Q_d}{Q_T}\right)} \quad (2.6)$$

The correlation fit relatively well with experimental data with an error less than 20%. The experimental friction factor and Reynolds number products, $(f_{exp}Re)_{TP}$, were calculated using the model developed by Walsh et al. [19] for the liquid-liquid data.

By using different correlations from the literature Jovanovic et al. [16], Kreutzer et al. [20], and Mac Giolla Eain et al. [18], the pressure drop of liquid-liquid slug flow in a microchannel with a diameter of 800 μm was calculated by Bandara et al. [2]. It was observed that there could fill a wide gap in understanding the basic dynamics of liquid-liquid two-phase flow because of the large differences in the calculated pressure drop.

Following the homogeneous flow approach and the separated flow approach, two-phase flow of oil-water in a T- junction horizontal microchannel was experimentally studied by Salim et al. [21]. Pressure drop was investigated by the use of two phase flow patterns and wettability of oil-water using quartz and glass microchannels. Injection of oil and water was done in the microchannel at a constant flow rate. The other fluid was then injected at a different flow rate. The homogeneous and Lockhart-Martinelli models [22] which are commonly used to describe the gas-liquid two-phase flow through pipes were used to compare the pressure drop. These models revealed that the pressure drop was dependent on flow rate, microchannel material and first injected fluid into the channel. In consideration of the flow pattern, these models revealed that liquid-liquid flow in a pipe was similar to gas-liquid flow in microchannels. An empirical

correlation was introduced for two-phase pressure in the case of injecting oil. The first flow drop was based on friction factor and Reynolds number for quartz ($C = 0.67$) and glass ($C = 0.8$) microchannels with an average error of 16 % and 18 %, respectively:

$$\left(\frac{\Delta P}{L}\right)_{Tp} = \left(\frac{\Delta P}{L}\right)_{w} + C\varepsilon_o \left(\frac{\Delta P}{L}\right)_{o} \tag{2.7}$$

where ε_o is the volume fraction of oil, Tp represents the two-phase pressure drop, and w and o represent water and oil, respectively.

In constructed polymer microfluidic channels, liquid-liquid segmented flows were investigated experimentally by Kim et al. [23]. The impact of this geometrical change on the development of the segmented flow was examined in three different cross-sectional expansion ratios which were obtained from injection into the test channels. The measured pressure drops have been underestimated by virtually all previous separated and homogeneous flow models built on viscous frictional pressure drop. Calculations of the dispersed fluid segment velocities and measurement of the length of the carrier and dispersed fluid segments were done in conjunction with identifying segmented flow patterns and their maps, as well as creating predictive geometrical models for these quantities. The pressure drop of the liquid-liquid segmented flow was measured. The measured data and those predicted based on the capillary and frictional pressure drop models were in much better agreement from those predicted by the homogeneous and Lockhart-Martinelli models.

Li and Angeli [24] conducted a systematic study on the hydrodynamics of liquid-liquid Taylor flow in small channels using bright field micro-PIV and CFD modelling. Pressure profiling was conducted along the channel with a series of plugs, this predicted the

numerical pressure gradients and agreed well with an asymptotic correlation, which included the dimensionless slug length and the ratio *Ca/Re* as parameters, to within 13%.

Table 2. 2 - Summarizes studies on the pressure drop of liquid-liquid Taylor flow in mini / micro channels.

Author(s)	Approach	Geometry	Working liquids & Flow conditions	Remarks
Kashid & Agar 2007	Experimental, Taylor flow and Lockhart-Martinelli approach	Capillary microreactor $D_h = 0.25 - 1\ mm$ PTFE Y-junction	Water / Cyclohexane $\dot{Q} = 5 - 200\ ml/h$	A theoretical prediction for pressure drop was developed with, without a wall film across capillary and Y-junction.
Salim et al. 2008	Experimental, Homogeneous & Lockhart-Martinelli approach	Quartz & glass microchannels $D_h = 793\ and\ 667\ \mu m$ *L=120 mm* Y-junction	Water / Oil $\beta = 0.8$ *Re<500*	Pressure drop a strong depends on flow rates, channel material, and the first fluid injected into the microchannel.
Aota et al. 2009	Experimental, Taylor flow approach	Microchips (glass microchannel) $D_h = 215 \times 33$ µm $L = 20\ mm$ Y-junction	Water / ethyl acetate $\dot{Q} = 1 - 180$ (µl/min)	Pressure loss model was proposed and verified for G–L and L-L interfaces of the two-phase slug flow.
Jovanovic et al. 2011	Experimental, Taylor flow approach	Microcapillary $D_h = 248\ and\ 498$ µm Stainless steel Y-mixer	Water / Toluene Ethylene glycol-water / Toluene $u = 0.03 - 0.5\ m/s$ $6.3 < Re < 84$ $9.2 \times 10^{4} < Ca < 1.9 \times 10^{-2}$ $2.7 \times 10^{-2} < We < 7 \times 10^{-1}$	The pressure drop was modeled for L-L Taylor flow as the sum of frictional pressure drop and interface pressure drop.
Tsaoulidis et al. 2013	Experimental approach	Teflon, glass microchannels $D_h = 200\ and\ 270$ µm $L = 200\ mm$ T- & Y-junction	Water / Ionic liquid $\dot{Q}_w = 0.0169 - 214.9\ cm^3/h$ $\dot{Q}_i = 0.065 - 11.31\ cm^3/h$ $0.05 \leq \alpha_L \leq 0.8$ $0.013 \leq Bo \leq 0.024$	Pressure drop model of L-L plug flow was improved by considering the film thickness.
Gupta et al. 2013	Experimental, Numerical (VOF), and Taylor flow approach	Circular minichannel $D_h = 1.06\ mm$ T-junction	Water / Hexadecane $0.3 \leq \alpha_L \leq 0.6$ $20 < Re < 42$ $4.5 \times 10^{-3} \leq Ca \leq 8.9 \times 10^{-3}$	An expression has been developed to calculate the total pressure drop in a fully- developed unit cell.
Kim et al. 2013	Experimental, Homogeneous & Lockhart-Martinelli approach	Polycarbonate microchips $D_h = 215 \times 33$ µm $L = 20$ mm Y-junction Polycarbonate chips	Deionized water with blue food-coloring / Perfluorocarbon with nonionic fluoro-soluble surfactant $0.11 < \beta_C < 0.97$ $2.3 < J_C(m/s) < 9.3$ $0.0002 < J_D(m/s) < 0.02$	Measurements of the L-L segmented flow pressure drops were carried out with varying the carrier fluid volumetric flow ratio.
Eain et al. 2015	Experimental, Taylor flow approach	Stainless steel & Teflon circular tubes $D_h = 50\ \mu m\ to\ 200\ \mu m$ X-junctions & segmenters	Water / Pd5, FC40, AR20, Dodecane $1.40 < Re < 100$ $4.5 \times 10^{-5} < Ca < 0.053$ $0.75 < L_c^* < 14.13$ $1.06 < L_d^* < 8.11$	Pressure drop models applied on G-L were reviewed and modified to the applicability to L–L Taylor flows.
Bandara et al. (2015)	Review, Taylor flow approach	Circular microchannels $D_h = 800\ \mu m$ $L = 50D_h$	$40 \leq Re \leq 100$ $\beta = 0.4$ $L_c/D = 3, L_{UC}/D = 5$	Review a general introduction of the hydrodynamics of slug flow in microchannels and showed little agreement between measured and predicted pressure drop.
Li and Angeli (2017)	Numerical, Taylor flow approach	Quartz microchannels $D_h = 0.2\ and\ 0.5\ mm$ T-junction	Ionic liquid / 1 M nitric acid solution $0.0224 < Ca < 0.299$ $\dot{Q}_C = \dot{Q}_D = 5 - 200\ ml/h$	The pressure profile along the channel with a series of slugs was predicted.

2.4 Film Thickness

Film thickness has been found to have a significant effect on heat transfer in liquid-liquid Taylor flow [7], [11], [25]. It also strongly affects hydrodynamics and pressure drop [14], [16,17], [24], as well as slug formation and slug shape [26–29]. The role of film thickness in a liquid-liquid Taylor flow regime is still poorly understood even though it has been addressed by numerous studies in gas-liquid flow regime.

Grimes et al. [30] used a wide experimental program to investigate the validity of the Taylor and Bretherton laws by using several potential carrier fluids (FC40, Tetradecane, Dodecane) to segment aqueous droplets (water) over different flow rates. The image of the aqueous plug was captured by a high-speed camera, and their corresponding velocities were calculated. The ratio of the carrier fluid's velocity to that of the aqueous plug was used to calculate the thickness of the films. Significant differences were found between the film thicknesses predicted by the Taylor and Bretherton law, and the measured data.

Eain et al. [25] experimentally calculated the film thickness for liquid-liquid slug flow in small-scale devices. Four combinations of oil as the carrier fluid with water as the segmented fluid were applied in their experiments. The film thickness and size were measured using optical macroscopy, in addition, it was used to measure the variation affected by aqueous slug length and also the carrier phase fluidic properties, as shown in the following correlation:

$$\frac{\delta}{R} = 0.35\ (Ca)^{0.354}(We)^{0.097} \tag{2.8}$$

where δ is the film thickness and Ca, R, and We are the capillary number, channel radius and Weber number respectively. The film thickness was measured by a direct optical macroscopy technique, and the results were compared with several published correlations.

Eain et al. [5] also examined the effect of film thickness on heat transfer of four different Taylor flows. The temperature of the flow fields with and without slugs was measured by Ashthana et al. [7] with the aid of a Laser Induced Fluorescence (*LIF*). In addition, the water velocity within a microchannel was measured using a micro-PIV, and the slug (oil) velocity was also estimated. The average flow velocity was less than the slug velocity, which implies that there is a thin film between the walls and slugs.

A numerical study was recently performed by Che et al. [11] to examine the shape and film thickness of liquid gutters formed between the curved interface of the droplets and the corners of a rectangular micro-channel. It was found that gutters reduce the rate of heat transfer, given the fact that conduction is solely responsible for the heat transfer from the wall to the center of the liquid in the gutters, and this is much slower than the heat transfer within the slug regions or droplets via advection. Recently, Dai et al. [13] conducted numerical and experimental research, where they applied a high grid resolution near the wall in numerical simulation and used a high-speed camera to capture the thickness of the liquid film. However, there was significant similarity between the correlations of Bretherton, Aussillous and Quéré [31] and the film thicknesses obtained from their numerical and experimental results for gas-liquid two phase flow. They illustrated that the flow conditions affect the heat transfer of the liquid-liquid slug flow.

Several studies have been conducted on the hydrodynamics and pressure drop of liquid-liquid slug flow both theoretically and experimentally. For example, Gupta et al. [17] studied hydrodynamics and pressure drop in liquid-liquid slug flow in circular capillaries with a diameter of 1.06 *mm* using water as a dispersed phase and hexadecane as the continuous phase (viscosity ratio = 0.3). They found that the film thickness around the droplet were in good agreement with Bretherton's expressions which were derived for the inviscid bubble, thereby suggesting the negligible effects of liquid viscosity for a low viscosity ratio. Similarly, Jovanovic´ et al. [16] investigated the effect of film thickness on the stagnant film model and the moving film model. In each model, a thin liquid film was introduced between the capillary wall and the phase distributed slug. The film velocity was found to have an insignificant impact on pressure drop. Thus, the pressure drop of liquid-liquid slug flow can be accurately predicted by the stagnant film model. Based on the model of Li et al. [24] and Eain et al. [25], they suggested an improved correlation, which predicts the film thickness with a deviation of 0.27% - 11.26% from experimental data. Using CFD and bright field micro-PIV modeling, a sequential and systematic study of the hydrodynamics of liquid-liquid plug flow in channels with an internal diameter of 0.2 *mm* and 0.5 *mm* was conducted. They measured the length and velocity of the plug as well as the thickness of the film around the plugs and made comparisons with the correlations in the literature. Under the same *Ca*, the dimensionless film thickness in the channel with a 0.2 *mm* diameter was found to be slightly smaller than that in the channel with a 0.5 *mm* diameter. The predicted values of pressure gradients agreed with existing correlation, which are a function of the ratio *Ca/Re* and the dimensionless slug length parameters. Similarly,

Kashid and Agar [14] developed a theoretical prediction for pressure drop in slug flow based on the capillary pressure and hydrodynamics pressure drop with and without a wall film and compared with experimental data. An overview of some of the recent measurement techniques used to measure liquid film thickness in liquid-liquid Taylor flow is summarized in Table (2.3).

Generally, the capillary number significantly affects the liquid film thickness of Taylor flow in a micro scale channel, as seen in the fact that a smaller *Ca* produces a very tiny film. Hence, it is difficult to obtain and measure very thin film even numerically since the film thickness should be bigger than the mesh elements. Also, the thin liquid film in the droplet / slug form, as well as the physical form of the droplet, can only be obtained by using the correct contact-angle value [2].

Table 2. 3 - Summarizes studies on the film thickness of liquid-liquid Taylor flow in mini / micro channels.

Author(s)	**Flow condition**	**Measuring technique**	**Correlation**
Soares et al. 2005	$2.0 \times 10^{-3} < \mathrm{Ca} < 1.0$	Video recording and Numerical predictions	Taylor's correlation
Grimes et al. 2006	$10^{-5} < \mathrm{Ca} < 10^{-1}$ $\mathrm{Ca}^{*} = 0.16, 0.24, 0.35$	Optical microscopy	Bretherton and Taylor correlations
Jovanovic´ et al. 2011	$1.9 \times 10^{4} < \mathrm{Ca} < 5.2 \times 10^{-2}$ $1.5 \times 10^{-2} < \mathrm{Ca} < 7.0 \times 10^{-1}$	Microscope video imaging (Matlab R2007b Image processing)	Bretherton's correlation
Ghaini et al. 2011	$10^{-4} < \mathrm{Ca} < 5 \times 10^{-3}$	Laser induced fluorescence (LIF)	Experimental approach
Dore et al. 2012	$7.0 \times 10^{-3} < \mathrm{Ca} < 1.59 \times 10^{-1}$	Micro-PIV	$\frac{\delta}{D_h} = 0.72[1 + \exp(-3.08\, Ca^{0.54})]$
Eain et al. 2013	$2.0 \times 10^{-3} < \mathrm{Ca} < 1.19 \times 10^{-1}$ $4.7 \times 10^{-2} < \mathrm{We} < 1.671$ $7.0 \times 10^{-4} < \mathrm{Ca}^{*} < 1.26 \times 10^{-1}$	Optical microscopy	$\frac{\delta}{D_h} = 0.72\, Ca^{0.354}\, We^{0.097}$
Tsaoulidis and Angeli 2015	$3.0 \times 10^{-2} < \mathrm{Ca} < 1.8$	High speed image capture	$\frac{\delta}{D_h} = 1.316\, Ca^{0.354}\, Re^{1.067}$

2.5 Other Aspects

This section reviews research that addresses the effects of various operating conditions on a liquid-liquid Taylor flow regime in mini / micro channels, slug size, interfacial area and mass transfer behavior including slug formation and circulation patterns [32].

Using computational fluid dynamics simulations, Kashid et al. [33] predicted the internal circulations within liquid slugs of a liquid-liquid slug flow. They also applied CFD particle tracing and PIV experimental methods to visualize the internal circulations. The PIV experimental methods showed the expected circulation patterns at low flow velocities. The position of the stagnant zone changed with changes in the flow velocity in the simulated results. Furthermore, they found there was no significant effect on the circulation time inside the slug at low flow velocities and the increase in flow velocity decreased the circulation time. They also found the particle tracing provides a quantitatively good prediction of internal circulations inside the liquid slugs. Kashid et al. [34] also used computational fluid dynamics simulations for predicting the mass transfer and internal flow patterns with slugs based on a finite element method, and it was performed with and without a chemical reaction in the liquid-liquid slug flow micro-reactor. The results conformed with the numerical and experimental results of Harries et al. [35].

Additionally, Kashid et al. [14] have an empirical study for liquid-liquid slug flow for three different non-reacting systems in a capillary micro-reactor. Experiments were conducted to determine how mass transfer coefficients and a flow splitter were affected by different operating conditions, such as flow rate, capillary diameter, and flow ratio. The liquid-liquid micro-extractor reactors used were observed provide better performance and

efficiency than conventional equipment. Additionally, the capillary micro-reactor provided large specific interfacial areas in comparison with other contactors, which enhances mass transfer rates.

Di Miceli Raimondi et al. [36]conducted a two-dimensional simulation to study the behavior of liquid-liquid slug flow systems in a square channel with a 50 to 960 μm depth. The authors found that the flow structures had a major impact on the mass transfer coefficient estimation. Furthermore, the rate of mass transfer was found to be better when droplets were constrained in the small channel than in macro channel.

Dessimoz et al., [37] conducted an experimental investigation to determine the influence of fluid properties on liquid-liquid two-phase flow patterns in Y- and T-shaped glass micro-channels. Figure (2.1) shows the fully developed hydrodynamics with internal circulation for slug flow regime. Furthermore, an instantaneous neutralization reaction was used to investigate the mass transfer performance for parallel and slug flow. They developed a model based on the mean capillary and Reynolds numbers. This model helps to predict flow patterns depending on fluid properties (Fig. 2.2).

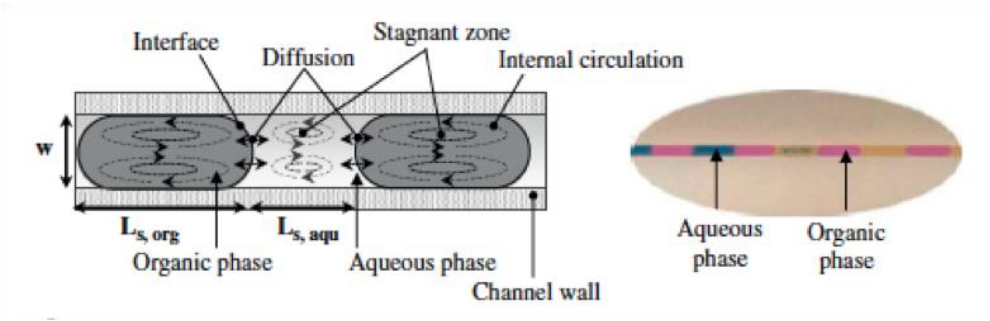

Fig. 2. 1 - Shows hydrodynamics with internal circulation and a photo of slug flow [37].

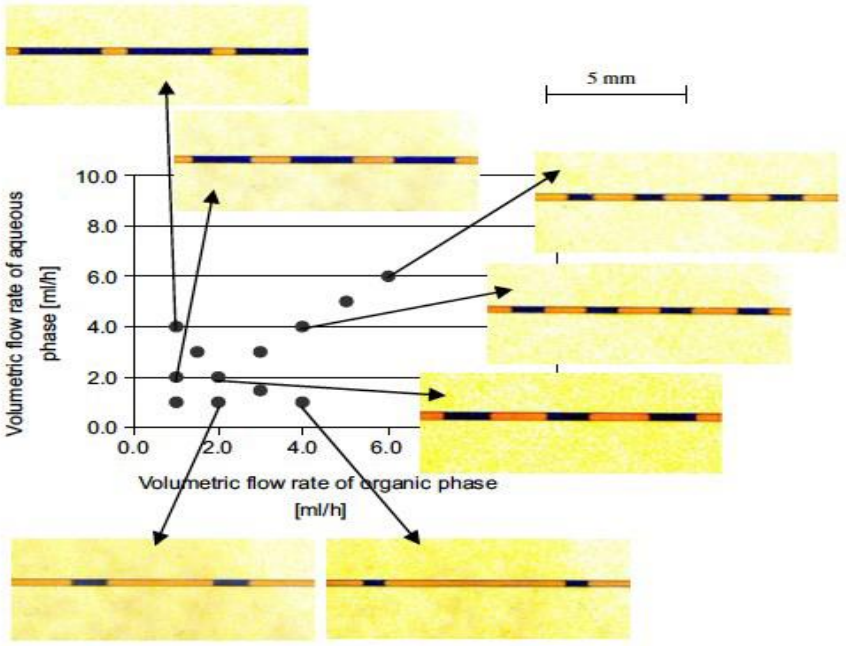

Fig. 2. 2 - Flow pattern map: for a T-shaped micro-reactor. Organic phase: toluene with Sudan III. Aqueous phase : water with NaOH 0.15 M and bromothymol [37].

Raj et al. [38] numerically investigated the liquid-liquid flow in three-dimensional (3-D) rectangular micro-channels using the VOF method and compared the results with an experiment done by Garstecki et al. [39]. They showed the effect of various parameters, such as liquid flow rates, wall contact angle, liquid properties (viscosity and interfacial tension), and channel size. The effects of distributor configurations (T-junction vs Y-junction), on the flow regimes and drop/slug lengths were examined by the results of the experiment. They obtained the slug flow regime when $\dot{Q}_{water}/\dot{Q}_{oil} < 1.7$, and a parallel flow regime when $\dot{Q}_{water}/\dot{Q}_{oil} > 1.7$ with considering of wall wettability. They found the predicted slug lengths independent of the channel size and the inlet distributor type when

$Ca > Ca_{\text{critical}}$; and almost independent of the continuous phase viscosity and also independent of the interfacial tension when $Ca < Ca_{\text{critical}}$.

Experimental and numerical studies on various flow regimes in liquid-liquid two-phase flows were conducted by Kumar et al. [40]. Rectangular micro-channels were used to perform the experiments under various operating conditions, such as different flow rates, channel sizes, and fluid systems with variable properties. The flow regimes were validated with numerical simulations, which are based on the VOF method, using a commercial package FLUENT.

The LIV methodology was employed by Ghaini et al. [27] to study the hydrodynamics within liquid slugs as well as capture the wall film. They examined the effect of the wall material using a hydrophilic glass capillary and a hydrophobic PTFE capillary. The volume of fluid (VOF) method, which is based on the incompressible Navier–Stokes equation with suitable boundary conditions between the two phases, was used to perform the CFD simulations. The importance of the wall film in the hydrodynamics and mass transfer liquid-liquid slug flow was shown in their results. The results also showed the presence of unsuspected complex patterns as opposed to the simple single Taylor vortex flow.

Kashid and Kiwi-Minsker [32] conducted experiments to produce flow patterns in liquid-liquid flow in four different micro channel designs. They showed that liquid-liquid flow pattern transition could be developed using the Capillary and Reynolds numbers proposed by Dessimoz et al. [41] for gas-liquid systems. Furthermore, a generic flow map for microchannels was produced, which included literature data and showed good agreement.

Dore et al. [29] conducted an experimental investigation on the circulation patterns by mixing characteristics within the water plugs in the liquid-liquid slug flow using the optical technique (micro-PIV). The experiments were performed in a circular glass micro channel with a radius of 100 μm, and the mixture velocities were varied from 0.0028 *m/s* to 0.0674 *m/s*. Two main circulation vortices were shown to exist within the slugs by the experimental results. Moreover, two other secondary vortices were found to exist in front of the plug at average mixture velocities. At the axial point of the vortex cores, which are located near the rear interface for shorter slugs (Fig. 2.3), a minimum circulation time, τ, was found using the circulation patterns. However, for longer plugs, a more uniform τ was found along the axial direction. The relationship between the maximum circulation velocity and *Ca* was determined to be almost linear.

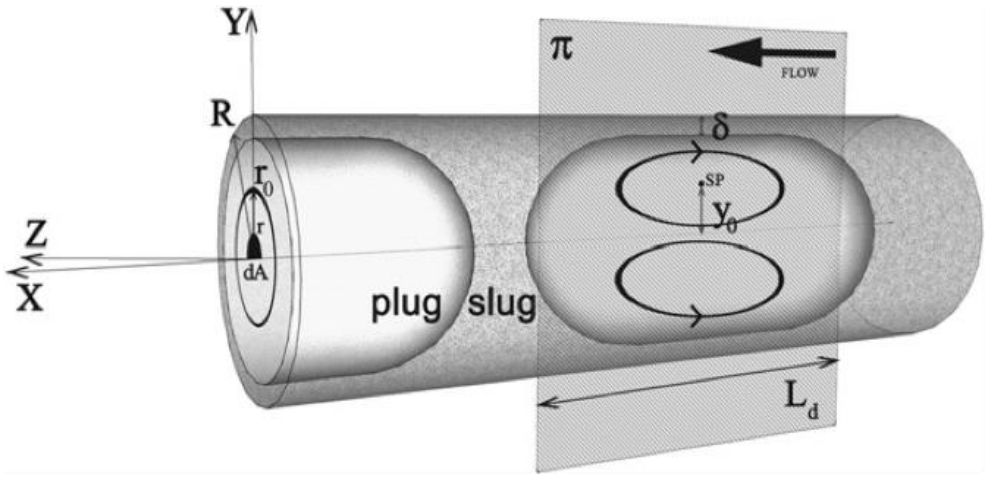

Fig. 2. 3 - A 3D schematic diagram of the Taylor flow pattern in a micro-channel. The interior recirculation parameters are indicated on the mid-XY plane (π) in water plug [29].

2.6 Research Objectives

The study of Taylor flow in small scales is important because of an increasing demand for the minimization of devices used in cooling systems, biological diagnostics, and other practical applications. Liquid-liquid Taylor flow has not been widely studied, and the number of articles found in this field is much less than on gas-liquid flow. Recent studies conducted by researchers on mini / micro scale channels with low speed or low Reynolds number flow have indicated that there is a lack of understanding concerning the mechanisms of this flow pattern. Many aspects of liquid-liquid Taylor flow, such as heat transfer characteristics, pressure drop and film thickness of continuous phase around slugs of dispersed phases, as well as the effect of channel path and geometries on these areas of liquid-liquid Taylor flow remain un-researched.

In particular, this work focuses on developing new models for liquid-liquid Taylor flow that will predict the pressure drop and heat transfer characteristics in small-scale channels using the effects of the channel geometry. These models will supplement the current prediction of manufacturing capability during various stages in the design of new small devices. The main objective of this work is to develop new models that will predict the behavior of liquid-liquid Taylor flow in mini-scale tubing based on the experimental and theoretical modeling methods. The work also aims at obtaining new fundamental knowledge of the hydrodynamics and heat transfer for non-boiling liquid-liquid slug flow through small-scale ducts of different geometry shapes to design an appropriate concept using experimental and theoretical techniques.

This thesis will examine the thermal and hydrodynamic properties of a liquid-liquid Taylor flow regime in mini-channel geometry. A continuous stream of monodispersed water slugs in an oil phase will be produced by pumping two immiscible liquids (an organic carrier phase and water) into a circular channel. The impacts of slug length and continuous oil phase variations on the thermal and hydrodynamic properties will then be examined. The following subjects in liquid-liquid Taylor flow will be addressed in this research.

- Definition of non-boiling liquid-liquid Taylor flow characteristics to better understand the mechanisms controlling this type of flow pattern in mini / micro channels that generate a steady uniform slug train.
- An experimental investigation of the thermal characteristics of a liquid-liquid Taylor flow regime confined to mini-scale tubing with isothermal boundary condition.
- A complete thorough thermal characterization of liquid-liquid Taylor flows subject to a constant wall temperature boundary condition. The experiments will be performed with mini scale curved and coiled tubing under different operating conditions, such as wide range of flow rates, tube dimensions, and Taylor flow with varying liquids properties.
- A development of a novel model to predict the thermal behavior of liquid-liquid Taylor flows over a wide range of parameters.
- A measurement of the pressure drop induced by a liquid-liquid Taylor flow regime in mini-scale tubing and determine the accuracy of analytical and empirical pressure drop models.

- A development of a novel model or correlation for predicting frictional pressure drop and describing the effect of interfacial surface shape, slug size, and Capillary diameter.
- Obtain new experimental data to supplement the development of theoretical models for pressure drop in small-scale coiled tubing.
- A development of new models and correlations for predicting heat transfer and pressure drop in mini-scale curved and coiled tubing flow, assessing the influence of secondary flow structure, and radius of curvature on the heat transfer rates attainable and pressure drop data.
- Characterize internal circulations and secondary flow for development of two-phase Taylor flow principle models in mini scale tubing.

The conclusions from these objectives will greatly contribute to the knowledge base pertaining to liquid-liquid Taylor flows in mini scale. These experimental and theoretical models will assist in optimizing the design of Taylor flow systems in mini / micro scale channels. The models will reduce the number of prototypes and experimentation required at various design stages, which will eventually lead to a reduction in design time and cost.

2.7 References

[1] Talimi, V., Muzychka, Y. S., and Kocabiyik, S., 2011, "A Review on Numerical Studies of Slug Flow Hydrodynamics and Heat Transfer in Microtubes and Microchannels," Int. J. Multiph. Flow, 39, pp. 88–104.

[2] Bandara, T., Nguyen, N. T., and Rosengarten, G., 2015, "Slug Flow Heat Transfer without Phase Change in Microchannels: A Review," Chem. Eng. Sci., 126, pp. 283–295.

[3] Asadi, M., Xie, G., and Sunden, B., 2014, "A Review of Heat Transfer and Pressure Drop Characteristics of Single and Two-Phase Microchannels," Int. J. Heat Mass Transf., 79, pp. 34–53.

[4] Abdollahi, A., Sharma, R. N., and Vatani, A., 2017, "Fluid Flow and Heat Transfer of Liquid-Liquid Two Phase Flow in Microchannels: A Review," Int. Commun. Heat Mass Transf., 84, pp. 66–74.

[5] Mac Giolla Eain, M., Egan, V., and Punch, J., 2015, "Local Nusselt Number Enhancements in Liquid-Liquid Taylor Flows," Int. J. Heat Mass Transf., 80, pp. 85–97.

[6] Muzychka, Y. S., Walsh, E. J., and Walsh, P., 2011, "Heat Transfer Enhancement Using Laminar Gas-Liquid Segmented Plug Flows," J. Heat Transfer, 133(4), p. 041902.

[7] Asthana, A., Zinovik, I., Weinmueller, C., and Poulikakos, D., 2011, "Significant Nusselt Number Increase in Microchannels with a Segmented Flow of Two Immiscible Liquids: An Experimental Study," Int. J. Heat Mass Transf., 54(7–8), pp. 1456–1464.

[8] Janes, N., Muzychka, Y. S., Guy, B., Walsh, E. J., and Walsh, P., 2010, "Heat Transfer in Gas-Liquid and Liquid-Liquid Two Phase Plug Flow Systems," 12th IEEE Intersoc. Conf. Therm. Thermomechanical Phenom. Electron. Syst., pp.1–11.

[9] Urbant, P., Leshansky, A., and Halupovich, Y., 2008, "On the Forced Convective

Heat Transport in a Droplet-Laden Flow in Microchannels," Microfluid. Nanofluidics, 4(6), pp. 533–542.

[10] Che, Z., Wong, T. N., and Nguyen, N. T., 2012, "Heat Transfer Enhancement by Recirculating Flow within Liquid Plugs in Microchannels," Int. J. Heat Mass Transf., 55(7–8), pp. 1947–1956.

[11] Che, Z., Wong, T. N., Nguyen, N. T., and Yang, C., 2015, "Three Dimensional Features of Convective Heat Transfer in Droplet-Based Microchannel Heat Sinks," Int. J. Heat Mass Transf., 86, pp. 455–464.

[12] Fischer, M., Juric, D., and Poulikakos, D., 2010, "Large Convective Heat Transfer Enhancement in Microchannels With a Train of Coflowing Immiscible or Colloidal Droplets," J. Heat Transfer, 132(11), p. 112402.

[13] Dai, Z., Guo, Z., Fletcher, D. F., and Haynes, B. S., 2015, "Taylor Flow Heat Transfer in Microchannels-Unification of Liquid-Liquid and Gas-Liquid Results," Chem. Eng. Sci., 138, pp. 140–152.

[14] Kashid, M. N., Harshe, Y. M., and Agar, D. W., 2007, "Liquid-Liquid Slug Flow in a Capillary: An Alternative to Suspended Drop or Film Contactors," Ind. Eng. Chem. Res., 46(25), pp. 8420–8430.

[15] Aota, A., Mawatari, K., Takahashi, S., Matsumoto, T., Kanda, K., Anraku, R., Hibara, A., Tokeshi, M., and Kitamori, T., 2009, "Phase Separation of Gas-Liquid and Liquid-Liquid Microflows in Microchips," Microchim. Acta, 164(3–4), pp. 249–255.

[16] Jovanović, J., Zhou, W., Rebrov, E. V., Nijhuis, T. A., Hessel, V., and Schouten, J. C., 2011, "Liquid-Liquid Slug Flow: Hydrodynamics and Pressure Drop," Chem. Eng. Sci., 66(1), pp. 42–54.

[17] Gupta, R., Leung, S. S. Y., Manica, R., Fletcher, D. F., and Haynes, B. S., 2013, "Hydrodynamics of Liquid-Liquid Taylor Flow in Microchannels," Chem. Eng. Sci., 92, pp. 180–189.

[18] Mac Giolla Eain, M., Egan, V., Howard, J., Walsh, P., Walsh, E., and Punch, J.,

2015, “Review and Extension of Pressure Drop Models Applied to Taylor Flow Regimes,” Int. J. Multiph. Flow, 68, pp. 1–9.

[19] Walsh, E., Muzychka, Y., Walsh, P., Egan, V., and Punch, J., 2009, “Pressure Drop in Two Phase Slug/Bubble Flows in Mini Scale Capillaries,” Int. J. Multiph. Flow, 35(10), pp. 879–884.

[20] Kreutzer, M. T., Kapteijn, F., Moulijn, J. A., Kleijn, C. R., and Heiszwolf, J. J., 2005, “Inertial and Interfacial Effects on Pressure Drop of Taylor Flow in Capillaries,” AIChE J., 51(9), pp. 2428–2440.

[21] Salim, A., Fourar, M., Pironon, J., and Sausse, J., 2008, “Oil-Water Two-Phase Flow in Microchannels: FLow Patterns and Pressure Drop Measurements,” Can. J. Chem. Eng., 86(6), pp. 978–988.

[22] Lockhart, R. W., and Martinelli, R. C., 1949, “Proposed Correlation of Data for Isothermal Two-Phase, Two-Component Flow in Pipes,” Chem. Eng. Prog., 45(1), pp. 39–48.

[23] Kim, N., Murphy, M. C., Soper, S. A., and Nikitopoulos, D. E., 2014, “Liquid-Liquid Segmented Flows in Polycarbonate Microchannels with Cross-Sectional Expansions,” Int. J. Multiph. Flow, 58, pp. 83–96.

[24] Li, Q., and Angeli, P., 2017, “Experimental and Numerical Hydrodynamic Studies of Ionic Liquid-Aqueous Plug Flow in Small Channels,” Chem. Eng. J., 328, pp. 717–736.

[25] Mac Giolla Eain, M., Egan, V., and Punch, J., 2013, “Film Thickness Measurements in Liquid-Liquid Slug Flow Regimes,” Int. J. Heat Fluid Flow, 44, pp. 515–523.

[26] Soares, E. J., Carvalho, M. S., and Mendes, P. R. S., 2005, “Immiscible Liquid-Liquid Displacement in Capillary Tubes,” J. Fluids Eng., 127(1), p. 24.

[27] Ghaini, A., Mescher, A., and Agar, D. W., 2011, “Hydrodynamic Studies of Liquid-Liquid Slug Flows in Circular Microchannels,” Chem. Eng. Sci., 66(6), pp. 1168–1178.

[28] Ufer, A., Mendorf, M., Ghaini, A., and Agar, D. W., 2011, “Liquid/Liquid Slug Flow Capillary Microreactor,” Chem. Eng. Technol.

[29] Dore, V., Tsaoulidis, D., and Angeli, P., 2012, “Mixing Patterns in Water Plugs during Water/Ionic Liquid Segmented Flow in Microchannels,” Chem. Eng. Sci., 80, pp. 334–341.

[30] Grimes, R., King, C., and Walsh, E., 2006, “Film Thickness for Two Phase Flow in a Microchannel,” pp. 1–5.

[31] Aussillous, P., and Quere, D., 2000, “Quick Deposition of a Fluid on the Wall of a Tube,” Phys. Fluids, 12(10), pp. 2367–2371.

[32] Kashid, M., and Kiwi-Minsker, L., 2011, “Quantitative Prediction of Flow Patterns in Liquid-Liquid Flow in Micro-Capillaries,” Chem. Eng. Process. Process Intensif., 50(10), pp. 972–978.

[33] Kashid, M. N., Gerlach, I., Goetz, S., Franzke, J., Acker, J. F., Agar, D. W., and Turek, S., 2005, “Internal Circulation within the Liquid Slugs of a Liquid-Liquid Slug-Flow Capillary Microreactor,” Ind. Eng. Chem. Res., 44(14), pp. 5003–5010.

[34] Kashid, M. N., Agar, D. W., and Turek, S., 2007, “CFD Modelling of Mass Transfer with and without Chemical Reaction in the Liquid-Liquid Slug Flow Microreactor,” Chem. Eng. Sci., 62(18–20), pp. 5102–5109.

[35] Harries, N., Burns, J. R., Barrow, D. A., and Ramshaw, C., 2003, “A Numerical Model for Segmented Flow in a Microreactor,” Int. J. Heat Mass Transf., 46(17), pp. 3313–3322.

[36] Di Miceli Raimondi, N., Prat, L., Gourdon, C., and Cognet, P., 2008, “Direct Numerical Simulations of Mass Transfer in Square Microchannels for Liquid-Liquid Slug Flow,” Chem. Eng. Sci., 63(22), pp. 5522–5530.

[37] Dessimoz, A. L., Cavin, L., Renken, A., and Kiwi-Minsker, L., 2008, “Liquid-Liquid Two-Phase Flow Patterns and Mass Transfer Characteristics in Rectangular Glass Microreactors,” Chem. Eng. Sci., 63(16), pp. 4035–4044.

[38] Raj, R., Mathur, N., and Buwa, V. V, 2006, “Numerical Simulations of Liquid - Liquid Flows in Microchannels,” (May), pp. 10606–10614.

[39] Garstecki, P., Fuerstman, M. J., Stone, H. A., and Whitesides, G. M., 2006, “Formation of Droplets and Bubbles in a Microfluidic T-Junction - Scaling and Mechanism of Break-Up,” Lab Chip, 6(3), pp. 437–446.

[40] Kumar, S., Cherlo, R., Kariveti, S., and Pushpavanam, S., 2010, “Experimental and Numerical Investigations of Two-Phase (Liquid - Liquid) Flow Behavior in Rectangular Microchannels,” Ind. Eng. Chem. Fundam., 49, pp. 893–899.

[41] Dessimoz, A. L., Raspail, P., Berguerand, C., and Kiwi-Minsker, L., 2010, “Quantitative Criteria to Define Flow Patterns in Micro-Capillaries,” Chem. Eng. J.,160(3),pp.882–890.

CHAPTER 3

Heat Transfer Enhancement Using Liquid-Liquid Taylor Flow in Mini-Scale Tubing*

3.1 Introduction

A segmented flow of immiscible liquids at small dimensional scales has emerged as a basic analysis area in recent years [1–4]. Cooling electronic devices with liquid flow in micro/mini channels effectively removes heat removal by utilizing the high heat capacity and conductivity of liquids, as well as the large surface area to volume ratio of the channels. As a result of the rise in the generation of large heat fluxes in electronic devices and systems and the reduction in available surface area from which to transfer heat, increasing demand for the development of high thermal flow removal technologies for maintaining components within safe operating temperature limits. These technologies can take advantage of the early studies in two phase flow heat transfer, which considered thermal

* Published in ASME 2015 13th International Conference on Nanochannels, Microchannels, and Mini channels, July 6-9, 2015, San Francisco, CA, USA; and submitted to Journal of Heat Transfer for publication.

enhancement using fluid plugs as a segmenting medium. It has long been known that, within the liquid plugs, internal circulations arise as a result of the gas-liquid, solid-liquid, or liquid-liquid interfaces. Consequently, enhanced heat transfer in mini-scale channels via segmented Taylor flows can be used in cooling systems to improve performance.

While there has been a lot of research aimed at understanding the hydrodynamics and mass transfer behavior of slug flows in mini / micro channels, very few researchers have studied heat transfer without phase change in liquid-liquid Taylor flow [5–7]. A small number of studies have been performed on liquid-liquid two-phase slug flows and a few representative works highlight the features of liquid-liquid flows, including hydrodynamics, pressure drop, and film thickness. Kashid et al. [8–11], Wu et al. [12], Mandal et al. [13], Kumar et al. [14], Dessimoz et al. [15] and Raimondi et al. [16] have identified flow patterns for non-boiling liquid-liquid segmented flows in channels and introduced a liquid-liquid flow pattern model. Pressure drop in a liquid-liquid two-phase segmented flow increases as compared to a single phase flow, as reported by Kashid et al. [17], Salim et al. [18], Jovanovic et al. [19], Asthana et al. [20], and Eain et al. [21]. In addition, Jovanovic et al. [22] and Eain et al. [23] examined the film thickness in a liquid-liquid Taylor flow and reported that the liquid film thickness around the slug increases as the Capillary number (*Ca*) increases. Other studies on liquid-liquid Taylor flow; such as slug formation and slug shape were performed by Kashid et al. [8,9], Wu et al. [12,24], Raj et al. [25], Mandal et al. [13], Ghaini et al. [26] and Kumar et al. [14].

Heat transfer is an important characteristic of liquid-liquid Taylor flow in small-scale channels. Two effects responsible for the enhancement of the heat transfer rate in a gas-

liquid segmented flow (Taylor flow) are internal circulation within the slugs (causing a greater radial heat transfer rate) and increased slug velocity when compared with the same single-phase mass flow rate (a consequence of reduced phase fraction). Therefore, using liquid-liquid Taylor flows for enhance heat transfer rate in mini-scale tubes is a promising technique for process optimization, since both fluid segments are participating. Eain et al. [21] considered the heat transfer characteristics of two-phase liquid-liquid non-boiling droplet flow. They used oil as the carrier fluid, segmented by water droplets in mini-scale tubes under constant heat flux boundary conditions. High resolution infrared thermography obtained external temperatures of the surface. Experiments were carried out with various values of the Reynolds number ($2.3 < Re < 92.1$), Capillary number ($0.001 < Ca < 0.120$), Prandtl number ($23.6 < Pr < 265.4$), droplet length, and droplet spacing. The results show that the droplet length has a major impact on attainable heat transfer rates due to a change in the internal circulations in the droplets with changes in length. To study convective heat transfer in micro-channels with segmented liquid-liquid flows, Asthana et al. [20] used Laser Induced Fluorescence (*LIF*) and micro-PIV to visualize the temperature of the coolant with and without droplets, as well as the velocity field. Their calculations of the Nusselt number show that heat sinks using the micro-channel geometry significantly enhanced the heat transfer rate compared to single phase liquid cooling. In addition, increased heat removal comes with a penalty of an increased pressure drop, which is strongly affected by the fluid temperature. Janes et al. [27] have experimentally investigated the heat transfer characteristics of two-phase slug flow (water-canola oil) in two different miniature heat

sinks. Their experimental data were presented graphically with dimensionless heat flux q^* vs dimensionless thermal length L^*, indicated an overall enhancement in heat transfer.

From a numerical perspective studies of heat transfer in slug flows have been conducted by Fischer et al. [28] at different flow conditions such as different velocity, slug size, and liquid type (with and without the use of nanoparticles). The local Nusselt number was used to determine the effect of different flow conditions and fluid systems on the heat transfer rate with single-phase flow. By using 3D simulations, the effect of the Peclet number on the heat transfer of a liquid-liquid two-phase flow in a rectangular micro-channel was studied by Che et al. [29]. There was an increase in the Nusselt number when the Peclet number was changed from 25 to 800. The speed of the heat transfer process decreased as the Peclet number increased. Fresh fluid moved to the high temperature wall from the middle of the plug at a high Peclet number and this cause the Nusselt numbers to exhibit an oscillatory behavior.

Although most studies do not control the slug length, doing so has been recognized as a key factor in determining the enhanced heat transfer rates offered by segmented flows. Recently, a small number of authors have experimentally [21] and numerically [29,30] investigated the influence of the slug length on heat transfer characteristics for liquid-liquid Taylor flows. The focus of the studies listed was on bulk tube heat transfer with an isoflux boundary condition, but for this study presents as equivalent isothermal data using the mean wall temperature. Each of these studies failed to successfully show good agreement with experimental data sets including varying slug lengths but did show increased heat transfer

rates for segmented flows with the same mass flow rate as compared with a continuous flow stream.

This work examines heat transfer rate in liquid-liquid Taylor flow inside copper tubing under a constant wall temperature boundary condition. This study demonstrates that the heat transfer is enhancement by using liquid-liquid slug flows and shortening the slug lengths of each phase. An experimental facility is designed to look at the problem and carefully control the volume fractions and slug lengths of the Taylor flow to show their significant impact on the rate of laminar heat transfer. Experimental data acquired from temperature measurements at the tube inlet, outlet, and wall surface are used to calculate the dimensionless mean wall heat flux and are compared with models proposed earlier by Muzychka et al. [31,32].

3.2 Experimental Setup

An experimental setup for internal flow in a heated copper tube with a small diameter at a constant wall temperature condition was built. As illustrated in Fig. (3.1), the experimental setup consists of a test section, two syringe pumps, thermocouples, an isothermal bath, segmentation device and a data acquisition system. The experiments were conducted with straight copper tubes of varying lengths and internal diameter (ID = 1.65 mm), hence different aspect ratios (L/D) of the test sections. A segmenter or T-junction was used to create a stream of liquid-liquid segmented flows to ensure that we have a slug flow pattern with high volumetric flow rates and thus increase liquid fraction. Three low viscosity silicone oils were used as carrier phases and water as dispersed phase in Taylor flow in order to provide a wide range of thermodynamic properties and thus to be varied of

Capillary number and Prandtl number. High precision pumps (Harvard Apparatus) with two glass syringes (100 *ml* capacity for each) were used to control the volumetric flow rates. Two separate syringe pumps allowed to be varied a wide range of the relative flow rate, and hence the slug lengths. Omega T-type thermocouples at both ends of the tube measure the temperature of the liquid stream. An isothermal bath (Fisher Scientific 3013) was used to maintain a constant wall temperature boundary condition for the test section. In addition, the high thermal conductivity of the copper tube helps to maintain the isothermal condition for the entire tube length. A Keithley data acquisition system (DAQ) was connected to a computer to collect and analyze the measured data of the inlet, outlet, and bath temperatures at different flow rates. A high-speed camera captured a series of images of the slug train for slug analysis to calculate liquid fractions.

The copper tubing was placed horizontally inside the constant temperature bath and was maintained at 40 °C ± 0.01 °C. Steady state conditions were reached by allowing a minimum of 4 minutes to pass for the flow to become thermally stable. The ambient temperature was approximately 23 °C. A series of experiments were performed with the flow rates adjusted according to the flow pattern and the hydrodynamic resistance of the system setup. A liquid-liquid Taylor flow was exhibited when two liquids were injected into the T-junction at different flow rates. Therefore, three liquid-liquid Taylor flow in mini scale tubes were obtained using three silicone oils of 0.65, 1, and 3 cSt viscosity segmented by water at a wide range of the volume fractions from 0.166 to 0.833. Figure (3.2) illustrates the photographs for the Taylor flow of 1 cSt silicone oil / dyed water with red color in a sample from the current experiments. Red dye enhances visualization of the water plugs.

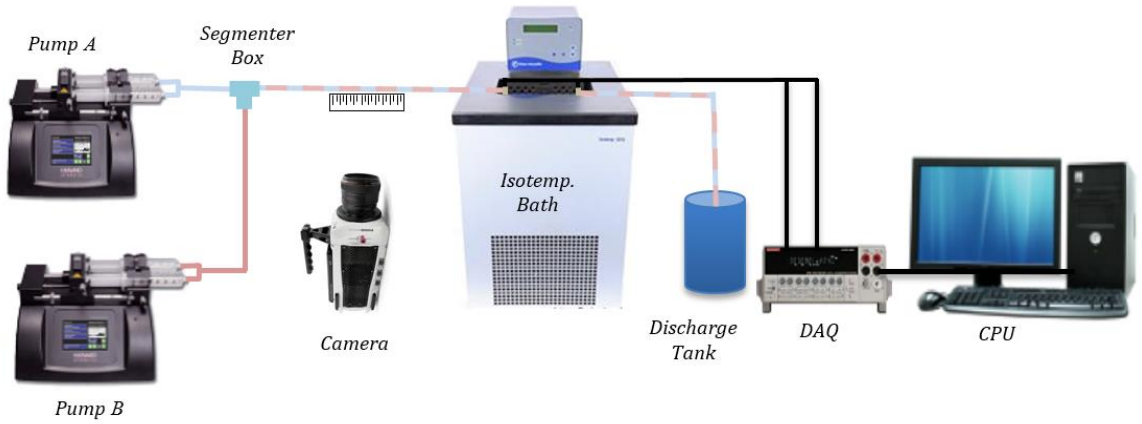

Fig. 3. 1 - System configuration.

The experiments were performed on Taylor flow in three different media (water / 0.65 cSt oil, water / 1 cSt oil or water / 3 cSt oil) in the straight heated copper tubes. A series of formed short slugs (Taylor flow) were injected into the test sections respectively at a variable flow rate for the first liquid phase and at a constant flow rate for the second liquid phase. Then the process was reversed in order to provide a wide range of liquid fractions. In this study, the flow was thermally developing and hydrodynamically fully developed. Several readings of the inlet and outlet temperatures were recorded for each flow rate to minimize errors in the readings.

Benchmark Test: To benchmark and verify the accuracy of the facility and then the experimental data, tests for a single-phase flow in a mini-scale tube were conducted with water and three low viscosity silicone oils (0.65 cSt, 1 cSt and 3 cSt). The experimental data of single-phase flow on heat transfer rate inside straight mini-scale tubes under a con stant wall temperature for different liquid flow rates is presented in Fig. (3.3) with classic

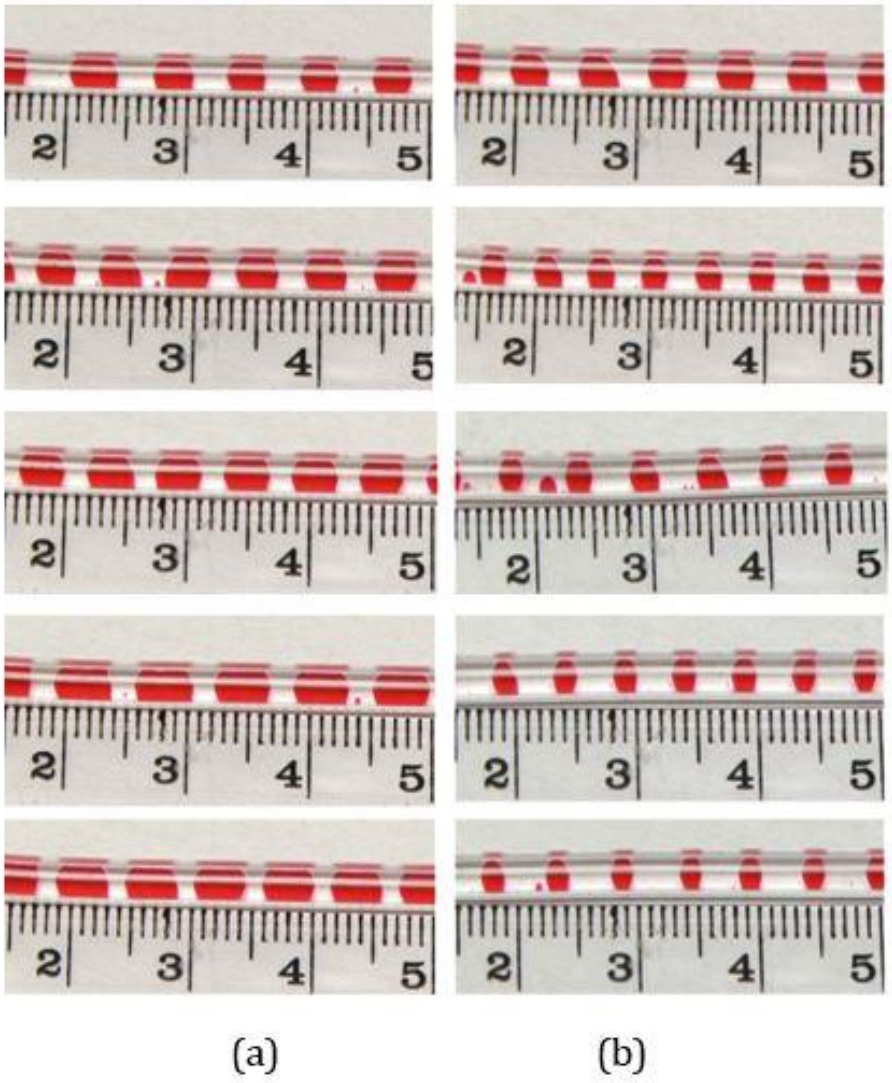

Fig. 3. 2 - Illustration of segmented flow for (a) variable flow rates of dyed water and constant flow rate of 1 cSt silicone oil (right column), and (b) variable flow rates of 1 cSt silicone oil and constant flow rate of water (left column).

Graetz-Poiseuille theory. As illustrated in Fig. (3.3), very good agreement with theory and the experimental data for all three fluids follows the Graetz model in the thermal developing region and approaches the fully developed limit of $q^* = 1/(4L^*)$ which is the maximum

heat that can be transferred to the fluids when $T_o \rightarrow T_w$. The results of single-phase flow in a mini-scale tube are used as a reference point for the new two-phase Taylor flow data.

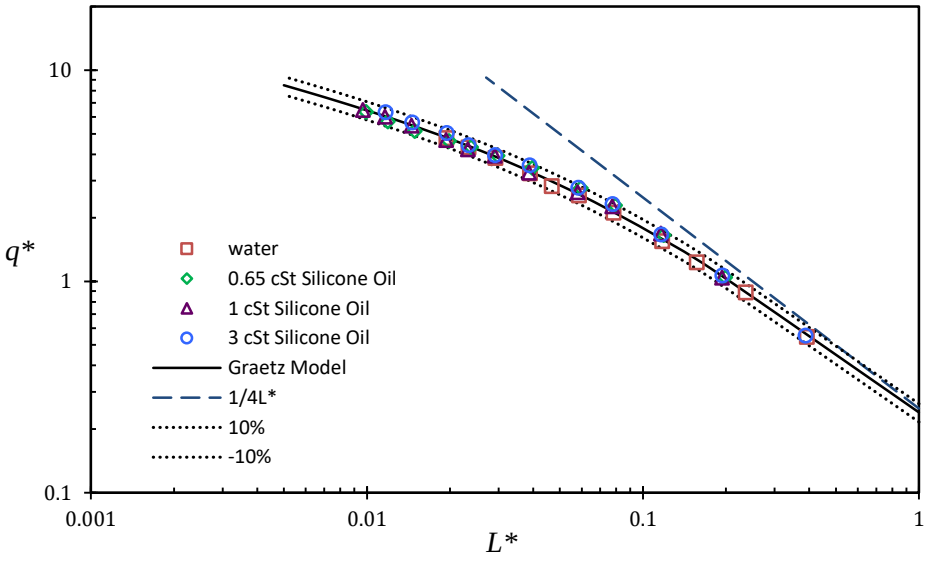

Fig. 3. 3 - Benchmarking results for a straight tube with 10 % error band.

Experimental Uncertainty: In this section, the experimental uncertainty is calculated using the method of Kline and McClintock [33,34]. The uncertainty analysis for this experiment was calculated for q^* and L^* based on uncertainties of the measuring equipment from manufacturer which was calibrated in our lab. The experimental uncertainty in these dimensionless parameters depends on the uncertainty in the experimental measurement of temperature, flow rate, geometric parameters, and properties of test fluids. The uncertainty analysis was performed using the root mean squares method and shows the estimated uncertainty for maximum and minimum flow rates in the experiment for the Taylor flow range. The uncertainty is estimated to be ± 4.51% to ± 7.51% for dimensionless thermal length L^* and ± 4.46% to 7.47% for dimensionless heat flux q^*.

3.3 Formulation of Heat Transfer for Taylor Flow

This section presents the analysis methodology for liquid-liquid Taylor flow based on the fundamental Graetz theory for both Poisueille and slug flow in the case of an isothermal wall [36,37]. The energy balance of the fluid flow can be represented by

$$Q = (\dot{m}c_p)_{L_c}\left(T_{o,L_c} - T_{i,L_c}\right) + (\dot{m}c_{p_{L_d}})\left(T_{o,L_d} - T_{i,L_d}\right) \tag{3.1}$$

where for this liquid-liquid Taylor flow, the same inlet temperature is maintained for both liquids (T_{i,L_c}=T_{i,L_d}), and the outlet temperature of the carrier liquid is approximately the same as the outlet temperature of the segmenting liquid (T_{o,L_c}~T_{o,L_d}).

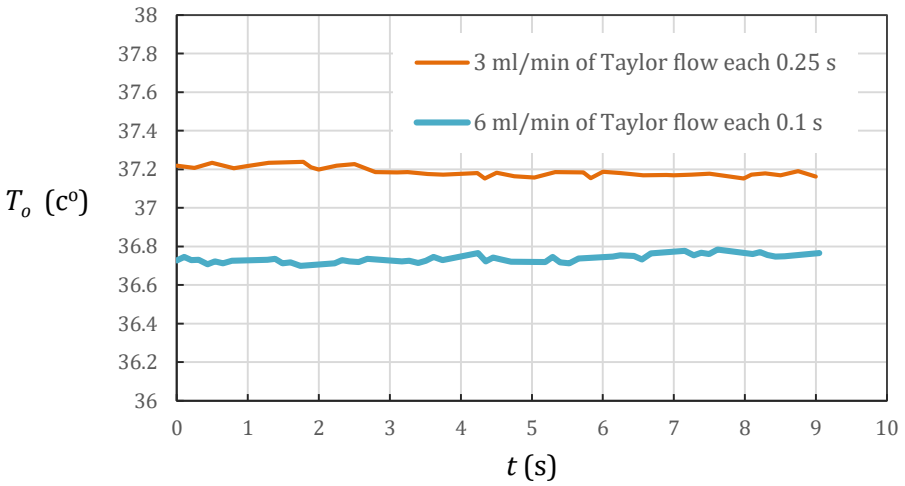

Fig. 3. 4 - Shows measured outlet temperature with time for a 1 cSt oil / water slug flow.

Figure (3.4) shows the measured outlet temperature with time for a 1 cSt oil/water slug flow at a 3 *ml/min* and 6 *ml/min* flow rate; readings are received every 0.1 sec and 0.25 sec in real-time. As shown in the figure, the variation of the outlet temperature is insignificant for both phases, which is reasonable due to the intimate thermal contact of the two phases,

where the heat transfers through the film and slug cap interfaces, and the fact that the thermal diffusion values of the liquids used in the slug flow are very close. This allows Eq. (3.1) to be written as:

$$Q = [(\dot{m}c_p)_{L_c} + (\dot{m}c_{p_{L_d}})](\bar{T}_o - T_i) \tag{3.2}$$

For constant wall temperature, reducing the data of a segmented liquid-liquid flow using the dimensionless mean wall heat flux approach which provides a more convenient method to study heat transfer enhancement of segmented flows for mini-channels than a Nusselt number approach [35]

$$q^* = \frac{\bar{q}\, D}{\bar{k}_e\,(T_w - T_i)} \tag{3.3}$$

where $\bar{q} = Q/A$ and $A = PL = \pi DL$ is the flow area of the copper tube, and D is the inner diameter of a standard circular tube.

In this case, the dimensionless mean wall heat flux (q^*) is a function of the dimensional thermal length (L^*)

$$L^* = \frac{L/D}{Re\ Pr} = \frac{L/D}{Pe} \tag{3.4}$$

where $Pe = UD/\bar{k}_e/\overline{\rho c_P}_e = UD/\bar{\alpha}_e$ is the Peclet number for liquid-liquid flow based on the effective properties of two-phase flow and the superficial velocity, i.e. $U = \left(\dot{Q}_{L_c} + \dot{Q}_{L_d}\right)/A$ and $A = \pi D^2/4$.

The following expressions are used to validate the results for the dimensionless mean wall heat flux for thermally developing flow under constant wall temperature condtion. For a Graetz- Poiseuille flow in a circular tube, Muzychka et al. [31,32] obtained

$$q^*_{pois} = \left[\left(\frac{1.614}{L^{*1/3}}\right)^{-3/2} + \left(\frac{1}{4L^*}\right)^{-3/2}\right]^{-2/3} \tag{3.5}$$

For Graetz-slug flow in a circular tube, the dimensionless heat transfer is

$$q^*_{slug} = \left[\left(\frac{1.128}{L^{*1/2}}\right)^{-2} + \left(\frac{1}{4L^*}\right)^{-2}\right]^{-1/2} \tag{3.6}$$

For a multicomponent liquid flow, the thermodynamic properties are calculated by the thermal equilibrium between the component liquids, which works well with the results compared with most commonly used formulas in two phase flows [36]. The thermal properties of two liquids in segmented flow using effective volume average:

$$\overline{\rho c_p}_e = \rho_{L_c} c_{p_{L_c}} \alpha_{L_c} + \rho_{L_d} c_{p_{L_d}} (1 - \alpha_{L_c}) \tag{3.7}$$

where $c_{p_{L_c}}$ and $c_{p_{L_d}}$ are the specific heat capacities of oil (carrier phase) and water (dispersed or segmented phase), respectively. The oil liquid fraction, α_{L_c}, is defined as:

$$\alpha_{L_c} = \frac{\dot{Q}_{L_c}}{\dot{Q}_{L_c} + \dot{Q}_{L_d}} \sim \frac{L_c}{L_c + L_d} \tag{3.8}$$

Finally, the effective thermal conductivity is calculated using the volume averaged value as follows:

$$\bar{k}_e = k_{L_c}\,\alpha_{L_c} + k_{L_d}\,(1-\alpha_{L_c}) \tag{3.9}$$

The heat transfer formulation provides an effective method to study and provide new insights on liquid-liquid Taylor flow.

3.4 Results and Discussion

This section presents new experimental data on liquid-liquid slug flows in heated tubes with a constant wall temperature boundary at varying volume fractions. Attainable heat transfer rates are augmented in a dimensionless format compared with the single-phase flow at different flow rates and tube lengths. Figures (3.5) to (3.7) illustrate the new experimental data in terms of q^* for different values of L^* in short and long mini-scale tubes. The magnitude of L^* is changed as the liquid flow rates or the ratio of the tube length to diameter is altered. The experimental data of liquid-liquid Taylor flows are presented using silicone oil of 1 cSt viscosity and segmented by water for tube lengths of $L = 163$ *mm*, 55 *mm,* and 46 *mm*, respectively. The obtained experimental data with using the liquid fraction in calculating the effective thermodynamic properties of Taylor flow are compared to models developed by Muzychka et al. [31] for Graetz Plug and Poiseuille flow. Initially, experiments were conducted for variable flow rates of water (3 to 7 *ml/min*) and a constant flow rate of silicone oils (3 *ml/min*), as well as for variable flow rates of silicone oils (3 to 7 *ml/min*) and a constant flow rate of water (3 *ml/min*), to show the effect of slug length ratio on the heat transfer process. The range of liquid fractions was $0.3 < \alpha_L < 0.7$, indicating varying slug lengths.

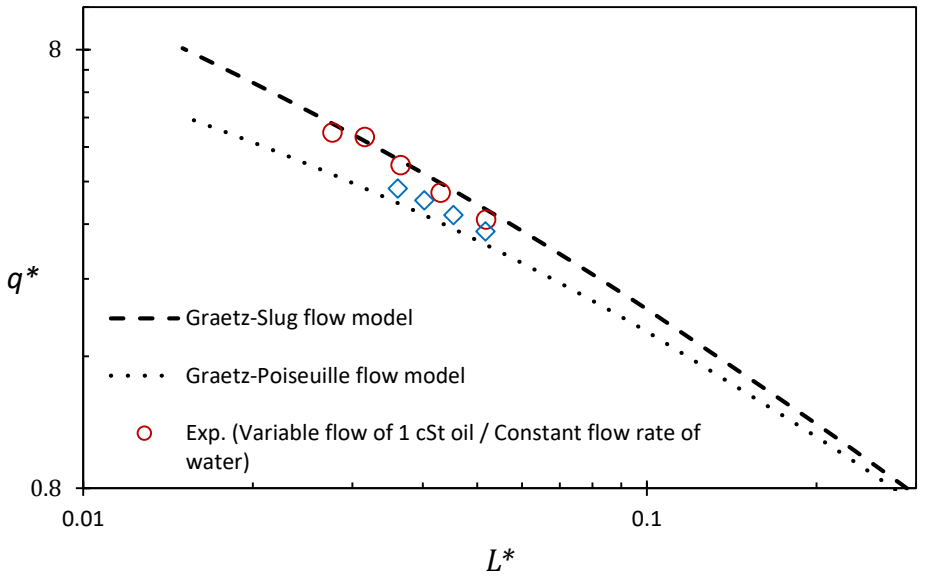

Fig. 3. 5 - Heat transfer effectiveness for liquid-liquid Taylor flow at various liquid fractions in a short length tube (L = 46 *mm*).

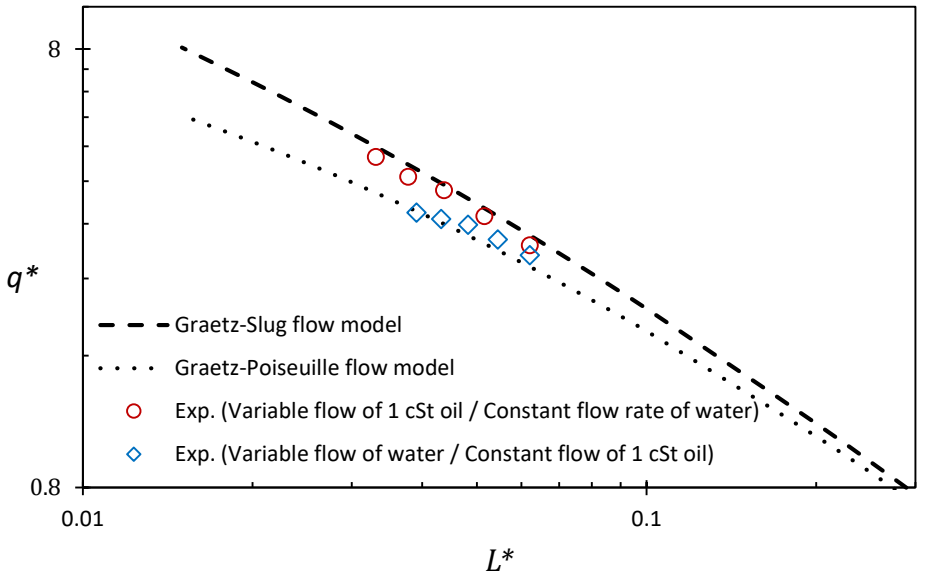

Fig. 3. 6 - Heat transfer effectiveness for liquid-liquid Taylor flow at various liquid fractions in a medium length tube (L = 55 mm).

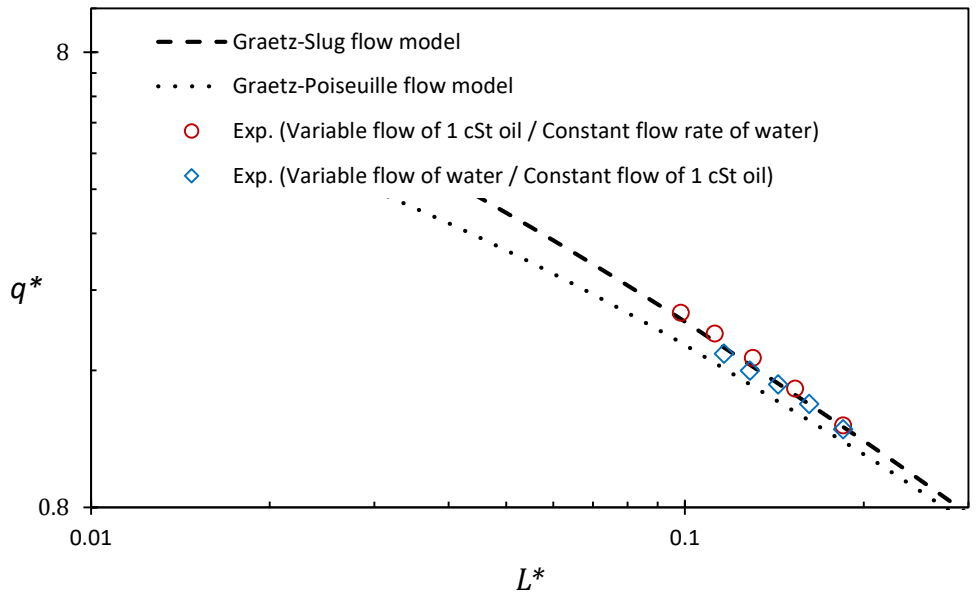

Fig. 3. 7 - Heat transfer effectiveness for liquid-liquid Taylor flow at various liquid fractions in a long length tube (L = 163 mm).

As illustrated in Figs. (3.5) to (3.7), the experimental data compares well with the predictions for Graetz-slug flow (Eq. 3.8) when oil is the variable phase and water is introduced at a constant flow rate. In contrast, the experimental data drop below the Graetz-slug flow curve when flow rates are increased, water is the variable phase and oil is the constant flow rate. All the experimental data are on or above the Graetz-Poiseuille flow curve, which demonstrates heat transfer enhancement significantly. Thermal enhancement for variable flow rate of water (increasing L_d) is significantly less than variable flow rate of silicone oil (increasing L_c). This is likely attributed that long slugs of segmented phase showed little enhancement over single-phase flow while short slugs resulted in almost an order of magnitude enhancement. It has been known that thermal enhancement occurs due to the internal circulation in the liquid plugs, leading to greater radial transport of heat or

mass, while the other mechanism as results from the reduced liquid fraction of segmented phase for a constant mass flow rate, leading to the increased velocity of liquid plugs and boundary layer renewal.

Based on the collected experimental results behavior and developed models earlier by second author [31] for Graetz-Poiseuille and -slug flow, new model is proposed using the Churchill and Usagi [37] asymptotic modelling approach and having the following form

$$q^*_{L-L\,Taylor\,flow} = \left[\left(\left(q^*_{Pois.}\right)_0 + \frac{\alpha_{L_c}}{2}\left(q^*_{Slug}\right)_0\right)^{-n} + \left(q^*_{\infty}\right)^{-n}\right]^{-1/n} \tag{3.10}$$

where α_{L_c} the liquid fraction of the carrier phase. Using the trial value of n~ $-3/2$ yields the best overall predictive mode. It is given here for completeness as follows

$$q^*_{L-L\,Taylor\,flow} = \left[\left(\left(\frac{1.614}{L^{*1}/_3}\right) + \frac{\alpha_{L_c}}{2}\left(\frac{1.128}{L^{*1}/_2}\right)\right)^{-3/2} + \left(\frac{1}{4L^*}\right)^{-3/2}\right]^{-2/3} \tag{3.11}$$

which has a root mean square (RMS) error typically less than 6%. This model captures the expected behavior of segmented Taylor flow in isothermal tubes by combining between the three asymptotic solutions for the boundary layer and fully developed regions. Thus, the proposed model is a function of the dimensionless tube length and the liquid fraction.

In order to properly validate the proposed model, now we can compare it with new experimental data covering a wide range of variables. In each experiment sets the working fluids of Taylor flow were changed inside different length of tubes. New experimental data for liquid-liquid Taylor flow in mini scale tubes were obtained using three silicone oils of 0.65, 1, and 3 cSt viscosity segmented by water for variable flow rates of water (3 to 15 *ml/min*) and constant flow rate of silicone oils (3 *ml/min*), as well as, variable flow rates of

silicone oils (3 to 15 *ml/min*) and constant flow rate of water (3 *ml/min*). Thus, the range of liquid fractions became $0.166 < \alpha_L < 0.833$ thus varying slug lengths.

Figures (3.8) and (3.9) show the experimental data with new model production for water / 0.65 cSt silicone oil of Taylor flow inside the constant tube length of 163 *mm* and 55 *mm*, respectively. The solid line shows the proposed correlation and the experimental data are plotted using the solid markers. Figs. (3.10) and (3.11) are the correlation prediction results for water / 1 cSt silicone oil of Taylor flow inside the constant tube length of 163 *mm* and 82 *mm*, respectively. Also, the experimental data and the proposed model for liquid-liquid Taylor flow in mini scale tubes are presented in Figures (3.12) and (3.13) using silicone oil of 3 cSt viscosity segmented by water at the wide range of liquid fractions for heated tube length of 82 *mm* and 55 *mm*, respectively.

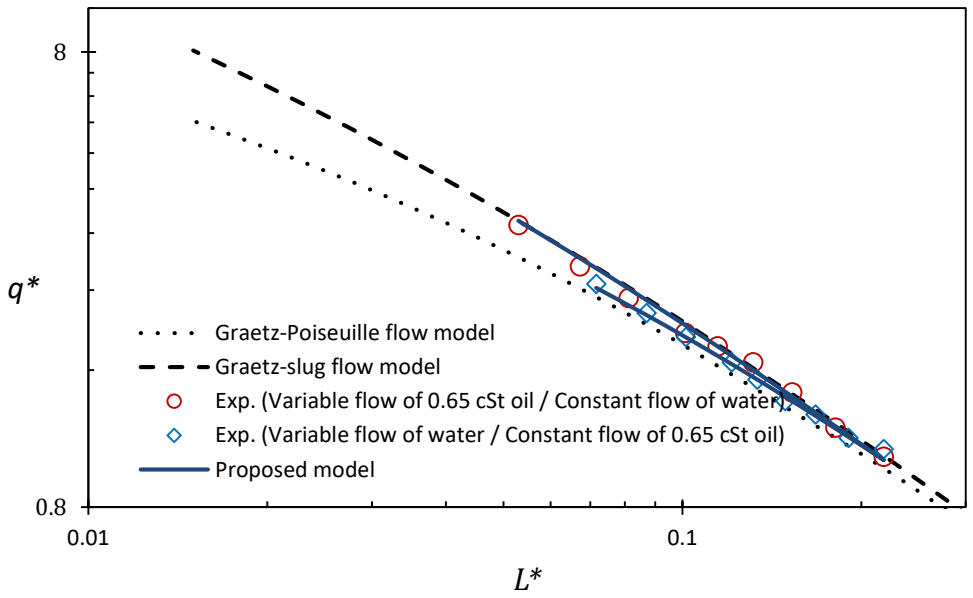

Fig. 3. 8 - Comparison of Taylor flow heat transfer data with proposed model at various liquid fractions in length tube of 163 *mm*.

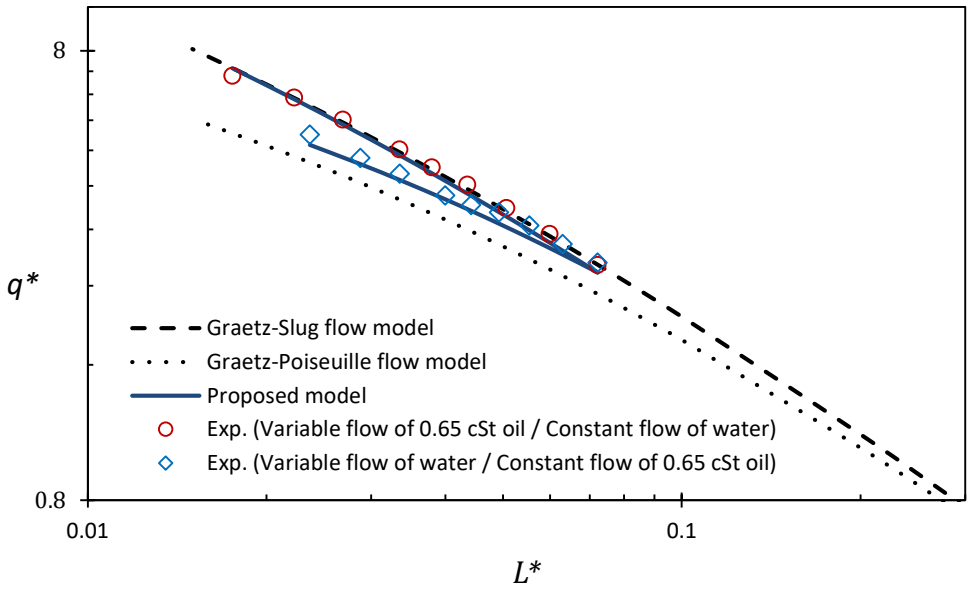

Fig. 3. 9 - Comparison of Taylor flow heat transfer data with proposed model at various liquid fractions in length tube of 55 *mm*.

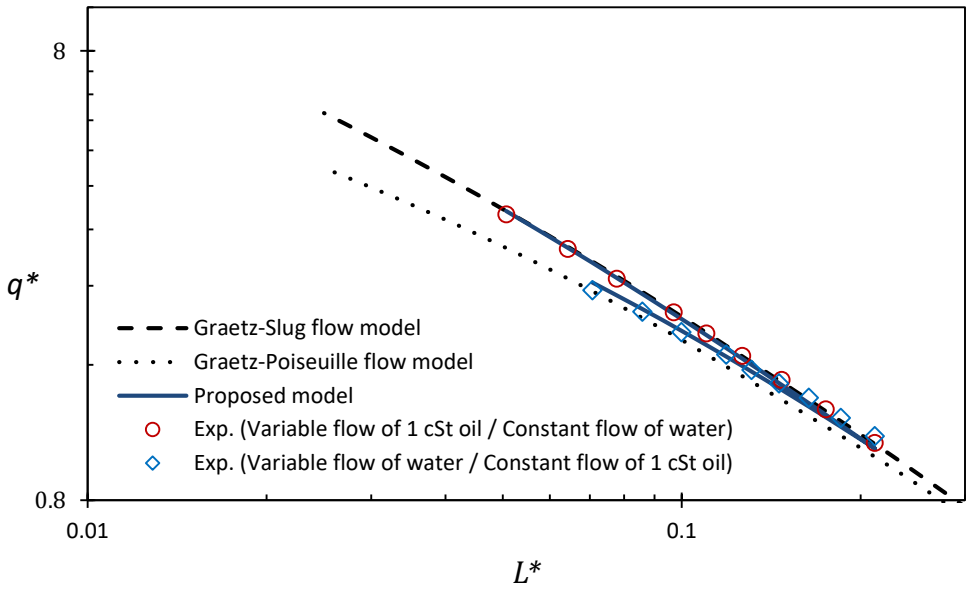

Fig. 3. 10 - Comparison of Taylor flow heat transfer data with proposed model at various liquid fractions in length tube of 163 *mm*.

Figures (3.9) to (3.13) provided comparisons the new model with the experimental data obtained. It can be seen from that the proposed model display the characteristics of the experimental data quite well. Good agreement is obtained between the proposed model and the experimental data although the varying of tube length and the Prandtl number. Note that the comparison of the model was obtained by considering a slug flow having the varying of liquid fraction and slug length. The data are also compared with the models of Graetz-Slug flow and Graetz-Poiseuille flow for the circular duct in all the figures with determining the percent difference between the data and the model predictions. The experimental data fall short of the model predictions at low Pr numbers as shown in Figs. (3.7) and (3.8) for water/1 cSt oil slug flow. However, all of the experimental data are in excellent agreement with the proposed model within $\pm$ 6% error.

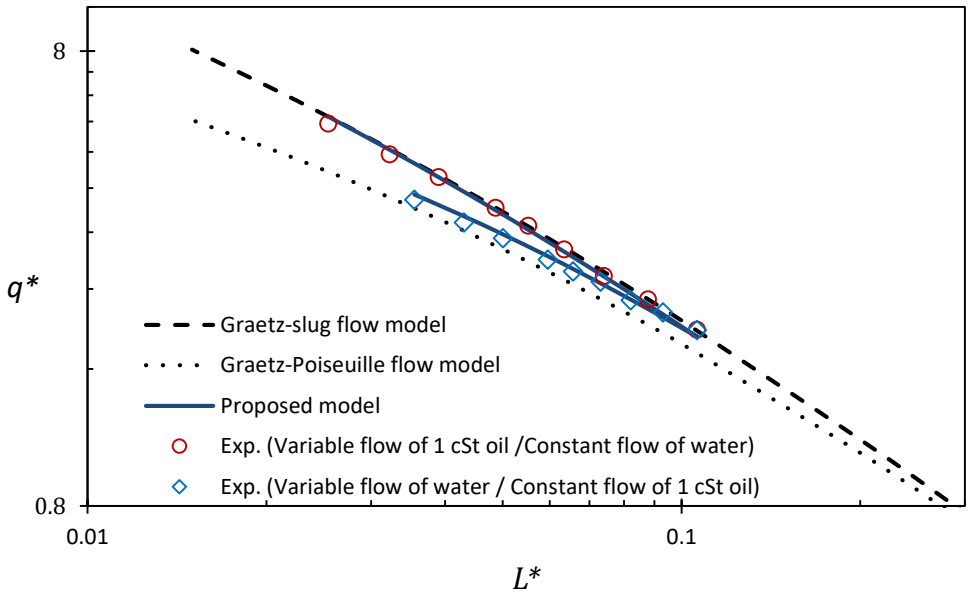

Fig. 3. 11 - Comparison of Taylor flow heat transfer data with proposed model at various liquid fractions in length tube of 82 *mm*.

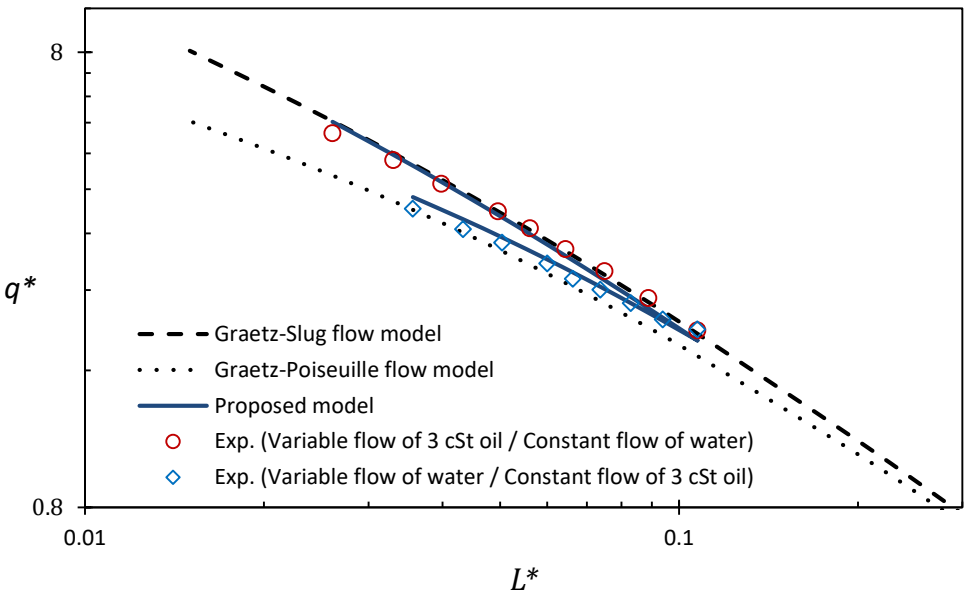

Fig. 3. 12 - Comparison of Taylor flow heat transfer data with proposed model at various liquid fractions in length tube of 82 *mm*.

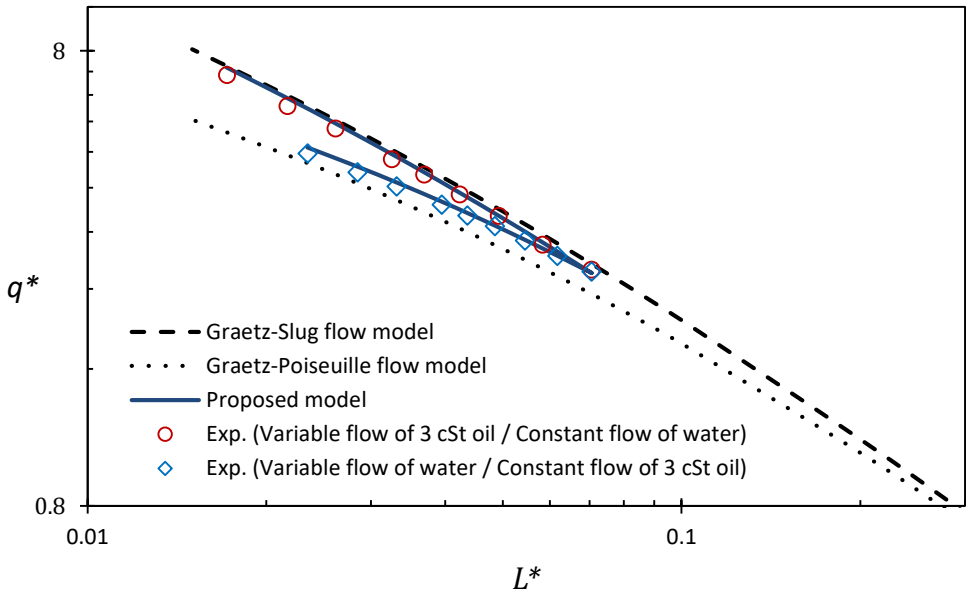

Fig. 3. 13 - Comparison of Taylor flow heat transfer data with proposed model at various liquid fractions in length tube of 55 *mm*.

Good agreement is also obtained for the case of the short and long tube for all Prandtl numbers. In general, the proposed model is quite robust in that it properly captures the expected trends of the data sets considered. The trend is towards Graetz-Slug flow model as a result of the reduced liquid fraction of segmented phase and resulting in the increased velocity of liquid slugs and the flow are becoming thermally saturated. While with the increased liquid fraction of segmented phase, it trends toward Graetz-Poiseuille flow model, which indicate that thermal saturation is not yet achieved.

3.5 Conclusions

With the growing need to develop alternative cooling techniques for electronic devices and systems in micro and mini-scale, use of non-boiling segmented slug flows has become one of the interesting methods for achieving higher cooling capacities. Heat transfer enhancement using non-boiling liquid-liquid segmented Taylor flow in straight mini-scale tubing was examined in this research. The laminar-flow heat transfer experiments were conducted in small diameter of heated copper tubes with constant wall temperature. The segmented flow was created using several fractions of low viscosity silicone oils (0.65 cSt, 1 cSt, 3 cSt) and water for a wide range of flow rates and slug lengths. The variety of liquids and flow rates change the Prandtl, Reynolds, and capillary numbers. The dimensionless mean wall flux and the dimensionless thermal flow length were used to analyze the experimental heat transfer data. The comparison has shown the heat transfer rate for Taylor flow is higher than in single-phase flow due to internal circulation in the fluid segments. Different mini-scale tubes were used which showed that tube length had no major effect on heat transfer enhancement if conditions prevented the flow from reaching the limit of

$1/(4L^*)$ which is the maximum heat transfer rate that can be achieved .

This study was performed also to demonstrate how heat transfer enhancement results due to shortening of the slug lengths of each phase in the segmented liquid-liquid Taylor flow. It was found that long slugs showed little improvement over single-phase flow whereas short slugs resulted in nearly an order of magnitude improvement. The results showed that when oil is the variable flow phase and water is introduced with constant flow, the two-phase flow exhibits Graetz-slug flow behaviour. Whereas, when water is the variable flow phase and oil is introduced at constant flow, the flow is approaching to Graetz-Poiseuille flow behavior. New model was developed using asymptotic modeling approach and based on the correlations proposed by Muzychka et al. [31], which predict heat transfer characteristics for the classic Graetz Poiseuille and slug flow in circular channels. The experimental data and proposed model results were found to be in good agreement with less than 6% error for most tube lengths and Taylor flows. The result highlights the constant / segmenting phase effect on heat transfer enhancement.

3.6 References

[1] Angeli, P., and Gavriilidis, A., 2008, "Hydrodynamics of Taylor Flow in Small Channels: A Review," Proc. Inst. Mech. Eng. Part C J. Mech. Eng. Sci., 222, pp. 737–751.

[2] Gupta, R., Fletcher, D. F., and Haynes, B. S., 2010, "Taylor Flow in Microchannels: A Review of Experimental and Computational Work," J. Comput. Multiph. Flows, 2(1), pp. 1–31.

[3] Talimi, V., Muzychka, Y. S., and Kocabiyik, S., 2011, "A Review on Numerical Studies of Slug Flow Hydrodynamics and Heat Transfer in Microtubes and Microchannels," Int. J. Multiph. Flow, 39, pp. 88–104.

[4] Muzychka, Y. S., Walsh, E., Walsh, P., and Egan, V., 2011, "Non-Boiling Two Phase Flow in Microchannels," *Microfluidics and Nanofluidics Handbook: Chemistry, Physics, and Life Science Principles*, S.K. Mitra, and S. Chakraborty, eds., CRC Press, Taylor & francis group, Boca Raton, FL.

[5] Asadi, M., Xie, G., and Sunden, B., 2014, "A Review of Heat Transfer and Pressure Drop Characteristics of Single and Two-Phase Microchannels," Int. J. Heat Mass Transf., 79, pp. 34–53.

[6] Bandara, T., Nguyen, N. T., and Rosengarten, G., 2015, "Slug Flow Heat Transfer without Phase Change in Microchannels: A Review," Chem. Eng. Sci., 126, pp. 283–295.

[7] Abdollahi, A., Sharma, R. N., and Vatani, A., 2017, "Fluid Flow and Heat Transfer of Liquid-Liquid Two Phase Flow in Microchannels: A Review," Int. Commun. Heat Mass Transf., 84, pp. 66–74.

[8] Kashid, M. N., and Agar, D. W., 2007, "Hydrodynamics of Liquid-Liquid Slug Flow Capillary Microreactor: Flow Regimes, Slug Size and Pressure Drop," Chem. Eng. J., 131(1–3), pp. 1–13.

[9] Kashid, M. N., Harshe, Y. M., and Agar, D. W., 2007, “Liquid-Liquid Slug Flow in a Capillary: An Alternative to Suspended Drop or Film Contactors,” Ind. Eng. Chem. Res., 46(25), pp. 8420–8430.

[10] Kashid, M. N., Agar, D. W., and Turek, S., 2007, “CFD Modelling of Mass Transfer with and without Chemical Reaction in the Liquid-Liquid Slug Flow Microreactor,” Chem. Eng. Sci., 62(18–20), pp. 5102–5109.

[11] Kashid, M., and Kiwi-Minsker, L., 2011, “Quantitative Prediction of Flow Patterns in Liquid-Liquid Flow in Micro-Capillaries,” Chem. Eng. Process. Process Intensif., 50(10), pp. 972–978.

[12] Wu, Z., Cao, Z., and Sundén, B., 2017, “Liquid-Liquid Flow Patterns and Slug Hydrodynamics in Square Microchannels of Cross-Shaped Junctions,” Chem. Eng. Sci., 174, pp. 56–66.

[13] Mandal, T. K., Das, G., and Das, P. K., 2010, “An Appraisal of Liquid-Liquid Slug Flow in Different Pipe Orientations,” Int. J. Multiph. Flow, 36(8), pp. 661–671.

[14] Kumar, S., Cherlo, R., Kariveti, S., and Pushpavanam, S., 2010, “Experimental and Numerical Investigations of Two-Phase (Liquid - Liquid) Flow Behavior in Rectangular Microchannels,” Ind. Eng. Chem. Fundam., 49, pp. 893–899.

[15] Dessimoz, A. L., Cavin, L., Renken, A., and Kiwi-Minsker, L., 2008, “Liquid-Liquid Two-Phase Flow Patterns and Mass Transfer Characteristics in Rectangular Glass Microreactors,” Chem. Eng. Sci., 63(16), pp. 4035–4044.

[16] Di Miceli Raimondi, N., Prat, L., Gourdon, C., and Cognet, P., 2008, “Direct Numerical Simulations of Mass Transfer in Square Microchannels for Liquid-Liquid Slug Flow,” Chem. Eng. Sci., 63(22), pp. 5522–5530.

[17] Kashid, M. N., Gerlach, I., Goetz, S., Franzke, J., Acker, J. F., Platte, F., Agar, D. W., and Turek, S., 2005, “Internal Circulation within the Liquid Slugs of a Liquid-Liquid Slug-Flow Capillary Microreactor,” Ind. Eng. Chem. Res., 44(14), pp. 5003–5010.

[18] Salim, A., Fourar, M., Pironon, J., and Sausse, J., 2008, “Oil-Water Two-Phase Flow in Microchannels: FLow Patterns and Pressure Drop Measurements,” Can. J. Chem. Eng., 86(6), pp. 978–988.

[19] Jovanović, J., Rebrov, E. V., Nijhuis, T. A., Hessel, V., and Schouten, J. C., 2010, “Phase-Transfer Catalysis in Segmented Flow in a Microchannel: Fluidic Control of Selectivity and Productivity,” Ind. Eng. Chem. Res., 49(6), pp. 2681–2687.

[20] Asthana, A., Zinovik, I., Weinmueller, C., and Poulikakos, D., 2011, “Significant Nusselt Number Increase in Microchannels with a Segmented Flow of Two Immiscible Liquids: An Experimental Study,” Int. J. Heat Mass Transf., 54(7–8), pp. 1456–1464.

[21] Mac Giolla Eain, M., Egan, V., and Punch, J., 2015, “Local Nusselt Number Enhancements in Liquid-Liquid Taylor Flows,” Int. J. Heat Mass Transf., 80, pp. 85–97.

[22] Jovanović, J., Zhou, W., Rebrov, E. V., Nijhuis, T. A., Hessel, V., and Schouten, J. C., 2011, “Liquid-Liquid Slug Flow: Hydrodynamics and Pressure Drop,” Chem. Eng. Sci., 66(1), pp. 42–54.

[23] Mac Giolla Eain, M., Egan, V., and Punch, J., 2013, “Film Thickness Measurements in Liquid-Liquid Slug Flow Regimes,” Int. J. Heat Fluid Flow, 44, pp. 515–523.

[24] Wu, L., Tsutahara, M., Kim, L. S., and Ha, M. Y., 2008, “Three-Dimensional Lattice Boltzmann Simulations of Droplet Formation in a Cross-Junction Microchannel,” Int. J. Multiph. Flow, 34(9), pp. 852–864.

[25] Raj, R., Mathur, N., and Buwa, V. V, 2010, “Numerical Simulations of Liquid - Liquid Flows in Microchannels,” Ind. Eng. Chem. Res., 49(21), pp. 10606–10614.

[26] Ghaini, A., Mescher, A., and Agar, D. W., 2011, “Hydrodynamic Studies of Liquid-Liquid Slug Flows in Circular Microchannels,” Chem. Eng. Sci., 66(6), pp. 1168–1178.

[27] Janes, N., Muzychka, Y. S., Guy, B., Walsh, E. J., and Walsh, P., 2010, “Heat

Transfer in Gas-Liquid and Liquid-Liquid Two Phase Plug Flow Systems," 12th IEEE Conf. Therm. Thermomechanical Phenom. Electron. Syst., pp. 1–11.

[28] Fischer, M., Juric, D., and Poulikakos, D., 2010, "Large Convective Heat Transfer Enhancement in Microchannels With a Train of Coflowing Immiscible or Colloidal Droplets," J. Heat Transfer, 132(11), p. 112402.

[29] Che, Z., Wong, T. N., Nguyen, N. T., and Yang, C., 2015, "Three Dimensional Features of Convective Heat Transfer in Droplet-Based Microchannel Heat Sinks," Int. J. Heat Mass Transf., 86, pp. 455–464.

[30] Urbant, P., Leshansky, A., and Halupovich, Y., 2008, "On the Forced Convective Heat Transport in a Droplet-Laden Flow in Microchannels," Microfluid. Nanofluidics, 4(6), pp. 533–542.

[31] Muzychka, Y. S., Walsh, E., and Walsh, P., 2010, "Simple Models for Laminar Thermally Developing Slug Flow in Noncircular Ducts and Channels," J. Heat Transfer, 132(111702–1).

[32] Muzychka, Y. S., Walsh, E. J., and Walsh, P., 2011, "Heat Transfer Enhancement Using Laminar Gas-Liquid Segmented Plug Flows," J. Heat Transfer, 133(4), p. 041902-1.

[33] Kline, S. J., and Mcclintock, F. A., 1953, "Describing Uncertainties in Single-Sample Experiments," J. Mech. Eng., 75, pp. 3–8.

[34] Holman, J. P., 2012, *Experimental Methods for Engineers*, McGraw-Hill, N. York.

[35] Muzychka, Y. S., and Ghobadi, M., 2016, "Measurement and Analysis of Laminar Heat Transfer Coefficients in Micro and Mini-Scale Ducts and Channels," Heat Transf. Eng., 37(11), pp. 938–94.

[36] Awad, M. M., and Muzychka, Y. S., 2008, "Effective Property Models for Homogeneous Two-Phase Flows," Exp. Therm. Fluid Sci., 33(1), pp. 106–113.

[37] Churchill, S. W., and Usagi, R., 1972, "A General Expression for the Correlation of Rates of Transfer and Other Phenomena," AIChE J., 18(6), pp. 1121–1128.

CHAPTER 4

Pressure Drop Modeling of Liquid-Liquid Taylor Flow in Mini-Scale Tubing*

4.1 Introduction

Taylor flow in small-scale channels is very important and in recent years has been used in a wide range of applications, such as in electronics cooling, heat exchange systems, pharmacology and biological microfluidics [1, 2]. Details on the flow hydrodynamics, pressure drop, and mass / heat transfer characteristics in the flow are required in the analysis and design of devices used for these applications. Expressions are needed to accurately predict the pressure drop in liquid-liquid Taylor flow in mini / micro scale channels because it is an important parameter needed for system design, the sizing of pumps, stability and flow rates as well as the total cost of the system. Numerous experimental and numerical investigations focusing on pressure drop of Taylor flows in small-scale channels have been conducted [3–7]. However, most research has focused on the interfacial pressure drop

* Submitted to ASME Journal of Fluids Engineering for publication.

associated with liquid-gas Taylor flow regimes [8, 9] and limited research has been conducted on liquid-liquid Taylor flow.

Many models and correlations were proposed to calculate the frictional pressure drop for two-phase flow in mini-channels [10]. Analysis of pressure drop modeling in Taylor flow is typically based on different approaches. The two most widely applied approaches are homogeneous flow and separated flow models. The homogeneous flow model assumes that the two-phase flow mixture behaves as a pseudo fluid, which has average defined properties and uses single-phase flow theory as reported by Salim et al. [11], Asthana et al. [12], Kim et al. [13], and Tsaoulidis et al. [14]. In a separated flow model, as in Salim et al. [11], Foroughi and Kawaji [15], Kim et al. [13], each phase is modeled separately or the Lockhart–Martinelli correlation is applied [16]. Additionally, there are studies that used both the homogeneous and separated approaches [11], [13].

While these approaches are widely applied for modeling a two-phase flow, they do not distinguish between the different flow regimes. There are models in the literature developed specifically for Taylor flow regimes [5, 6, 17 – 21]. As known Taylor flow consists of a series of slug unit cells and pressure drop of Taylor flow combines the frictional pressure drop of both phases as well as the interfacial pressure drop. Because in most of these studies the original correlations have been modified to fit the data, or because the proposed correlations may be valid only for the specific conditions studied, there is no generalized model for liquid-liquid Taylor flow in mini / micro scale channels.

Based on the homogeneous flow model and the separated flow model, Salim et al. [11] experimentally investigated two-phase oil-water flow pressure drop in micro T-junctions made of quartz and glass with different hydraulic diameters. Three flow patterns (drop, slug, and

annular flow) were obtained by injecting one fluid at a constant flow rate and a second with a pulsed flow rate. The pressure drop was measured by using homogeneous and Lockhart-Martinelli models [22], which are commonly used to describe the gas-liquid two-phase flow through the tubes. Their results showed that pressure drop was strongly dependent on flow rate, micro-channel material, and thermophysical properties of the carrier fluid. Kim et al. [13] conducted an experimental investigation of liquid–liquid segmented flows in fabricated polymer microfluidic channels. Three different cross-sectional expansion ratios from the injection to the test channels were used to observe the effect of the geometrical transition on the evolution of segmented flow in the test channel. The study includes identification of segmented flow regimes and their maps, length of dispersed and carrier fluid segments, development of predictive geometrical models for these quantities, and measurement of the dispersed fluid segment velocities. Velocity and pressure drop measurements of the liquid–liquid segmented flows were conducted for all flow regimes, and the associated trends were correlated with changes in the flow topology. The measured data agreed well with the prediction from the capillary pressure drop (interfacial pressure drop) model of Bretherton [23].

In the Taylor flow modeling approach, Kashid and Agar [17] experimentally studied the effects of various operating conditions on the flow regimes, including slug size, interfacial area and pressure drop for different Y-junction mixing elements. They used a snapshot approach under similar operating conditions and a corresponding interfacial area to measure the slug length and contact angles. The experimental snapshots were obtained by a photographic system comprised of a commercial camera to capture several slugs in an exposure; and were analyzed using the Adobe Photoshop® and Image Tool software.

They developed a theoretical prediction for pressure drop along the slug flow capillary based on the capillary pressure and hydrodynamic pressure drop without a wall film and compared it with experimental data. The experimental results were in good agreement with the theoretical model and they identified an organic wall film affecting the flow. Aota et al. [18] proposed that for gas-liquid and liquid-liquid flows laminar pipe flow theory predicts the pressure within each phase with reasonable accuracy when the pressure drop at the interface is balanced by the Laplace pressure. Their models were demonstrated good agreement with the experimental data.

Jovanovic et al. [19] numerically and experimentally investigated hydrodynamics and pressure drop of liquid-liquid slug flow in micro capillaries. They developed a liquid-liquid slug flow pressure drop model describing the effect of interface surface shape, slug size and capillary diameter. Also, experiments were performed to measure pressure drops and slug sizes in capillaries with diameters of 248 μm and 498 μm by several immiscible liquids of two phases slug flow such as water/toluene and ethylene glycol-water/toluene. The results showed that the film velocity has no significant effect on pressure drop; therefore, the stagnant film model accurately predicted the liquid-liquid slug flow pressure drop. The experimental and modified model results agreed well, with a mean relative error of less than 7%.

An experimental study of slug flow pressure drop in mini scale capillaries has been published by Eain et al. [6]. They reviewed the previous works of pressure drop models applied to Taylor flow. They also pointed out the lack of data while calculating pressure drop of liquid-liquid slug flow. According to their results, the comparison between experimental liquid-liquid data and the existence of gas-liquid correlations was limiting the

results, despite good agreement. They proposed a modification to Warnier et al. [24] model and Walsh et al. [25] model for liquid-gas pressure drop to extend the applicability of the correlation to liquid-liquid flows. These modified models agree with the experimental data to within ±20%.

Furthermore, the pressure drop of liquid-liquid slug flow in a microchannel, with a diameter of 800 μm, was calculated by Bandara et al. [5] in a review paper associated with Taylor flow. They used four different correlations from the literature: Eain et al. [6], Kreutzer et al. [9], and Jovanovic et al. [19], in addition to single-phase flow pressure drop. It was observed that there is a wide gap in understanding of the basic dynamics of liquid-liquid two-phase flow because of the large differences in how the pressure drop was calculated.

The main objective of this work is to propose a new model for predicting frictional pressure drop of liquid-liquid Taylor flow in small diameter tubes based on the interfacial pressure drop modeling approach, with a focus on interface surface shape, slug size and Capillary number. The slug length and contact angles will be measured using a snapshot approach under similar operating conditions and the corresponding interfacial area will be determined. Experimentally measured pressure drops and slug sizes in mini-scale tubing with several immiscible liquids used for model validation. The simplified theory will be employed to calculate the pressure drop along the length of the channel and the predictions will be compared with experimental results.

4.2 Formulation of Pressure Drop Model for Taylor Flow

This section presents the analysis methodology for pressure drop of segmented liquid-liquid Taylor flow. The total pressure drop in a Taylor flow regime is expressed as the sum of the single-phase pressure drops of different phases, and the additional pressure drop caused by the interface between the phases [25]. The analytical solution is developed for the total pressure drop of liquid-liquid Taylor flow in a capillary tube under the assumption that the film thickness is very thin. As illustrated in Fig. (4.1), the flow is divided into unit cells consisting of a liquid slug for carrier phase (L_c), and liquid slug for dispersed phase (L_d), and effective length of a unit cell is L_e.

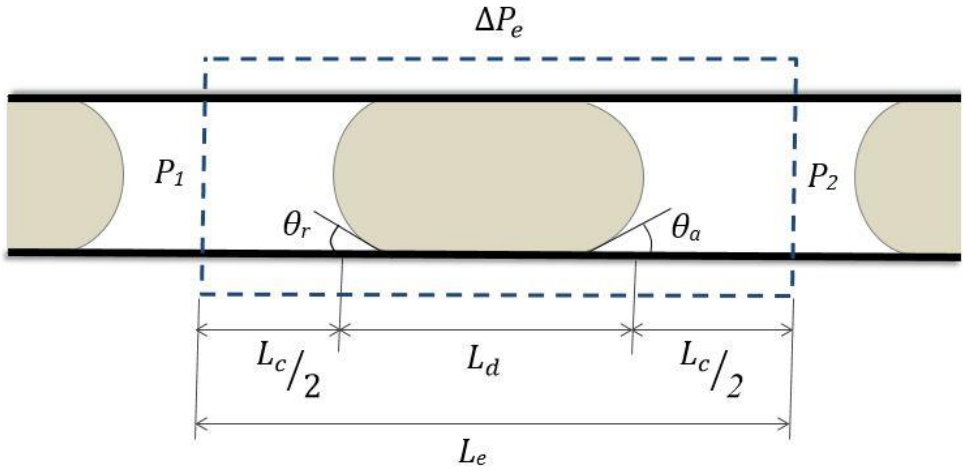

Fig. 4. 1 - Pressure drop in slug unit cell.

The pressure gradient is applied on a slug unit cell to properly account for the total pressure drop of segmented flow through a duct or channel, and the force balance in a unit cell of the slug flow can be expressed as

$$(P_1 - P_2)_e\, A = \tau_w\, P L_e + \Delta P_{Int}\, A \tag{4.1}$$

where P_1 and P_2 are the inlet and outlet pressure in the unit cell, respectively. The variable A is the area of the channel cross-section. The expression can be rewritten as

$$\frac{\Delta P_e}{L_e}\frac{A}{P} = \tau_w + \frac{\Delta P_{Int}}{L_e}\frac{A}{P} \tag{4.2}$$

For fully developed flow in a circular channel, the wall shear stress is related to the friction pressure gradient $\tau_w = f\left(\frac{1}{2}\bar{\rho}_e\, U^2\right)$ and $A/P = D/4$. By substituting these values into Eq. (4.2), the pressure drop per unit length in a circular channel becomes

$$\frac{\Delta P_e}{L_e}\frac{D}{4} = f\left(\frac{1}{2}\bar{\rho}_e\, U^2\right) + \frac{\Delta P_{Int}}{L_e}\frac{D}{4} \tag{4.3}$$

where f is the Fanning friction factor. Introducing $Re = \bar{\rho}_e\, U\, D/\bar{\mu}_e$ into Eq. (4.3) provides the following form

$$\frac{\Delta P_e}{L_e}\frac{D^2}{2\,\bar{\mu}_e\, U} = fRe + \frac{\Delta P_{Int}}{L_e}\frac{D^2}{2\,\bar{\mu}_e\, U} \tag{4.4}$$

The superficial velocity, U, is determined from the total flow rate

$$U = \frac{(\dot{Q}_c + \dot{Q}_d)}{A} \tag{4.5}$$

where $\dot{Q}_c$ and $\dot{Q}_d$ are the volumetric flow rates of carrier and dispersed phase, respectively.

Several models have been proposed to evaluate the dynamic viscosity of two-phase flow [26,27]. Typically, the dynamic viscosity of two-phase flow is assumed to depend on the structure of each phase, their interconnection, and volume fractions. According to the series

of slugs' structure in narrow tubes for liquid-liquid Taylor flow, the effective viscosity, $\bar{\mu}_e$, is replaced by the McAdams model [28], which is in reasonable agreement with experimental data, defined as

$$\bar{\mu}_e = \left[\frac{x}{\mu_c} + \frac{1-x}{\mu_d}\right]^{-1} \tag{4.6}$$

The effective density of liquid-liquid two-phase flow, $\bar{\rho}_e$, can be also calculated using liquid fraction of dispersed phase, α_L, or mass fraction, x:

$$\bar{\rho}_e = \left[\frac{x}{\rho_c} + \frac{1-x}{\rho_d}\right]^{-1} = \rho_c\, \alpha_{L_c} + \rho_d\, (1 - \alpha_{L_c}) \tag{4.7}$$

where the mass quality is $x = \dot{m}_c/(\dot{m}_d + \dot{m}_c)$ and the liquid fraction $\alpha_{L_c} = \dot{Q}_c/(\dot{Q}_d + \dot{Q}_c)$. The interface pressure, ΔP_{Int} is obtained from the Young-Laplace equation; thus, the pressure drop due to the liquid-liquid interfaces on the motion of one or more liquid slugs inside a capillary tube corresponds to the Laplace pressure,

$$\Delta P_{Int} = \frac{2\sigma}{R}\cos\theta \tag{4.8}$$

where R, σ and θ represent the radius of the liquid–liquid interface, interfacial tension between the respective phases, and contact angle, respectively. This equation assumes the film thickness was much less than the tube radius, then $D = 2R$.

For a slug moving inside a capillary tube, the interface pressure drop is due to the difference of the capillary forces between advancing and receding fronts because of the two different contact angles (advancing and receding) [18,29], as illustrated in Fig. (4. 1). The interface pressure drop of liquid-liquid slug flow is given by

$$\Delta P_{Int} = \frac{4\,\sigma}{D}\,(-\cos\theta_a + \cos\theta_r), \quad P_1 > P_2 \tag{4.9}$$

where θ_a and θ_r are the advancing and receding contact angle, respectively. By combining Eq. (4.9) and Eq. (4.4), the slug flow pressure drop per unit length in a circular channel becomes

$$\frac{\Delta P_e}{L_e}\frac{D^2}{2\,\bar{\mu}_e\,U} = fRe + \frac{D}{\bar{\mu}_e\,U}\frac{2\sigma}{L_e}\,(cos\,\theta_r - cos\,\theta_a) \tag{4.10}$$

Equation (4.10) can also be expressed in the following way

$$\frac{\Delta P_e}{L_e}\frac{D^2}{2\,\bar{\mu}_e\,U} = fRe + \frac{2\,D}{L_e}\,\frac{(\cos\theta_r - \cos\theta_a)}{Ca} \tag{4. 11}$$

where Ca is the Capillary number based on the two-phase Taylor flow model, which can be expressed as

$$Ca = \frac{\bar{\mu}_e\,U}{\sigma} \tag{4. 12}$$

At low capillary numbers, the pressure drop due to friction is much smaller than that due to the interface.

The dimensionless total pressure drop per unit length can be represented by

$$\Delta P_T^* = \frac{\Delta P_e}{L_e}\frac{D^2}{2\,\bar{\mu}_e\,U} \tag{4. 13}$$

and the dimensionless length of a unit cell can be expressed as

$$L_e^* = \frac{L_e}{D}\frac{Ca}{2(\cos\theta_r - \cos\theta_a)} \tag{4. 14}$$

These dimensionless substitutions for the general expression of the total pressure drop for Taylor flow in mini-scale tubing is a function of all effective variables on pressure drop in mini and micro scale channels. A model for Eq. (4.11) can be developed by combining the two dimensionless groups, which has the form

$$\Delta P_T^* = fRe + \frac{1}{L_e^*} \tag{4. 15}$$

For fully developed laminar flow in a circular channel, the frictional pressure drop of single-phase flow is

$$f = \frac{16}{Re} \tag{4. 16}$$

Thus, the proposed model for the total pressure drop per unit length is

$$\Delta P_T^* = 16 + \frac{1}{L_e^*} \tag{4. 17}$$

Finally, the analytical solution is presented in terms of the dimensionless groups, ΔP_T^*, to predict the total pressure drop in Taylor flow. The general proposed model takes the form

$$\Delta P_T^* = \Delta P_{Sp}^* + \Delta P_{Int}^* \tag{4. 18}$$

where ΔP_{Sp}^* and ΔP_{Int}^* are the dimensionless pressure drop of single-phase flow and interface between the phases, respectively. The total pressure drop is expressed as a function of the effective unit length (L_e). The Taylor flow is modeled as a series of slug unit cells, where $\Delta P_e / L_e = \Delta P / L$. Hence, the pressure drop of Taylor flow through mini / micro channels can be expressed as a function of all effective parameters (i.e.., Ca, L_e,

and θ) rather than using the Bretherton solution to account for the interfacial pressure drop, as in previous models.

4.3 Experimental Setup

The experimental setup for liquid-liquid two-phase flow in small-scale tubing is presented in Fig. (4.2). The experiments are conducted on mini-scale smooth-tubing (Nalgene™ 180 Clear Plastic PVC Tubing) with an internal diameter of 1.59 *mm*, and tube lengths of 0.5 *m* and 1 *m*. Two high-precision syringe pumps (Harvard Apparatus pumps) with glass syringes. The pumps control the relative flow rate of both phases and hence the infusion rates of liquids cause different slug lengths in the tubing. A box segmenter (T-junction) creates a slug train of liquid-liquid Taylor flow. Water and three silicone oils with low viscosity (1 cSt, 3 cSt, and 5 cSt) are used in this study. In all experiments, the silicone oils are the carrier phase and the segmented or dispersed phase is water. The thermophysical properties of liquids, at standard temperature and pressure, are presented in Table (4.1). Properties were obtained from the supplier of the silicone oils (Clear Co.). A digital high-speed camera (Phantom v611) with a light source is used for flow visualisation. The slug length and dynamic contact angles are measured, for each test, with the camera images to analyze the effect of slug length on pressure drop.

Figure (4.3) illustrates photographs for Taylor flow of water / 1 cSt silicone oil with different slug lengths in a sample. Depending on the pressure range for each dimension of the tubes and liquids, two pressure transducers with an accuracy of 1%, for ranges of 0 to 1 psi and 0 to 5 psi, are used and located at the test tube ends to measure the pressure drop

of the liquid stream. A Keithley data acquisition system is connected to a computer to collect and analyze the measured data of pressure drop at different flow rates.

Table 4. 1 - Carrier fluid properties

Oils	***ρ (kg/m^3)***	***μ (kg/m.s)***	***σ(N/m)***	***Pr***
1 cSt	815	0.00081	0.0427	13
3 cSt	895	0.00268	0.0424	39.1
5 cSt	915	0.00457	0.0428	64.4

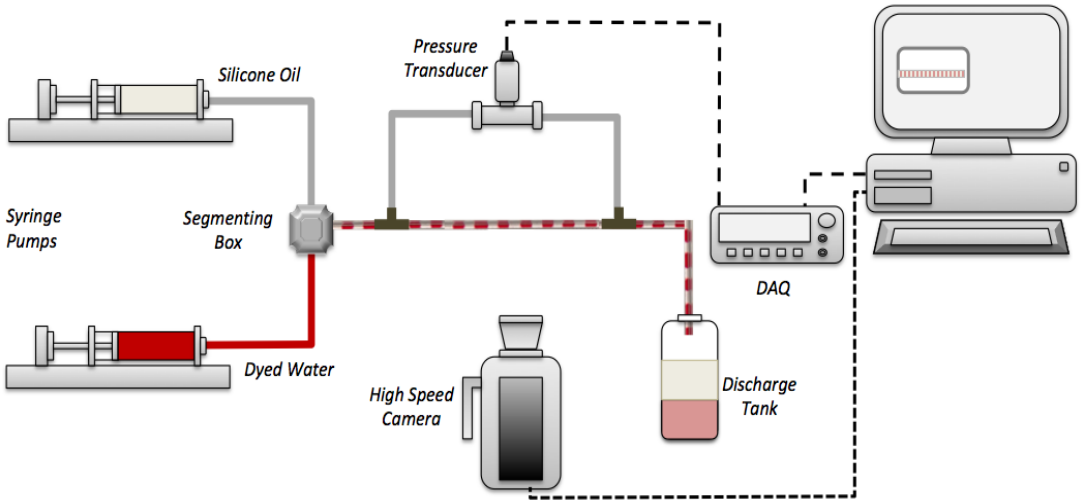

Fig. 4. 2 - Schematic of experimental setup.

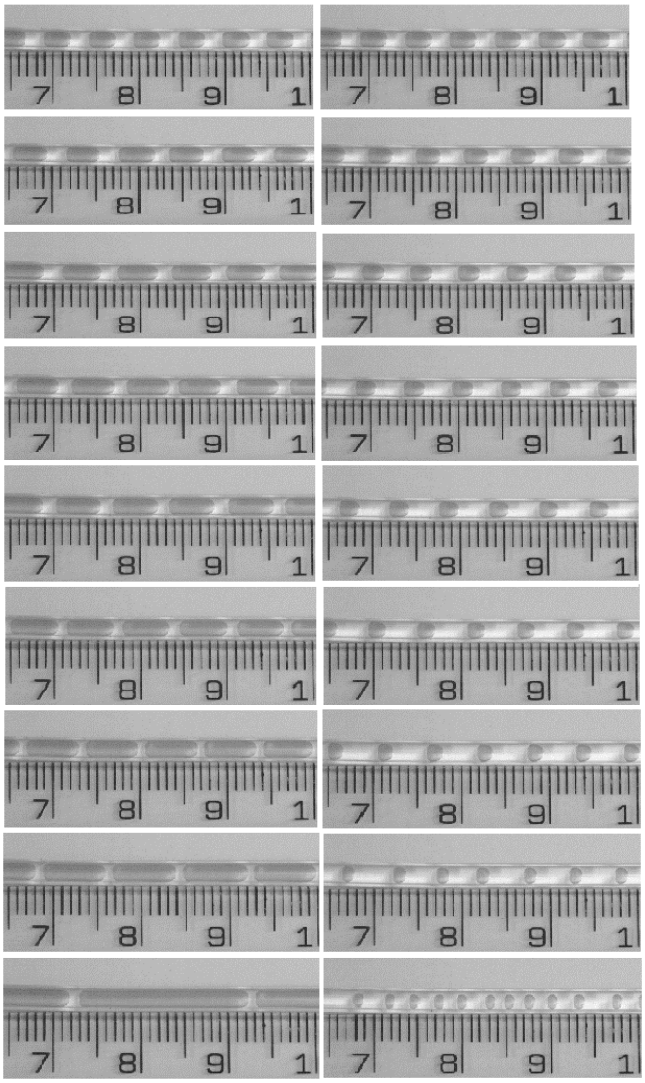

Fig. 4. 3 - Illustration of slug flows for (a) variable flow rates of water and constant flow rate of 1 cSt silicone oil (right column), and (b) variable flow rates of 1 cSt silicone oil and constant flow rate of water (left column).

A series of experiments are performed with the flow rates adjusted according to Taylor flow range and hydrodynamic resistance of system setup. Two-phase flow is exhibited when two liquids are injected into a T-junction at limited flow rates. The liquid flow rates

are selected to ensure the flow pattern in the main section is in the liquid-liquid slug flow regime. The liquids are pumped directly into mini tubes with steady state conditions to become liquid-liquid two phase flow with a velocity profile of laminar fully developed flows and an ambient temperature of approximately 23°C. The experiments are repeated, and two snapshots are taken for each set of flow conditions to confirm the reproducibility of the snapshots and pressure drop measurements. The snapshots for contact angle and slug length measurements are taken for both flowing and stationary conditions. The uncertainty of the friction factor measurements are between 4.46% and 7.47% using the Kline and McClintock approach [30].

4.4 Results and Discussion

This section presents the results of the pressure drop on liquid-liquid Taylor flow in capillary tubes. The results of single-phase flow in a mini-scale tube are used as a benchmark test for the new two-phase Taylor flow data. All measured pressure data are compared to the single-phase flow model and the proposed theoretical models for Taylor flow using the dimensionless variables. The comparison provides validation of the model for predicting pressure drop in liquid-liquid Taylor flow in small-scale tubes. The new results provide insights on the effects of slug length and Capillary number on pressure drop in a small-scale tube.

Benchmark tests for single-phase fully developed flow are conducted with different flow rates of water and 3 cSt viscosity silicone oil. As illustrated in Fig. (4.4), the experimental data for all test fluids follows the theoretical model in a mini-scale tube with ~ 10 % error.

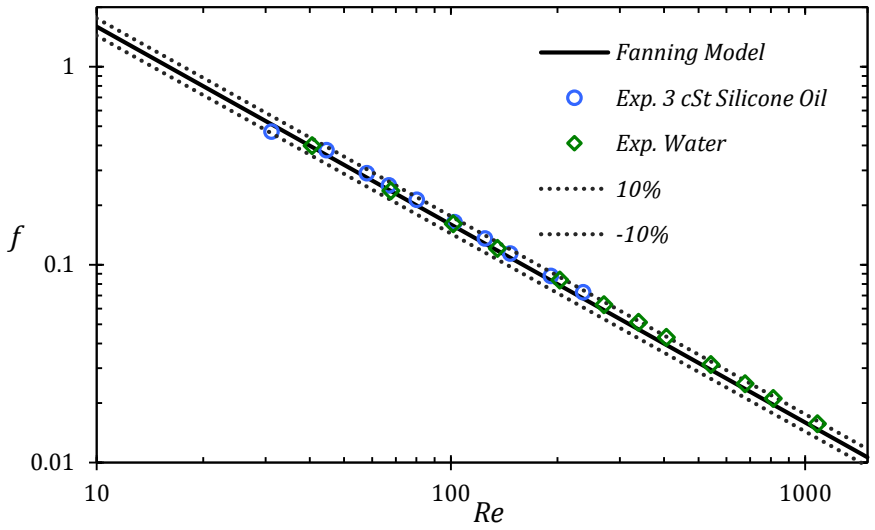

Fig. 4. 4 - Benchmarking test for friction factor in a straight tube with ± 10 % error band.

For two-phase flow, the experiments are conducted for variable flow rates of water (3 *ml/min* to 15 *ml/min*) and constant flow rate of silicone oil (3 *ml/min*), as well as variable flow rates of silicone oil (3 *ml/min* to 15 *ml/min*) and constant flow rate of water (3 *ml/min*), respectively. The range of liquid fraction is $0.16 < \alpha_L < 0.83$. Additionally, experiments are conducted with Taylor flow of water and silicone oil in the channel with α_L maintained at 0.5, and the range of each liquid flow rate is 3 *ml/min* to 20 *ml/min*.

Initially, the experimental results are presented in terms of friction factor with different values of Reynolds number for Taylor flow in mini-scale tubes. The magnitude of *Re* and *Ca* are changed by altering the liquid flow rates and liquid used. The experimental data are considered for the range of Reynolds number ($55 < \mathrm{Re} < 850$) and Capillary number ($0.001 < \mathrm{Ca} < 0.03$), which is Taylor flow range in this scale with different liquids and segmenter junctions. As illustrated in Fig. (4.5), the experimental data points are higher

than the theoretical model for laminar flow in a circular tube (Eq. 4.16). Figure (4.5) shows all data follows the same trend at lower values of Reynolds number, $Re < 100$. The results diverge for variable flow rate of silicone oil with a constant flow rate of water, compared to variable flow rate of silicone oil with a constant flow rate of water. The large increase of friction in Taylor flow is due to the pressure drop at the interface of fluids, which is neglected in the single-phase model. Therefore, in this study, a theoretical model is developed for describing the pressure drop of liquid-liquid Taylor flows in mini-scale tubes, with negligible liquid film thickness, which accounts for the effects of interfacial pressure with changing the mean slugs' velocity, U, and the effective unit length, L_e.

The results of the proposed model are presented in Fig. (4.6) along with the Walsh model [25] for gas-liquid Taylor flows. The theoretical solution for the pressure drop of liquid-liquid Taylor flow based on the theoretical force balance model is presented, while the model developed by Walsh et al. [25], based on a scale analysis of the Bretherton model is used to determine the interfacial pressure drop. The plot presents the total pressure drop dimensionless of fRe or ΔP^* against dimensionless unit effective length of the channel for the present model and the dimensionless groups $L_c^* \ (Ca/Re)^{1/3}$ for the Walsh model. Although a comparison of the models shows a similar trend of data, both models underestimate the magnitude of the pressure drop at high L_e^*, where the dominant flow turns from Taylor flow to single-phase flow. The flows are subject to reduced interfacial effects and the slugs are of sufficient length for the pressure drop in the capillary to be characteristically Poiseuille flow.

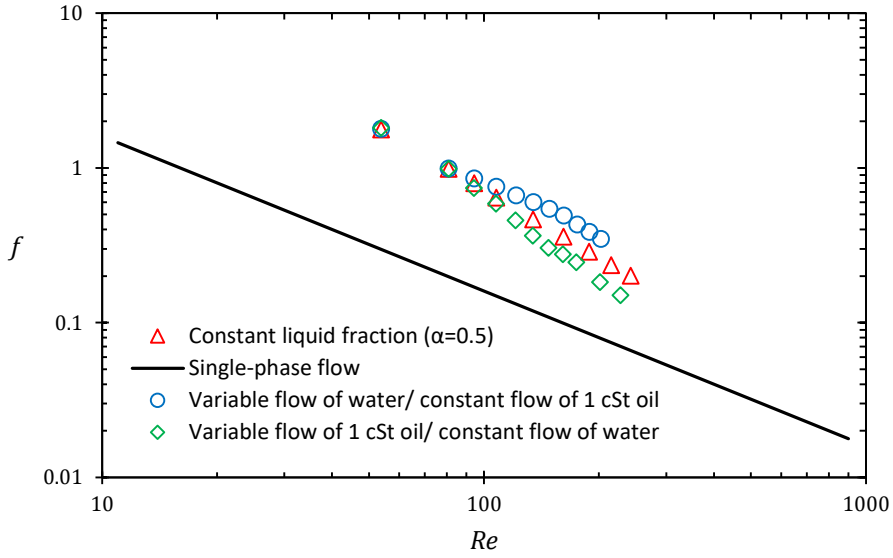

Fig. 4. 5 - Friction factor for liquid-liquid slug flow in variable flow rates of liquids.

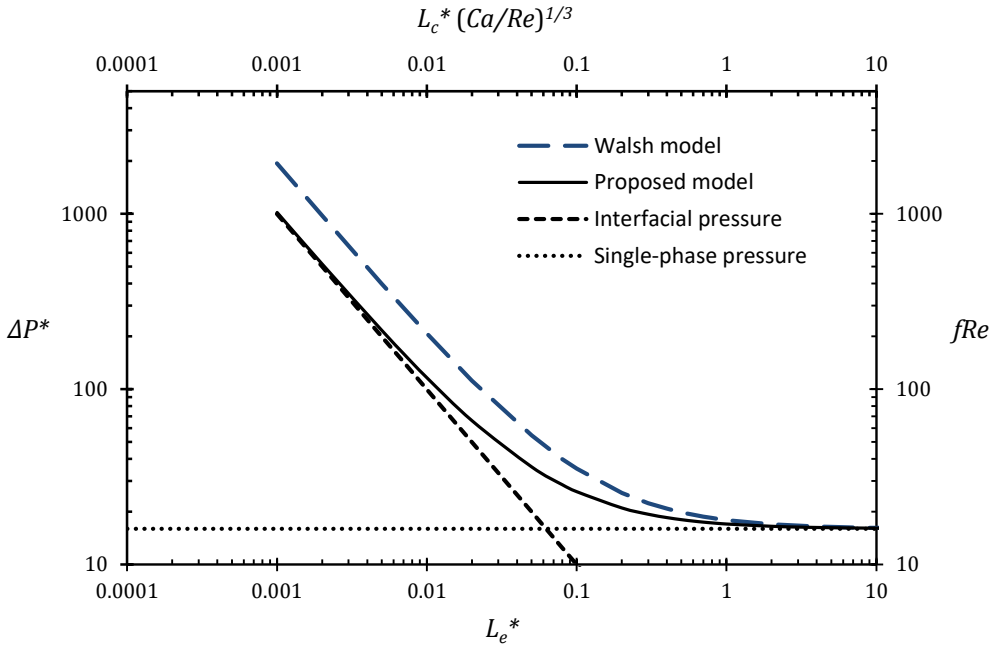

Fig. 4. 6 - Proposed model predication (Eq. 4.17) for pressure drop of liquid-liquid slug flow compared with Walsh model [25] where both the single-phase and interfacial pressure dominant the total pressure drop.

The new theoretical model, using the interfacial pressure drop is illustrated in Fig. (4.7). As illustrated in Fig. (4.7), changing the flow rates of 1 cSt viscosity silicone oil and water, causes the experimental pressure drop data to follow the same trend as the liquid-liquid Taylor flow model. Where the dimensionless total pressure drop, ΔP^*, for the variable flow rate of 1 cSt silicone oil and the constant flow rate of water is slightly less than the variable flow rate of water and constant flow rate of 1 cSt silicone oil. Thus, when the flow rates of 1 cSt silicone oil varies with constant water flow rate, the slug length of water is the dominate phase. In the opposite case, the slug length of 1 cSt silicone oil is characteristically Taylor flow, when variable flow rates of water with constant oil flow rate is the dominate phase.

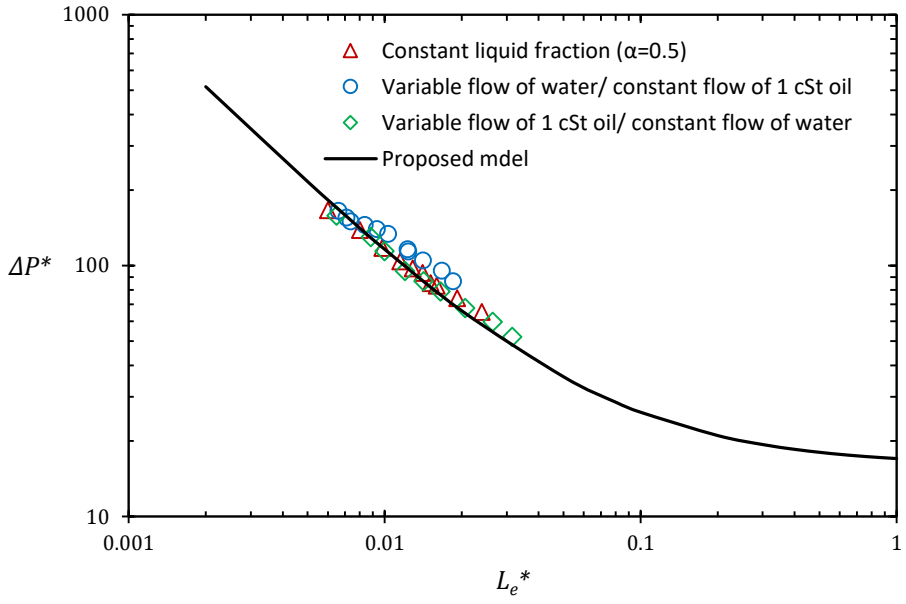

Fig. 4. 7 - Non-dimensional pressure drop (ΔP^*) compared with the experimental data of water / 1 cSt oil slug flow.

For further validation of the proposed model, two additional liquid-liquid combinations were used with varying effective viscosity. Figs. (4.8) and (4.9) show the comparison between the proposed model and new experimental data of pressure drop for water / 3 cSt silicone oil and water / 5 cSt silicone oil slug flow inside mini scale tubing at different volume fractions. Excellent agreement is achieved between the experimental data and the proposed model. The theoretical model performance continues regardless of the liquids used and the viscosity ratios, with all of the Taylor flow data within ± 20 % of the predictive model. This highlights the applicability of this model for low or high viscosity ratio flows.

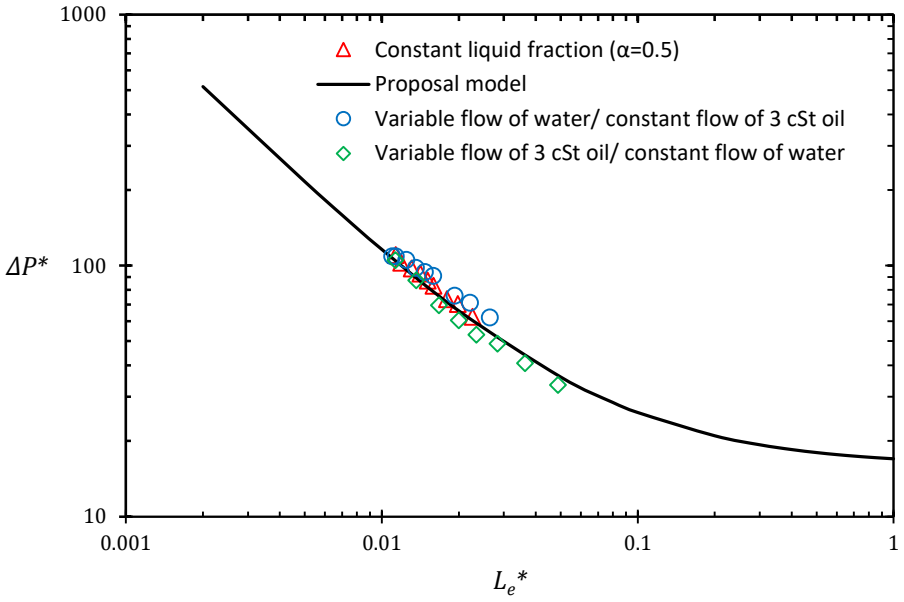

Fig. 4. 8 - Non-dimensional pressure drop (ΔP^*) compared with the experimental data of water / 3 cSt oil slug flow.

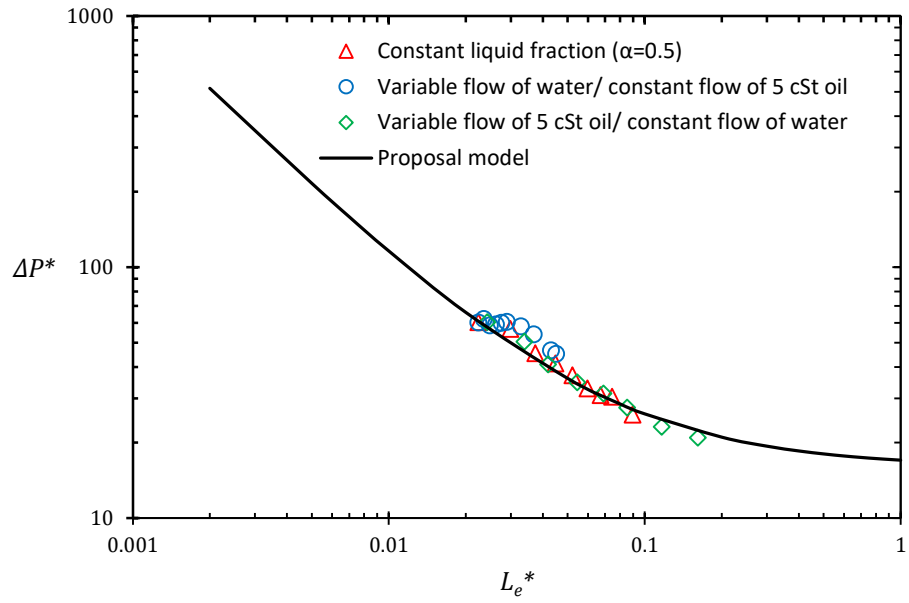

Fig. 4. 9 - Non-dimensional pressure drop (ΔP^*) compared with the experimental data of water / 5 cSt oil slug flow.

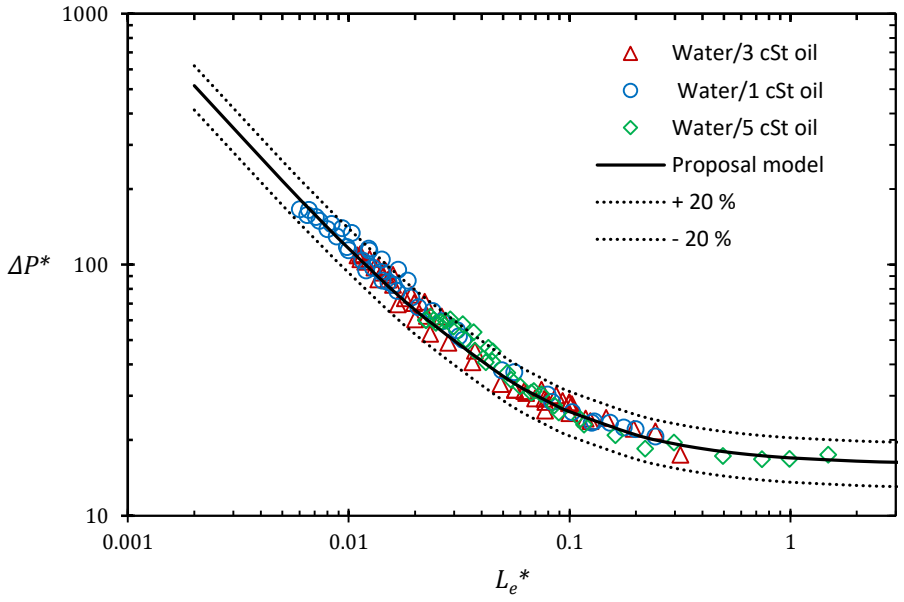

Fig. 4. 10 - All data repotted considering slug length and liquid fraction in the data reduction with the predicted model.

As illustrated in Fig. (4.10), the experimental data has the same general trend as the predicted results of the new model. For $L_e^* < 0.1$, the effect of slug length is not significant, and the pressure drop in the flow is dominated by the characteristically single phase Poiseuille flow. For $L_e^* > 0.1$, the slug effect is significant, and the pressure drop in the flow is characteristically Taylor flow. As illustrated in Fig. (4.10), there is good agreement between the predicted and experimental results, within ± 20%. The root mean square (RMS) error was found to be 14% for all experimental data with different liquids used of Taylor flow. The differences between measured and predicted results can likely be attributed to measurement accuracy, or the calculation method used to determine the average two-phase viscosity.

4.5 Conclusions

In this chapter, the pressure drop of segmented liquid-liquid Taylor flow in small-scale tubing was investigated. A new theoretical model was developed to describe the pressure drop of Taylor flows based on pressure forces balance model into a unit cell of a slug flow. The proposed model takes into account the pressure drop due to friction between each fluid and the tube wall, in addition to the capillary pressure drop at the interface of the fluids. The flows are subject to reduced interfacial effects when the slugs are of sufficient length for the pressure drop in the capillary to be characteristically Poiseuille flow. New experimental data for liquid-liquid Taylor flow in mini-scale tubes were obtained using three silicone oils of 1, 3, and 5 cSt viscosity segmented by water at varying volume fractions from 0.16 to, 0.83. Varying slug lengths were obtained by careful controlled of volume fractions show a significant impact on the pressure drop.

It can be concluded that introducing two immiscible liquids to mini scale channels significantly increases pressure drop and the pressure drop for two-phase flow is much higher than the pressure drop for single-phase flow. However, the effect of slug length has been shown for the continuous and dispersed phases and the range of each liquid flow rate on the transition from a Taylor-dominated flow to Poiseuille single-phase-dominated flow. The dependence of pressure drop on the bubble velocity is not incorporated in the model of Walsh et al., while is included in the model developed in this work. The present model is in good agreement with the experimental data and the fitted model predicts the measured pressure drop, both to within ± 20%. It provides useful new insights into liquid-liquid Taylor flow in mini / micro scale channels. The new proposed model of pressure drop is valuable for general liquid-liquid Taylor flows in mini scale tubing.

4.6 References

[1] Kim, S. M., and Mudawar, I., 2014, "Review of Databases and Predictive Methods for Heat Transfer in Condensing and Boiling Mini/Micro-Channel Flows," Int. J. Heat Mass Transf., 77, pp. 627–652.

[2] Gupta, R., Fletcher, D. F., and Haynes, B. S., 2010, "Taylor Flow in Microchannels: A Review of Experimental and Computational Work," J. Comput. Multiph. Flows, 2(1), pp. 1–31.

[3] Talimi, V., Muzychka, Y. S., and Kocabiyik, S., 2011, "A Review on Numerical Studies of Slug Flow Hydrodynamics and Heat Transfer in Microtubes and Microchannels," Int. J. Multiph. Flow, 39, pp. 88–104.

[4] Asadi, M., Xie, G., and Sunden, B., 2014, "A Review of Heat Transfer and Pressure Drop Characteristics of Single and Two-Phase Microchannels," Int. J. Heat Mass Transf., 79, pp. 34–53.

[5] Bandara, T., Nguyen, N. T., and Rosengarten, G., 2015, "Slug Flow Heat Transfer without Phase Change in Microchannels: A Review," Chem. Eng. Sci., 126, pp. 283–295.

[6] Mac Giolla Eain, M., Egan, V., Howard, J., Walsh, P., Walsh, E., and Punch, J., 2015, "Review and Extension of Pressure Drop Models Applied to Taylor Flow Regimes," Int. J. Multiph. Flow, 68, pp. 1–9.

[7] Abdollahi, A., Sharma, R. N., and Vatani, A., 2017, "Fluid Flow and Heat Transfer of Liquid-Liquid Two Phase Flow in Microchannels: A Review," Int. Commun. Heat Mass Transf., 84, pp. 66–74.

[8] Yue, J., Luo, L., Gonthier, Y., Chen, G., and Yuan, Q., 2009, "An Experimental Study of Air-Water Taylor Flow and Mass Transfer inside Square Microchannels," Chem. Eng. Sci., 64(16), pp. 3697–3708.

[9] Kreutzer, M. T., Kapteijn, F., Moulijn, J. A., Kleijn, C. R., and Heiszwolf, J. J., 2005, "Inertial and Interfacial Effects on Pressure Drop of Taylor Flow in Capillaries,"

AIChE J., 51(9), pp. 2428–2440.

[10] Sun, L., and Mishima, K., 2009, "Evaluation Analysis of Prediction Methods for Two-Phase Flow Pressure Drop in Mini-Channels," Int. J. Multiph. Flow, 35(1), pp. 47–54.

[11] Salim, A., Fourar, M., Pironon, J., and Sausse, J., 2008, "Oil-Water Two-Phase Flow in Microchannels: FLow Patterns and Pressure Drop Measurements," Can. J. Chem. Eng., 86(6), pp. 978–988.

[12] Asthana, A., Zinovik, I., Weinmueller, C., and Poulikakos, D., 2011, "Significant Nusselt Number Increase in Microchannels with a Segmented Flow of Two Immiscible Liquids: An Experimental Study," Int. J. Heat Mass Transf., 54(7–8), pp. 1456–1464.

[13] Kim, N., Murphy, M. C., Soper, S. A., and Nikitopoulos, D. E., 2014, "Liquid-Liquid Segmented Flows in Polycarbonate Microchannels with Cross-Sectional Expansions," Int. J. Multiph. Flow, 58, pp. 83–96.

[14] Tsaoulidis, D., Dore, V., Angeli, P., Plechkova, N. V., and Seddon, K. R., 2013, "Flow Patterns and Pressure Drop of Ionic Liquid-Water Two-Phase Flows in Microchannels," Int. J. Multiph. Flow, 54, pp. 1–10.

[15] Foroughi, H., and Kawaji, M., 2011, "Viscous Oil-Water Flows in a Microchannel Initially Saturated with Oil: Flow Patterns and Pressure Drop Characteristics," Int. J. Multiph. Flow, 37(9), pp. 1147–1155.

[16] Muzychka, Y. S., Walsh, E., Walsh, P., and Egan, V., 2011, "Non-Boiling Two Phase Flow in Microchannels," Microfluidics and Nanofluidics Handbook: Chemistry, Physics, and Life Science Principles, S.K. Mitra, and S. Chakraborty, eds., CRC Press, Taylor & francis group, Boca Raton, FL.

[17] Kashid, M. N., and Agar, D. W., 2007, "Hydrodynamics of Liquid-Liquid Slug Flow Capillary Microreactor: Flow Regimes, Slug Size and Pressure Drop," Chem. Eng. J., 131(1–3), pp. 1–13.

[18] Aota, A., Mawatari, K., Takahashi, S., Matsumoto, T., Kanda, K., Anraku, R., Hibara, A., Tokeshi, M., and Kitamori, T., 2009, "Phase Separation of Gas-Liquid and Liquid-Liquid Microflows in Microchips," Microchim. Acta, 164(3–4), pp. 249–255.

[19] Jovanović, J., Zhou, W., Rebrov, E. V., Nijhuis, T. A., Hessel, V., and Schouten, J. C., 2011, "Liquid-Liquid Slug Flow: Hydrodynamics and Pressure Drop," Chem. Eng. Sci., 66(1), pp. 42–54.

[20] Gupta, R., Leung, S. S. Y., Manica, R., Fletcher, D. F., and Haynes, B. S., 2013, "Hydrodynamics of Liquid-Liquid Taylor Flow in Microchannels," Chem. Eng. Sci., 92, pp. 180–189.

[21] Li, Q., and Angeli, P., 2017, "Experimental and Numerical Hydrodynamic Studies of Ionic Liquid-Aqueous Plug Flow in Small Channels," Chem. Eng. J., 328, pp. 717–736.

[22] Lockhart, R. W., and Martinelli, R. C., 1949, "Proposed Correlation of Data for Isothermal Two-Phase, Two-Component Flow in Pipes," Chem. Eng. Prog., 45(1), pp. 39–48.

[23] Bretherton, F. P., 1961, "The Motion of Long Bubbles in Tubes," J. Fluid Mech., pp. 166–188.

[24] Warnier, M. J. F., De Croon, M. H. J. M., Rebrov, E. V., and Schouten, J. C., 2010, "Pressure Drop of Gas-Liquid Taylor Flow in Round Micro-Capillaries for Low to Intermediate Reynolds Numbers," Microfluid. Nanofluidics, 8(1), pp. 33–45.

[25] Walsh, E., Muzychka, Y., Walsh, P., Egan, V., and Punch, J., 2009, "Pressure Drop in Two Phase Slug/Bubble Flows in Mini Scale Capillaries," Int. J. Multiph. Flow, 35(10), pp. 879–884.

[26] Awad, M. M., and Muzychka, Y. S., 2008, "Effective Property Models for Homogeneous Two-Phase Flows," Exp. Therm. Fluid Sci., 33(1), pp. 106–113.

[27] Yue, J., Chen, G., and Yuan, Q., 2004, “Pressure Drops of Single and Two-Phase Flows through T-Type Microchannel Mixers,” Chem. Eng. J., 102(1), pp. 11–24.

[28] McAdams, W. H., Woods, W. K., Heroman Jr, L. C., and Heroman L C, J., 1942, “Vaporization inside Horizontal Tubes II-Benzene-Oil Mixtures,” Trans. ASME, 64(3), pp. 193–200.

[29] Berthier, J., and Silberzan, P., 2006, *Microfluidics for Biotechnology*, Artech House, London

[30] Kline, S. J., and McClintock, F. A., 1953, “Describing Uncertainties in Single-Sample Experiments,” Mech. Eng., 75, pp. 3–8.

CHAPTER 5

Heat Transfer in Liquid-Liquid Taylor Flow in Curved Mini-Scale Tubing for Constant Wall Temperature*

5.1 Introduction

In recent years, two-phase flow in a curved flow path has been investigated extensively for lab-on-chip applications and cooling purposes at small scales [1]. Segmented (Taylor) flow is a passive heat transfer enhancement technique that aligns well with several heat transfer applications. Using a curved flow path is also a passive technique to enhance heat transfer in a mini-scale channel. Passive cooling techniques are a promising technique to effectively remove heat from hot spots [2].

Most of the research on two-phase flow at mini-scales for curved channels is for gas–liquid flow, and only a few studies consider liquid–liquid two-phase flow. Large gaps in

* Published in Journal of Electronic Packaging, June 2017, Vol. 139 / 020909-1. It has been chosen to be an outstanding paper at the ASME 2016 International Mechanical Engineering Congress and Exposition (IMECE 2016), Nov. 11-17, 2016, Phoenix, AZ, USA.

the research exist for liquid–liquid slug flow in curved tubing [3]. Donaldson et al. [4] and Kirpalani et al. [5] have predicted and identified flow patterns with secondary flow for gas–liquid two-phase flows in small curved channels, while Yue et al. [1] investigated the flow patterns in a glass microfluidic chip with curved microchannels and 98 μm hydraulic diameter for the two-phase (gas–liquid and liquid–liquid) and three-phase flow (gas–liquid–liquid). They identified the slug flow pattern and flow regime transition boundaries based on the velocity of bubbles or slugs and average volumetric flow rates of the gas and the liquid phases. This regime can be seen as slug flow for three-phase flow and parallel-slug flow for two-phase flow. Pressure drop correlations in two-phase flow are proposed for curved and helically coiled tubes by Yue et al. [1], Vashisth and Nigam [6], Zhao and Guo [7], Guo [8], and Saxena et al. [9]. Other studies on two-phase flow in curved or helically coiled channels such as slug formation and interfacial structure were performed by Murai et al. [10], Kumar et al. [11], Dogan et al. [12], Wang et al. [13], and Vashisth and Nigam [6,14]. There are a few studies on the thermal behavior of liquid–liquid mixture flows on the refrigerant side [15–17].

Two effects responsible for the enhancement of heat transfer rate in gas–liquid slug flow are internal circulations within the slugs, which cause a greater radial heat transfer rate and increased slug velocity due to the gas when compared with the same single-phase mass flow rate. Therefore, the application of liquid–liquid Taylor flow for heat transfer in miniscale tubes is a promising technique for process optimization as both fluid segments have high heat capacities. Theoretical and experimental studies [2,18] of single-phase flow have been performed to investigate the hydrodynamic and thermal behavior of cooling methods in small-scale tubing. The geometry of ducts can significantly affect the behavior

of two-phase flow and subsequently the mass, momentum, and heat transport within the plugs. In this rresearch, the heat transfer in liquid–liquid Taylor flows inside copper tubing for constant wall temperature boundary conditions is examined. Heat transfer rate is determined by a dimensionless approach at different flow rates for different lengths and curvatures in miniscale tubing. A wide range of flow rates of water / 1 cS oil slug flow and water / 3 cS oil slug flow are used as working fluids. The method is based on temperature measurements at the tube inlet, outlet, and surface. The dimensionless mean wall flux, q^*, [19] and Nusselt number, Nu, are used to analyze the experimental data and compare with single-phase flow models. The experimental results reveal the effect of the curvature and the length in curve tubes on the heat transfer rate, as well as the nature of fluid, which have substantially different Prandtl numbers.

5.2 Experimental Setup

Experiments are performed with liquid–liquid Taylor flow in curved mini-scale tubing at isothermal boundary conditions. As illustrated in Fig. (5.1), the measurement facility consists of a test section, pumping device, test fluids, thermocouples, isothermal bath, and data acquisition system. The test section is a series of tubes of different lengths and radius of curvature for mini-scale copper tubing with $D = 1.65\,mm$ and $t = 0.79\,mm$. The system uses two dual syringe pumps (High Precision Harvard Apparatus pumps) to produce liquid-liquid Taylor flow. Each pump is equipped with two glass syringes of 100 *ml* capacity. The liquids are water and low viscosity silicone oils, (1 cSt or 3 cSt). For each experimental run, two syringes are filled with the test fluid and the pumps are set to the desirable flow rate. A T-junction creates liquid-liquid segmented flows. Two Omega T-

type thermocouples at each end of the test section measure the inlet and outlet temperature. A Fisher Scientific Isotemp 3013D digital constant temperature bath provides a symmetric and constant wall temperature with ± 1% temperature stability; hence, an isothermal boundary condition can be created. The high thermal conductivity of copper tube with a thin-wall helps maintain the isothermal condition for the whole tube length. Plastic tubing connects the fluid flow during the experiment, as illustrated in Fig. (5.1). A high-speed camera is used for recording videos of the two-phase segmented flow during each experimental run. This camera allows us to capture the images of the slug train. The function of this camera is more important when we are working with high flow rates.

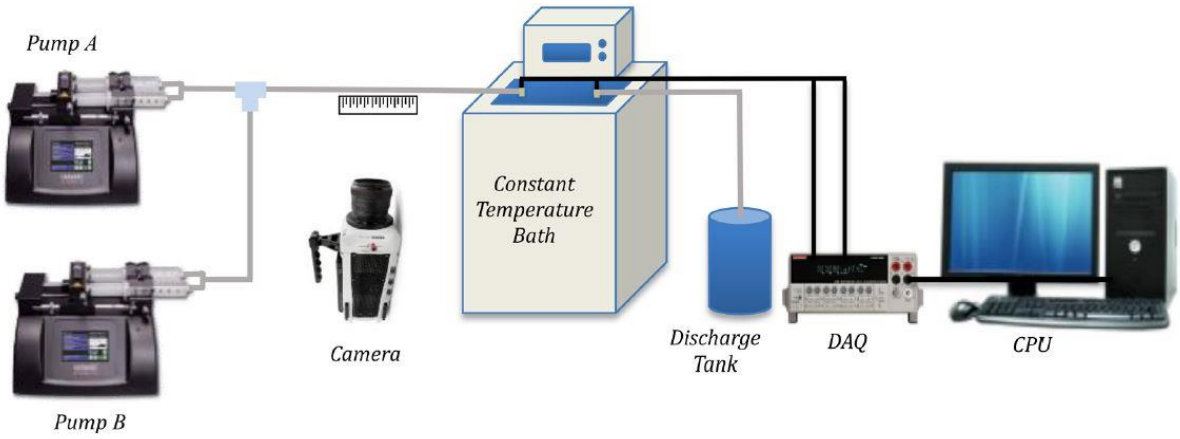

Fig. 5. 1 - System configuration.

The copper tubing is placed inside the thermal bath for isothermal conditions and the isothermal bath is maintained at 40 °C ± 0.1 °C. The curved copper tubes have four different radii (1, 2, 4, and 8 *cm*) and in different lengths as presented in Table (5.1) and Fig. (5.2). During the experiments, thermal stability is achieved in approximately 4 minutes and with

an ambient temperature of approximately 22 °C. For liquid-liquid Taylor flow, two liquids are injected into a T-junction and the syringe pumps adjusted for the required flow rates of liquids to adjust the slug lengths (Fig. 5.3).

The liquids (water / 1 cSt oil or water / 3 cSt oil) are injected into the tubing at the same flow rate from 3 *ml/min* to 30 *ml/min* for each liquid, in which the liquid fraction (α_L) is approximately 0.5. It is assumed the flow is thermally developing and hydrodynamically fully developed. Several readings of the inlet and the outlet temperatures are recorded for each run of flow rate to minimize the error in reading. The uncertainty analysis is carried out at maximum and minimum possible flow rates in the experiment. This yields an uncertainty using the root mean squares method of ± (4.51% - 7.52%) in the dimensionless heat transfer and ± (4.46% - 7.47%) for the dimensionless thermal length.

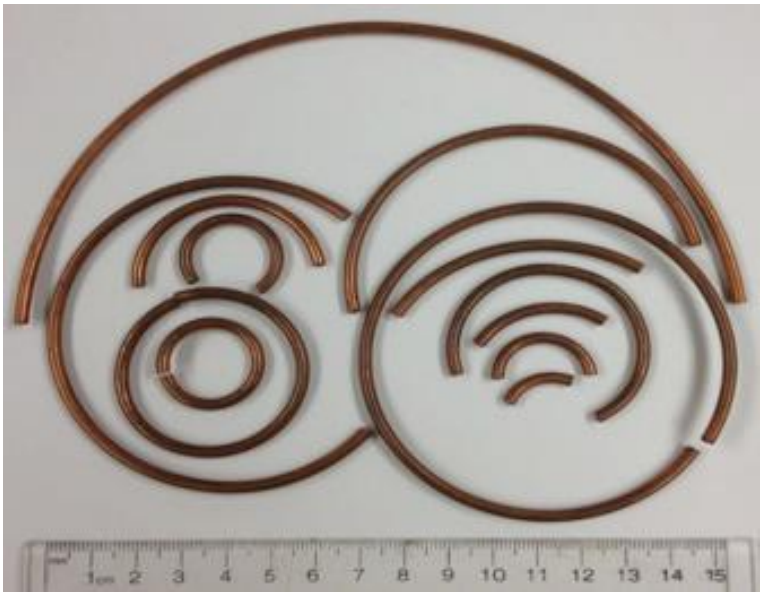

Fig. 5. 2 - Test geometries of different lengths and radii.

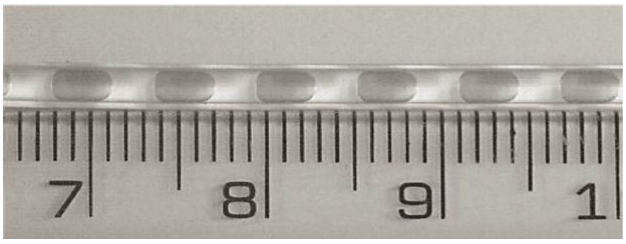

Fig. 5. 3 - Illustration of water / 1 cSt silicone oil of segmented flow for $\alpha_L = 0.5$. The water has been tinted for enhanced visualization of the interface.

Table 5. 1 - Curved tubes lengths (*cm***)**

Radius (cm)	***θ = 90º***	***θ = 180º***	***θ = 270º***	***θ = 360º***
1		3.14	4.71	6.28
2	3.14	6.28	9.42	12.56
4	6.28	12.56	18.84	25.12
8		25.12		

5.3 Analysis of Heat Transfer for Taylor Flow

In this section, the analysis methodology is presented for heat transfer rate of liquid-liquid Taylor flow in a curved mini-channel with constant wall temperature. The energy balance is applied to determine the total convection heat transfer in relation to the difference in temperatures at the tube inlet and outlet. The energy balance equation is used to determine the total heat transfer rate

$$Q = (\dot{m}c_p)_{L_c}\left(T_{o,L_c} - T_{i,L_c}\right) + (\dot{m}c_{p_{L_d}})\left(T_{o,L_d} - T_{i,L_d}\right) \tag{5.1}$$

where the same inlet temperature is maintained for both liquids ($T_{i,L_c} = T_{i,L_d}$) and the outlet temperature of the carrier liquid is measured to be approximately the same as the outlet temperature of the segmenting liquid ($T_{o,L_c} \sim T_{o,L_d}$), which is reasonable due to the thermal

contact between the two liquids, as well as internal circulation in each liquid. Therefore, allows Eq. (5.1) can be simplified in the follow:

$$Q = [(\dot{m}c_p)_{L_c} + (\dot{m}c_p)_{L_d}](\bar{T}_o - T_i) \tag{5.2}$$

The heat transfer per unit area is defined by

$$\bar{q} = \frac{Q}{PL} = \frac{Q}{\pi DL} \tag{5.3}$$

where $PL = \pi\, DL$ is the surface area in the curved tube, and the hydraulic diameter of a standard circular tube is the inner diameter, D.

For a constant temperature wall condition in segmented liquid-liquid flow, the heat transfer rate is defined by the mean Nusselt number,

$$\overline{Nu} = \frac{\bar{h}\, D}{\bar{k}_e} = \frac{\bar{q}\, D}{\bar{k}_e\, \Delta T_{lm}} \tag{5.4}$$

For $\bar{h}$ to be defined for wall to bulk fluid temperature difference, the log mean temperature difference is used.

$$\Delta T_{lm} = \frac{(T_w - T_i) - (T_w - T_o)}{\ln\left(\frac{T_w - T_i}{T_w - T_o}\right)} \tag{5.5}$$

However, for the dimensionless mean wall heat flux approach (rather than a Nusselt number approach) and working with the classical heat transfer rate, the dimensionless mean wall flux is defined by [20]

$$q^* = \frac{\bar{q}\, D}{\bar{k}_e\, (T_w - T_i)} \tag{5.6}$$

and the dimensionless thermal length is

$$L^* = \frac{L/D}{Pe} \tag{5.7}$$

The Peclet number for liquid-liquid flow is defined by

$$Pe = Pr\,Re = \frac{UD}{\bar{k}_e/\overline{\rho c_P}_e} = \frac{UD}{\bar{\alpha}_e} \tag{5.8}$$

The average liquid velocity for Taylor flow is

$$U = \frac{\dot{Q}_{L_c} - \dot{Q}_{L_d}}{A} \tag{5.9}$$

where $A = \pi D^2/4$ is the cross-sectional area of the curved tubing.

The following expressions are used to validate and compare the results for the dimensionless mean wall flux for constant wall temperature. For Graetz-Poiseuille flow in a straight circular tube, Muzychka et al. [20] obtained

$$q^*_{pois} = \left[\left(\frac{1.614}{L^{*1/3}}\right)^{-3/2} + \left(\frac{1}{4L^*}\right)^{-3/2}\right]^{-2/3} \tag{5.10}$$

The experimental results are compared with single-phase flow in curved tube results at same condition to show Taylor flow effect on heat transfer enhancement. The following correlation was proposed for the Nusselt number in the laminar flow through curved tubes [18, 21]:

$$Nu_c = \left[3.66^4 + \left(0.91375\sqrt{De}\,Pr^{-0.1}\right)^4\right]^{1/4} \tag{5.11}$$

where Nu_c is Nusselt number in the curved tubes and the following asymptotes are

determined:

$$Nu_c = \begin{cases} 3.66 & \text{If } De < 10 \\ 0.91375\sqrt{De}\, Pr^{-0.1} & \text{If } De \geq 50 \end{cases} \quad (5.12)$$

The validity of the model is examined with the present experimental results. The Dean number (*De*) accounts for the secondary flow patterns in a curved tube and is defined as

$$De = Re\sqrt{\frac{D}{2R}} \quad (5.13)$$

For multicomponent liquid flow, the thermodynamic properties are calculated by thermal equilibrium between the component liquids which works well with the present results compared with most commonly used formulas in two phase flows [22, 23]. The thermal properties of two liquids in segmented flow using volume averaging are

$$\overline{\rho c_P}_e = \rho_{L_c} c_{p_{L_c}} \alpha_{L_c} + \rho_{L_d} c_{p_{L_d}} (1 - \alpha_{L_c}) \quad (5.14)$$

where $c_{p_{L_c}}$ and $c_{p_{L_d}}$ are specific heat capacities of oil and water, respectively. The oil liquid fraction, α_{L_c}, is defined as

$$\alpha_{L_c} = \frac{\dot{Q}_{L_c}}{\dot{Q}_{L_c} - \dot{Q}_{L_d}} \quad (5.15)$$

where $\dot{Q}_{L_i}$ is the volumetric flow of each phase.

The thermal conductivity is calculated by taking the volume averaged value of the two conductivities in segmented flow

$$\bar{k}_e = k_{L_c}\alpha_{L_c} + k_{L_d}(1 - \alpha_{L_c}) \quad (5.16)$$

The heat transfer formulation provides an effective method to study and provide new insights on liquid-liquid Taylor flow in curved mini-tubes.

5.4 Results and Discussion

In this section, the experimental results are presented based on four different conditions, including (i) the experimental results of liquid-liquid slug flow are compared with a model [21] for single-phase flow, (ii) the effect of tube curvature on the heat transfer augmentation is examined, (iii) the effect of different lengths with the same curvature on heat transfer augmentation is examined, and (iv) the Prandtl number effect on heat transfer enhancement in curved tubing is studied by using different liquids in Taylor flow.

To benchmark and verify the accuracy of the experimental data, tests for single-phase flow in a mini-scale tube are conducted with water and 1 cSt viscosity silicone oil. As illustrated in Fig. (5.4), the new experimental data on heat transfer rate inside straight mini-scale tubes (inner diameter, D=1.65 *mm* and length L=163 *mm*) with a constant wall temperature, for different flow rates, compares very well with Graetz-Poiseuille's theory [20]. The experimental data for all three fluids follows the Graetz model in the thermal developing region and approaches the fully developed limit of $q^* = 1/(4L^*)$, which is the maximum heat transfer that can be achieved when $T_o \to T_w$.

Figure (5.5) shows the heat transfer results for water / 1 cSt silicone oil slug flow inside the curved tubing with a 4 cm radius and a length of 25.12 *cm*. The experimental results are compared with the Ghobadi and Muzychka model [21] for single-phase flow at constant wall temperature in a curved tube with an identical cross section and length. The

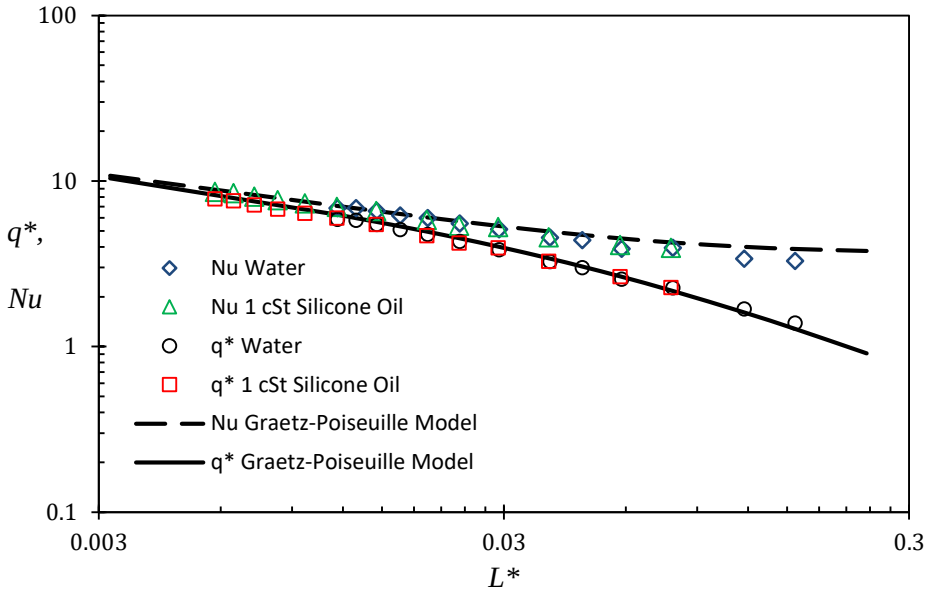

Fig. 5. 4 - Benchmarking results for laminar heat transfer in a straight tube.

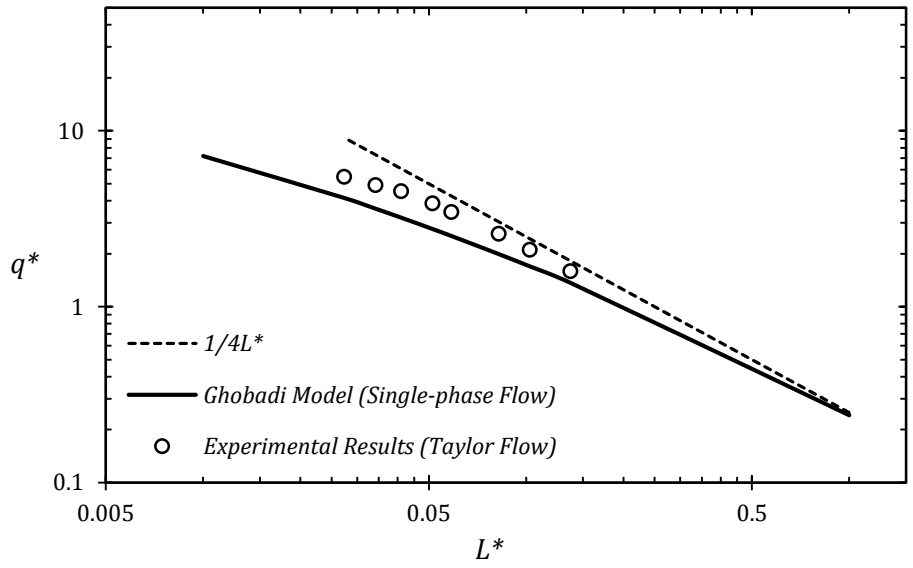

Fig. 5. 5 - Heat Single-phase flow model comparison for the experimental results of water / 1 cS oil Taylor flow at *R*= 4 *cm* and L= 25.12 *cm*.

experimental data are above the single-phase prediction and show heat transfer enhancement compared to single-phase flow. The Prandtl number of water / 1 cSt oil slug flow is $Pr \approx 12.5$ and the constant wall temperature is maintained at 40 ^{o}C. The asymptote of $q^* = 1/4L^*$ shows the maximum heat transfer rate in the limit of $T_o \rightarrow T_w$.

Figure (5.6) illustrates the experimental data for water / 3 cSt silicone oil flowing inside a 4 cm radius of curvature with a 12.56 *cm* length. The Prandtl number is ($Pr \approx 25.2$) and the wall temperature is maintained at 40 ^{o}C. Other comparisons of the experimental results have also shown similar behavior. Thus, one may observe a noticeable heat transfer enhancement by using liquid-liquid Taylor flow in small curved tubing in comparison to single-phase flow.

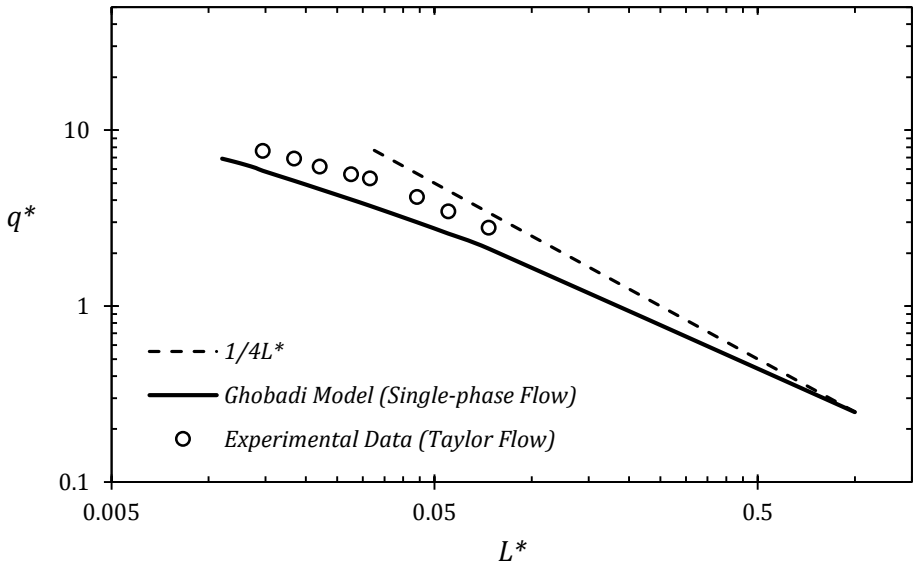

Fig. 5. 6 - Single-phase flow model comparison for the experimental results for water / 3 cS oil Taylor flow at *R*=4 *cm* and *L=12.56 cm.*

Figure (5.7) illustrates the results of water / 1 cSt silicone oil Taylor flow for different curvatures of copper tubing with a constant length of 6.28 *cm*. A smaller radius of curvature (higher curvature) causes an increased heat transfer rate. The dimensionless mean wall flux is highest for a 1 *cm* radius, and is higher in a 2 *cm* radius compared to a 4 *cm* radius. This enhancement is the result of an increase in the secondary flow pattern inside the tubing by increasing the curvature, as well as from the internal circulation caused by Taylor flow.

Data for water / 3 cSt silicone oil Taylor flow in curved tubes having a constant length of 6.28 *cm* is shown in Fig. (5.8). A full circle with a 1 *cm* radius, a half circle with a 2 *cm* radius and a quarter circle a 4 *cm* radius have the same length and a similar trend is also observed in this figure compared to Fig. (5.7). The 1 *cm* radius shows better augmentation than 2 *cm* and 4 *cm* radius.

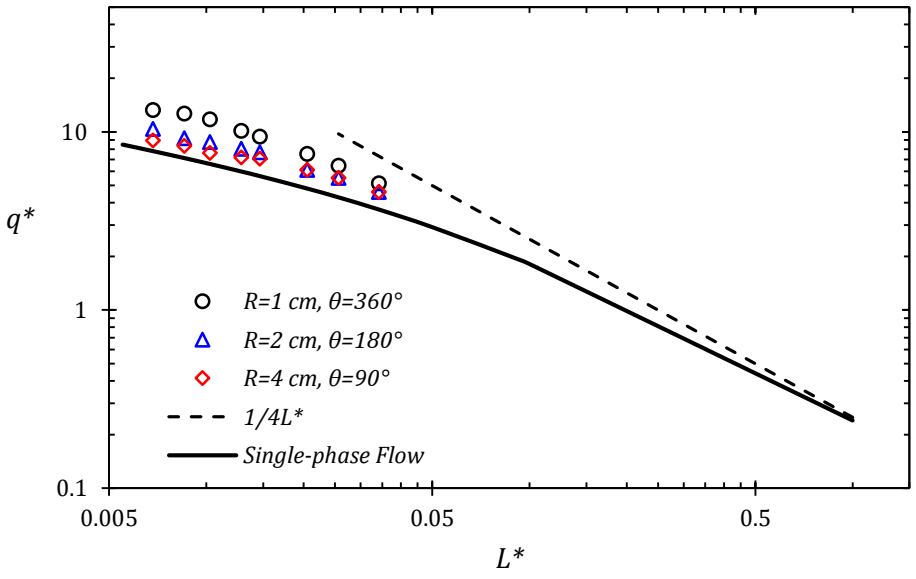

Fig. 5. 7 - Heat transfer enhancement with different radius of curvature for water / 1 cS oil Taylor flow with L=6.28 *cm.*

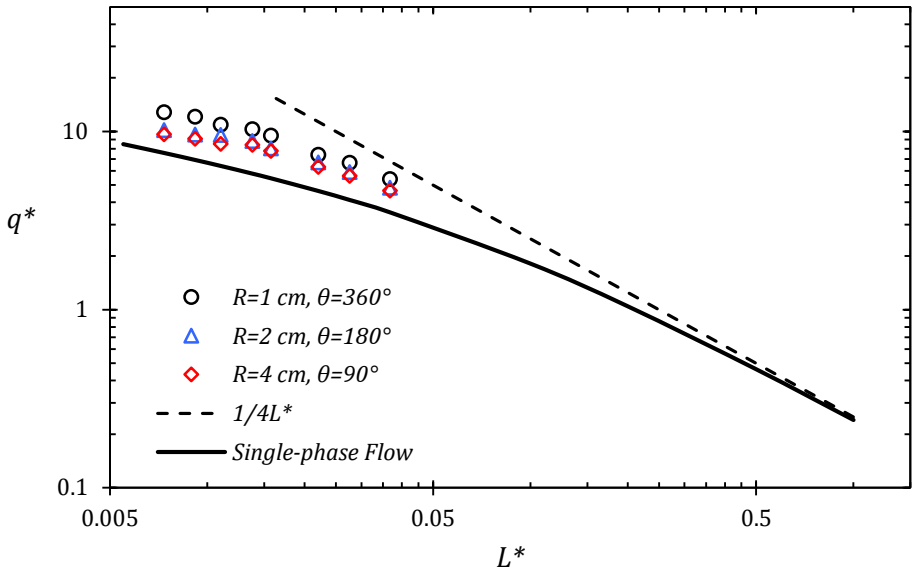

Fig. 5. 8 - Heat transfer enhancement with different radius of curvature for water / 3 cS oil Taylor flow with L=6.28 *cm*.

Figures (5.7) and (5.8) compare experimental heat transfer rate for curved tubes in liquid-liquid Taylor flow to single-phase flow predictions. The figures (5.7) and (5.8) also show that at very low flow rates, all the experimental data approaches the single-phase model [21]. The secondary flow patterns are only effective when the flow velocity is high enough to initiate it.

The effect of the tube length on heat transfer enhancement is investigated with four different tube lengths: a quarter, half, three quarters and full circle (θ = 90^o, 180^o, 270^o and 360^o) with the same radius of curvature. Hence, convection heat transfer is compared in the different lengths for the same curvature. In this part of the investigation, the experimental data is presented in terms of Nusselt number instead of the dimensionless mean wall flux

q^* (X-axis) and the Dean number or Reynolds number instead of the dimensionless length L^* (Y-axis).

Due to the dimensionless L^* being a function of the length in addition to the Reynolds number and Prandtl number, it can not work in order to examine the length effect on heat transfer enhancement. Hence, any observed augmentation for the different lengths at a same curvature in comparison may be due the higher flow rate with a constant Prandtl number, which is the high Reynolds number. From Eq. (5.7) for the Dean number, there is a linear correlation between Reynolds number and Dean number and the range of both dimensionless numbers are the same for all four lengths. This means that the Dean number is proportional to flow rate with the same curvature.

Figures (5.9) and (5.10) show the length effect at a constant curvature for two different conditions of a liquid-liquid slug flow heat transfer rate. Figure (5.9) illustrates the length effect on 4 *cm* radius of curvature tube employing water / 1 cSt silicone oil slug flow as a working fluid and the average Prandtl number is 13.4. Figure (5.10) illustrates the length effect on the 4 *cm* radius of curvature with water / 3 cSt silicone oil slug flow, which has an average Prandtl number of 25.2. The heat transfer rate for the liquid-liquid slug flow in the curved tubes with constant curvature and different lengths identifies the length effects, as well as the secondary flow patterns caused by the curved tubes in addition to internal circulation declared from the liquid-liquid interfaces.

As illustrated in Figs. (5.9) and (5.10), the Nusselt number is higher for liquid-liquid slug flow in the curved tubes with a shorter length. The enhanced heat transfer rate caused by the secondary flow pattern and entrance effect in addition to internal circulation within

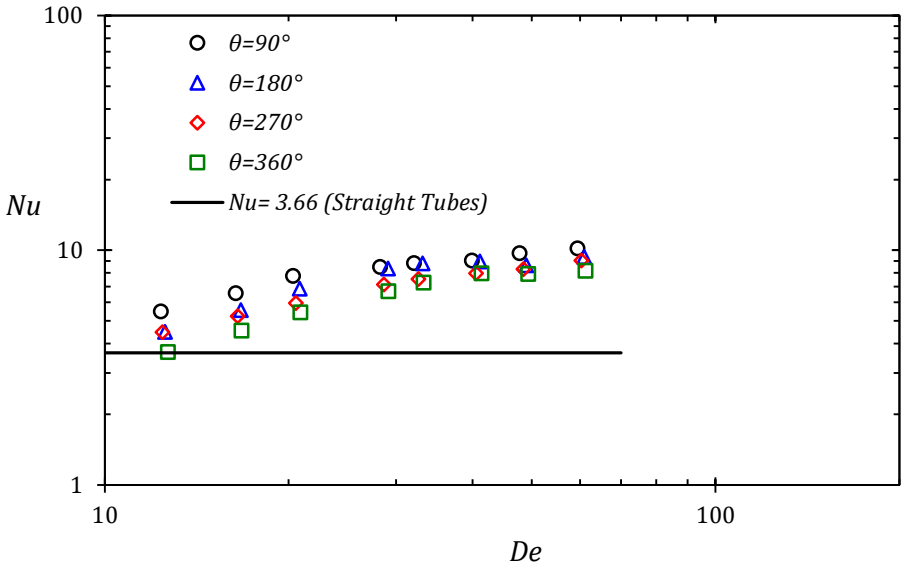

Fig. 5. 9 - Length effect on heat transfer enhancement for water / 1 cSt oil Taylor flow with R= 4 *cm*.

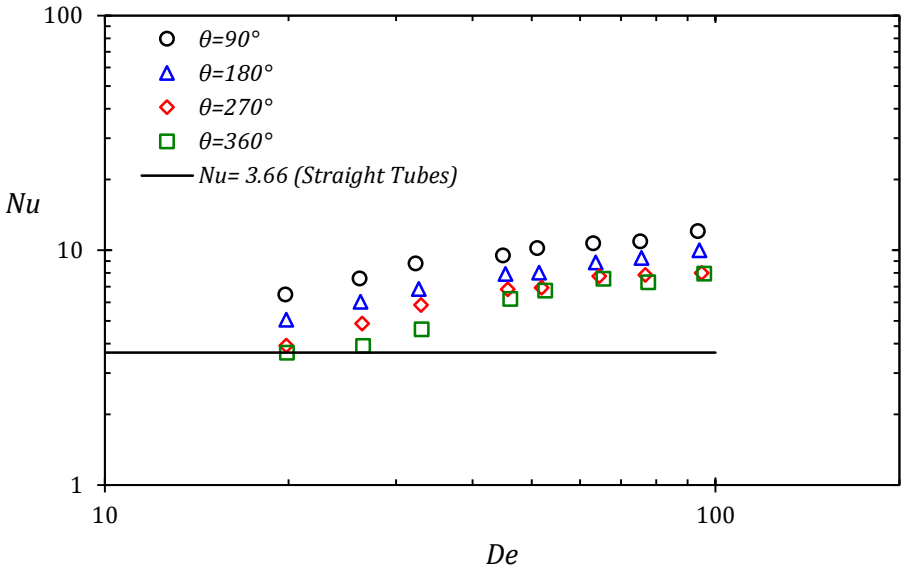

Fig. 5. 10 - Length effect on heat transfer enhancement for water / 3 cSt oil Taylor flow with *R= 4 cm*.

liquid slugs is indicated. The entrance effect dominates the enhancement at shorter lengths and the difference between longer curved tubes and short curved tubes is evident in both figures. Although the data of the longer curved tubes with $\theta = 270^{o}$ and 360^{o} is very close for each other, it demonstrates the decay of the entrance effect and the increase of the secondary flow effect on the total Nusselt number.

To study the effect of Prandtl number on heat transfer enhancement, Figs. (5.11) and (5.12) illustrate the dimensionless mean wall flux versus the dimensionless thermal length of liquid-liquid Taylor flow with different lengths and curvatures. The Taylor flows are water / 1 cSt silicone oil and water / 3 cSt silicone oil. Figure (5.11) illustrates the experimental results for a curved tube with $L = 9.42\ cm$ and $R = 2\ cm$ at a wide range of flow rates of water/1 cSt oil slug flow and water/3 cSt oil slug flow, compared to the Ghobadi and Muzychka model [19] for single phase flow. Significant changes in Prandtl and Reynolds numbers lead to variations in the heat transfer rate.

For curved tubing with 4 *cm* radius and $L = 18.84\ cm$ (Fig. 5.12), the results agree very well with Fig. (5.11). Water / 1 cSt oil slug flow with the average Prandtl number of 13.4 has the highest heat transfer enhancement, and it is follow by water / 3 cSt oil slug flow with the average Prandtl number of 25.2. Obviously, increasing the Prandtl number reduces heat transfer enhancement. Hence, the less viscous the segmenting fluid is in curved tubing, the greater the heat transfer enhancement. However, by increasing the flow rate (decreasing L^{*}), the difference of the heat transfer augmentation becomes more noticeable. The viscosity of fluid strongly affects the secondary flow and the working fluid with the lower viscosity cause an increase in the secondary flows with increasing flow rate, thus raising

heat transfer rates. The results of these experiments show that the highest heat transfer augmentation is achieved for Taylor flow with a low effective Prandtl number.

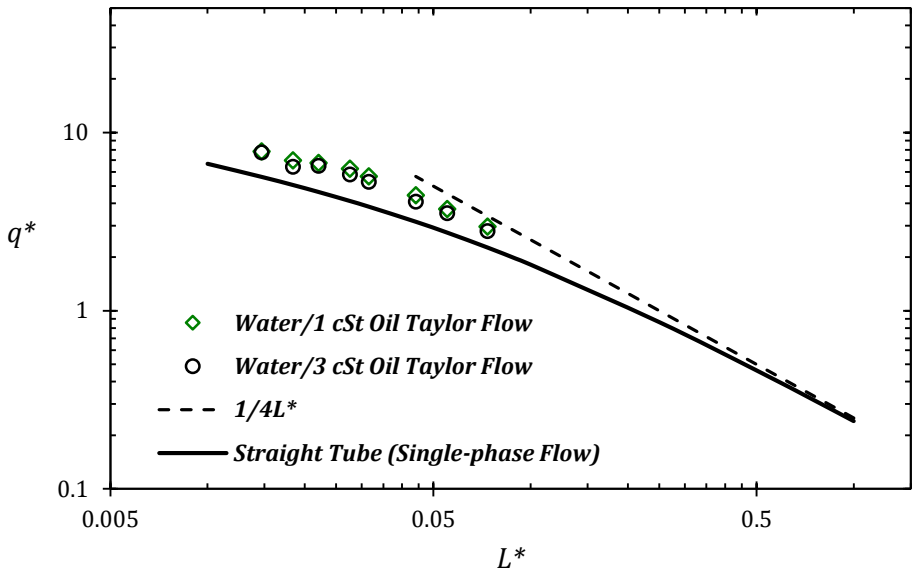

Fig. 5. 11 - Prandtl number effect on the curved tube with *R= 2 cm* and *L= 9.42 cm*.

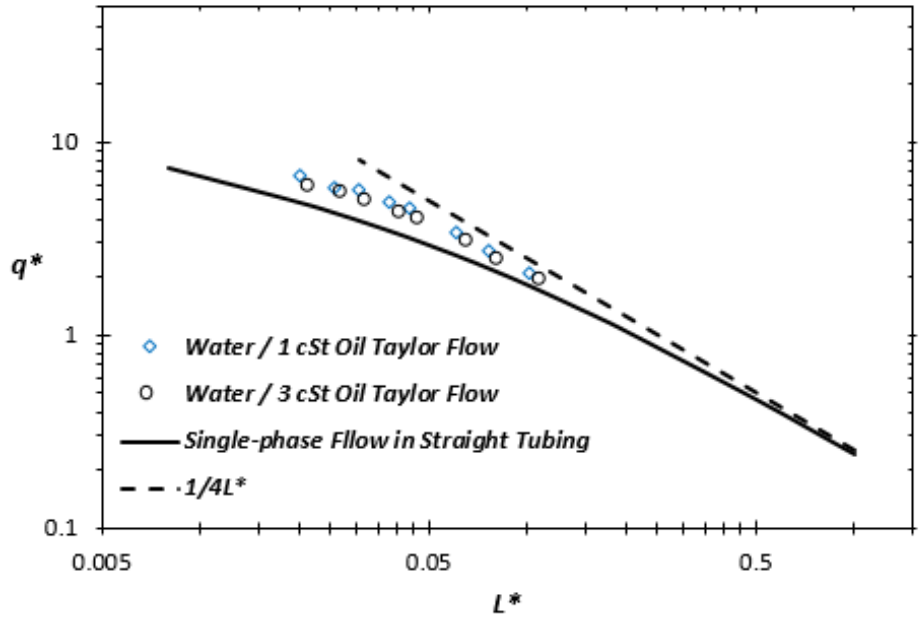

Fig. 5. 12 - Prandtl number effect on the curved tube with *R= 2 cm* and *L= 18.84 cm*.

5.5 Conclusions

This study used experimental methods to study heat transfer rates with liquid-liquid Taylor flow in miniscale curved tubes with a constant wall temperature. Several copper tubes have been used with different radii of curvature and lengths. The effect of the tube curvature on heat transfer enhancement in liquid-liquid Taylor flow was compared with a model for single-phase flow in curved tubing. The results showed that using liquid-liquid Taylor flow in mini scale curved tubes enhances heat transfer rates compared to single-phase flow. Heat transfer with liquid-liquid Taylor flow in curved tubes with a constant length and different curvatures was examined. Also, experimental results for heat transfer in liquid-liquid Taylor flow were produced with constant curvature and different lengths in miniscale curved tubing. Experimental results were also compared with a single-phase model for curved tubing. Water / 1 cSt silicone oil and water / 3 cSt silicone oil slug flow were used in the experiments to examine the effect of Prandtl number on curved tubing heat transfer augmentation. The results highlight the heat transfer enhancement from liquid-liquid Taylor flow inside mini scale curved tubes.

5.6 References

[1] Yue, J., Rebrov, E. V., and Schouten, J. C., 2014, “Gas-liquid–liquid three-phase flow pattern and pressure drop in a microfluidic chip: similarities with gas–liquid / liquid-liquid flows”, The Royal Society of Chem. J., 14, pp.1632-1649.

[2] Ghobadi Mehdi, “Experimental Measurement and Modeling of Heat Transfer in Spiral and Curved Channels”, PhD thesis, Memorial University, St. John’s, NL, Canada, May 2014.

[3] Talimi, V., Muzychka, Y. S., and Kocabiyik, S., 2012, “A Review on Numerical Studies of Slug Flow Hydrodynamics and Heat Transfer in Microtubes and Microchannels", Int. J. of Multiphase Flow, 39, pp. 88-104.

[4] Donaldson, A. A., Kirpalani, D. M., and Macchi A., 2012, “Curvature induced flow pattern transitions in serpentine mini-channels”. Int. J. of Multiphase Flow, 39, pp. 88-104.

[5] Kirpalani, D. M., Patel, T., Mehrani, M., and Macchi A., 2008, “Experimental analysis of the unit cell approach for two-phase flow dynamics in curved flow channels”, Int. J. of Heat and Mass Transfer, 51, pp. 1095-1103.

[6] Vashisth, S., and Nigam, K., 2009, “Prediction of flow profiles and interfacial phenomena for two-phase flow in coiled tubes”, Che. Eng. and Proc., 48, pp. 452-463.

[7] Zhao, L., and Guo, L. J., 2003, “Convective boiling heat transfer and two-phase flow characteristics inside a small horizontal helically coiled tubing once-through steam generator”, Int. J. Heat Mass Transf., 46, pp. 4779–4788.

[8] Guo, L., 2002, "Oil-air-water multiphase flow in helically coiled tube and the theory of sand separation from crude oil (in Chinese)", J. Eng. Thermophys, (China), pp. 107-110.

[9] Saxena, A. K., Nigam, K. D. P., Schumpe, A., and Deckwer, W. D., 1996, "Liquid phase residence time distribution for two phase flow in coiled tubes", The Canadian J. of Chem. Eng., 74 (6), pp. 861-866.

[10] Murai, Y., Yoshikawa S., Toda S., Ishikawa, M., and Yamamoto, F., 2006, "Structure of air-water two-phase flow in helically coiled tubes", Nuclear Eng. and Design, 236, pp. 94-106.

[11] Kumar, V., Vashisth, S., Hoarau, Y., and Nigam, P., 2007, "Slug flow in curved microreactors: Hydrodynamic study", Chem. Eng. Science, 62, pp. 7494-7504.

[12] Dogan, H., Nas, S., and Muradoglu, M., 2008, "Mixing of miscible liquids in gas-segmented serpentine channels", Int. J. of Multiphase Flow, pp. 1149-1158.

[13] Wanga, C., Chenb, I., Linc, Y., and Chang, Y., 2008, "A visual observation of the air-water two-phase flow in small diameter tubes subject to the influence of vertical return bends", Chem. Eng. research and design, 86, pp. 1223-1235.

[14] Vashisth, S., and Nigam, K., 2009, "Liquid-Phase Residence Time Distribution for Two-Phase Flow in Coiled Flow Inverter", Ind. Eng. Ch. Res, 47, pp. 3630-3638.

[15] Nadim, N., and Chandratilleke, T., 2014, "Secondary flow structure and thermal behaviour of immiscible two-phase fluid flow in curved channels", Int. J. of Thermal Sciences, 82, pp. 9-22.

[16] Wongwises, S., Polsongkram, M., 2006, "Condensation heat transfer and pressure drop of HFC-134a in a helically coiled concentric tube-in-tube heat exchanger", Int. J. Heat & Mass Transfer, 49, pp. 4386-4398.

[17] Kang, T. G., Hulsen, M. A., Anderson, P. D., and den Toonder, J., Meijer H., 2007, "Chaotic advection using passive and externally actuated particles in a serpentine flow", Chem. Eng. Sci., 62, pp. 6677-6686.

[18] Ghobadi, M., and Muzychka, Y. S., 2013, "Effect of entrance region and curvature on heat transfer in mini scale curved tubing at constant wall temperature", Int. J. of Heat and Mass Transfer, 65, pp. 357-365.

[19] Muzychka, Y. S., and Ghobadi, M., 2016, “Measurement and Analysis of Laminar Heat Transfer Coefficients in Micro and Mini-Scale Ducts and Channels,” Int. J. Heat Transfer Eng., 37(11), pp. 938–946.

[20] Muzychka, Y. S., Walsh, E., and Walsh, P., 2011, “Heat Transfer Enhancement Using Laminar Gas-Liquid Segmented Plug Flows,” ASME J. Heat Transfer, 133(4), p. 041902.

[21] Ghobadi, M., and Muzychka, Y. S., 2014, “Fully Developed Heat Transfer in Mini Scale Coiled Tubing for Constant Wall Temperature,” Int. J. Heat Mass Transfer, 72, pp. 87–97.

[22] Muzychka, Y. S., Walsh, E., Walsh, P., and Egan, V., 2011, “Non-Boiling Two Phase Flow in Microchannels,” Microfluidics and Nanofluidics Handbook: Chemistry, Physics, and Life Science Principles, S. K. Mitra and S. Chakraborty, eds., CRC Press, Boca Raton, FL.

[23] Awad, M. M., and Muzychka, Y. S., 2008, “Effective Property Models for Homogeneous Two-Phase Flows,” Exp. Therm. Fluid Sci., 33(1), pp. 106–113.

[24] Adrugi, M. W., Muzychka, Y. S., and Pope, K., 2016, “Heat Transfer in Liquid–Liquid Taylor Flow in a Mini-Scale Tube with Constant Wall Temperature,” ASME Paper No. ICNMM2015-48272.

[25] Ghaini, A., Mescher, A., and David, A., 2011, “Hydrodynamics of Liquid–Liquid Slug Flow in Circular Microchannels,” Chem. Eng. Sci., 66(6), pp. 1168–1178.

[26] Eain, M. G., Egan, V., and Punch, J., 2015, “Local Nusselt Number Enhancements in Liquid–Liquid Taylor Flow,” Int. J. Heat Mass Transfer, 80, pp. 85–97.

[27] Flores, A. G., Crowe, K. E., and Griffith, P., 1995, “Gas-Phase Secondary Flow in Horizontal, Stratified and Annular Two-Phase Flow,” Int. J. Multiphase Flow, 21(2), pp. 207–221.

CHAPTER 6

Heat Transfer Model for Liquid-Liquid Taylor Flow in Coiled Mini-Scale Tubing*

6.1 Introduction

Taylor flow (or slug flow) at small-scale tubing has important applications in environmental, industrial and medical applications. These applications include electronics cooling, heat exchange systems and biological micro-fluidics, among others [1-3]. Two-phase Taylor flow systems are among passive techniques of heat transfer enhancement by causing internal circulation within the liquid slugs. These internal circulations improve heat and mass transfer between the tube wall to liquid and interfacial from slug to another [4]. Fluid flow through coiled tubes is also a passive technique for heat transfer enhancement, which causes rotating vortices due to the influence of channel curvatures on flow (secondary flow) [5-7]. The secondary flow appears in curved or coiled channels due to

* Published in ASME 2018 16th International Conference on Nanochannels, Microchannels, and Mini channels, June 10-13, 2018 in Dubrovnik, Croatia.

centrifugal forces on the fluid. The dimensionless Dean number is often used to determine the intensity of the secondary flow. Surface geometry and segmented Taylor flow effectively enhance heat transfer in mini / micro channels [8-12].

This chapter examines heat transfer in liquid-liquid Taylor flow in coiled tubing for a constant wall temperature boundary condition. A survey of the previous literature shows that several experimental and theoretical studies have been conducted on two-phase slug flow in different geometries [13-16]. However, limited data are available for liquid-liquid slug flow in helical coiled channels, especially for heat transfer and hydrodynamic characteristics in small-scale coiled tubing. Most of the researches on thermal behavior of two-phase slug flow at small-scale for coiled or helically coiled channels are for gas-liquid flow. Only a few studies of liquid-liquid slug flow have dealt with mass transfer rate in helical coiled tubular devices [17-18]. Recently, the authors predicted thermal behavior with secondary flow for liquid-liquid Taylor flows in curved mini-channels [19].

Liquid-liquid Taylor flow in mini-scale tubes is a promising technique for heat transfer enhancement as both fluid segments have high heat capacities. The geometry of ducts can significantly affect the behavior of Taylor flow path and subsequently the mass, momentum and heat transport within the plugs. In this investigation, heat transfer enhancement in liquid-liquid Taylor flows inside copper tubing coils for constant wall temperature boundary conditions is examined. Heat transfer rate is determined by a dimensionless approach at different flow rates for different lengths and curvature, which make different number of turns that can enhance heat transfer in mini-scale tubing. The method is based on temperature measurements at the tube inlet and outlet. The dimensionless mean wall

heat flux, q^*, and Nusselt number, *Nu*, are used to analyze the experimental data and compare with theoretical models.

6.2 Experimental Setup

An experimental system was designed to conduct the operation of the liquid-liquid flow in mini-scale tubing for isothermal boundary conditions. As presented in Fig. (6.1), the main components of the experimental setup are a test section (coiled copper tubes with an inner diameter of 1.65 *mm*), two high-precision pumping devices, test fluids, T-junction, thermocouples, isothermal bath, and data acquisition system. The dimensions of the mini-scale copper tubing with different radius of curvature and number of turns in each coil are presented in Table (6.1) Fig. (6.2). Two dual syringe pumps (Harvard pumps) produce liquid-liquid Taylor flow are used in this system. Each pump is equipped with two glass syringes of 100 *ml* capacity. The liquids are water and three low viscosity silicone oils, 1 cSt, 3 cSt and 5 cSt. A T-junction creates liquid-liquid segmented flows. Two thermocouples are attached at both ends of the test section to measure the inlet and outlet temperature. These thermocouples are insulated by Epoxy, which has very high thermal resistance. Thus, the effect of heating current on the thermocouple readings is avoided. An isothermal bath is used, to maintain a uniform constant wall temperature on the copper tube, which has high thermal conductivity. As illustrated in Fig. (6.1), plastic tubing connects the fluid flow during the experiment and a high-speed camera captures the segmented flow images.

The thermal bath is set at 40 °C within ± 0.1 °C uncertainty, and the copper tube is placed inside the bath for isothermal conditions. The ambient temperature is approximately

22 °C. Two liquids are injected into a T-junction to get liquid-liquid Taylor flow, and the syringe pumps control the liquid flow rates to adjust the slug lengths.

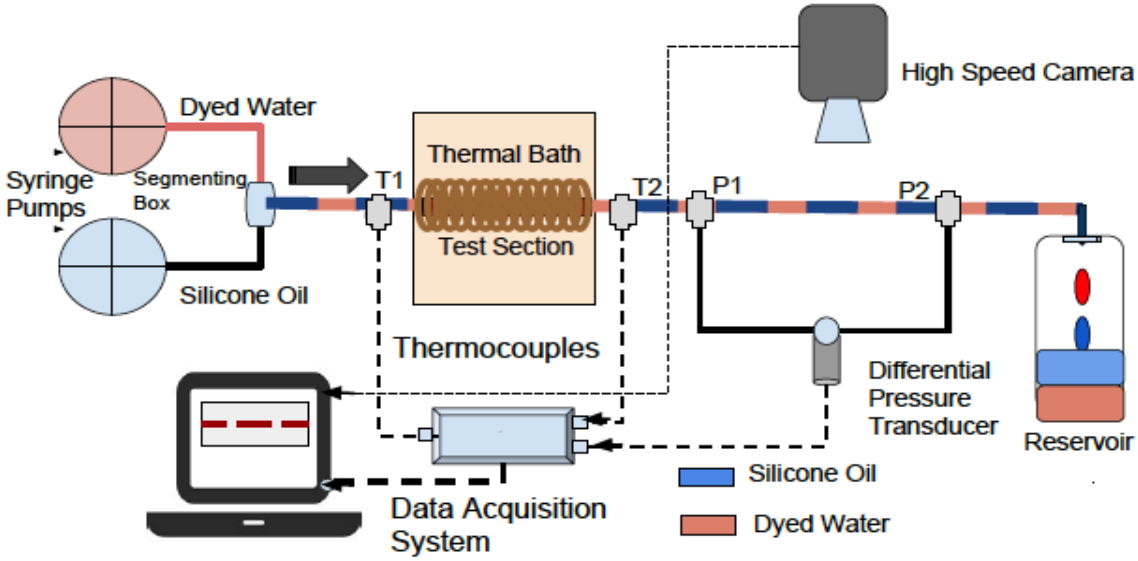

Fig. 6. 1 - Experimental apparatus used in present study.

Fig. 6. 2 - Test geometries of different lengths and radii.

Table 6. 1 - Mini-scale coiled tubes

Coil Radius (*cm*)	1 Turn	2 Turns	3 Turns	4 Turns
1		12.56	18.84	25.12
2	12.56	25.12	37.68	50.24
4	25.12	50.24	75.36	

Fig. 6. 3 - Water / 1 cSt silicone oil slug flow ($\alpha_{L_c} = \alpha_{L_d} = 0.5$) in mini-scale tubing.

The liquids (water / 1 cSt oil, water / 3 cSt oil or water / 5 cSt oil) are injected into the tubing at the same flow rate from 4 *ml/min* to 30 *ml*/*min* for each liquid, in which the liquid fraction (α_{L_c}) was 0.5. Conditions were then allowed to reach steady state before data acquisition began. Each liquid flow rate was then increased by 1 or 2 *ml*/*min* increments and the procedure repeated until the maximum flow rate was reached. It is assumed the flow is thermally developing and hydro-dynamically fully developed. Several readings of the inlet and the outlet temperatures are recorded for each run of flow rate to minimize the

error in reading. The uncertainty analysis is carried out at maximum and minimum possible flow rates in the experiment by using the Kline and McClintock [20] method. This yields an uncertainty using the root mean squares method of ± 4.51 % to 7.52 % in the dimensionless heat transfer (q^* and Nu).

6.3 Formulation of Heat Transfer of Taylor Flow

In this section, the analysis methodology is presented for heat transfer rate of liquid-liquid Taylor flow in a coiled mini -tube with constant wall temperature. The energy balance is applied to determine the total convection heat transfer in relation to the difference in temperatures at the tube inlet and outlet. The energy balance equation is used to determine the total heat transfer rate:

$$Q = (\dot{m}c_p)_{L_c}\left(T_{o,L_c} - T_{i,L_c}\right) + (\dot{m}c_{p_{L_d}})\left(T_{o,L_d} - T_{i,L_d}\right) \tag{6.1}$$

where the same inlet temperature is maintained for both liquids (T_{i,L_c} = T_{i,L_d}) and the outlet temperature of the carrier liquid is measured to be approximately the same as the outlet temperature of the segmenting liquid ($T_{o,L_c} \sim T_{o,L_d}$), which is reasonable due to the thermal contact between the two liquids, as well as internal circulation in each liquid. Therefore, Eq. (6.1) can be simplified in the follow way:

$$Q = [(\dot{m}c_p)_{L_c} + (\dot{m}c_p)_{L_d}](\bar{T}_o - T_i) \tag{6.2}$$

The heat transfer per unit surface area in the coiled tube is defined by:

$$\bar{q} = \frac{Q}{PL} = \frac{Q}{\pi DL} \tag{6.3}$$

where *D*, the diameter of a standard circular tube is the inner diameter.

For a constant temperature wall condition in segmented liquid-liquid flow, the dimensionless heat transfer rate is defined by the mean Nusselt number:

$$\overline{Nu} = \frac{\bar{h}\, D}{\bar{k}_e} = \frac{\bar{q}\, D}{\bar{k}_e\, \Delta T_{lm}} \tag{6.4}$$

For $\bar{h}$ to be defined for wall to bulk fluid temperature difference, the log mean temperature difference is used

$$\Delta T_{lm} = \frac{(T_w - T_i) - (T_w - T_o)}{\ln\left(\frac{T_w - T_i}{T_w - T_o}\right)} \tag{6.5}$$

However, for the dimensionless mean wall heat flux approach (rather than a Nusselt number approach) the dimensionless mean wall flux is defined by [21]:

$$q^* = \frac{\bar{q}\, D}{\bar{k}_e\, (T_w - T_i)} \tag{6.6}$$

and the dimensionless thermal length is:

$$L^* = \frac{L/D}{Pe_D} \tag{6.7}$$

where the Peclet number for liquid-liquid flow is defined by

$$Pe_D = Pr\, Re = \frac{UD}{\bar{k}_e/\overline{\rho c_P}_e} = \frac{UD}{\bar{\alpha}_e} \tag{6.8}$$

The average liquid velocity for Taylor flow is

$$U = \frac{\dot{Q}_{L_c} + \dot{Q}_{L_d}}{A} \tag{6.9}$$

where $A = \pi D^2/4$ is the cross-sectional area of the coiled tubing.

The following expressions are used to compare the results for the dimensionless mean wall flux for a constant wall temperature. For Graetz-Poiseuille flow in a straight circular tube, Muzychka et al. [22] obtained:

$$\overline{Nu}_{pois} = \left[\left(\frac{1.614}{L^{*1/3}}\right)^5 + (3.66)^5\right]^{1/5} \tag{6.10}$$

and

$$q^*_{pois} = \left[\left(\frac{1.614}{L^{*1/3}}\right)^{-3/2} + \left(\frac{1}{4L^*}\right)^{-3/2}\right]^{-2/3} \tag{6.11}$$

To show the secondary flow effect with Taylor flow on heat transfer enhancement, the collected experimental results are compared with the model by Ghobadi and Muzychka [23] for a single-phase flow in mini-scale coiled tubing. The following correlation was proposed based on their experimental results for the Nusselt number in the fully developed laminar and theoretical asymptote:

$$Nu_c = \left[3.66^4 + \left(0.91375\sqrt{De}\,Pr^{-0.1}\right)^4\right]^{1/4} \tag{6.12}$$

The validity of the model was examined with experimental results and in the range of *De* < 700. The Dean number (*De*) accounts for the secondary flow patterns in a curved or coiled tube and is defined as:

$$De = Re\sqrt{\frac{D}{2R}} \tag{6.13}$$

where the Dean number is related to the Reynolds number and radius of curvature, R.

For multicomponent liquid flow, the thermodynamic properties are calculated by thermal equilibrium between the component liquids, which works well with the present results compared with most commonly used formulas in two phase flows [24, 25]. The thermal properties of two liquids in segmented flow using volume averaging are:

$$\overline{\rho c_p}_e = \rho_{L_c} c_{p_{L_c}} \alpha_{L_c} + \rho_{L_d} c_{p_{L_d}} (1 - \alpha_{L_c}) \tag{6.14}$$

where $c_{p_{L_c}}$ and $c_{p_{L_d}}$ are the specific heat capacities of oil and water, respectively. The oil liquid fraction, α_{L_c}, is defined as

$$\alpha_{L_c} = \frac{\dot{Q}_{L_c}}{\dot{Q}_{L_c} + \dot{Q}_{L_d}} \tag{6.15}$$

where $\dot{Q}_{L_i}$ is the volumetric flow of each phase.

The effective thermal conductivity is calculated by Cicchitti model of the two conductivities in segmented flow based slug flow based on the structure of the slug flow inside mini circle tubes [24], which was a reasonable agreement with our experimental data, defined as:

$$\bar{k}_e = k_{L_c} \alpha_{L_c} + k_{L_d} (1 - \alpha_{L_c}) \tag{6.16}$$

The Prandtl number based on the two-phase flow model can be expressed as:

$$Pr = \frac{\bar{\mu}_e \bar{c_p}_e}{\bar{k}_e} \tag{6.17}$$

The Prandtl number depends on the fluid properties, which, heat capacity, viscosity and conductivity, changes mostly with the viscosity change, as the other two parameters are almost the same for different silicone oils. As properties are a function of temperature, the correlations given by the provider were used to calculate the effective properties in each experiment and the average of the entrance and the exit temperature were used.

The heat transfer formulation provides an effective method to study and provide new insights on liquid-liquid Taylor flow in coiled mini/micro channels.

6.4 Results and Discussion

This section presents new experimental data for three different liquid-liquid Taylor flows in mini-scale coiled tubes. As stated before, water and three different silicone oils were used to create two-phase Taylor flow with wide range of flow rates in the experiments. This means a broad range of the different dimensionless numbers (Pr, Re, De, and L^*) were obtained in the experiments. The experimental data is presented using the dimensionless variables. The Y-axis is the dimensionless Nusselt number, *Nu*, which represents the convection heat transfer between the fluid and the tube wall. The X-axis shows the dimensionless Dean number, Reynolds number, or the dimensionless thermal length. This means that the dimensionless variables on the x-axis are proportional to flow rate with different conditions in the experiments. All plots are in Log–Log base.

The experimental results are presented based on four different conditions, in addition to the experimental results of the benchmarking test for a single-phase flow in a mini-scale

tube are used as a reference point to the new two-phase Taylor flow data. First, the experimental results of liquid-liquid slug flow are compared with a single-phase flow in mini scale coiled tubing. Second the effect of tube curvature on the heat transfer augmentation is examined. Third, the effect of curvature and length change with the different turns of coil on heat transfer augmentation is examined. Finally, the Prandtl number effect on heat transfer enhancement in mini scale coiled tubing is studied by using different liquids in Taylor flow.

To benchmark and verify the accuracy of the experimental data, tests for single-phase flow in a mini-scale tube are conducted with water and 1 cSt low viscosity silicone oils. As illustrated in Fig. (6.4), the new experimental data on heat transfer rate inside straight mini-scale tubes (inner diameter, D = 1.65 *mm* and length L = 163 *mm*) with a constant wall temperature, for different flow rates, compares very well with Graetz-Poiseuille's theory

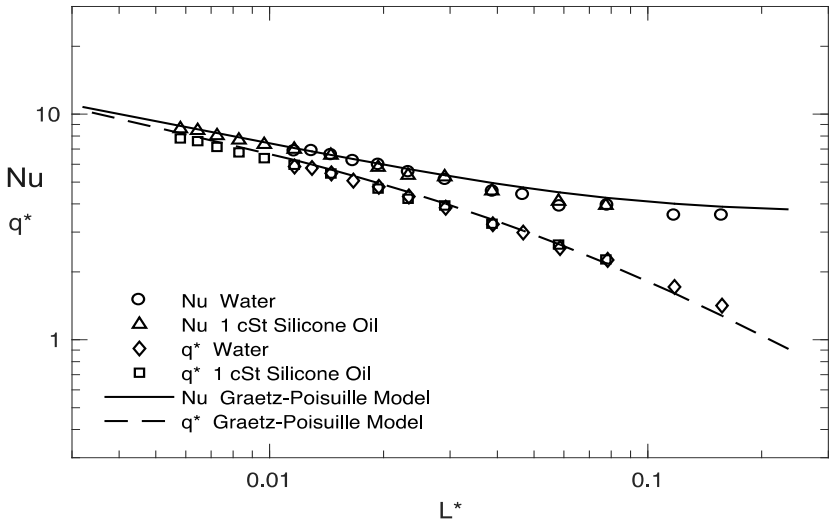

Fig. 6. 4 - Benchmarking results for a straight tube.

[22]. The experimental data for all four liquids follows the Graetz models in the thermal developing region with less than 10 % error.

Figure (6.5) illustrates the experimental data for water / 1 cSt silicone oil flowing inside a different curvatures of copper tubing with a constant length of 50.24 *cm*. The experimental results are compared with the Ghobadi and Muzychka [23] model for single-phase flow in a coiled tube at constant wall temperature. The Nusselt number for the fully developed flow inside a straight tube, Nu = 3.66, is also plotted to show the heat transfer enhancement of different curvatures. The experimental data are above the Ghobadi and Muzychka [23] model prediction and show heat transfer enhancement compared to single-phase flow. The Prandtl number of water / 1 cSt oil slug flow is ($Pr \approx 12.5$) and the constant wall temperature is maintained at 40 ^{o}C.

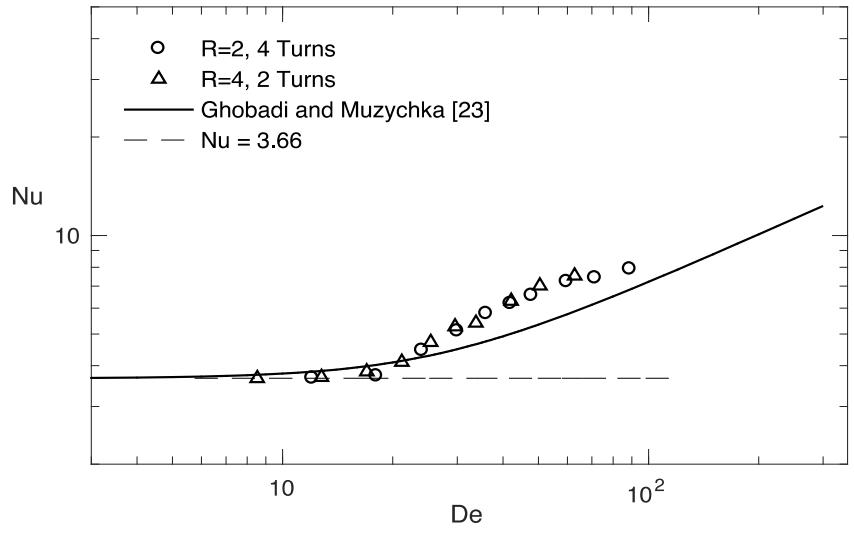

Fig. 6. 5 - Single-phase flow model comparison for the experimental results for water / 1cSt oil Taylor flow at L = 50.24 *cm.*

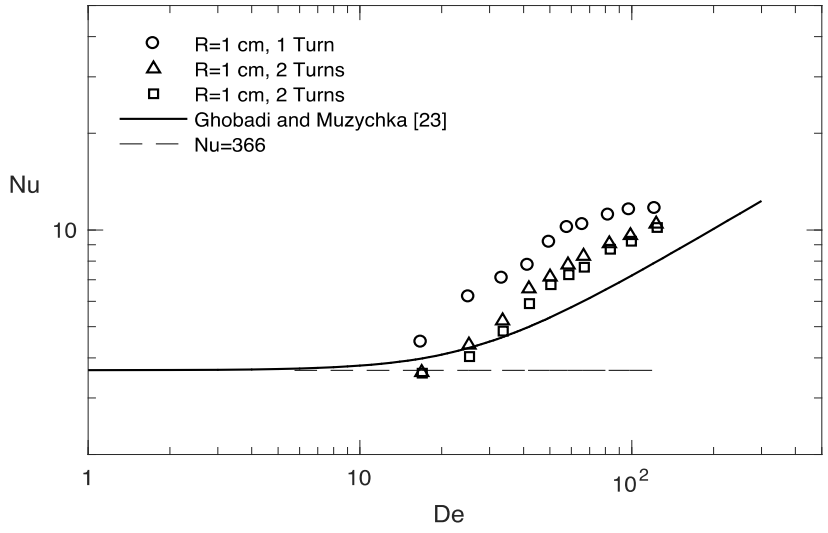

Fig. 6. 6 - Single-phase flow model comparison for the experimental results for water / 5cSt oil Taylor flow at $R = 1\ cm$.

Figure (6.6) shows the heat transfer results for water / 5 cSt silicone oil slug flow inside the coiled tubing with varying lengths and the same radius of curvature (R = 1 *cm*), thus different coil turns. The Prandtl number is ($Pr \approx 38.9$) and the wall temperature is maintained at 40 ^{o}C. Other comparisons of the experimental results have also shown similar behavior. Thus, one may observe a noticeable heat transfer enhancement by using liquid-liquid Taylor flow in small coiled tubing in comparison to single-phase flow.

Figures (6.5) and (6.6) also show that at very low flow rates, the experimental data approaches the single-phase model $Nu = 3.66$. The secondary flow patterns are only effective when the flow velocity and / or curvature is high enough to initiate it.

Based on the collected results, a simple empirical model for predicting the Nusselt number in coiled tubes with small scale is developed for liquid-liquid Taylor flow.

Employing an empirical approach, and based on the results for large curvature region, the following correlation is obtained:

$$Nu_c = 0.75\sqrt{De}\,Pr^{0.1} \tag{6.20}$$

where $Nu_c = 3.66$ for the fully developed Nusselt number in constant wall temperature boundary condition and small curvature region $De < 10$. Consequently, using the asymptotic correlation method, the proposed model takes the form:

$$Nu_c = \left[3.66^{15} + \left(0.75\sqrt{De}\,Pr^{0.1}\right)^{15}\right]^{1/15} \tag{6.21}$$

The above model is valid for various *Pr*, which is typical for most low Reynolds number flow in mini scale tubing based on the present experimental results.

Now in terms of the changing the curvature of copper tubes with a constant length, the experimental results are presented to show the effect of curvature in coiled tubing on the heat transfer augmentation and are compared with the proposed correlation. The experimental data is presented in terms of Nusselt number (Y-axis) and the Dean number or the Reynolds number (X-axis).

Figures (6.7) and (6.8) illustrate the results of water / 1 cSt silicone oil Taylor flow for different curvatures of copper tubing (1 *cm*, 2 *cm*, and 4 *cm*) with a constant length of 25.12 *cm* thus different number of turns in each coil. A smaller radius of curvature causes an increased heat transfer rate. The heat transfer performance for all three radii of curvature is enhanced in comparison to the heat transfer rate in straight tubing; however,

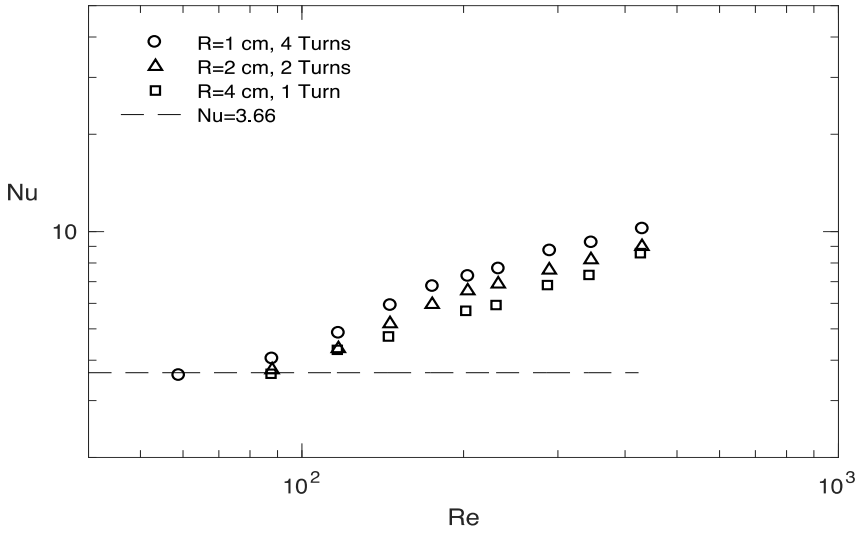

Fig. 6. 7 - Heat transfer enhancement with different radius of curvature for water / 1 cSt oil Taylor flow with L = 25.12 *cm.*

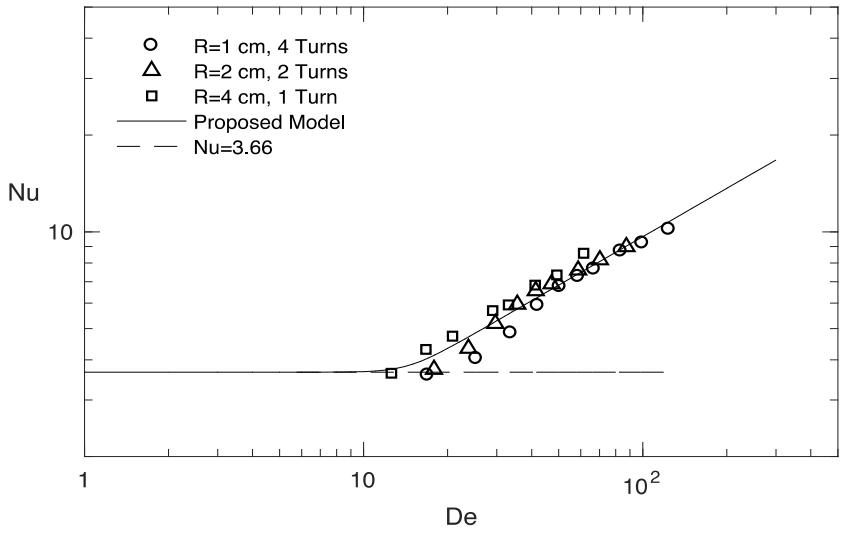

Fig. 6. 8 - Proposed model comparison for the experimental results for water / 1 cSt oil Taylor flow with L = 25.12 *cm.*

the dimensionless a 2 *cm* Nusselt number is highest for a 1 *cm* radius (a greater number of turns) and is higher in radius compared to a 4 *cm* radius (less turns). These enhancements are the result of an increase in the secondary flow pattern inside the tubing by increasing the curvature 1/*R*, as well as from the internal circulation and boundary layer renewal within liquid slugs caused by Taylor flow. All the experimental results of the predicted Nusselt number are in good agreement with the proposed model.

For experimental data of water / 3 cSt silicone oil Taylor flow in coiled tubes having a same length of 25.12 *cm* and various radii of curvature with a 1 *cm*, 2 *cm*, and 4 *cm* is shown in Figs. (6.9) and (6.10). These data have a similar trend is also observed in this figure compared to Figs. (6.7) and (6.8) with same boundary condition (T_w = 40 ^{o}C) and different Prandtl number (Pr $\approx$ 25.2). The 4 turns of coils (R = 1 *cm*) shows better augmentation than the 1 turn (R = 2 *cm*) and 2 turns (R = 4 *cm*). This enhancement occurs as a result of internal circulation and secondary flow within liquid slugs. The intensity of these circulations and secondary flow is a function of different parameters, including radii of curvature. Other comparisons of the experimental results in coiled tubing with different radii of curvature. Thus, various turns of the coil to make the equal lengths have also shown similar behavior with different Taylor flow (change the Prandtl number). Therefore, one may observe a noticeable heat transfer enhancement by using liquid-liquid Taylor flow in small coiled tubing in comparison to single-phase flow. Figures (6.8) and (6.10) also show that at different flow rates, all the experimental data approaches the proposed model prediction.

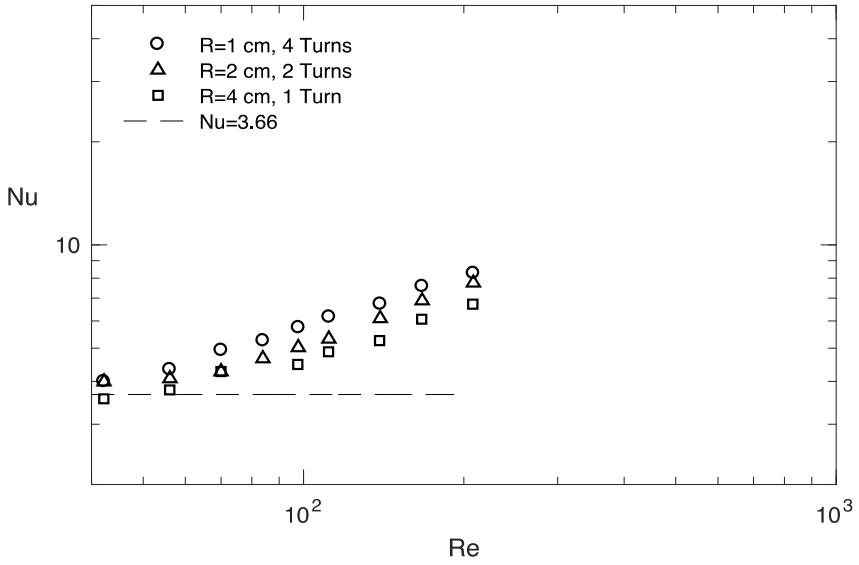

Fig. 6. 10 - Heat transfer enhancement with different radius of curvature for water /3 cSt oil Taylor flow with L = 25.12 *cm*.

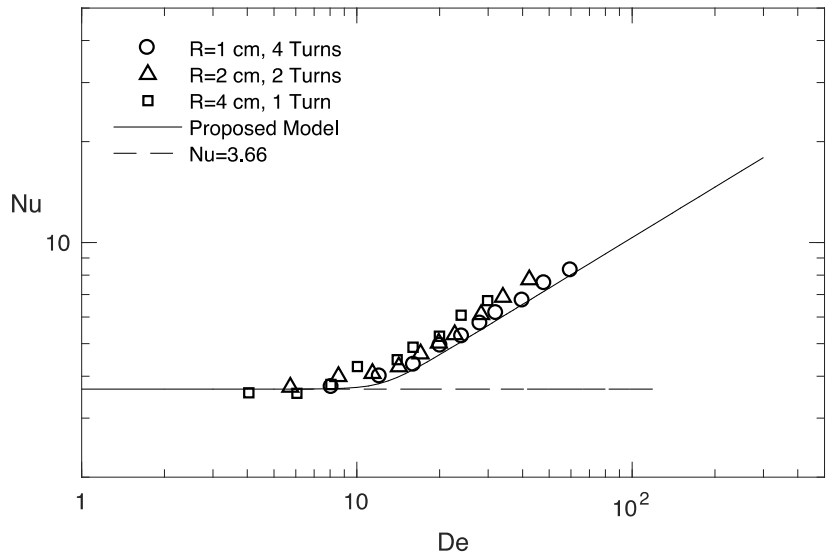

Fig. 6. 9 - Proposed model comparison for the experimental results for water / 3 cSt oil Taylor flow with L = 25.12 *cm*.

As the third discussion for the experimental results is the effect of tube length on the augmentation using different lengths with the same curvature, which make a different number of turns. Hence, any observed for the different lengths at a same curvature in comparison may be due the higher flow rate with a constant Prandtl number, which is the high Reynolds number. Figures (6.11) and (6.12) show the length effect at a constant curvature for two different conditions of a liquid-liquid slug flow heat transfer rate. Hence, convection heat transfer is compared in the different lengths for the same curvature in coiled tubing and with the proposal model.

Figure (6.11) depicts the effect of the tube length on heat transfer enhancement is investigated with four different tube lengths (12.56 *cm*, 25.12 *cm*, 37.68 *cm* and 50.24 *cm*) with a 2 *cm* radius of curvature tube. These coiled mini scale tubing are employing water/1 cSt silicone oil slug flow as a working fluid and the average Prandtl number is 13.4. Figure (6.12) illustrates the length effect on the 1 cm radius of curvature with water/3 cSt silicone oil slug flow, which has an average Prandtl number of 25.2. The heat transfer rate for the liquid-liquid slug flow in the coiled tubes with constant curvature and different lengths (12.56 *cm*, 18.84 *cm*, and 25.12 *cm*) identifies the length effects, as well as the secondary flow patterns caused by the coiled tubes in addition to internal circulation declared from the liquid-liquid interfaces.

As illustrated in Figs. (6.11) and (6.12), the Nusselt number is higher for liquid-liquid slug flow in the coiled tubes with a shorter length (L = 12.56 *cm*). The enhanced heat transfer rate caused by the entrance effect in addition to internal circulation within liquid slugs is indicated. The entrance effect dominates the enhancement at shorter lengths and

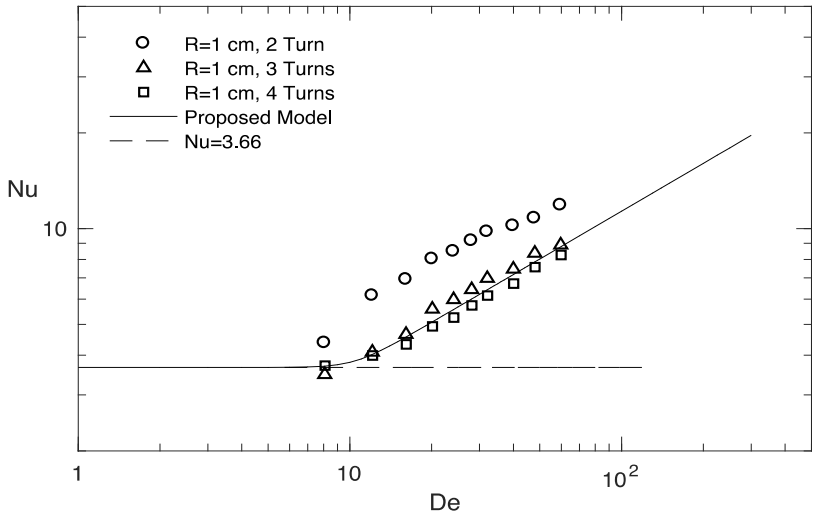

Fig. 6. 12 - Length effect on heat transfer enhancement for water / 3 cSt oil Taylor flow with $R = 1\ cm$.

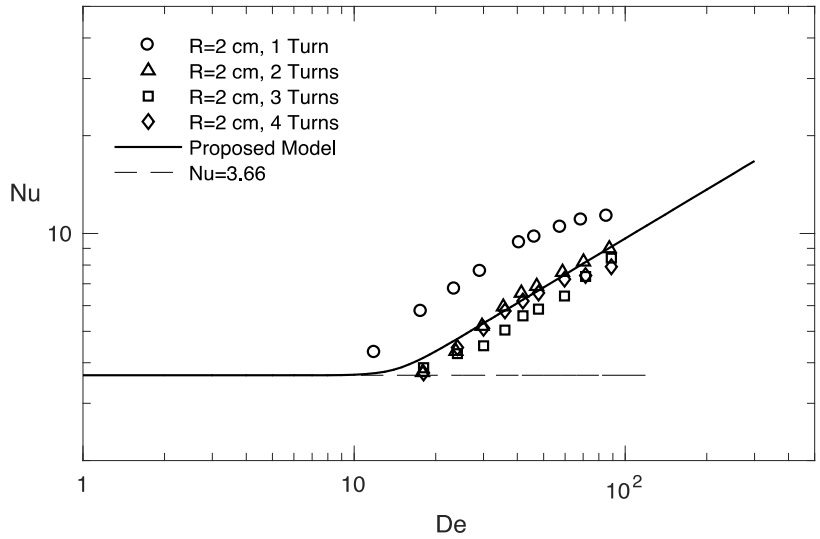

Fig. 6. 11 - Length effect on heat transfer enhancement for water / 1 cSt oil Taylor flow with $R = 2\ cm$.

the difference between longer curved tubes and short curved tubes is evident Ghobadi and Muzychka [22]. Although the data of the longer coiled tubes with (L = 18.84 *cm*, and 25.12 *cm*) and (L = 25.12 *cm*, 37.68 *cm* and 50.24 *cm*) is very close for each other, which demonstrate the decay of the entrance effect and the increase of the secondary flow effect on the total Nusselt number.

Another important issue in this investigation is in the effect of changing Prandtl number on the augmentation. The experimental results of the effect of liquid viscosity on heat transfer enhancement in two-phase liquid-liquid slug flow in mini scale coiled tubing are studied. Figs. (6.13) and (6.14) illustrate the dimensionless Nusselt number versus the dimensionless length instead of the Dean number or Reynolds number for liquid-liquid Taylor flow with different lengths and number of turns in a coil. The Taylor flows are water / 1 cSt silicone oil, water / 3 cSt silicone oil and water / 5 cSt silicone oil. Figure 6.13 illustrates the experimental results for a coiled tube with L =18.84 *cm* and R = 1 *cm* (3 Turns) at a wide range of flow rates of water / 1 cSt oil slug flow, water / 3 cSt silicone oil slug flow and water / 5 cSt oil slug flow. Significant changes in Prandtl and flow rates of liquids lead to variations in the heat transfer rate.

For coiled tubing with 1 *cm* radius and $L = 25.12$ *cm* (4 Turns) in Fig. (6.14), the results agree very well with Fig. (6.13). Water / 1 cSt oil slug flow with the average Prandtl number of 12.5 has the highest heat transfer enhancement, and it is following by water / 3 cSt oil slug flow with the average Prandtl number of 25.2 and then water / 5 cSt oil slug flow with the average Prandtl number of 38.9.

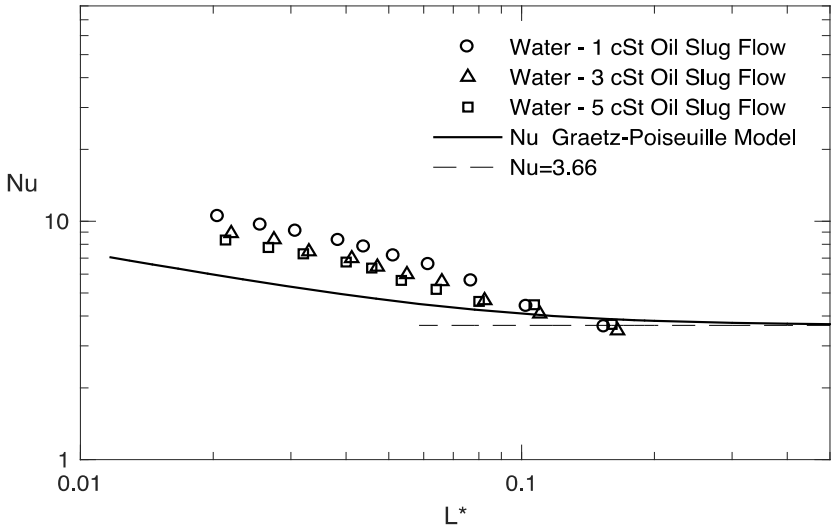

Fig. 6. 13 - Viscosity effect on the mini scale coiled tube with R = 1 *cm* and L = 18.84 *cm*.

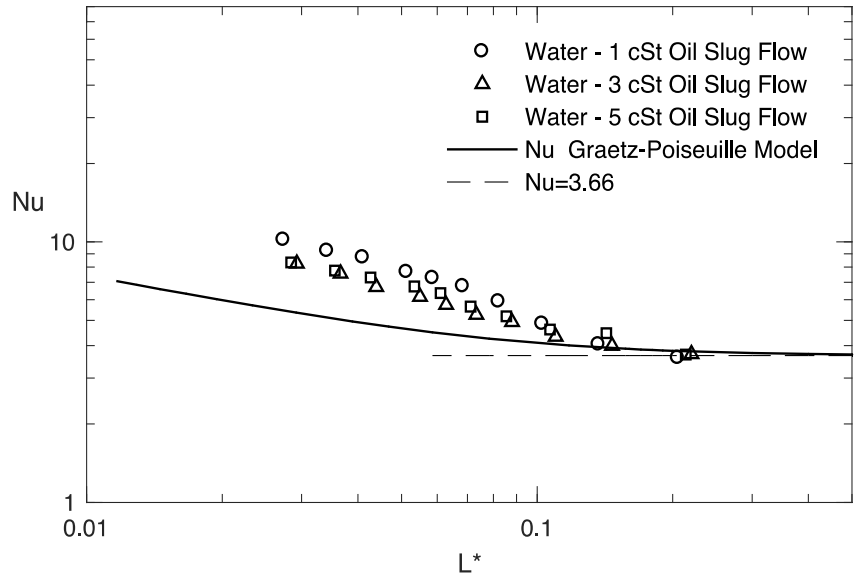

Fig. 6. 14 - Viscosity effect on the mini scale coiled tube with R = 1 *cm* and L = 25.12 *cm*.

Obviously, increasing the Prandtl number reduces heat transfer enhancement. Hence, the less viscous the segmenting fluid is in coiled tubing, the greater the heat transfer enhancement. However, by increasing the flow rate (decreasing L^*), the difference of the heat transfer augmentation becomes more noticeable. The viscosity of fluid strongly affects the secondary flow and the working fluid with the lower viscosity cause an increase in the secondary flows with increasing flow rate, thus raising heat transfer rates. The results show that the highest thermal performance augmentation is achieved with a lower effective viscosity of Taylor flow.

6.5 Conclusions

The experimental study on heat transfer enhancement using non-boiling liquid-liquid segmented (Taylor) flow in coiled mini scale tubing was conducted. An experimental setup was assembled using mini scale copper tubes in which liquid-liquid Taylor flow is heated under a constant wall temperature condition. Coiled copper tubing with different radii of curvature and lengths were used as test sections. Laminar heat transfer of liquid-liquid Taylor flow in coiled tubes with a constant length and different curvatures was examined. Also, experimental results for heat transfer in liquid-liquid Taylor flow were produced with constant curvature and different lengths in coiled tubing. To examine the effect of Prandtl number on heat transfer rates in coiled tubing, three low viscosity silicone oils (1 cSt, 3 cSt, 5 cSt) segmented by water were used to obtain the segmented slug flow. The experiments were performed with liquid fraction maintained constant at 0.5 and Reynolds numbers from 20 to 440. Additionally, benchmark tests were conducted of single-phase flow in a straight tube. The experimental results are compared with models for liquid-liquid Taylor flow in

straight and coiled tubing. The effect of the tube curvature on heat transfer enhancement in liquid-liquid Taylor flow was compared with a model for single-phase flow in coiled tubing.

The new results showed that using liquid-liquid Taylor flow in coiled mini scale tubes enhances heat transfer rates compared to single-phase flow. This enhancement occurs due to internal circulation, secondary flow, and boundary layer renewal within liquid slugs. The experimental model was developed to describe the heat transfer of Taylor flows in mini scale coiled tubing based on a *De* number and *Pr* number. The present model is in good agreement with the experimental data and the fitted model predicts the measured heat transfer within ± 15% for thermally fully developed flow. The new model and experimental data provide useful new insights into liquid-liquid Taylor flows in curved and coiled channels with small scale.

6.6 References

[1] Yue J., Rebrov E. V., and Schouten J. C., 2014, "Gas-liquid–liquid three-phase flow pattern and pressure drop in a microfluidic chip: similarities with gas–liquid / liquid-liquid flows", The Royal Society of Chemistry Journal, 14, pp.1632-1649.

[2] Murai Y., Yoshikawa S., Toda S., Ishikawa M., and Yamamoto F., 2006, "Structure of air–water two-phase flow in helically coiled tubes", Nuclear Engineering and Design 236, pp. 94-106.

[3] Donaldson A. A., Kirpalani D. M. and Macchi A., 2012, "Curvature induced flow pattern transitions in serpentine mini-channels". Int. J. of Multiphase Flow, 39, pp. 88-104.

[4] Talimi V., Muzychka Y. S., Kocabiyik S., 2012, "A review on numerical studies of slug flow hydrodynamics and heat transfer in Microtubes and microchannels", Int. Journal of Multiphase Flow, 39, pp. 88-104.

[5] Ghobadi M., Muzychka Y. S., 2013, "Effect of entrance region and curvature on heat transfer in mini scale curved tubing at constant wall temperature", Int. J. of Heat and Mass Transfer, 65, pp. 357–365.

[6] Kirpalani D. M., Patel T., Mehrani M., Macchi A., 2008, "Experimental analysis of the unit cell approach for two-phase flow dynamics in curved flow channels", Int. Journal of Heat and Mass Transfer, 51, pp. 1095–1103.

[7] Jayakumar J.S., Mahajani S.M., Mandal J.C., Iyer K. N., Vijayan P.K., 2010, "CFD analysis of single-phase flows inside helically coiled tubes", Computers and Chemical Engineering, 65, pp. 357–365.

[8] Vashisth S., Nigam K., 2009, "Prediction of flow profiles and interfacial phenomena for two-phase flow in coiled tubes", Che. Eng. and Proc., 48, pp. 452-463.

[9] Adrugi, M. W., Muzychka, Y. S., and Pope, K., 2016, "Heat transfer in liquid–liquid Taylor flow in a mini-scale tube with constant wall temperature," ASME Paper No. ICNMM 2015-48272.

[10] Guo L., 2002, "Oil–air–water multiphase flow in helically coiled tube and the theory of sand separation from crude oil (in Chinese)", J. Eng. Thermophys, pp. 107–110.

[11] Eain M. G, Egan V., Punch J., 2015, “Local Nusselt number enhancements in liquid-liquid Taylor flow”, Int. J. of Heat and Mass Transfer, 80, pp. 85-97.

[12] Saxena A. K., Nigam K. D. P., Schumpe A., Deckwer W. D 1996, “Liquid phase residence time distribution for two phase flow in coiled tubes”, The Canadian Journal of Chemical Engineering, Vol.74 (6), pp. 861-866.

[13] Kumar V., Vashisth, S., Hoarau, Y., Nigam, P., 2007, “Slug flow in curved microreactors: Hydrodynamic study. Chemical Eng. Science, 62, pp. 7494-7504.

[14] Dogan H., Nas S., Muradoglu M., 2008, “Mixing of miscible liquids in gas-segmented serpentine channels”, International J. of Multiphase Flow, pp. 1149–1158.

[15] Wanga C., Chenb I., Linc Y., Chang Y., 2008, “A visual observation of the air–water two-phase flow in small diameter tubes subject to the influence of vertical return bends”, chemical engineering research and design, 86, pp. 1223–1235.

[16] Vashisth S., Nigam K., 2009, “Liquid-phase residence time distribution for two-phase flow in coiled flow Inverter”, Ind. Eng. Chem. Res, 47, pp. 3630-3638.

[17] Nadim N and Chandratilleke T., 2014, “Secondary flow structure and thermal behaviour of immiscible two-phase fluid flow in curved channels”, Int. J. of Thermal Sciences, 82, pp. 9-22.

[18] Wongwises S., Polsongkram M., 2006, “Condensation heat transfer and pressure drop of HFC-134a in a helically coiled concentric tube-in-tube heat exchanger”, Int. J. Heat & Mass Transfer, 49, pp. 4386-4398.

[19] Adrugi W., Muzychka Y. S., and Pope K., 2017, “Heat transfer in liquid-liquid Taylor flow in a miniscale curved tubing for constant wall temperature”, ASME Journal of Electronic Packaging, Vol. 139, 020909-2.

[20] Kline, S. J. and McClintock, F. A., 1953, "Describing uncertainties in single-sample experiments," Mech. Eng., Jan., p. 3-8.

[21] Muzychka Y. S. and Ghobadi M., 2016, “Measurement and analysis of laminar heat transfer coefficients in micro and mini-scale ducts and channels”, Heat Transfer Engineering, 37(11): 938–946, Taylor & Francis Group.

[22] Muzychka Y. S., Walsh E., Walsh P., 2009, “Heat transfer enhancement using laminar gas-liquid segmented fluid stream”, Proceedings of Inter Pack, San Francisco, July 19-23.

[23] Ghobadi M., Muzychka Y. S., 2014, “Fully developed heat transfer in mini scale coiled tubing for constant wall temperature”, Int. J. of Heat and Mass Transfer, 72, pp. 87–97.

[24] Awad, M. M., and Muzychka, Y. S., 2008, “Effective property models for homogeneous Two-Phase Flows,” Exp. Therm. Fluid Sci., 33(1), pp. 106–113.

[25] Muzychka, Y. S., Walsh, E., Walsh, P., and Egan, V., 2011, “Non-boiling two phase flow in microchannels,” Microfluidics and Nanofluidics Handbook: Chemistry, Physics, and Life Science Principles, S. K. Mitra and S. Chakraborty, eds., CRC Press, Boca Raton, FL.

CHAPTER 7

Pressure Drop of Liquid-Liquid Taylor Flow in Coiled and Curved Mini-Scale Tubing*

7.1 Introduction

Small-scale coiled channels and Taylor flow (or slug flow) are effective and compact, and accordingly, have a wide applications in cooling systems, chemical engineering, and microfluidics biomedical devices [1–3]. Numerous researchers have studied fluid flow in curved and coiled mini / micro channels. Much of the work on pressure drop in two-phase flows in helically coiled tubes has been summarized by Fsadni and Whitty [4]. They presented a review of the pertinent literature on the pressure drop characteristics of boiling / non-boiling air-water two-phase flow and nanofluid flows with correlations. The present work is focused upon the pressure drop associated with liquid-liquid segmented Taylor flow regimes in mini scale coiled tubing. The pressure drop associated with a non-boiling

* Accepted to ASME 2019 17th International Conference on Nanochannels, Microchannels, and Mini channels, June 23-26, St. John's, Newfoundland, Canada

two-phase flow regime in coiled geometry has received significant attention in the literature and has been the subject of numerous numerical and experimental studies, including Czop et al. [5], Awwad et al. [6], Xin et al. [7], Mandal and Das [8] and Vashisth and Nigam [9]. However, the prediction of pressure drop in Taylor flows regime in any helical spiral mini or micro channels has received almost no attention.

For gas-liquid Taylor flow characteristics in curved or coiled channels, Xin et al. [10], Murai et al. [11], Vashisth and Nigam [9], and Gourma and Verdin [12] have performed numeral and experimental studies. The numerical results of Jayakumar et al. [13] and Zohurul Islam et al. [14] suggest that there is a significant difference between the slug flow in helical and straight tubing due to centrifugal force causing secondary flow patterns [15,16]. The differences in heat transfer coefficients and friction factor between the main flow and secondary flow occur due to the differences in their flow patterns. Several experimental and numerical studies have addressed the pressure drop of single-phase flow in small-scale coiled tubing [13],[17].

Slug or Taylor flow regimes in mini / micro-scale tubes can provide significant heat transfer enhancement over equivalent single phase systems such as those studied by Adrugi et al. [18] and Eain et al., [19]. Few studies have been conducted on the heat and mass transfer characteristics of liquid-liquid Taylor flow in small curved and coiled tubing [20–23]. In previous chapters, we have reported new experimental data, which considers increases in heat transfer rates for two phase slug flows in curved [9] and coiled [10] mini scale tubes with a constant wall temperature. We have developed a model which addresses the effect of secondary flow (Dean number) on the Nusselt number.

The behavior of Taylor flow depends to a large extent on the ducts geometry. Accordingly, duct geometry also affects hydrodynamic and thermal characteristics in the channels. Although similar behavior is observed within liquid slugs in curved mini / microchannels, flow induction within liquid slugs is asymmetric as a result of the channel curvature other than straight channels. This produces more complex flow fields and results in a faster mass transfer over the whole slugs and an improved mixing efficiency [24]. This study experimentally explores the pressure drop of liquid-liquid Taylor flow in coiled and curved mini-scale tubing and develops a new predictive correlation. The study also investigates the effects of the number of coils in the tubing on the liquid-liquid slug flow. It reviews and addresses the experimental and theoretical study of pressure drop in liquid-liquid Taylor flow in mini scale straight tubing by Adrugi et al. [25] for comparison purposes. A dimensionless approach is used to predict pressure drop in coiled tubing across a wide range of Reynolds, Dean, and Capillary numbers.

7.2 Experimentation

An experimental setup for two-phase flow in mini / micro channel geometries was designed in the Microfluidics and Multiphase Flow Research Laboratory. The setup can create a steady slug flow regime with accurately controlled inlet flow rates and can monitor and record variations in transient pressure drop to ensure that steady state conditions are achieved. The experiment, shown in Fig. (7.1), consists of two syringe pumps, pressure sensors, test sections, T-junctions, a high-speed camera, and related instrumentations. Two precision syringe pumps (Harvard Apparatus PHD Ultra™) with glass syringes were employed to set the volumetric flow rates and, accordingly, slug lengths. A T-junction was

employed to ensure sufficient control of droplet size and spacing. To acquire precise results, the experiment employed two calibrated pressure sensors with pressure ranges of 0-5 psi and 0-1 psi.

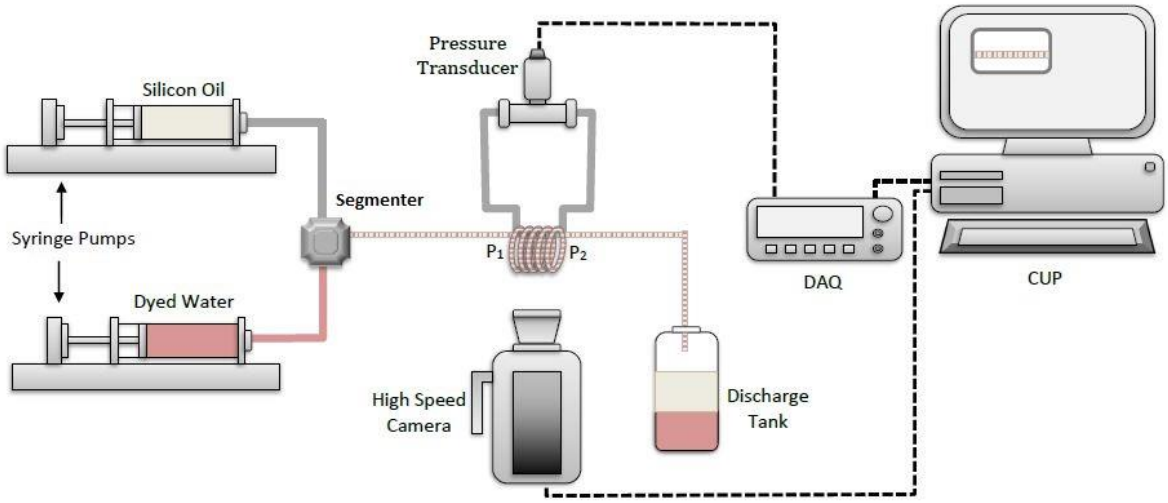

Fig. 7. 1 - Schematic of experimental setup for liquid-liquid slug flow.

The test sections consisted of flexible smooth-tubes (Nalgene™ 180 Clear Plastic PVC Tubing) of 0.5 *m* and 1 *m* length that were coiled around cylinders in three radii (8.14 *mm*, 12.10 *mm*, and 14.72 *mm*). Different radii of curvature were used to explore their impact on the pressure gradient of Taylor flow with different internal tube diameters (1.02 *mm*, 1.27 *mm*, and 1.59 *mm*). It was necessary to have a thick and firm tube wall to maintain a constant cross sectional area after coiling. Table (7.1) presents the dimensions of the test sections. The majority of experiments used 1 cSt silicone oil segmented by water to generate liquid-liquid Taylor flow. The fluid properties based on the room (bulk)

temperature of approximately 24°C. The flow visualization section comprised a digital high-speed camera (Phantom v611) connected to a computer for data acquisition.

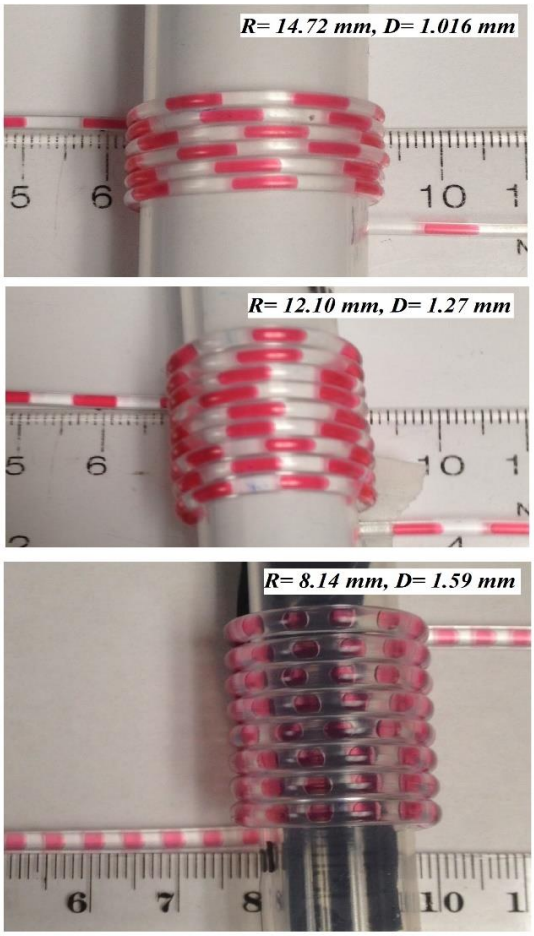

Fig. 7. 2 - Dyed water / 1 cSt slugs flow in coiled tubes with varying radii of curvature and internal diameters.

Table 7. 1 - Coiled tubes dimensions

Lengths (*m*)	Tube Diameters (*mm*)	Coil Radius (*mm*)
0.5 1	1.59	8.14
	1.27	12.10
	1.016	14.72

After the syringes were filled with test liquids and mounted on syringe pumps, the system took approximately 10 minutes to reach a steady state. The experiments were performed with a liquid volume fraction maintained constantly at 0.5 and a liquid flow rate from 3 *ml/min* to 30 *ml/min* for each phase (Fig. 7.2). The camera with a light source was placed and adjusted at a set distance ~ 50 *cm* from the setup to record a straight section of tubing and to receive data on the size of slug lengths. Various flow rates of Taylor flow in all test sections were set to perform pressure drop measurements. To eliminate the noise effect on the readings, several readings for each pressure drop were recorded. The uncertainty of the friction factor measurements was determined to be ~ 6.05 % using the Kline and McClintock approach [26], with a 1% uncertainty for the pressure gauges.

7.3 Formulation of Pressure Drop for Taylor Flow

This section presents the analysis methodology for pressure drop of liquid-liquid Taylor flow in a coiled and curved mini-scale channel. As a benchmark for the experiments, the initial measurements were performed on pressure drop of a single-phase flow in a straight tube. Afterwards, the pressures drop in liquid-liquid Taylor flow was subsequently measured for each test section. Pressure gradient correlations for single-phase flow in coiled tubing and Taylor flow in straight tubing were used as the bases for the Taylor flow analysis in coiled tubing, due to a lack of correlation for this type of flow in the literature. The resulting data was correlated as a function of the Dean number due to the secondary flow in coiled Taylor flow. As the Dean number is proportional to the channel curvature, it changes with the flow rate and curvature. The Dean number (*De*) is defined as

$$De = Re\sqrt{\frac{D}{2R}} \tag{7.19}$$

In all the experimental tests reported in this research, the Dean number (*De*) was used instead of a helical coil number (*He*) for coiled tubes or helical coil due to the coil pitch was very small. Thus, the effect of the effective radius (*Rc*) is often the same as the radius of the tube curvature (R), which can be neglected. This study considers a wide range of Dean numbers and Reynolds numbers.

In a previous study [25], we have proposed and verified a phase separation model focused on single-phase pressure drop and the additional pressure drop caused by the liquid-liquid interfaces. This study models the pressure drop associated with a liquid-liquid Taylor flow regime in mini-scale. As a consequence, the following correlation was proposed to express the total pressure drop in the channel as the sum of the single-phase pressure drop contributions of each phase and the interfacial pressure that exists between the two phases:

$$\Delta P^* = (fRe_D)_{sp} + \left(\frac{1}{L_e^*}\right)_{Int.} \tag{7.2}$$

where ΔP^*, the dimensionless total pressure drop, can be expressed as

$$\Delta P^* = \frac{\Delta P_e}{L_e}\frac{D^2}{2\,U\bar{\mu}_e} \tag{7.3}$$

where ΔP_e, is the difference between the inlet and outlet pressure in the unit cell, and L_e is the length of a unit cell ($L_e = L_c + L_d$). The variable U is the superficial velocity of the total flow rate:

$$U = \frac{(\dot{Q}_c + \dot{Q}_d)}{A} \tag{7.4}$$

where $\dot{Q}_c$ and $\dot{Q}_d$ are the volumetric flow rates of the carrier and dispersed phase and A is the cross-sectional area of the curved tube.

In accordance with the liquid-liquid two-phase flow structure (series of slugs) in capillary tubing, the effective viscosity, $\bar{\mu}_e$, was replaced by the McAdams model [27], defined as

$$\bar{\mu}_e = \left[\frac{x}{\mu_c} + \frac{1-x}{\mu_d}\right]^{-1} \tag{7.5}$$

where the mass quality is $x = \dot{m}_c/(\dot{m}_d + \dot{m}_c)$, and the effective density of liquid-liquid two-phase flow, $\bar{\rho}_e$, can be calculated using liquid fraction (α_L)or the mass quality (x) of dispersed phase, are defined as

$$\bar{\rho}_e = \rho_c\, \alpha_{L_c} + \rho_d\left(1 - \alpha_{L_c}\right) = \left[\frac{x}{\rho_c} + \frac{1-x}{\rho_d}\right]^{-1} \tag{7.6}$$

The dimensionless length of a unit cell is

$$L_e^* = \frac{L_e}{D}\frac{Ca}{2(\cos\theta_r - \cos\theta_a)} \tag{7.7}$$

where θ_a and θ_r are the advancing and receding contact angle, respectively and Ca is the Capillary number. Based on the two-phase Taylor flow model, Ca can be expressed as

$$Ca = \frac{\bar{\mu}_e\, U}{\sigma} \tag{7.8}$$

where σ is the interfacial tension of two liquids.

For the fully developed laminar flow in a circular channel, the frictional pressure drop is

$$\Delta P = \frac{4\,f\,L}{D}\frac{1}{2}\bar{\rho}_e\,U^2 \quad or \quad fRe_D = 16 \tag{7.9}$$

where f is the Fanning friction factor and the Reynolds number is $Re_D = \bar{\rho}_e\,U\,D/\bar{\mu}_e$.

Based on the empirical model of Ghobadi & Muzychka [17] for fully developed laminar flow in a helical coiled tube, the pressure drop is presented in the form of fRe and can be expressed as:

$$fRe = 16\left[1 + \left(0.45De^{1/3}\right)^5\right]^{1/5} \tag{7.10}$$

The correlation is valid for Dean numbers up to 400. Another important correlation to predict the secondary flow's effect on increasing frictional losses (pressure drop) in fully developed laminar flow in helically coiled tubes, relative to straight tubes is given by Incropera et al. [28],

$$fRe = \begin{cases} 16 & \text{If } De \le 30 \\ 6.75\,De^{0.275} & \text{If } 30 \le De \le 300 \\ 1.8\,De^{0.5} & \text{If } De \ge 300 \end{cases} \tag{7.11}$$

These correlations are reasonable and recommended with $2R/D \ge 3$.

The pressure drop formulation provides an effective method to study and provide new insights into liquid-liquid Taylor flows in curved and coiled mini / micro channels.

7.4 Results and Discussion

In this section, new experimental data for pressure drop rate in liquid-liquid Taylor flows in mini-scale coiled tubes are presented. The experiments used silicone oil segmented by water to generate two-phase Taylor flows with liquid fraction maintained constant at 0.5 with Reynolds numbers from 80 to 840. The results were obtained with a variety of dimensionless variables (ΔP_T^*, L_e^*, and De) to present the experimental data.

The experimental results of the benchmarking test for single-phase flow in a mini-scale tube are used as a reference for the new Taylor flow data. The experimental results are compared with the Adrugi et al. model [25] for liquid-liquid Taylor flow in mini scale straight tubing and with the Fanning correlation for single-phase Poiseuille flow. The effect of tube curvature and the number of turns in the coil on the pressure drop augmentation is investigated by the length and curvature change of tubing used. Subsequently, the proposed correlation is employed to predict the results and the discussion of the results is provided.

Water and 3 cSt viscosity silicone oil are used to perform tests for single-phase flow in a mini-scale tube to benchmark and verify the accuracy of the experimental data. Figure (7.3) illustrates the new experimental data on pressure drop for laminar flow inside a straight mini-scale tube (inner diameter, D=1.59 mm and length, L= 1 m) with various flow rates and compared with the Fanning equation. The theoretical model of fully developed laminar flows agrees well with the experimental data for all fluids used.

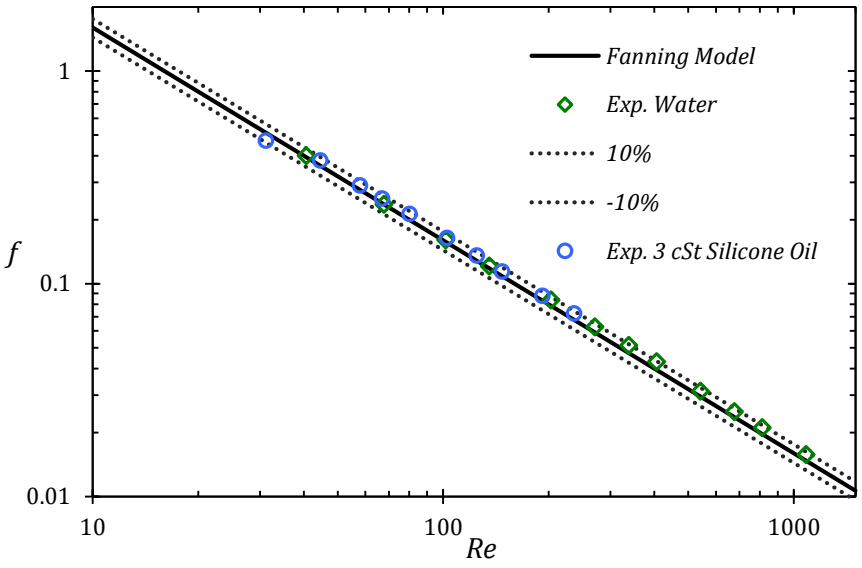

Fig. 7. 3 - Benchmarking results for laminar friction factor in a straight tube with ± 10 % error band.

For coiled tubing using 1cSt / water slug flow into a constant length of tubing with respective diameters of 1.59 *mm*, 1.27 *mm* and 1.016 *mm* are shown in Figures (7.4 – 7.6). The effect of curvature on the pressure drop in Taylor flow is shown by the plot between the dimensionless pressure drop (ΔP^*) versus the dimensionless effective length (L_e^*). The pressure drop correlation for Taylor flow in straight tubes is also plotted to show the pressure drop increase in coil tubes in addition to the friction pressure drop model for laminar single-phase flow ($\Delta P^* = fRe = 16$).

As shown in Figures (7.4 – 7.6), the experimental data of pressure drop for Taylor flow in coiled tubing is higher than the predictive model of Taylor flow in straight tubing with the same limit of flow. The result indicates that the secondary flow inside the tubing increases the pressure drop and the curvature is the main factor with causes the increase.

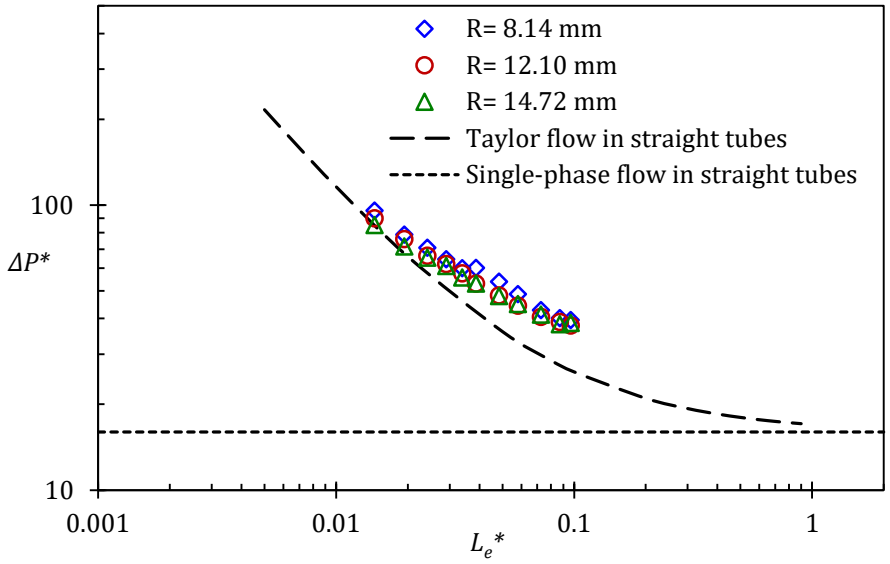

Fig. 7. 4 - ΔP^* vs L_e^* for 1.59 *mm* tube diameter and 1 m length with different radii of curvature in each coil.

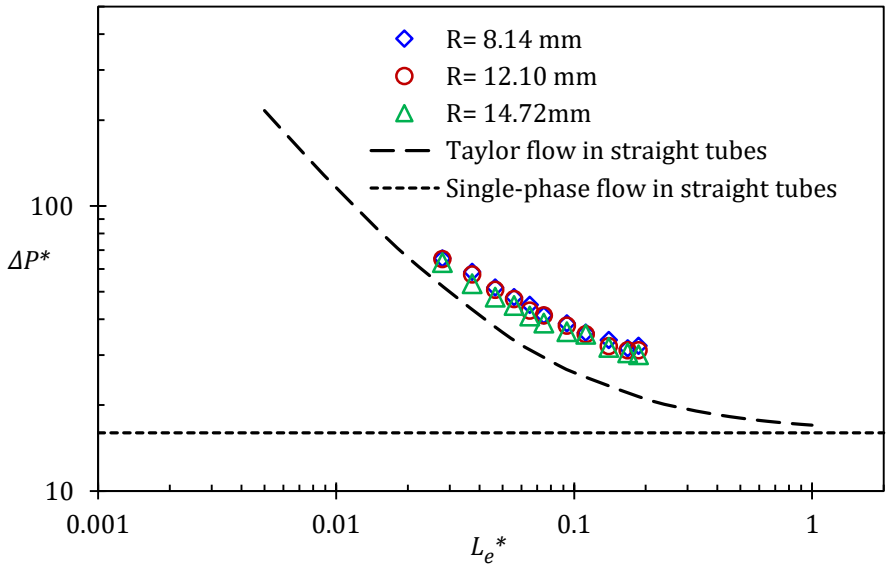

Fig. 7. 5 - ΔP^* vs L_e^* for 1.27 *mm* tube diameter and 1 *m* length with different radii of curvature in each coil.

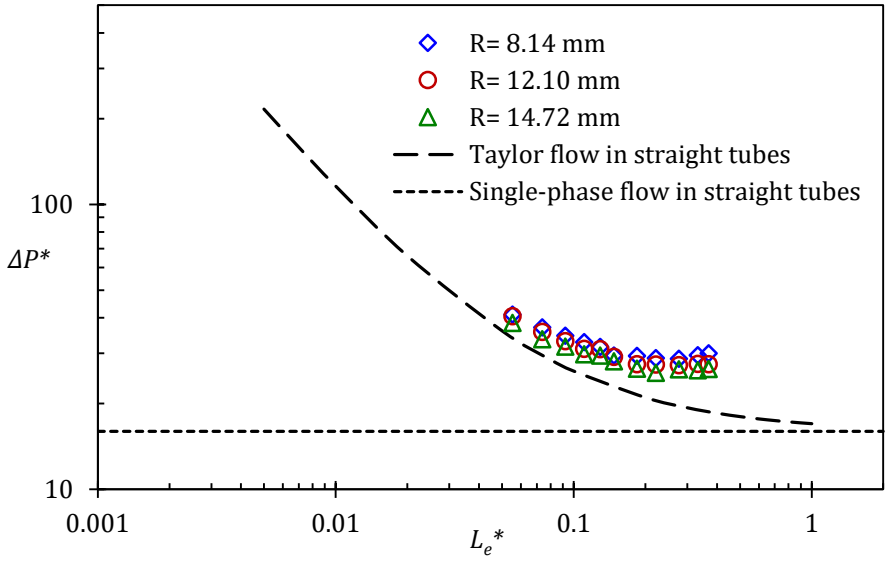

Fig. 7. 6 - ΔP^* vs L_e^* for 1.016 *mm* tube diameter and 1 *m* length with different radii of curvature in each coil.

7.4.1 Proposed Model

Previous studies lacked correlations to describe the pressure drop of two-phase Taylor flow in small coiled tubing. Therefore, correlations are established based on the Adrugi et.al model [25] for Taylor flow in mini scale straight tubes, as well as the Ghobadi and Muzychka model [17] and the Incropera et al. model [28] for single-phase Poiseuille flow in small scale coiled tubes to compare with the experimental results. Thus, combining the two models using the asymptotic correlation method shows a transitional behavior:

$$\Delta P^* = 16\left[1 + \left(0.45\, De^{1/3}\right)^5\right]^{1/5} + \left(\frac{1}{L_e^*}\right) \tag{7.12}$$

and

$$\Delta P^* = 16\ \left[1 + \left(0.421\ De^{1/4}\right)\right] + \left(\frac{1}{L_e^*}\right) \tag{7.13}$$

Based on the comparison between the path of the new experimental data and modified models (Eqs. 7.12 and 7.13), we propose a new empirical prediction for the pressure drop of liquid-liquid Taylor flow in small curved and coiled tubes by asymptotes expressed in the form

$$\Delta P^* = 16\ \left[1 + \left(0.421\ De^{1/4}\right)^n\right]^{1/n} + \left(\frac{1}{L_e^*}\right) \tag{7.14}$$

where n = 2, and this value was chosen to minimize the root mean square (RMS) error between the model prediction and the experimental data; and the most accurate transitional results are predicted.

Since the dimensionless pressure drop, ΔP^*, is a function of two dimensionless groups, De and L_e^*, this correlation (Eq. 7.14) may be rewritten as only a function of one dimensionless variable De or L_e^*. Given the pressure gradient relates to the average velocity U for Taylor flow. Thus, the capillary number can be substituted into Eq. (7.8) as follows:

$$L_e^* = \frac{L_e}{D}\frac{\bar{\mu}_e U}{2\sigma\ (cos\ \theta_r - cos\ \theta_a)} \tag{7.15}$$

where U is defined from Eq. (7.1) and takes the form

$$U = \frac{De\ \bar{\mu}_e}{\bar{\rho}_e\ D}\sqrt{2R/_D} \tag{7.16}$$

Using Eq. (7.15) for the dimensionless effective tube length L_e^* and substituting for the velocity variable U from Eq. (7.16):

$$L_e^* = \frac{L_e \bar{\mu}_e^2}{2\, D^2 \bar{\rho}\, \sigma\, (cos\, \theta_r - cos\, \theta_a)} \sqrt{2R/_D}\; De \tag{7.17}$$

and thus, the dimensionless effective tube length L_e^* can be expressed

$$L_e^* = C\, De \quad or \quad De = {L_e^*}/_C \tag{7.18}$$

where C represents all depended parameters at x-axis (L_e^*) and is defined as

$$C = \frac{L_e\, \bar{\mu}_e^2}{2\, D^2 \bar{\rho}_{\,e} \sigma\, (cos\, \theta_r - cos\, \theta_a)} \sqrt{2R/_D} \tag{7.19}$$

The proposed model is now only a function of the dimensionless Dean number or effective tube length, whereas the correlation (7.14) is functions of the dimensionless duct length (L_e^*) and Dean number *De*. Thus, the proposed model takes the form

$$\Delta P^* = 16 \left[1 + \left(0.421\, De^{1/4}\right)^2\right]^{1/2} + \left(\frac{1}{C\, De}\right) \tag{7.20}$$

which acknowledges that the dimensionless pressure gradient ΔP^* in a coiled tube is a function of the Dean number. This dependence is evident from Figures (7.7 - 7.9) and has been determined experimentally for selected values of the Dean number with radii of curvature in coils. The results have been correlated to within ± 10% of the proposed correlation. The new correlation can accurately predict the pressure gradient of Taylor flow in small-scale coiled tubing systems.

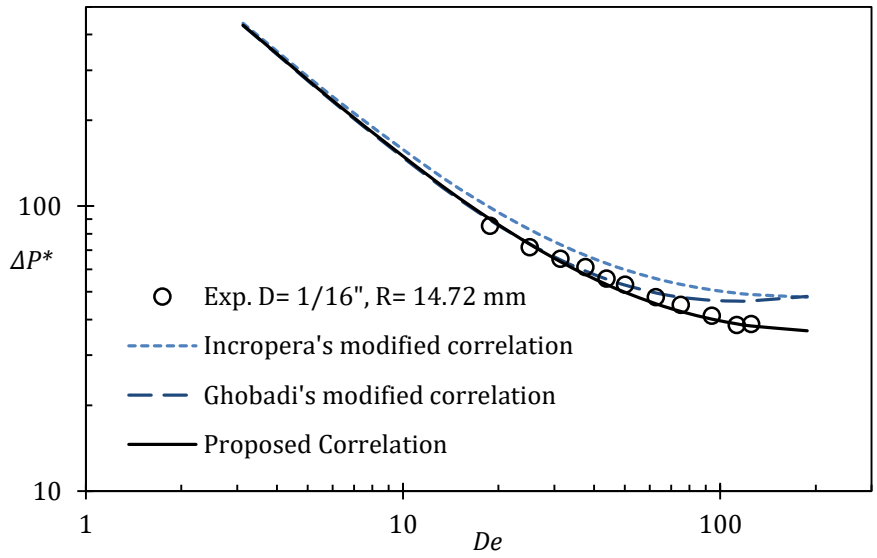

Fig. 7. 7 - Comparison between experimental data for 1.59 *mm* tube diameter and 14.72 *mm* radii of curvature in coiled tube with proposed correlations.

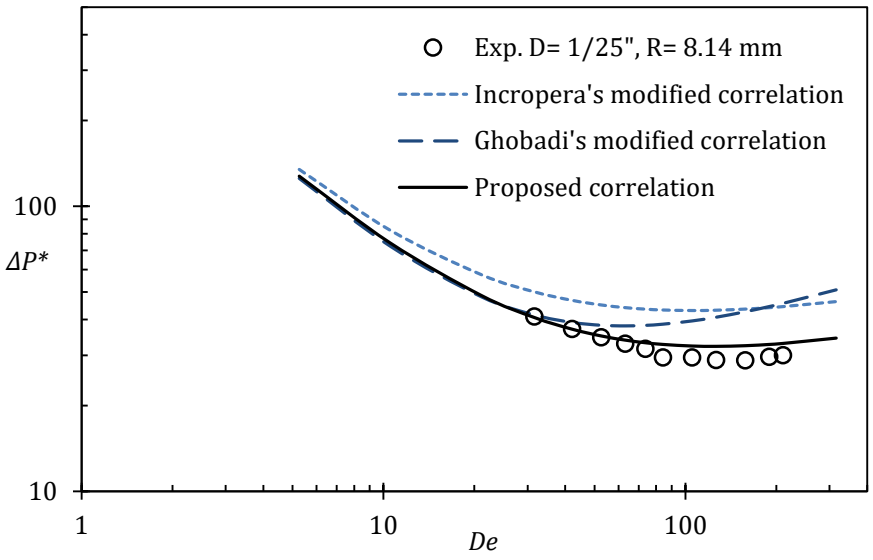

Fig. 7. 8 - Comparison between experimental data for 1.016 *mm* tube diameter and 8.14 *mm* radii of curvature in coiled tube with proposed correlations.

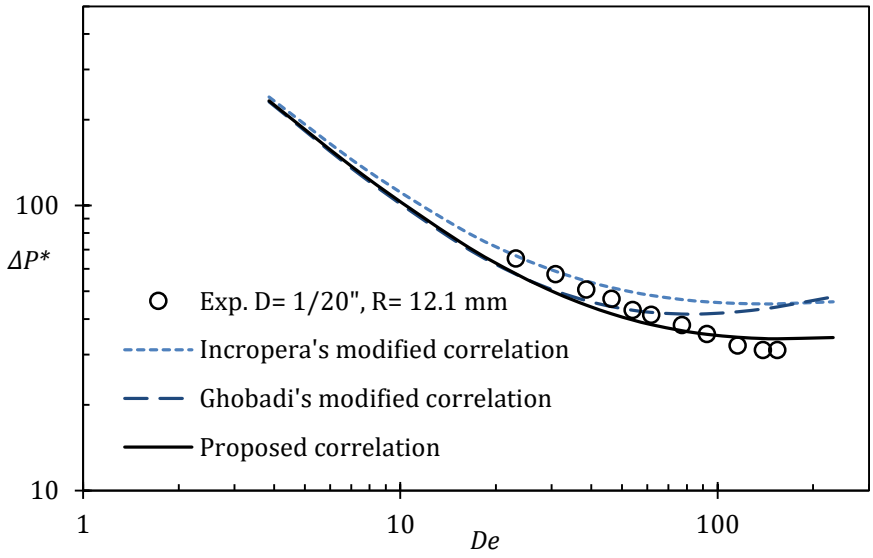

Fig. 7. 9 - Comparison between experimental data for 1.27 *mm* tube diameter and 12.10 *mm* radii of curvature in coiled tube with proposed correlations.

The experimental data with correlated predictions for coiled tubes with 0.5 *m* length and 1.016 *mm*, 1.27 *mm*, and 1.59 *mm* diameters are illustrated in Figs (7.7 – 7.9). The dashed line illustrates previously introduced combined correlations, while the continuous line shows the new proposed model for pressure drop prediction of liquid-liquid Taylor flow in mini-scale coiled tubing. In all figures, there is an improved agreement for the proposed correlation (Eq. 7.14) with the experimental data. It is also noted that the high Dean number flows the correlations (Eq. 7.14) offer better predictions than the correlations presented in (Eq. 7.12) and (Eq. 7.13). According to the results, the proposed correlation predicts the experimental results in a mini scale with the average of less than 7.7% RMS error and 10% was the maximum deviation.

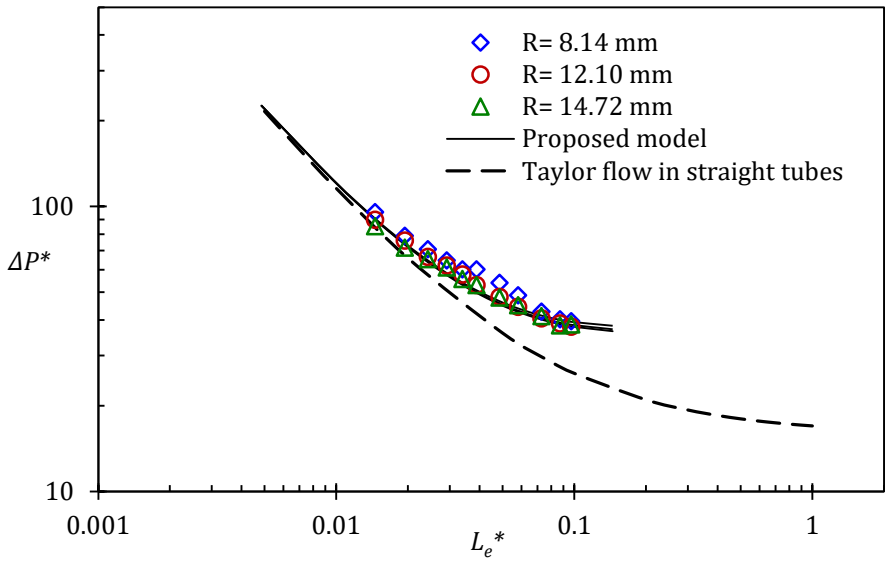

Fig. 7. 10 - ΔP^* vs L_e^* for experimental data of different radii of curvature in each coil ($D = 1.59\ mm, L = 1\ m$) with proposed model.

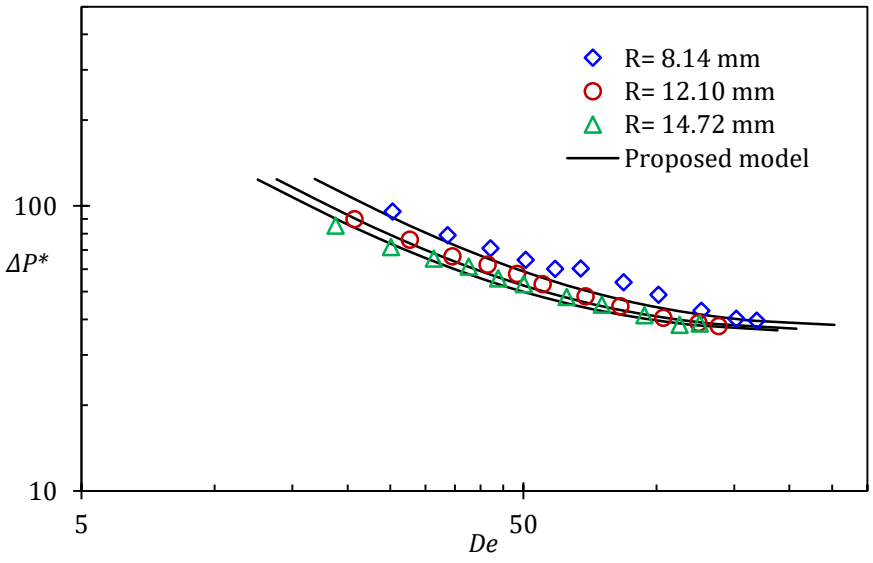

Fig. 7. 11 - ΔP^* vs De for experimental data of different curvature in each coil ($D = 1.59\ mm, L = 1\ m$) with proposed model.

The impact of curvature on the pressure drop increase is illustrated by the experimental results using the different radius of curvatures in coiled tubes. Furthermore, results are compared with the proposed correlation using the dimensionless pressure drop as a function in the dimensionless effective length as shown in Figs. (7.10), (7.12), and (7.14); and as a function in Dean number instead of dimensionless effective length as shown in Figs. (7.11), (7.13), and (7.15).

The results of water / 1 cSt silicone oil slug flow for the different radius of curvatures of coiled tubing (14.72 *mm*, 12.1 *mm*, and 8.14 *mm*) with a constant length of 0.5 *m* or 1 *m* are shown in Figs. (7.10 – 7.15). A different radius of curvature and the same tube length result in more numbers of turns in coils, which, in turn leads to increased pressure drop. The experimental data points correspond to the proposed model trend as it was noted pressure drop expresses comparable behavior for coiled tubes with different diameters (1.016 *mm*, 1.27 *mm*, and 1,59 *mm*).

An increase in the pressure drop for all of the coiled tubes is the result of increasing curvature. The coiled tubing with the largest curvature, *1/R*, i.e. when $R = 8.14$ *mm* achieved the maximum pressure drop. The next highest pressure drop was for $R = 12.1$ *mm*. The smallest pressure drop was for a coiled tube with $R = 14.72$ *mm*. As the curvature of the tube increases, intensify of the secondary flow increases, and then leads to increase mass transfer rates. Therefore, the pressure drop increases are caused by the additional momentum transport.

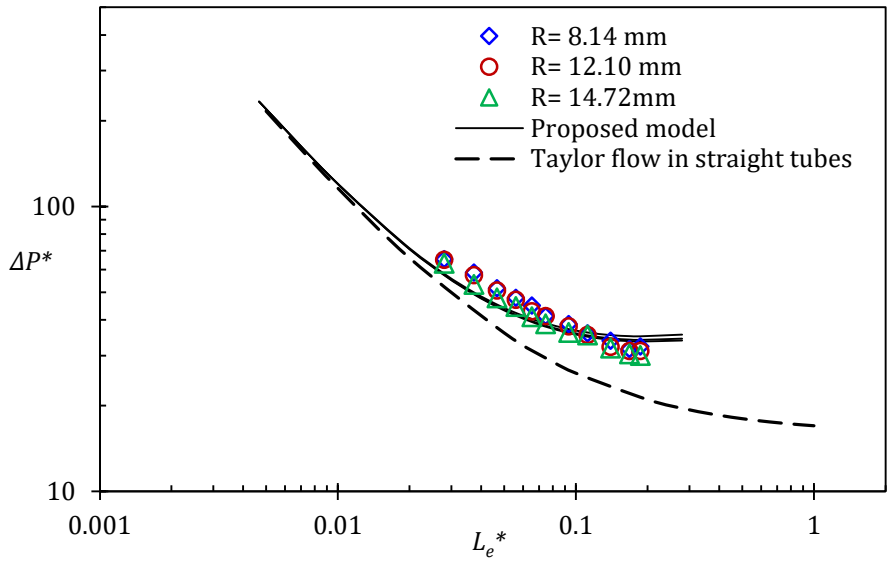

Fig. 7. 12- ΔP^* vs L_e^* for experimental data of different radii of curvature in each coil ($D = 1.27\ mm, L = 0.5\ m$) with proposed model.

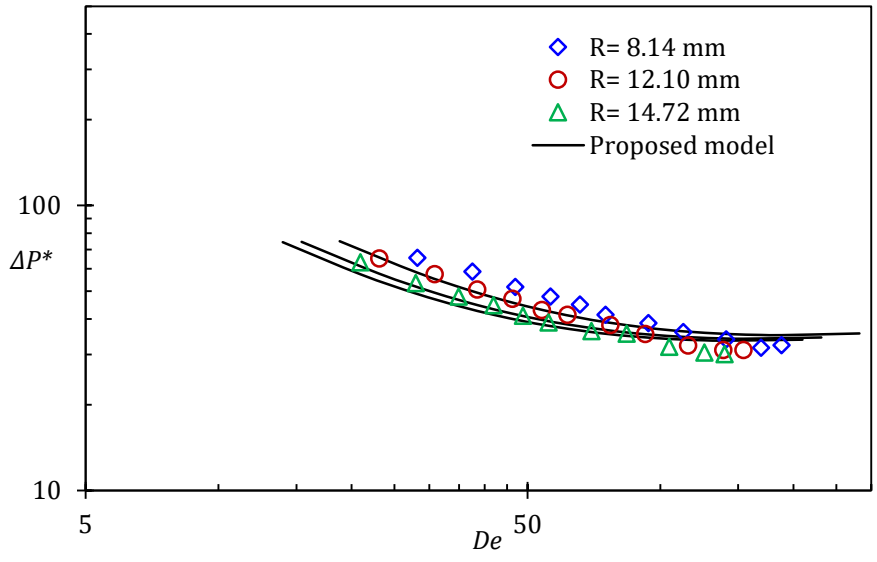

Fig. 7. 13 - ΔP^* vs De for experimental data of different curvature in each coil ($D = 1.27\ mm, L = 1\ m$) with proposed model.

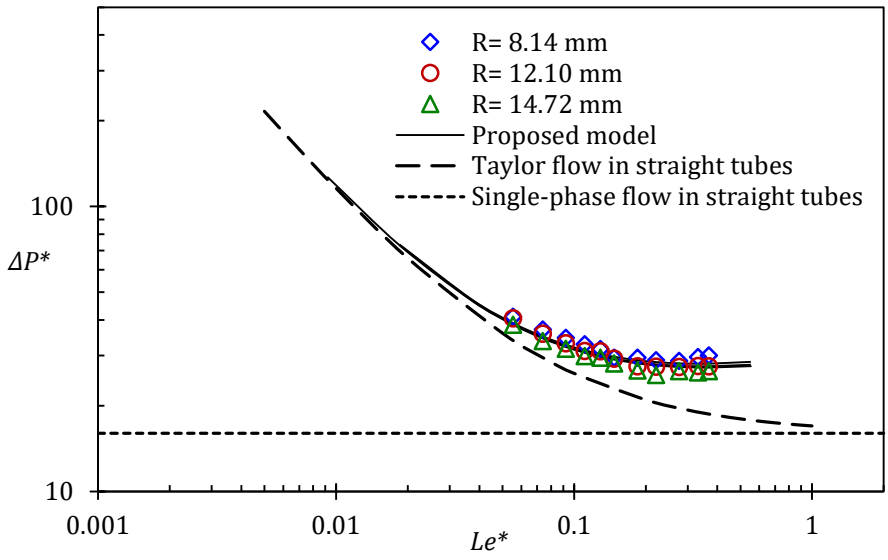

Fig. 7.14 - ΔP^* vs L_e^* for experimental data of different radii of curvature in each coil ($D = 1.016\ mm, L = 1\ m$) with proposed model.

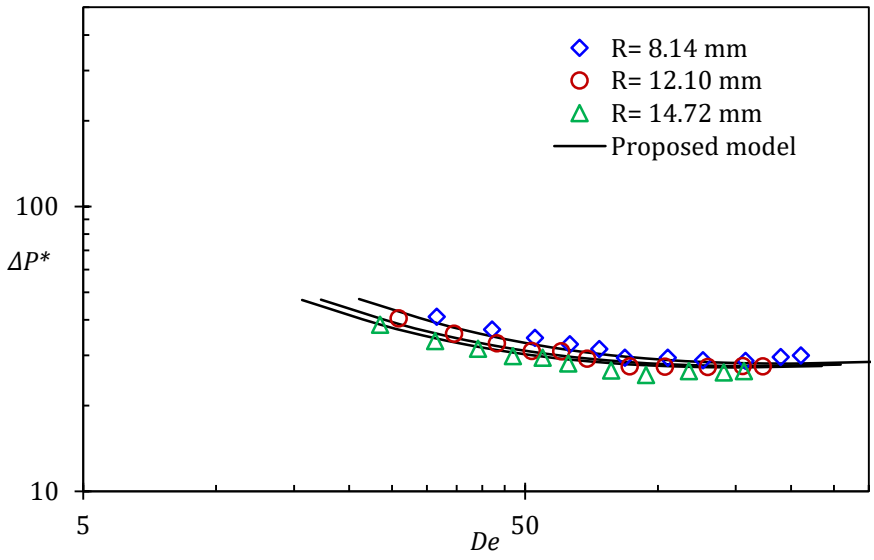

Fig. 7. 15 - ΔP^* vs De for experimental data of different curvature in each coil ($D = 1.016\ mm, L = 1\ m$) with proposed model.

The discussion will also address the effect of the tube diameter on increasing pressure drop through the collected new experimental data and for more validation to the proposed model. Figures (7.16 – 7.21) present the dimensionless pressure drop with the Dean number and / or the dimensionless length for a water / 1 cSt oil slug flow at a constant curvature of a coiled tube. Three different tube diameters, 1.016 *mm*, 1.27 *mm*, and 1.59 *mm* with 14.72 *mm*, 12.1 *mm*, and 8.14 *mm* radius of curvature were used to examine the pressure drop in coiled mini scale tubing.

The results of Taylor flow in coiled tubes having a constant radius of curvature, $R = 8.14$ *mm* is shown in Figs. (7.16) and (7.17). As illustrated in the figures (7.18 – 7.21), similar trends were noted for diameters with radii of curvature, namely $R = 14.72$ *mm* and $R = 12.1$ *mm*, in comparison to $R = 8.14$ *mm*. As are the proposed model expectations, the big diameter exceeds in terms of pressure drop increase the small diameter with increased the dimensionless effective tube length. Accordingly, any observed increased pressure drop for the different tube diameters at the same curvature and length in comparison may be due the higher flow rate caused by a smaller diameter, which is caused by the effect of slug length is not significant and the pressure drop in the flow is dominated by the characteristically Poiseuille flow.

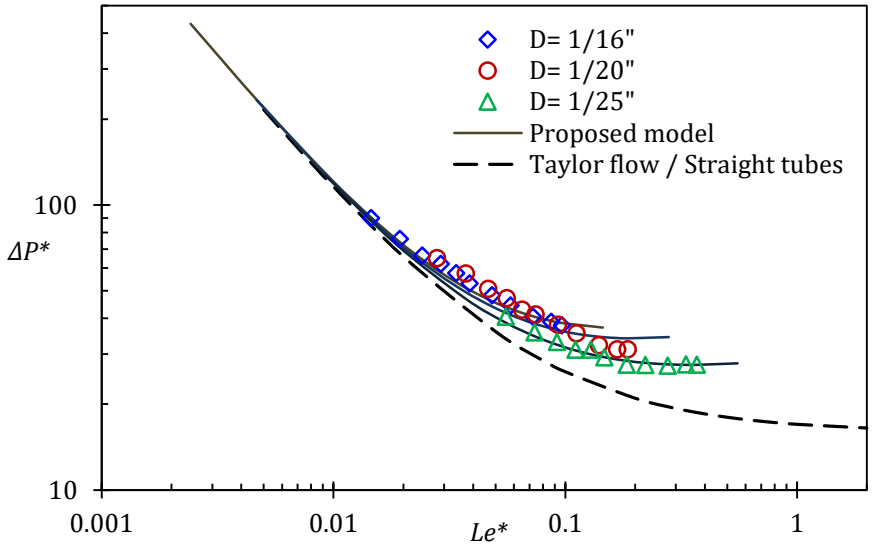

Fig. 7. 16 - ΔP^* vs L_e^* for experimental data of different coiled tube diameter and constant radii of curvature ($R = 14.72\ mm$) with proposed model.

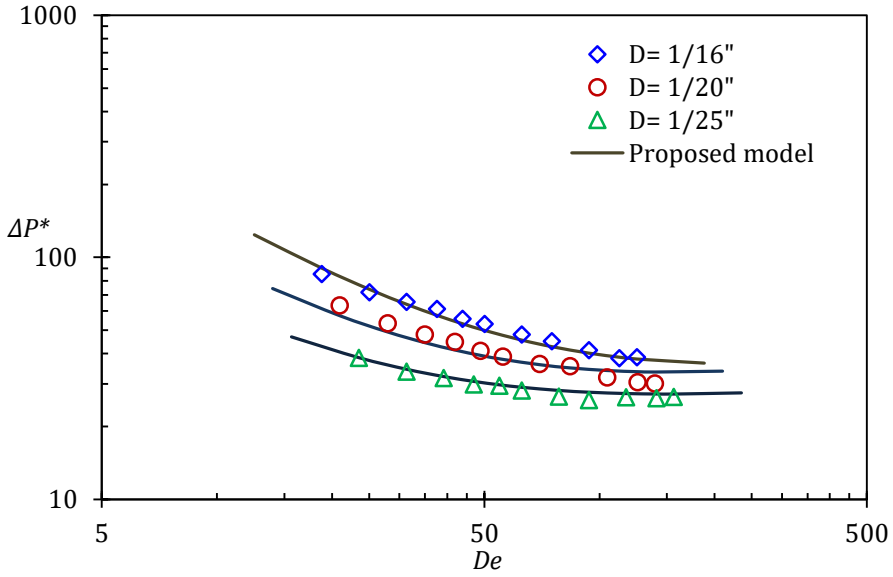

Fig. 7. 17 - ΔP^* vs De for experimental data of different coiled tube diameter and constant radii of curvature ($R = 14.72\ mm$) with proposed model.

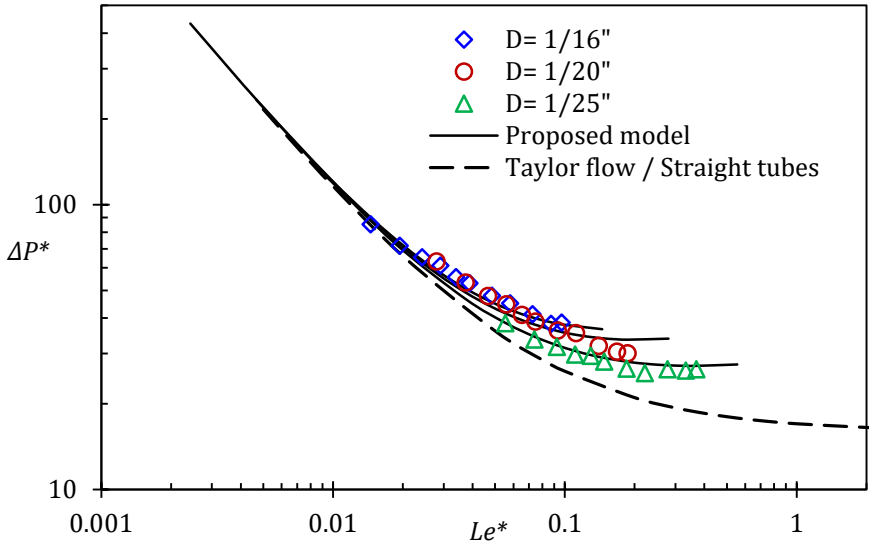

Fig. 7. 18 vs L_e^* for experimental data of different coiled tube diameter and constant radii of curvature ($R = 12.10\ mm$) with proposed model.

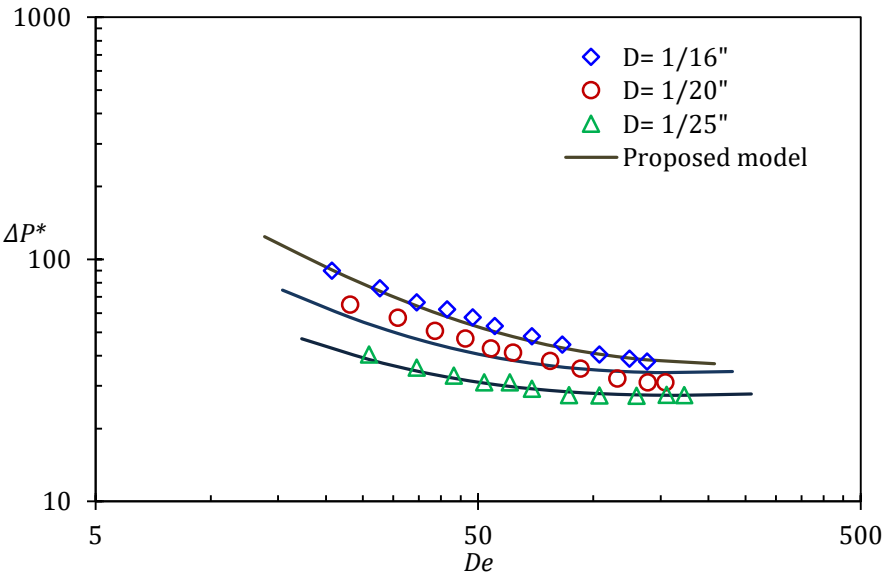

Fig. 7. 19 - ΔP^* vs De for experimental data of different coiled tube diameter and constant radii of curvature ($R = 12.10\ mm$) with proposed model.

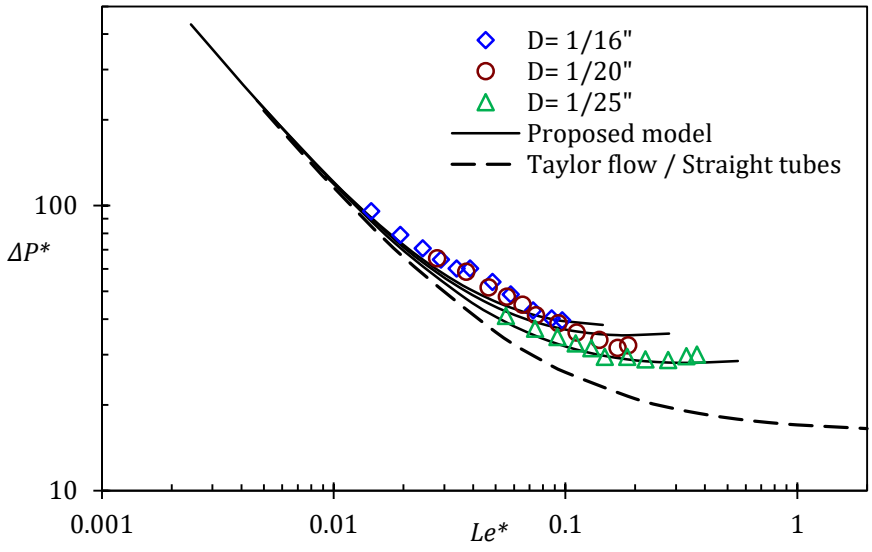

Fig. 7. 20 - ΔP^* vs L_e^* for experimental data of different coiled tube diameter and constant radii of curvature ($R = 8.14\ mm$) with proposed model.

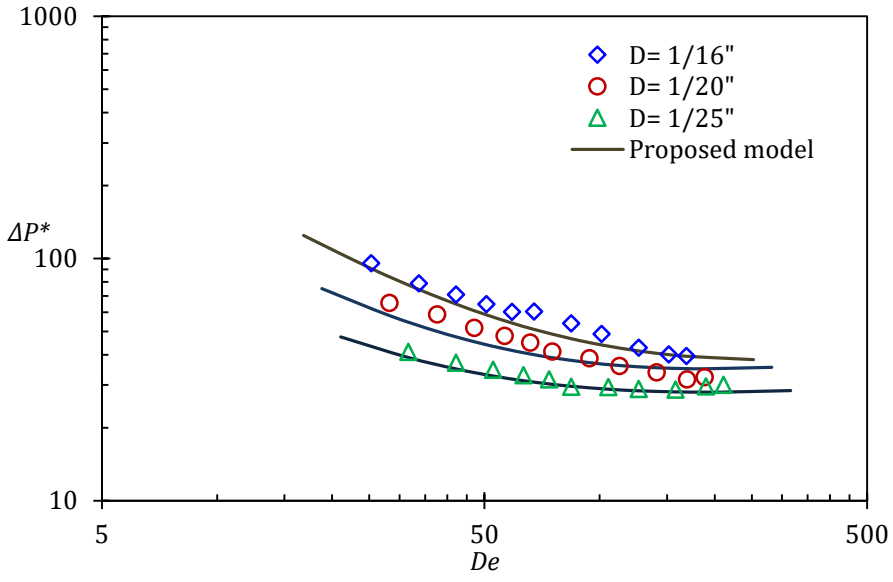

Fig. 7. 21 - ΔP^* vs De for experimental data of different coiled tube diameter and constant radii of curvature ($R = 8.14\ mm$) with proposed model.

7.5 For Curved Tubing

To validate the proposed model in curved tubing, Figures (7.22 to 7.28) illustrate the dimensionless pressure drop of liquid-liquid Taylor flow in a set of curved tubes with different lengths and curvatures. The Taylor flows are water / 1 cSt silicone oil in mini scale tubing with four different tube lengths: a quarter, half, three quarters, and a full circle ($\theta = 90^o, 180^o, 270^o,$ and 360^o), with the same radius of curvature (R = 14.15 *cm*, 10.55 *cm*, or 7.03 *cm*). Figures (7.22) and (7.23) illustrate the experimental results for curved tubes with a radius of curvature ($R = 14.15\ cm$) and different lengths ($L = 88.86\ cm$, 66.64 cm, 44.43 cm and $22.21\ cm$); and for curved tubing with $10.55\ cm$ radius, and its lengths are 66.33 cm, 49.75 cm, 33.16 cm and 16.58 cm (Figs. 7.24 and 7.25). However, Figures (7.26) and (7.27) also depict the effect of the tube length on pressure drop are investigated with four different tube lengths (44.22 *cm*, 33.16 *cm*, 22.11 *cm*, and 11.05 *cm*) with a 7.03 *cm* radius of curvature.

At a wide range of flow rates of slug flow compared to the proposed correlation, the results of dimensionless pressure drop agree very well in all figures. Significant changes in Dean number lead to variations in the pressure drop. Obviously, increasing the Dean number reduces pressure drop to a certain extent as expected in coiled tubing. Hence, the tube curvature affects the Taylor flow and cause an increase in the secondary flows with increasing flow rate, thus raising pressure drop. However, by increasing the flow rate (increasing L^* and De), the pressure drop is significantly increased compared to Taylor flow in a straight tube.

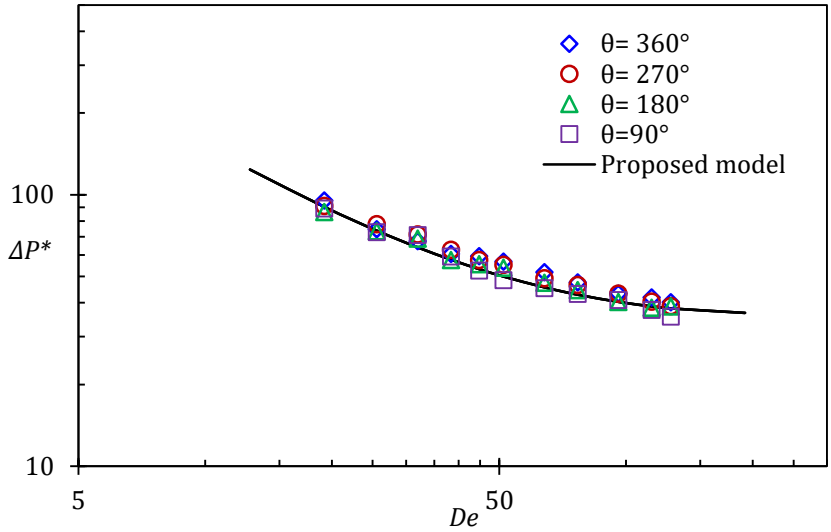

Fig. 7. 22 - ΔP^* vs De for experimental data of different length curved tube and constant radii of curvature ($R = 14.15\ cm$) with proposed model.

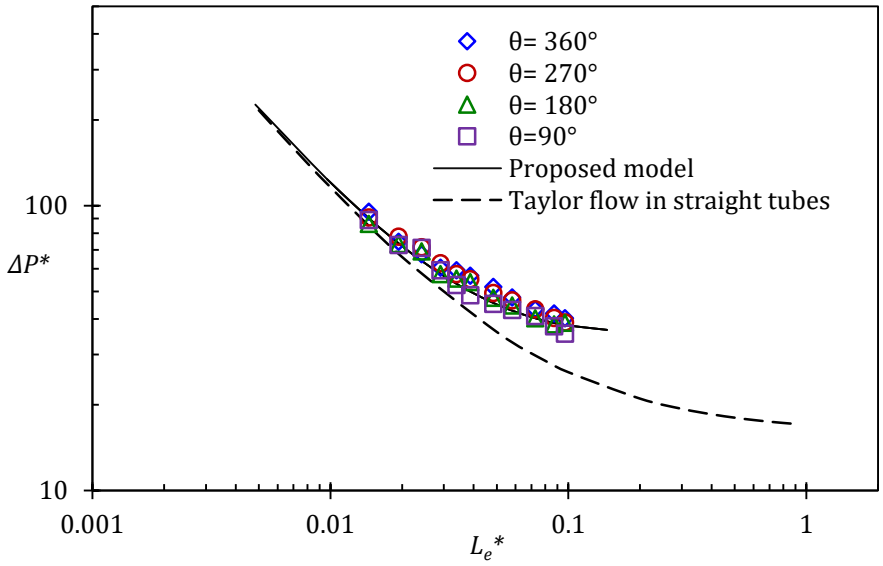

Fig. 7. 23 - ΔP^* vs L_e^* for experimental data of different length curved tube and constant radii of curvature ($R = 14.15\ cm$) with proposed model.

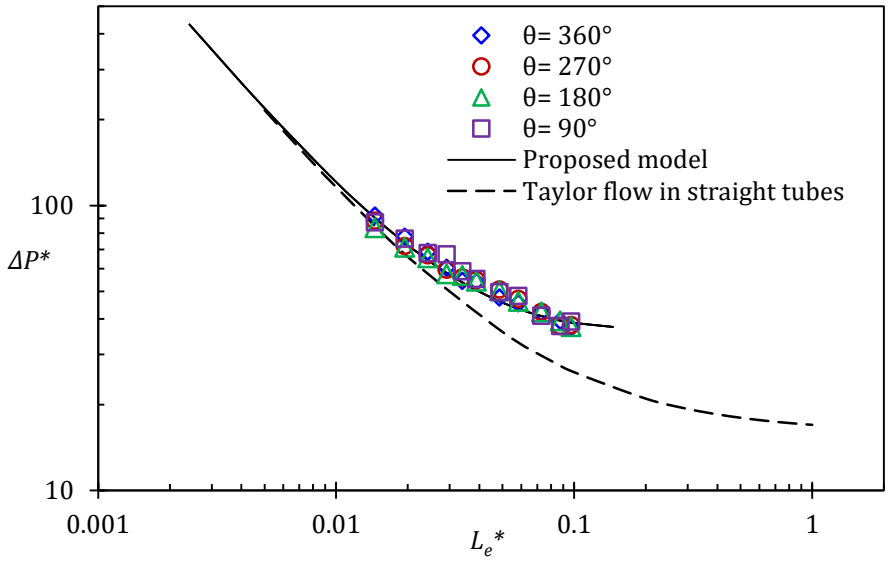

Fig. 7. 24 - ΔP^* vs L_e^* for experimental data of different length curved tube and constant radii of curvature ($R = 10.55\ cm$) with proposed model.

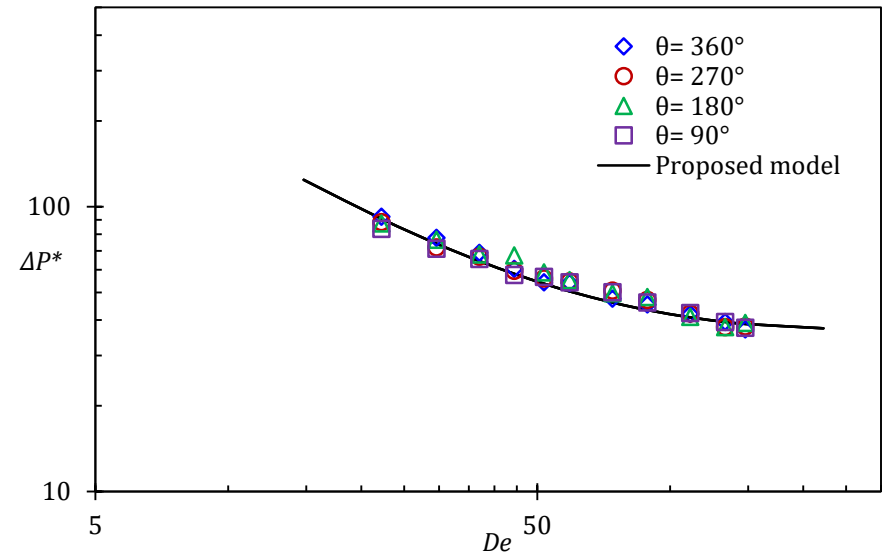

Fig. 7. 25 - ΔP^* vs De for experimental data of different length curved tube and constant radii of curvature ($R = 10.55\ cm$) with proposed model.

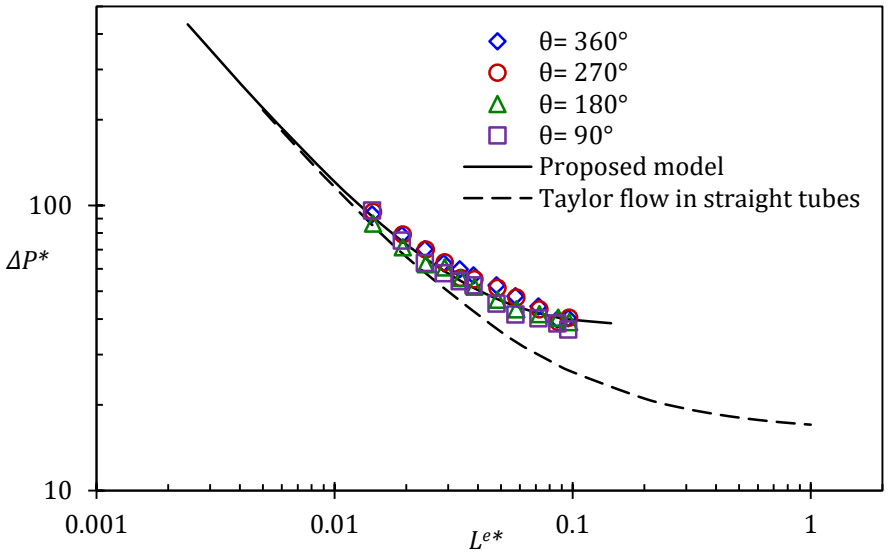

Fig. 7. 26 - ΔP^* vs L_e^* for experimental data of different length curved tube and constant radii of curvature ($R = 7.03\ cm$) with proposed model.

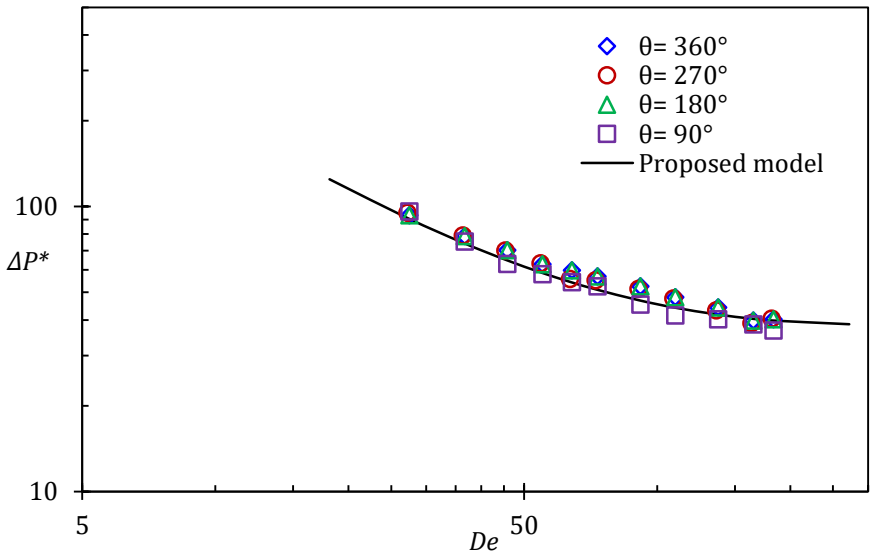

Fig. 7. 27 - ΔP^* vs De for experimental data of different length curved tube and constant radii of curvature ($R = 7.03\ cm$) with proposed model.

The experimental results show that all the data approaches the single-phase Poiseuille model in mini-scale coiled tubing at very high flow rates and two-phase Taylor flow in coiled mini scale tubing with a different Dean number has the greatest pressure drop, where the single phase and interfacial pressure drop dominate in the total pressure drop.

7.6 Conclusions

This experimental study focused on liquid-liquid Taylor flow in coiled and curved mini-scale tubing with inner diameters of 1.59 *mm*, 1.27 *mm*, and 1.016 *mm*. The experiment used coiled flexible tubes with different lengths and radii of curvature. The study investigated the effects of tube size and curvature on the Taylor flow pattern and pressure drop. The experimental data were compared with correlations found in the relevant literature. The comparison revealed the lack of segmented flow physics related to these models and underlined that they are not applicable to liquid-liquid slug flow regimes.

According to the results, it is possible to accurately predict the frictional pressure drop by the flow pattern-based models. This prediction is more precise than predictions by two-phase flow in coiled tubing and Taylor flow in straight tubing models. The frictional pressure gradient was measured, and the data compared well with predictions from the new correlation proposed in this work. The results showed excellent agreement across a wide range of Reynolds, Dean, and Capillary numbers using these scaling parameters. The new model predicted the measured pressure gradient within ± 10 % error. The model and new experimental results provide new insights into liquid-liquid Taylor flow in small scale curved and coiled tubes.

7.7 References

[1] Muzychka, Y. S., Walsh, E. J., and Walsh, P., 2011, "Heat Transfer Enhancement Using Laminar Gas-Liquid Segmented Plug Flows," J. Heat Transfer, 133(4), p. 041902.

[2] Kreutzer, M. T., Kapteijn, F., Moulijn, J. A., Kleijn, C. R., and Heiszwolf, J. J., 2005, "Inertial and Interfacial Effects on Pressure Drop of Taylor Flow in Capillaries," AIChE J., 51(9), pp. 2428–2440.

[3] Abolhasani, M., and Jensen, K. F., 2016, "Oscillatory Multiphase Flow Strategy for Chemistry and Biology," Lab Chip, 16(15), pp. 2775–2784.

[4] Fsadni, A. M., and Whitty, J. P. M., 2016, "A Review on the Two-Phase Pressure Drop Characteristics in Helically Coiled Tubes," Appl. Therm. Eng., 103, pp. 616–638.

[5] Czop, V., Barbier, D., and Dong, S., 1994, "Pressure Drop, Void Fraction and Shear Stress Measurements in an Adiabatic Two-Phase Flow in a Coiled Tube," Nucl. Eng. Des., 149(1–3), pp. 323–333.

[6] Awwad, a., Xin, R. C., Dong, Z. F., Ebadian, M. a., and Soliman, H. M., 1995, "Flow Patterns and Pressure Drop in Air/Water Two-Phase Flow in Horizontal Helicoidal Pipes," J. Fluids Eng., 117(4), p. 720.

[7] Xin, R. C., A, A., Dong, Z. F., and Ebadian, M. A., 1997, "An Experimental Study of Single-Phase and Two-Phase Flow Pressure Drop in Annular Helicoidal Pipes," Int. J. Heat Fluid, 18(5), pp. 482–488.

[8] Mandal, S. N., and Das, S. K., 2003, "Gas-Liquid Flow through Coils," Korean J. Chem. Eng., 20(4), pp. 624–630.

[9] Vashisth, S., and Nigam, K. D. P., 2009, "Prediction of Flow Profiles and Interfacial Phenomena for Two-Phase Flow in Coiled Tubes," Chem. Eng. Process. Process Intensif., 48(1), pp. 452–463.

[10] Xin, R. C., Dong, Z. F., and Ebadian, M. A., 1996, “Heat Transfer of Air/Water Two- Phase Flow in Helicoidal Pipes,” J. Heat Transfer, 118(2), pp. 442–448.

[11] Murai, Y., Inaba, K., Takeda, Y., and Yamamoto, F., 2007, “Backlight Imaging Tomography for Slug Flows in Straight and Helical Tubes,” Flow Meas. Instrum., 18(5–6), pp. 223–229.

[12] Gourma, M., and Verdin, P. G., 2016, “Two-Phase Slug Flows in Helical Pipes: Slug Frequency Alterations and Helicity Fluctuations,” J. Multiph. Flow, 86, pp. 10–20.

[13] Jayakumar, J. S., Mahajani, S. M., Mandal, J. C., Iyer, K. N., and Vijayan, P. K., 2010, “Thermal Hydraulic Characteristics of Air-Water Two-Phase Flows in Helical Pipes,” Chem. Eng. Res. Des., 88(4), pp. 501–512.

[14] Zohurul Islam, M., Mondal, R. N., and Rashidi, M. M., 2017, “Dean-Taylor Flow with Convective Heat Transfer through a Coiled Duct,” Comput. Fluids, 149, pp. 41–55.

[15] Vashisth, S., and Nigam, K. D. P., 2008, “Experimental Investigation of Void Fraction and Flow Patterns in Coiled Flow Inverter,” Chem. Eng. Process. Process Intensif., 47(8), pp. 1287–1297.

[16] Vashisth, S., and Nigam, K. D. P., 2008, “Liquid-Phase Residence Time Distribution for Two-Phase Flow in Coiled Flow Inverter,” Ind. Eng. Chem. Res., 47(10), pp. 3630–3638.

[17] Ghobadi, M., and Muzychka, Y. S., 2014, “Pressure Drop in Mini-Scale Coiled Tubing,” Exp. Therm. Fluid Sci., 57, pp. 57–64.

[18] Adrugi, W. M., Muzychka, Y. S., and Pope, K., 2015, “Heat Transfer in Liquid-Liquid Taylor Flow in a Mini-Scale Tube with Constant Wall Temperature,” ASME 13th International Conference on Nanochannels, Microchannels, and Minichannels.

[19] Mac Giolla Eain, M., Egan, V., and Punch, J., 2015, “Local Nusselt Number Enhancements in Liquid-Liquid Taylor Flows,” Int. J. Heat Mass Transf., 80, pp. 85–97.

[20] Adrugi, W., Muzychka, Y., and Pope, K., 2017, “Heat Transfer in Liquid-Liquid Taylor Flow in Miniscale Curved Tubing for Constant Wall Temperature,” J. Electron. Packag. Trans. ASME, 139(2).

[21] Adrugi, W. M., Muzychka, Y. S., and Pope, K., 2018, “Heat Transfer Model for Liquid-Liquid Taylor Flow in Mini-Scale Coiled Tubing,” ASME Pap. No ICNMM2018-7743.

[22] Vural Gürsel, I., Kurt, S. K., Aalders, J., Wang, Q., Noël, T., Nigam, K. D. P., Kockmann, N., and Hessel, V., 2016, “Utilization of Milli-Scale Coiled Flow Inverter in Combination with Phase Separator for Continuous Flow Liquid-Liquid Extraction Processes,” Chem. Eng. J., 283, pp. 855–868.

[23] Kurt, S. K., Vural Gürsel, I., Hessel, V., Nigam, K. D. P., and Kockmann, N., 2016, “Liquid-Liquid Extraction System with Microstructured Coiled Flow Inverter and Other Capillary Setups for Single-Stage Extraction Applications,” Chem. Eng. J., 284, pp. 764–777.

[24] Malsch, D., Kielpinski, M., Merthan, R., Albert, J., Mayer, G., Köhler, J. M., Süße, H., Stahl, M., and Henkel, T., 2008, “MPIV-Analysis of Taylor Flow in Micro Channels,” Chem. Eng. J., 135(SUPPL. 1), pp. 166–172.

[25] Adrugi, W., Muzychka, Y. S., and Pope, K., 2016, “Pressure Drop of Liquid-Liquid Taylor Flow in Mini-Scale Tubing,” ASME International Mechanical Engineering Congress and Exposition, Proceedings (IMECE).

[26] Holman, J. P., 2012, Experimental Methods for Engineers, McGraw-Hill, New York.

[27] Awad, M. M., and Muzychka, Y. S., 2008, “Effective Property Models for Homogeneous Two-Phase Flows,” Exp. Therm. Fluid Sci., 33(1), pp. 106–113.

[28] Incropera, F. P., DeWitt, D. P., Bergman, T. L., and Lavine, A. S., 2007, Fundamentals of Heat and Mass Transfer, John Wiley & Sons.

CHAPTER 8

Conclusions and Recommendation

The present chapter is concerned with the main conclusions drawn from the whole research presented in this thesis as well as the recommendations for further investigations are presented. The principal objective of the study is to examine and understand the fundamental thermal and hydrodynamic characteristics of the liquid-liquid Taylor flows confined to geometries of the mini-scale tubing. This thesis investigates the fluid friction and heat transfer characteristics for three typical small-scale geometries namely, straight, curved, and coiled which are employed in practical design applications. The experimental programme that was conducted allowed the flow to be investigated and studied under a broad range of operational and geometrical parameters.

8.1 Summary and Conclusions

This section presents a summary of discussing the findings of the thermally and hydrodynamic studies, namely the heat transfer and pressure drop associated with liquid-liquid Taylor flows in short and long straight heat sinks. Then this section will address an overview of the findings of the effect of entrance region and curvature on heat transfer of

liquid-liquid Taylor flow in the curved mini-scale tubing at a constant wall temperature. Finally, this section summarizes thermal behavior and pressure drop using liquid-liquid Taylor flows in the coiled curved mini scale tubing.

For laminar heat transfer study of liquid-liquid Taylor flow in straight mini-scale tubes, copper tubes of different length with constant wall temperature were employed using the experimental approach. For single phase Poiseuille flow as a benchmarking test, the experimental data and theoretical model results were found to be in acceptable agreement with a mean relative error of less than 7%. The results demonstrate that the two-phase flow exhibits Graetz-Slug flow behavior when silicon oil is the variable flow phase and water is introduced with constant flow. However, the flow exhibits Graetz-Poiseuille flow behavior when water is the variable flow phase, and silicon oil is introduced at constant flow. The result highlights the effect of the liquid-liquid Taylor flow in mini scale tubes on heat transfer enhancement with different slug lengths. The mini scale tubes that were used show that the tube length had no significant effect on the heat transfer enhancement when the flow reached the fully developed flow region and the fluid too thermally saturated to produce reasonable results.

Furthermore, the pressure drops of the liquid-liquid segmented flow in the small-scale tubing was investigated. To predict the pressure drop of Taylor flows in small-scale tubes or channels, a theoretical model was developed based on a force balance model into a unit cell, L_e. The model took into consideration the pressure drop due to friction between each fluid and the tube wall, in addition to the capillary pressure drop at the interface of the fluids. Reduced interfacial effects were subjected to the flows when the slugs were of sufficient length for the pressure drop in the capillary to be characteristically Poiseuille law.

As expected, the pressure drop for the two phase flow was much higher than the pressure drop for the single-phase flow.

Moreover, the effect of slug length in continuous and dispersed phases and the range of each liquid flow rate on the transition from Taylor dominated flow to Poiseuille single-phase dominated flow were also shown. According to comparisons with slug flow models, the Walsh et al. model failed to incorporate the dependence of pressure drop on the slug velocity but was included in this model presented in this work. The presented model was in acceptable agreement with the experimental data. New insights into liquid-liquid Taylor flow were provided by the new theoretical model and experimental data for pressure drop in a small scale.

The effect of curvature on the heat transfer of liquid-liquid Taylor flow was studied by using the experimental approach in coiled mini scale tubes with the use of a constant wall temperature. Copper tubes with different radii of curvature and lengths were employed, and the effect of the tube curvature on heat transfer enhancement in liquid-liquid Taylor flow was compared with a model for single-phase flow in the curved tubing. As a result, liquid-liquid Taylor flow in curved and coiled mini scale tubes enhanced heat transfer rates compared to single-phase flow models. The effect of curvature and tube length on the heat transfer associated with liquid-liquid Taylor flow in curved and coiled tubes was discussed in detail. The data analysis reveals more interesting results, showing that the entrance effect dominates the augmentation in short lengths; however, the secondary flow effect becomes greater by increasing the curved tubing length. Also, the viscosity effect on curved tubing heat transfer augmentation was examined using the experimental water / 1 cSt silicone oil, water / 3 cSt silicone oil, and water / 5 cSt silicone oil slug flows. The experimental model

was developed as a function of a *De* number and *Pr* number to describe the heat transfer of Taylor flows in mini scale coiled tubing.

Taking into considerations that this study used coiled tubes of different lengths and radii of curvature, the focus of this study was hence based upon the non-boiling liquid-liquid Taylor flow in the coiled mini scale tubing having inner diameters of 1.59 *mm*, 12.7 *mm* and 1.016 *mm*. The pressure drop study conducted an investigation of the effects of the tubing size, curvature on the Taylor flow pattern and pressure drop. The experimental data obtained were then compared with the modified correlations presented in the relevant literature section. The results led to the conclusion that the frictional pressure drop can be accurately predicted by the flow pattern-based models in coiled tubes. The data for the friction pressure gradient was obtained and compared with the predictions from the proposed correlation of the different curvatures. The numbers of turns in coiled tubes and the lengths of curved tubes of less than one turn with varying values in low Reynolds number were used to evaluate how critical and applicable the proposed model is. The anticipated outcome of the proposed model was based on an asymptotic approach to describe the pressure drop of Taylor flows in curved and coiled mini scale tubing as a function of dimensionless slug length and a Dean number. The results provide new insights into the effect of coiling and secondary flow on pressure drop for liquid-liquid Taylor flow in mini scale systems.

Finally, the proposed models for heat transfer and pressure gradient corresponded to the experimental data and the fitted model predicted the measured data with ± 15% error. The new insights about liquid-liquid Taylor flow in curved and coiled channels with a small

scale provided by the models and the associated experimental results are demonstrating a significant contribution to the field.

8.2 Recommendations for Future Studies

Based on the results of this research, there are still many questions and possible discussions concerning thermal and hydrodynamic characteristics of liquid-liquid Taylor flow in small-scale channel geometries. This section outlines some of the most important questions/ recommendations that should be considered and addresses to improve the current database of results and proposed models. It is therefore recommended to focus on the following aspects in future studies:

- **Taylor Flow in Micro Scale Channels**

All of the results presented in this dissertation were in the mini scale range. However, with the recent advancement in microfabrication technologies, the size of electronic and digital microfluidic devices is decreasing. Therefore, all of the models developed in this research for mini-scale geometries tubing may be used to predict the heat transfer characteristics and pressure gradient in micro-scale channels.

- **Particle Image Velocimetry in Curved Geometry**

Although few investigations have conducted Taylor flow using PIV, there are still many gaps that need to be filled. Few studies were performed to understand the nature of the flow in a curved channel from a heat transfer point of view and also a hydrodynamic point. Micro-PIV observation is needed to find liquid-liquid Taylor flow field change for different Reynolds number and curved geometries.

- **Effects on Film Thickness on Heat Transfer and Pressure Drop**

It has been observed that the liquid film around slugs could have a significant impact on heat transfer and pressure drop in two-phase slug flows by changing the portion of the liquid in circulation and bypass. Further evidence has recently been published by Zhang et al. [1], and Jovanovic´ [2], but additional research is necessary to evaluate the significance of this effect quantitatively. Therefore, future work is required on this phenomenon to improve the current database of models.

- **Using Nanofluids Taylor flow in Mini and Micro Scale Ducts**

Nanofluids are a new class of fluids engineered by dispersing nanometer-size solid particles in base fluids. As a new research frontier, nanofluid two-phase flow and thermal physics have the potential to improve heat transfer and energy efficiency in thermal management systems for many applications. So far, the study of nanofluid two-phase flow and thermal physics is still in its infancy. The physical properties of nanofluids such as surface tension, liquid thermal conductivity, viscosity, and density have significant effects on the nanofluid two-phase flow and heat transfer characteristics [3] [4]. Therefore, using nanofluids Taylor flow for enhancing heat transfer rates at mini and micro scales channels can also be considered in the future studies.

In addition to aspects mentioned above for future studies, and to improve the current database of results and proposed models, extend the scope of this study to provide alternative parameters including the testing of different channel materials, the use of alternative Taylor flows (including gas-liquid), and the different cross sections of test

sections. By using the same inlet conditions, the current study can be extended to determine the effect of these parameters on both the heat transfer and the pressure drop.

8.3 References

[1] Zhang, J., Fletcher, D. F., and Li, W., 2016, "Heat Transfer and Pressure Drop Characteristics of Gas-Liquid Taylor Flow in Mini Ducts of Square and Rectangular Cross-Sections," Int. J. Heat Mass Transf., 103, pp. 45–56.

[2] Jovanović, J., Zhou, W., Rebrov, E. V., Nijhuis, T. A., Hessel, V., and Schouten, J. C., 2011, "Liquid-Liquid Slug Flow: Hydrodynamics and Pressure Drop," Chem. Eng. Sci., 66(1), pp. 42–54.

[3] Cheng, L., Bandarra Filho, E. P., and Thome, J. R., 2008, "Nanofluid Two-Phase Flow and Thermal Physics: A New Research Frontier of Nanotechnology and Its Challenges," J. Nanosci. Nanotechnol., 8(7), pp. 3315–32.

[4] Muzychka, Y. S., Walsh, E., Walsh, P., and Egan, V., 2011, "Non-Boiling Two Phase Flow in Microchannels," *Microfluidics and Nanofluidics Handbook: Chemistry, Physics, and Life Science Principles*, S.K. Mitra, and S. Chakraborty, eds., CRC Press, Taylor & francis group, Boca Raton, FL.

Appendices

Appendix A: Experimental Method

The previous chapters had examined general configurations of the experiments; however, this section explains more details about the various experimental setups employed in conducting this research in addition to experimental uncertainty analysis. A picture was added to vividly illustrate the experimental setup.

A.1 Benchmarking Tests

The process of comparison between employed processes and performance metrics with known best practices is defined as benchmarking. The best-known practices are used as a reference point for evaluating performance or level of quality of the used processes and results. The main purpose of benchmarking tests is to determine the uncertainty of our apparatus used for the measurements. In this study, benchmarking was applied to undertake the tests under similar conditions. Since the correct results had already been established, a comparison was conducted between the obtained experimental results and the expected answers or results. The comparison enabled the verification of the accurate experimental procedure. Fully developed laminar flow in straight tubing is mostly used since the exact results of this study are widely available. This section described how the experimental procedure was benchmarked. Two tests were conducted regarding the benchmarking process: (1) Heat transfer. (2) Pressure drop. These two tests were all conducted on the straight tube but under different working conditions.

A.1.1 Experimental Facilities and Setup

An experimental setup was assembled to measure heat transfer and pressure drop for the laminar internal flow. The experiment facility was assembled at Memorial University in the Micro-fluidics lab. The shown in Fig. (A.1) shows this setup.

The system employs two high-accuracy pumps (Harvard Syringe Pumps) to provide flow accuracy within 0.25 %. These pumps are configured to the specified flow rates. In this system, as a result of the fluids were volumetrically pumped while the pressure could not be adjusted, the maximum volumetric flow rate is proportional to the hydrodynamic resistance of the system setup. However, the pumps could work simultaneously in parallel to provide higher flow rates. Two or four syringes (Hamilton Glass Gastight Syringes) with 100 ml capacity each are employed in this case, however, were dependent on the flow rate. For heat transfer inside copper tubing with a constant wall temperature boundary condition (isothermal tests), a 3013 Isotemp refrigerated circulator from Fisher Scientific Co. (Fig. A.2) is available in the lab, that can provide a constant temperature between -30 to +150 ^{o}C, with ± 1 ^{o}C temperature stability. The copper tube was used as a test section for its high thermal conductivity and then uniform temperature distribution in the tube can be assumed. Two Omega T-type thermocouples are used to measure the inlet and outlet bulk temperature using a simple T-junction with a thermocouple embedded in the flow stream. Three pressure sensors with pressure range from 0-1 psi, 0-5 psi and 0-15 psi were used in conjunction with a plastic PVC tubing to take the pressure drop measurements. A data collection system known as Keithley Data Acquisition system (DAQ) was used to collects data during the experiments.

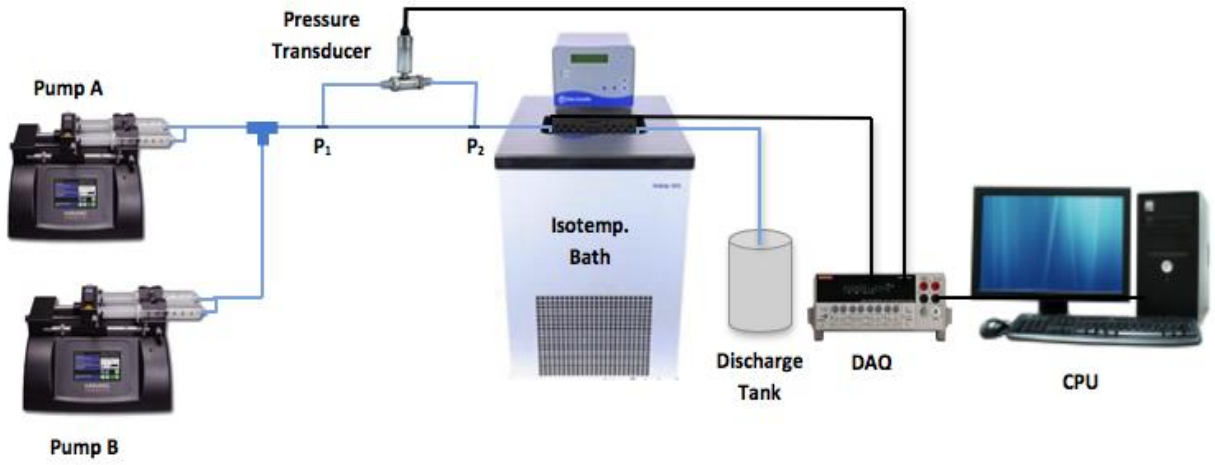

Fig. A. 1 - Schematic of the experimental setup in the microfluidic lab.

Fig. A. 2 - Isotemperature bath.

A.1.2 Heat Transfer

A straight copper tube with163 *mm* long and the diameter of 1.65 *mm* was used to conduct the test. The tube was accurately cut, and the edges were smoothed. Thermocouples were then positioned with the minimum distance at each side from the copper tubing. Since the plastic tubing conductivity is too low relative to copper, it was assumed that the exit temperatures measured were equal to the temperature of the fluids at the end of the copper tubing. The constant wall temperature condition was considered with a surface temperature of 40 ^{o}C while the ambient temperature was around 23 ^{o}C.

The tube was placed in the thermal bath horizontally. The flow assumed to be hydrodynamically developed and thermally developing at the copper tube entrance. The working fluids examined were Water, 0.65 cSt oil, 1 cSt and 3 cSt viscosity silicone oils.

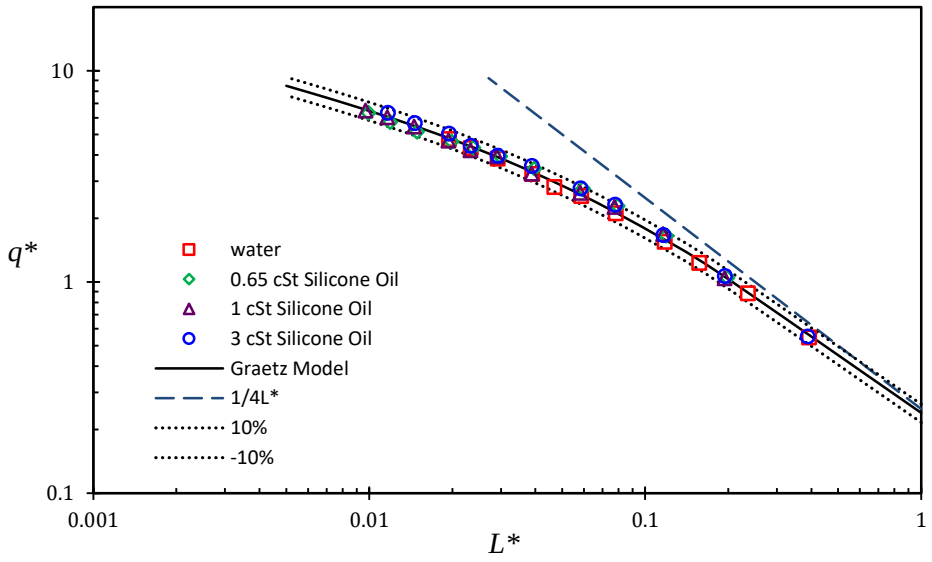

Fig. A. 3 – Heat transfer benchmark test in a straight tube for different liquids with ±10% error band.

The results between the measured heat transfer coefficient and the calculated coefficient revealed a good agreement. The following figures Fig. A.3 reveal the comparison between the Graetz model and the examined fluids.

A.1.3 Pressure Drop

The verification of the pressure drop was done on 0.5 m to 3 m pieces of plastic PVC and copper tubes with 1.59 *mm* and 1.65 *mm* the tube diameter, respectively. The flow was assumed to be hydrodynamic fully developed through tubes. The working fluids employed at the room temperature (24 ^{o}C) were water and three low viscosity silicone oils (1 cSt, 3 cSt, 5 cSt). The flow was laminar flow as Reynolds numbers from 10 up to 1500 was examined, and according to Graetz and Fanning theory:

$$f = \frac{16}{Re} \tag{A.1}$$

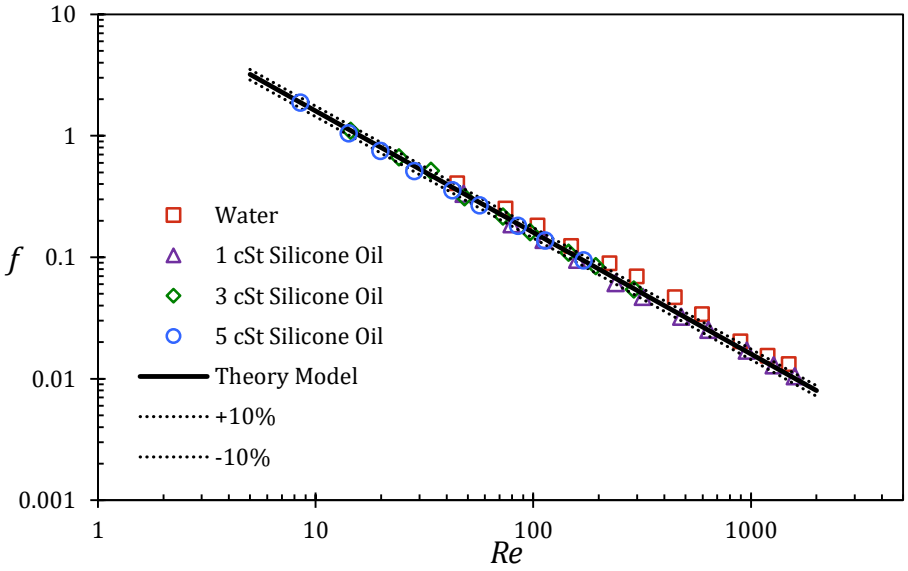

Fig. A. 4 – Fanning friction factor benchmark test in a straight tube for different liquids with $\pm 10\%$ error band.

Pressure drop at each velocity was measured using the most accurate sensor. This was because the pressure drop was measure using the differential pressure sensors having different pressure ranges. The Fig. A.4 revealed the benchmarking summary within the 1 m straight tube. The collected points were within the 15 % range of the straight tube model.

A.1.4 Viscosity

In order to verify the reported values by the company providers, the qualities of working fluids were measured using a precise instrument during the verification process. The manufacturers had provided the viscosity of the silicone oils, as well as their temperature dependencies. However, to confirm the provided data by the providers, (Physica MCR 301 from Rheosys Company) at room temperature was used to confirm the viscosities of the oils. This is a very accurate instrument for conducting these measurements. The following process was used to measure the required torque as different rates of rotational speed were applied to the disk rotating on a film of the fluid. The apparatus then converted measured given torque to the viscosity relating to each speed. Measuring the water's viscosity benchmarked the accuracy of the equipment. The mean viscosity of a fluid could be calculated from of the previously collected data. The measured viscosity at the temperature of 22 ^{o}C and corresponding deviations in addition to the provided viscosity are available in the table A.1.

Table A. 1 - Silicone oils benchmarking results

Fluid	Measured Viscosity	Reported Viscosity	Difference
0.65 cSt	0. 505 cSt	0. 526 cSt	4. 18 %
1 cSt	0. 895 cSt	0. 872 cSt	2. 51 %
3 cSt	2. 616 cSt	2. 717 cSt	3. 87 %
10 cSt	9. 415 cSt	9. 406 cSt	1. 02 %

A.2 Tests Sections

Generally, during the experiments, two types of straight and curved tubing were employed: copper tubing and plastic PVC tubing. Copper tubes were mostly employed in the heat transfer calculation purpose, while the plastic tubing was employed to measure the pressure drop.

During the first part of the experiments, a short and long straight tube that were explained and depicted in Chapter 3 and 4 were employed. The tubes used in Chapter 5, 6 and 7, were curved and coiled. They were cut and curved in the manufacturing shop at MUN. The ends of these tubes were polished; this was to minimize the effect of entrance disturbance. Fig. A.6. shows several the curved and coiled tubes.

In order to investigate the pressure gradient inside mini scale coiled tubes, mini scale plastic tubes were curved around cylinders with different diameters. The Fig. A.7 shows how the tubes for the pressure drop measurement study were coiled.

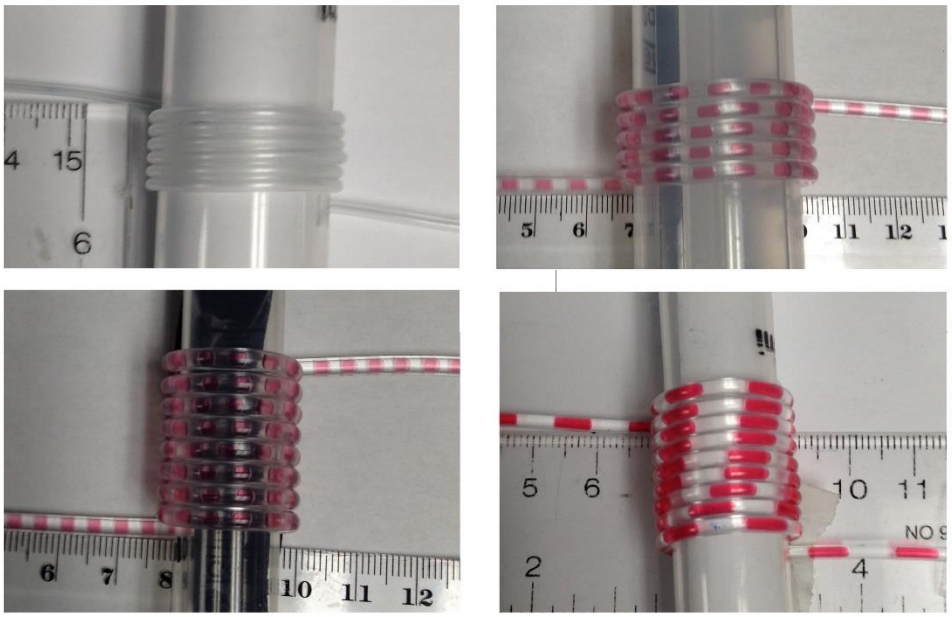

Fig. A. 5 - Samples of the test sections for pressure experiments of Taylor flow in coiled tubing.

Fig. A. 6 - Some of the examined shapes for different lengths and radii of test heat sections.

A.3 Creating Liquid-Liquid Slug flow

Creating a uniform slug train in small-scale tubing has difficulties and challenges. Several segmenters and junctions (T, Y, and X) were used during these experiments to obtain a liquid-liquid slug flow regime (Fig. A.7). Segmenters boxes / segmentation device have already been designed, manufactured and examined in the university labs. The junctions and segmenters with different directions for injecting liquids are shown in Figs. A.8 and A.9.

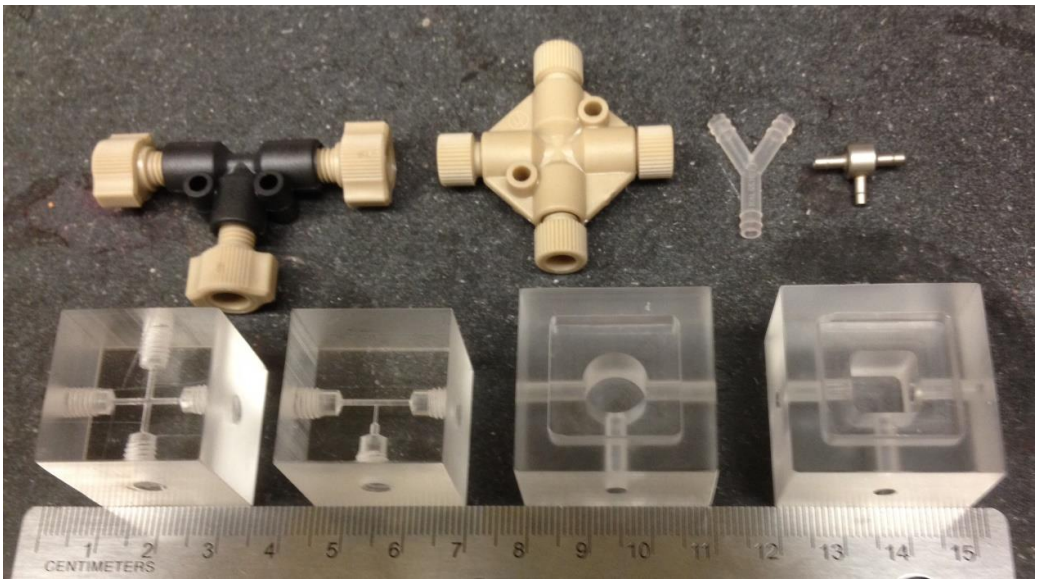

Fig. A. 7 - Junctions and segmenters used in the present work.

One fluid is the dispersed or discontinuous phase and the other will work as the carrier or continuous phase (Fig. A.9). The difficulty is two immiscible liquids becomes the segmented flow, especially in high flow rates that are maintaining the flow pattern. The lab is equipped with a high-speed camera (Phantom v611) that captures images of the plug

train to analysis and calculates liquid fractions. Fig. A.10 shows the snapshot taken from of the Phantom Camera Control software during the experiment.

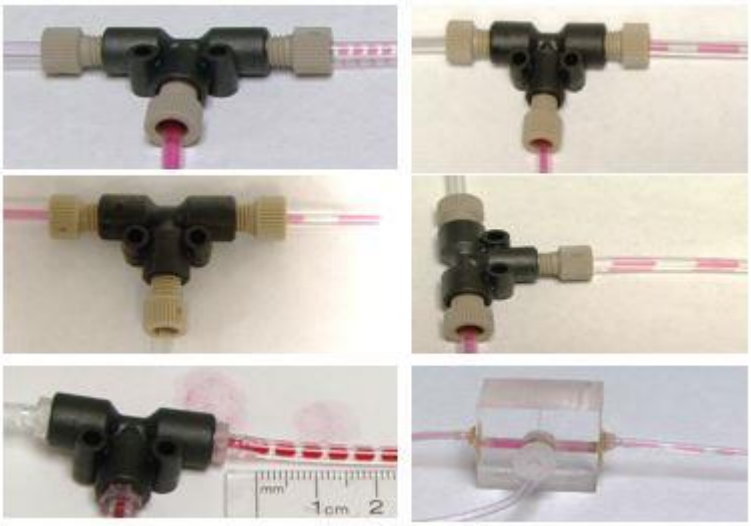

Fig. A. 8 - T-Junction and segmenter box with different directions for injecting liquids.

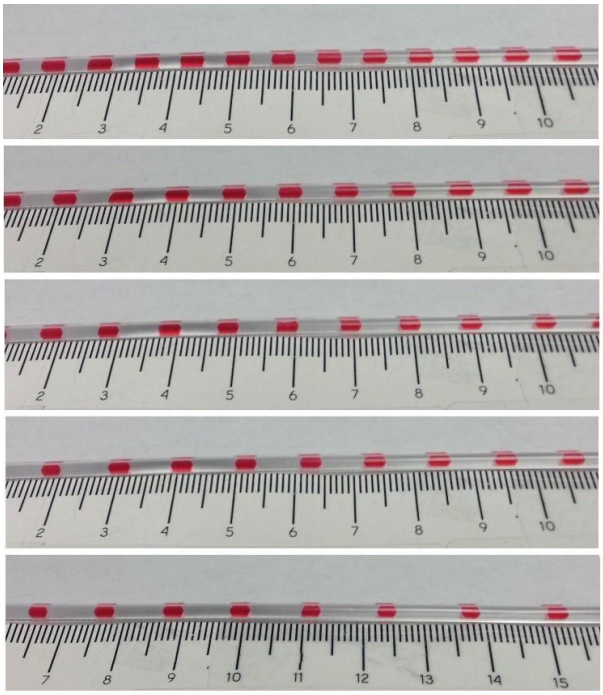

Fig. A. 9 - Images of dyed water/1 cSt silicone oil slug flow for with variable flow rates of silicone oil and constant flow rate of water.

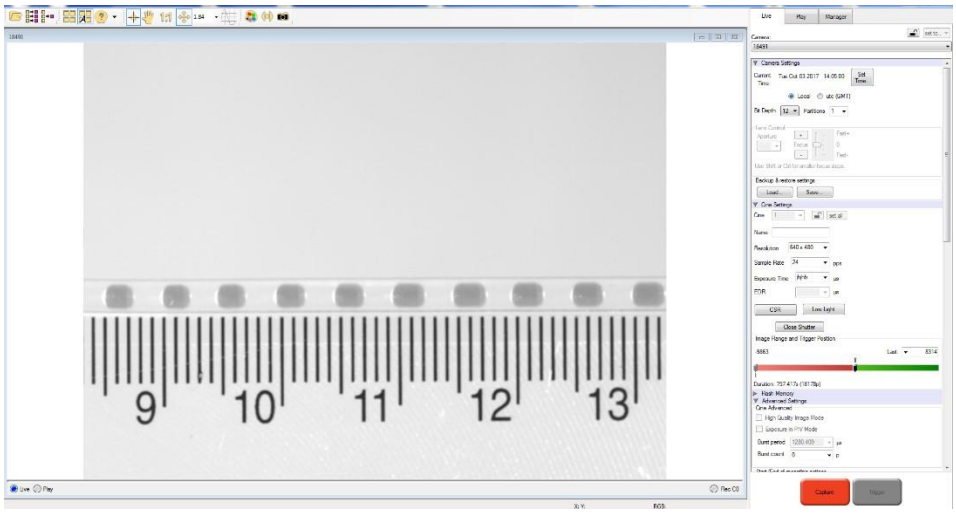

Fig. A. 10 - Snapshot of the Phantom Camera Control software during the experiment.

Appendix B: Uncertainty Analysis

Uncertainties of the reported quantities have been analyzed and reported in each experiment section. The root sum square method by Kline and McClintock [1953] had been used to determine the uncertainties in the experimental measurements and the propagation of errors.

$$R = R(x_1, x_2, x_3, \dots, x_n) \tag{B.1}$$

where x_i are independent measured quantities, the uncertain w_R in the result R is given by

$$w_R = \left[\left(\frac{\partial R}{\partial x_1} w_1\right)^2 + \left(\frac{\partial R}{\partial x_2} w_2\right)^2 + \left(\frac{\partial R}{\partial x_3} w_3\right)^2 + \cdots \left(\frac{\partial R}{\partial x_n} w_n\right)^2\right]^{1/2} \tag{B.2}$$

where w_i are the uncertainties in the independent variables x_i.

Estimating uncertainty of experimental results of single phase and two-phase flows were performed for both hydrodynamic and thermal parameters. The major four parameters were

determined through calculations as samples: Re, f, L^* and q^*or Nu. In each of the above cases the uncertainty of the results is calculated. These include the uncertainties of measuring equipment, such as temperature, mass flow rate, pressure, etc. Uncertainties of the measuring equipment used in the experiment setup which are specified by manufacturer. This happens as an amount for each independent variable was assigned depending on the uncertainties of each variable. This method was applied to the parameters above, hence through calculations the expressions for the uncertainty due to experimental measurements could be determined. The uncertainty in the independent variables affected the uncertainty of the experimental measurements of temperature and pressure. They are summarized in Table B.1.

Table B. 1 - Uncertainty in Measurements.

Measurement	Uncertainty
Temperature [^oC]	$\pm 0.1\ ^oC$
Pressure [Pa]	$\pm 1\ \%$
Flow Rate [*ml/min*]	$\pm 0.25\ \%$
Dimension Tolerance [mm]	$\pm 0.02\ mm$
Fluid Properties	$\pm 2 - 5\ \%$

B.1 Uncertainty in Reynolds Number and Friction Factor

The Reynolds number can be defined as:

$$Re = \frac{\rho\, u\, D_h}{\mu} \tag{B.3}$$

The overall uncertainty in the Reynolds number may be computed from

$$\frac{w_{Re}}{Re} = \left[\left(\frac{w_\rho}{\rho}\right)^2 + \left(\frac{w_u}{u}\right)^2 + \left(\frac{w_{D_h}}{D_h}\right)^2 + \left(\frac{w_\mu}{\mu}\right)^2\right]^{1/2} \tag{B.4}$$

or

$$\frac{w_{Re}}{Re} = \left[\left(\frac{w_{\dot{m}}}{\dot{m}}\right)^2 + \left(\frac{w_{D_h}}{D_h}\right)^2 + \left(\frac{w_\mu}{\mu}\right)^2 + \left(\frac{w_A}{A}\right)^2\right]^{1/2} \tag{B.5}$$

The friction factor can be defined as:

$$f = \frac{\Delta P}{2\,\rho\, u^2}\,\frac{D_h}{L} \tag{B.6}$$

The uncertainty in the overall pressure drop may be determined from the following expression for the uncertainty in the friction factor:

$$\frac{w_f}{f} = \left[\left(\frac{w_{\Delta P}}{\Delta P}\right)^2 + \left(-2\frac{w_u}{u}\right)^2 + \left(\frac{w_\rho}{\rho}\right)^2 + \left(\frac{w_L}{L}\right)^2 + \left(\frac{w_{D_h}}{D_h}\right)^2\right]^{1/2} \tag{B.7}$$

where

$$\frac{w_u}{u} = \left[\left(\frac{w_{\dot{m}}}{\dot{m}}\right)^2 + \left(\frac{w_\rho}{\rho}\right)^2 + \left(\frac{w_A}{A}\right)^2\right]^{1/2} \tag{B.8}$$

B.2 Uncertainty in Dimensionless Thermal Length and Mean Heat Flux

The uncertainty in the overall heat transfer coefficient may be determined by the uncertainty in the dimensionless thermal length and mean heat flux or Nusselt number.

The dimensionless thermal length can be defined as:

$$L^* = \frac{L/D_h}{Pr\,Re} \tag{B.9}$$

The overall uncertainty in the L^* may be computed from

$$\frac{w_{L^*}}{L^*} = \left[\left(\frac{w_L}{L}\right)^2 + \left(\frac{w_{D_h}}{D_h}\right)^2 + \left(\frac{w_{Pr}}{Pr}\right)^2 + \left(\frac{w_{Re}}{Re}\right)^2\right]^{1/2} \tag{B.10}$$

where

$$\frac{w_{Pr}}{Pr} = \left[\left(\frac{w_\mu}{\mu}\right)^2 + \left(\frac{w_{c_p}}{c_p}\right)^2 + \left(\frac{w_k}{k}\right)^2\right]^{1/2} \tag{B.11}$$

The dimensionless mean heat flux can be defined as:

$$q^* = \frac{\bar{q}/D_h}{k\,\Delta T} \tag{B.12}$$

The overall uncertainty in the q^* may be computed from

$$\frac{w_{q^*}}{q^*} = \left[\left(\frac{w_{\bar{q}}}{\bar{q}}\right)^2 + \left(\frac{w_{D_h}}{D_h}\right)^2 + \left(\frac{w_k}{k}\right)^2 + \left(\frac{w_{\Delta T}}{\Delta T}\right)^2\right]^{1/2} \tag{B.13}$$

where $\bar{q} = {}^{Q}/_{A}$ and $Q = \dot{m}c_p\Delta T$.

$$\frac{w_{\bar{q}}}{\bar{q}} = \left[\left(\frac{w_A}{A}\right)^2 + \left(\frac{w_{\dot{m}}}{\dot{m}}\right)^2 + \left(\frac{w_{c_p}}{c_p}\right)^2 + \left(\frac{w_{\Delta T}}{\Delta T}\right)^2\right]^{1/2} \tag{B.14}$$

and

$$\frac{w_{\Delta T}}{\Delta T} = \left[\left(\frac{w_{T_i}}{T_i}\right)^2 + \left(\frac{w_{T_o}}{T_o}\right)^2\right]^{1/2} \tag{B.15}$$

The above equations are applied to the two data sets for lower flow rate $\dot{Q}_{min} = 3\,ml/min$ and at higher flow rate $\dot{Q}_{max} = 100\,ml/min$. Considerations are taken to

account for all the parameters changes between the two data sets except for Prandtl number. The Prandtl number uncertainty does not change between the data sets. All the uncertainties for important parameters are shown in Table B.2.

Table B. 2 - Uncertainty in Parameters.

Parameters	Uncertainty
Re	3.98 % - 6.31 %
f	5.64 % - 6.62 %
q^*	4.51 % - 7.51 %
Nu	4.52 % - 7.52 %
L^*	4.46 % - 7.47 %
Pr	3.46 % - 6.92 %